Investigation of pathomechanisms and treatment safety of age-related and juvenile macular degeneration

Dissertation

der Mathematisch-Naturwissenschaftlichen Fakultät
der Eberhard Karls Universität Tübingen
zur Erlangung des Grades eines
Doktors der Naturwissenschaften
(Dr. rer. nat.)

vorgelegt von
Tatjana Taubitz
aus
Bad Neustadt a. d. Saale

Tübingen
2019

Gedruckt mit Genehmigung der Mathematisch-Naturwissenschaftlichen Fakultät der Eberhard Karls Universität Tübingen.

Tag der mündlichen Qualifikation:	03.03.2020
Dekan:	Prof. Dr. Wolfgang Rosenstiel
1. Berichterstatter:	Prof. Dr. Ulrich Schraermeyer
2. Berichterstatter:	Prof. Dr. Michael Duszenko
3. Berichterstatter:	Prof. Dr. Thomas Langmann

Table of contents

Table of figures

Abbreviations

A2E	N-retinylidene-N-retinylethanolamin
ABCA4	ATP-binding cassette A4
AF	autofluorescence
AMD	age-related macular degeneration
Ang-2	angiopoietin 2
ARVO	Association for Research in Vision and Ophthalmology
ATP	adenosine triphosphate
atRAL	all-*trans*-retinal
atROL	all-*trans*-retinol
CC	choriocapillaris
CNV	choroidal neovascularisation
DARPin	designed ankyrin repeat protein
DNA	deoxyribonucleic acid
ELOVL4	Elongation of very long chain fatty acids-like 4
EMA	European Medicines Agency
EudraCT	European Union Drug Regulating Authorities Clinical Trials
Fc	fragment crystallisable
FcγRIIa	low affinity immunoglobulin gamma Fc region receptor II-a
FDA	Food and Drug Administration
GA	geographic atrophy
IgG	Immunoglobulin G
IUPAC	International Union of Pure and Applied Chemistry
NIR	near-infrared
NretPE	N-retinylidene-phosphatidylethanolamine
OCT	optical coherence tomography
OMIM	Online Mendelian Inheritance in Man
PEDF	pigment epithelium-derived factor
PROM1	prominin-1
RDH8	retinol dehydrogenase 8
RPE	retinal pigment epithelium
scFv	single-chain variable fragment
STGD1	Stargardt disease 1
SW	short-wavelength
VEGF	vascular endothelial growth factor

Zusammenfassung

Im Menschen basiert das hochaufgelöste Sehen auf einer spezialisierten anatomischen Struktur der Netzhaut, der sogenannten Makula. Obwohl sie nur einen Durchmesser von 5,5 mm hat, ist die Makula unentbehrlich für Sehvorgänge bei denen ein Objekt fixiert wird, wie zum Beispiel beim Lesen oder dem Erkennen von Gesichtern. Ein Verlust der Makula führt daher bei Betroffenen zu starken Einschränkungen im Alltag, auch wenn das periphere Sehen erhalten ist und so zumindest eine räumliche Orientierung noch möglich ist.

Makuladegeneration tritt für gewöhnlich entweder als multifaktorielle Alterserkrankung (altersbedingte Makuladegeneration, AMD) oder aber als vererbte, seltene Erkrankung auf (die häufigste ist dabei Morbus Stargardt, STGD1). AMD kann in eine „feuchte“ (exudative) Form und eine „trockene“ (nicht-exudative) Form unterteilt werden. Die feuchte Form ist charakterisiert durch die Neubildung von Blutgefäßen mit dadurch bedingter Ödembildung und Einblutungen, während die trockene Form durch eine örtliche Degeneration von Photorezeptoren, retinalen Pigmentepithelzellen und des versorgenden Kapillarbetts gekennzeichnet ist. Der erbliche M. Stargardt hat ein ähnliches klinisches Bild wie die trockene AMD, obwohl die zugrundeliegenden Krankheitsmechanismen unterschiedlich sind. Bislang sind sowohl AMD, als auch M. Stargardt nicht heilbar. Da die feuchte AMD aber von einen Überschuss an Wachstumsfaktoren, wie z. B. dem *vascular endothelial growth factor* (VEGF), begleitet ist, erlaubt eine wiederholte intravitreale Gabe von anti-VEGF Therapeutika die akuten, durch das Ödem bedingten Sehstörungen zu beseitigen und den Krankheitsverlauf zu verlangsamen.

Die vorliegende Doktorarbeit beschäftigt sich mit den pathologischen Veränderungen und der pharmakologischen Therapie der Makuladegeneration und untersucht dabei drei Aspekte:

1) Licht- und elektronenmikroskopische Untersuchung der Pathomechanismen bei AMD und M. Stargardt anhand von menschlichem Spendermaterial bzw. von drei Stargardt Mausmodellen
2) Aufklärung der subzellulären Ursprungs der Nahinfrarot-Autofluoreszenz (NIR-AF), die zur Diagnostik und Verlaufsbeobachtung bei retinalen Erkrankungen wie AMD und M. Stargardt eingesetzt wird

3) Untersuchung der unerwünschte Arzneimittelwirkungen auf ultrastruktureller Ebene nach der intravitrealen Gabe von anti-VEGF Wirkstoffen für die Behandlung der feuchten AMD

Eine licht- und elektronenmikroskopische Untersuchung von menschlichem Augengewebe mit und ohne AMD zeigte, dass sowohl in der trockenen, als auch der feuchten Form der AMD, der Verlust der Choriocapillaris, dem versorgenden Kapillarbett, der retinalen Degeneration vorausgeht. Diese Studie beantwortete die lange unbeantwortete Frage welches retinale Gewebe bei der AMD zuerst degeneriert. Der Verlauf von M. Stargardt wurde mit Hilfe von 3 häufig verwendeten Stargardt Mausmodellen untersucht. Diese Untersuchung zeigte auffällige pathologische Veränderungen, die aber nur in einem albino und nicht in zwei pigmentierten Mausmodellen auftraten. Dies unterstreicht den vorteilhaften Einfluss, den okulares Melanin womöglich auf die Krankheitsausprägung hat.

Weiterhin konnte gezeigt werden, dass NIR-AF keine intrinsische Eigenschaft von Melanin ist, wie bislang angenommen wurde, sondern vielmehr eine Konsequenz von Melaninschädigung aufgrund von Licht und/oder oxidativem Stress. Weiterhin stellte sich heraus, dass NIR-AF nicht nur von Melanosomen, sondern auch von Lipofuszin, einem Nebenprodukt des Sehzyklus, das sich im Alter oder bei bestimmten Krankheiten im retinalen Pigmentepithel ansammelt, herrühren kann. Diese Erkenntnisse sind sowohl für die Aufklärung der Pathomechanismen bei Melanin- und Lipofuszin-assoziierten Krankheiten, als auch für die Verbesserung der NIR-AF basierten Diagnostik relevant.

Darüber hinaus legten frühere ultrastrukturelle Untersuchungen von unerwünschten Arzneimittelwirkungen des Immunglobulin G (IgG)-basierten anti-VEGF Wirkstoffes Bevacizumab nahe, dass das IgG-Fc Fragment (engl. *fragment crystallisable*) an der Entstehung der beobachteten unerwünschten Wirkungen beteiligt ist. Dies wurde anhand von Studien bestätigt, bei denen ultrastrukturelle Veränderungen nach intravitrealer Gabe von anti-VEGF Wirkstoffen mit und ohne Fc Fragment in Affenaugen bzw. nach intravitrealer Gabe von isoliertem Fc Fragment in Rattenaugen untersucht wurden. Diese Arbeiten unterstreichen die Rolle des Fc Fragments bei unerwünschten Arzneimittelwirkungen von IgG-basierten pharmakologischen Wirkstoffen, die in der Augenheilkunde Anwendung finden.

Zusammengefasst untersucht die vorliegende Doktorarbeit Schlüsselereignisse im Pathomechanismus der AMD (Reihenfolge des Gewebeverlustes) und des M. Stargardt (angedeutete Schutzwirkung des Melanins), klärt die subzelluläre Herkunft des NIR-AF Signals auf, das für augenheilkundliche Diagnostik und Verlaufsbeobachtung herangezogen wird, und bestätigt die Beteiligung des Fc Fragments an unerwünschten Arzneimittelwirkungen, die nach der intravitrealen Gabe von anti-VEGF Wirkstoffen beobachtet wurden.

Summary

In humans, high-resolution vision relies on a specialised anatomical structure of the retina, the so called macula. While only 5.5 mm in diameter, the macula is indispensable for visual tasks depending on visual fixation of an object, such as reading and facial recognition. Loss of the macula therefore heavily impairs affected individuals, even though peripheral vision is not inhibited and spatial orientation is still possible.

Macular degeneration usually arises either as multifactorial age-dependent disease (age-related macular degeneration, AMD) or as rare hereditary disease (the most common one being Stargardt disease, STGD1). AMD can be sub-classified in a "wet" (exudative) form that is characterised by neovascularisation with collateral oedema and bleeding, and a "dry" (non-exudative) form defined by local degeneration of photoreceptors, retinal pigment epithelium cells and the supporting capillary bed. Inherited Stargardt disease has a similar clinical presentation to dry AMD, even though the underlying disease mechanisms differ. To date, no cure for AMD or Stargardt disease is available. However, since wet AMD is accompanied with a surplus of growth factors, e.g. vascular endothelial growth factor (VEGF), the repeated intravitreal application of anti-VEGF therapeutics allows for a reversal of acute visual distortions due to oedema and a reduction of disease progression.

This thesis deals with the pathologic processes and pharmacological therapy of macular degeneration and therefore investigates three aspects:

1) pathomechanisms in AMD and Stargardt disease, investigated by light- and electron microscopy on human donor samples and three Stargardt mouse models, respectively
2) resolving the subcellular origin of near-infrared autofluorescence (NIR-AF) used in diagnostics and monitoring of retinal diseases, such as AMD and STGD1
3) adverse events on the ultrastructural level after intravitreal use of anti-VEGF compounds for treatment of wet AMD

A light and electron microscopic investigation of human ocular tissue with and without AMD revealed that a loss of choriocapillaris, the nourishing capillary bed

underneath the retina, precedes retinal degeneration in both the wet and the dry form of AMD. This study answered the open question of which retinal tissue is the first to degenerate in AMD. Stargardt disease progression was investigated in three commonly used Stargardt mouse models and revealed distinctive pathologic changes only present in an albino, but not in two pigmented mouse models, highlighting the potential beneficial impact of ocular melanin in disease modulation.

NIR-AF was shown to not be an intrinsic property of melanin, as previously thought, but rather a consequence of melanin damage due to photic and/or oxidative stress. Furthermore, NIR-AF was found to not only stem from melanosomes, but also partly from lipofuscin, a byproduct of the visual cycle that accumulates with age and/or disease in the retinal pigment epithelium. These findings are relevant for both elucidating the pathomechanisms in melanin- and lipofuscin-associated retinal diseases and the refinement of NIR-AF based diagnostics.

And lastly, previous ultrastructural investigations of adverse events of the immunoglobulin G (IgG)-based anti-VEGF compound bevacizumab suggested that the fragment crystallisable (Fc) unit is involved in the development of said adverse events. This was confirmed by studies analysing ultrastructural changes after intravitreal application of anti-VEGF compounds with and without Fc fragment in monkey eyes and intravitreal application of isolated Fc fragments in rat eyes. These works emphasize the role of the Fc fragment in adverse events of IgG-based pharmacological compounds used in ophthalmology.

To conclude, the present thesis investigates key events in the pathomechanisms of AMD (order of tissue loss) and STGD1 (indicated protective role of melanin), identifies the subcellular origin of the NIR-AF signal used in ophthalmologic diagnostics and disease monitoring and confirms the involvement of the Fc fragment in adverse events observed after intravitreal application of anti-VEGF compounds.

List of publications enclosed in this thesis

The present thesis encompasses in total six peer-reviewed publications. The first two [1, 2] were published during my time as a student research assistant (*studentische Hilfskraft*) in the group of Prof. Dr. Schraermeyer and contain considerable contributions by me regarding the experimental work. These articles present groundwork to the later publications and were therefore included in the present thesis. The final four articles [3-6], resulted from my work as a PhD student. All publications are independent of my diploma thesis that was also conducted in the laboratory of Prof. Dr. Schraermeyer.

For better understanding, the main text of this thesis does not deal with the manuscripts in chronological order, but arranged by topic.

A) Articles based on work that was conducted during my time as a student research assistant.

1) Biesemeier, A., Taubitz, T., Julien, S., Yoeruek, E. & Schraermeyer, U. **Choriocapillaris breakdown precedes retinal degeneration in age-related macular degeneration.** *Neurobiology of aging* 35, 2562-2573, DOI: 10.1016/j.neurobiolaging.2014.05.003 (2014).

2) Julien, S., Biesemeier, A., Taubitz, T. & Schraermeyer, U. **Different effects of intravitreally injected ranibizumab and aflibercept on retinal and choroidal tissues of monkey eyes.** *The British journal of ophthalmology* 98, 813-825, DOI: 10.1136/bjophthalmol-2013-304019 (2014).

B) Articles based on work that was conducted during my time as a PhD student.

3) Ludinsky, M., Christner, S., Su, N., Taubitz, T., Tschulakow, A., Biesemeier, A., Julien-Schraermeyer, S. & Schraermeyer, U. **The effects of VEGF-A-inhibitors aflibercept and ranibizumab on the ciliary body and iris of monkeys.** *Graefe's archive for clinical and experimental ophthalmology* 254, 1117-1125, DOI: 10.1007/s00417-016-3344-8 (2016).

4) Taubitz, T., Steinbrenner, L. P., Tschulakow, A. V., Biesemeier, A., Julien-Schraermeyer, S. & Schraermeyer, U. **Effects of intravitreally injected**

Fc fragment on rat eyes. *Graefe's archive for clinical and experimental ophthalmology* 254, 2401-2409, DOI:10.1007/s00417-016-3511-y (2016).

5) Taubitz, T., Tschulakow, A. V., Tikhonovich, M., Illing, B., Fang, Y., Biesemeier, A., Julien-Schraermeyer, S. & Schraermeyer, U. **Ultrastructural alterations in the retinal pigment epithelium and photoreceptors of a Stargardt patient and three Stargardt mouse models: indication for the central role of RPE melanin in oxidative stress.** *PeerJ* 6, e5215, DOI: 10.7717/peerj.5215 (2018).
6) Taubitz, T., Fang, Y., Biesemeier, A., Julien-Schraermeyer, S. & Schraermeyer, U. **Age, lipofuscin and melanin oxidation affect fundus near-infrared autofluorescence.** *EBioMedicine* 48, 592-604, DOI: 10.1016/j.ebiom.2019.09.048 (2019).

All manuscripts are enclosed as subsections in the results and discussion section (section 3) of this thesis. Comments about my particular contributions for each manuscript can be found at the beginning of the respective subsections.

1 Introduction

1.1 Ocular anatomy

The mammalian eyeball is enclosed by a three-layered wall consisting of the exterior fibrous tunic (subdivided into cornea and sclera), the uvea in the middle (consisting of choroid, ciliary body, iris) and the retina, the innermost layer (Fig. 1). The space inside the eyeball between lens and retina is filled by a clear, gelatinous mass called vitreous body.

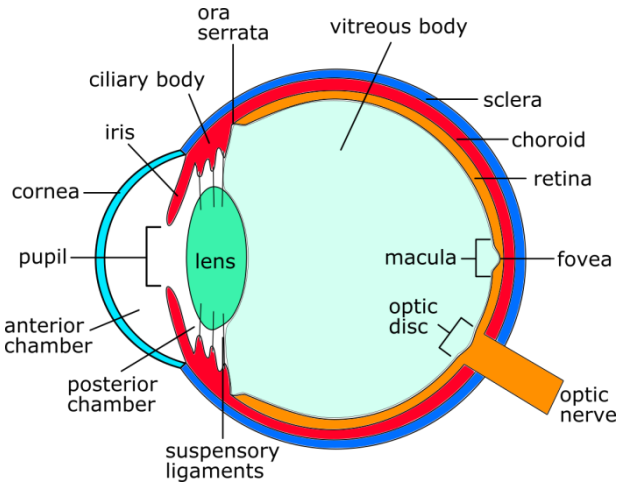

Figure 1: Schematic view of the primate eye (not to scale). Own work.

The retina is a highly organised nervous tissue consisting of light-sensitive photoreceptor cells, bipolar, horizontal and amacrine cells that are the first processing unit for the visual signal, Müller glia that are essential for structural integrity and light transmission and ganglion cells that transmit the visual signal towards the brain (Fig. 2). The big vessels of the retinal vasculature can be found in the innermost layers, the nerve fibre layer and the ganglion cell layer, while retinal capillaries can be found above and below the inner nuclear layer.

There are two types of photoreceptors: rod cells that function in low-light conditions and mediate night vision and cone cells that function in bright-light conditions and are responsible for colour vision. Both photoreceptor types are not equally distributed in the human retina. While rods are mostly present in the peripheral part of the retina, cones are predominantly found in the central parts. An outstanding anatomic feature of the primate central retina, that also has the highest density of cones, is the macula that will be described below in section 1.3.

A specialised subunit of the photoreceptor cell, the so-called outer segment, contains 1000 – 2000 stacked discs. In rod cells, these discs are separate and not connected to the plasma membrane, while in cone cells, the discs are continuous invaginations of the plasma membrane. In the disc membranes, the visual pigments, the most well-known being rhodopsin in rods, and further auxiliary proteins are located.

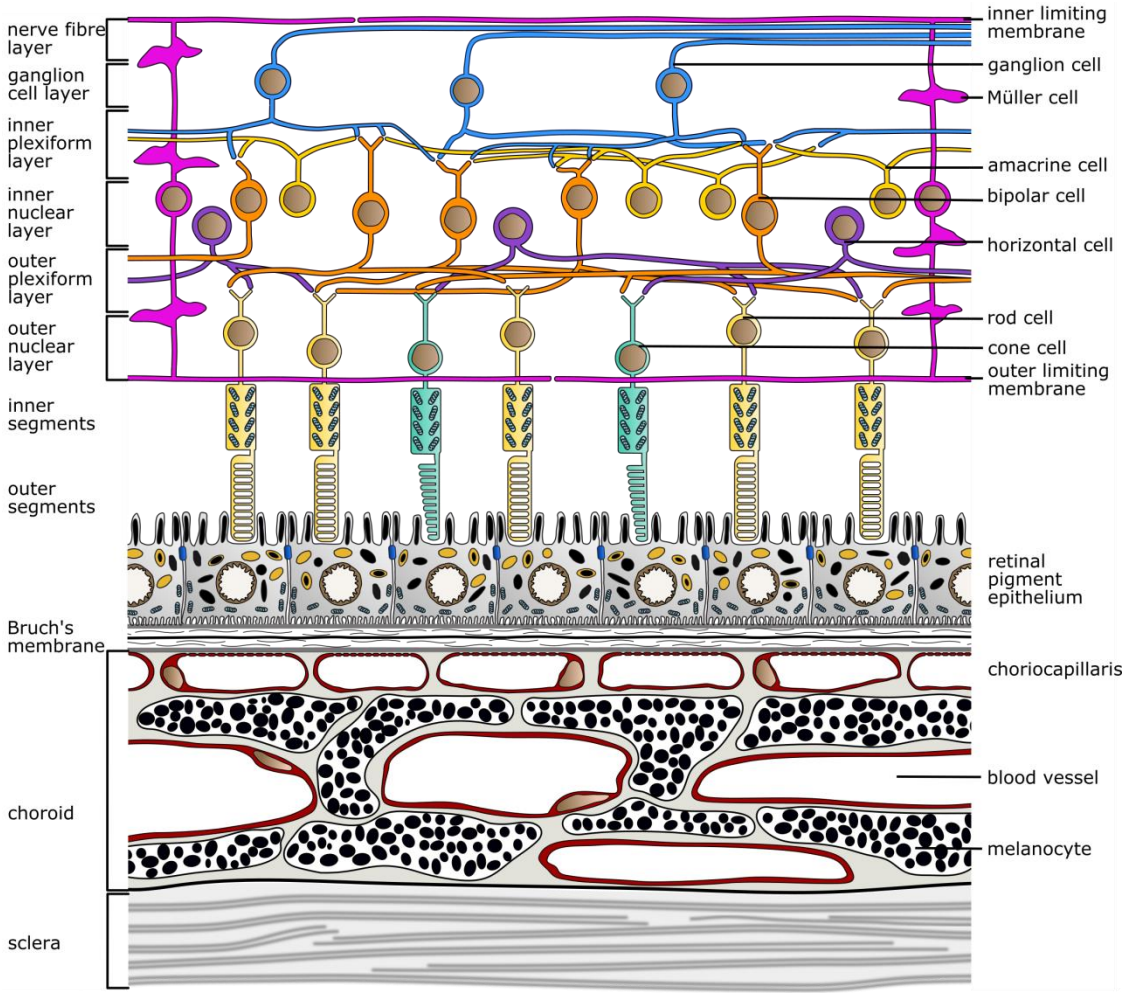

Figure 2: Schematic view of the human retina and underlying structures (not to scale). Own work, partially based on data published in [7].

The photoreceptors and the underlying retinal pigment epithelium (RPE) form a functional unit (reviewed in [8]). The main functions of the RPE comprise:

- The visual cycle, the "recycling" of all-*trans*-retinal released by the photoreceptors after photo transduction to 11-*cis*-retinal that can be reused to form new visual pigments (reviewed in [9]).
- Formation of the outer blood-retina barrier while transporting water and lactate from the retina to the blood and nutrients like glucose and do-

cosahexaenoic acid from the blood to the retina. In fact, recent findings indicate that RPE and photoreceptors share a "metabolic ecosystem" in which the RPE transports glucose to the photoreceptors that convert it to lactate by glycolysis; the lactate is then partly used by Müller cells and the RPE as fuel [10].

- Phagocytosis of photoreceptor outer segment tips that are shed as part of the continual renewal of the outer segment. Since photoreceptor outer segments contain high levels of photosensitive material like polyunsaturated fatty acids and are exposed to intense light levels each day, photo-damaged material can accumulate. Thus, outer segment tips are shed each morning after light onset and phagocytosed by the RPE, while the outer segment is replenished at its base (reviewed in [11]). A complete renewal of the outer segment is thereby achieved within 10 days [12]. Since each adult human RPE cell covers about 35 photoreceptors, it is estimated that each RPE cell phagocytoses hundreds of thousands outer segment discs during its lifetime [11].
- Secretion of a variety of growth factors such as fibroblast growth factors, pigment epithelium-derived factor, ciliary neurotrophic factor, platelet-derived growth factor, vascular endothelial growth factor, tissue inhibitor matrix protease, complement factor H, interleukin 8 and monocyte chemotactic protein 1 among others. These factors are closely regulated in the healthy eye to ensure the stability of the photoreceptors, the stability of the supplying capillary bed (the so-called choriocapillaris, see below) and the immune modulation.

The RPE forms a cuboidal monolayer and gained its name "pigment epithelium" from the fact that the RPE cells are highly pigmented. An overview over the RPE pigmentation will be given in section 1.2.

The RPE is situated on Bruch's membrane, which is not a membrane in the molecular biological sense, but in the histological sense; it is composed of 5 distinct layers of extracellular matrix material as illustrated in Fig. 3: 1) the basement membrane of the RPE, 2) the inner collagenous zone, 3) the central band of elastic fibres, 4) the outer collagenous zone and 5) the basement membrane of the endothelial cells of the choriocapillaris. With age, undegradable material beneath the RPE can accumulate either between the plasma membrane and the basement

membrane of the RPE (basal laminar deposits) or between the basement membrane of the RPE and the inner collagenous zone (basal linear deposits) [13]. The latter type of deposit can form so-called drusen that are big enough to be observable by funduscopy and, when being large or present in high numbers, can be associated with age-related retinal disease, as will be expanded on in section 1.4.1 [13, 14].

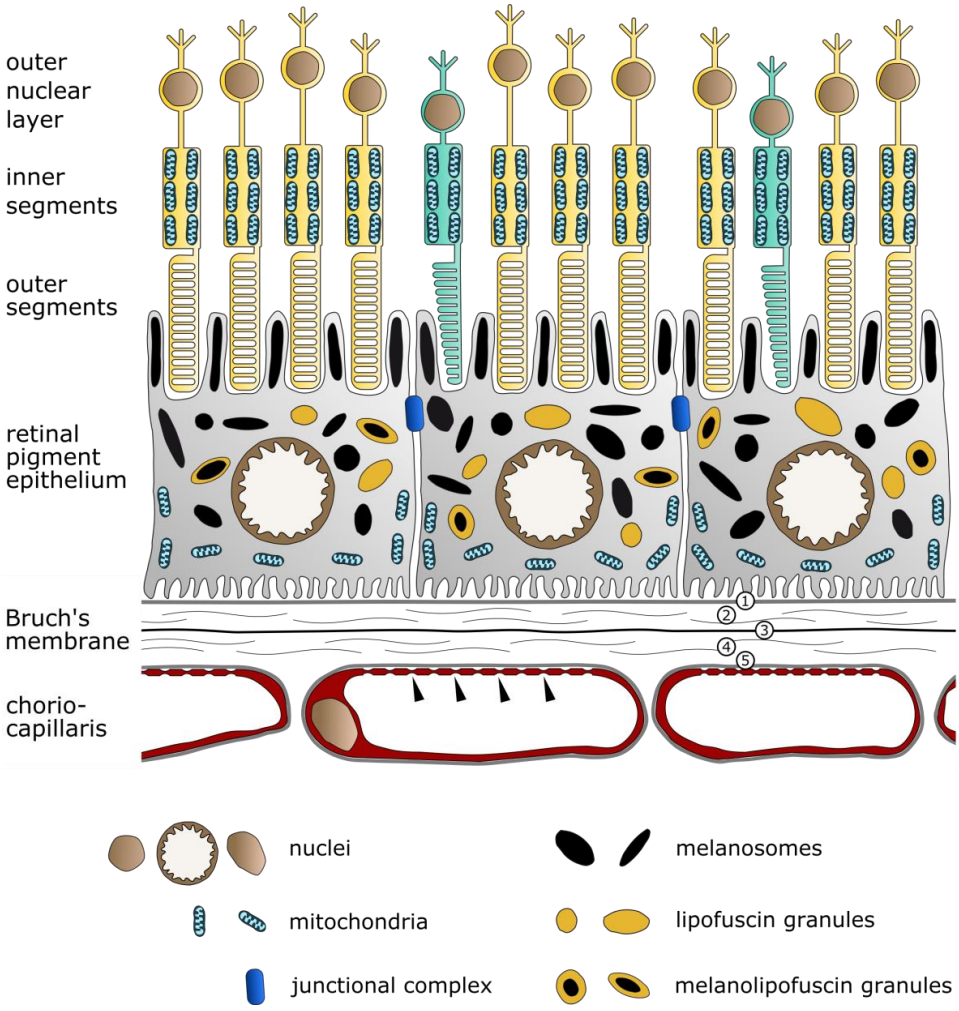

Figure 3: Schematic view of the choriocapillaris/RPE/photoreceptor-interface (not to scale). RPE cells contain melanin (black), lipofuscin (yellow-orange) and melanolipofuscin (yellow-orange with black core) granules in the apical part of the cytoplasm. Microvilli contain elongated spindle-shaped melanin granules. Bruch's membrane consists of five distinct layers (for details, please refer to the main text). Fenestration of choriocapillaris predominantly exists on the RPE-side of the vessels (arrowheads). Own work.

Directly beneath Bruch's membrane, the choriocapillaris, a capillary bed, is located. The choriocapillaris supplies approximately 50% of the needed oxygen during dark adaption [15]. To facilitate this, the blood flow rate in the choriocapillaris is remarkably high and the vessels are fenestrated (Fig. 3). Since the retina is one of

the most metabolically active tissues in the human body with a high oxygen consumption, a generous supply of oxygen and nutrients from the choriocapillaris allows for a less dense retinal vasculature hence reducing light scattering effects by retinal blood vessels.

Photoreceptors, RPE, Bruch's membrane and choriocapillaris share a mutualistic relationship: impairment/loss of one structure leads to impairment/loss of the other structures [16]. The choriocapillaris marks the beginning of the choroid that consists of connective tissue, blood vessels and melanocytes with melanosomes. The melanin in the melanocytes is assumed to have two main functions: reducing uncontrolled scattered light that might result in disrupted perception and acting as an antioxidant, since the choroid is highly perfused due to the high oxygen need of the retina. However, in many vertebrates, part of the choroidal pigmentation is missing and replaced by a special structure named *tapetum lucidum*, which reflects light in a controlled manner and supports superior night vision in these species (reviewed in [17]).

1.2 Pigmentation of the retinal pigment epithelium

The RPE differs from all other pigmented cells in its embryonic origin: while melanocytes (including the melanocytes of the choroid) are derived from the neural crest, the RPE is derived from the neural ectoderm [18].

Most melanised tissues, such as hair and skin, express tyrosinase, the canonical key enzyme of melanogenesis, over the entire lifespan and therefore can continuously synthesise melanin. In the RPE however, tyrosinase-expression was only found pre-natal (reviewed in [19]) and thus, according to established scientific doctrine, there is no melanin biosynthesis in the RPE after birth [20-22]. However, post-natal melanin biosynthesis has been described in several species [19, 23-26] and tyrosinase-independent melanin biosynthesis in RPE cells was seen *in vitro* [27].

RPE melanosomes are located both within the cell body and within the microvilli that encircle the photoreceptor outer segments (Fig. 3). Melanosomes can be spindle-shaped (in microvilli, cell body) or spherical (only in cell body). The amount of melanin in the RPE in humans is independent of race [28]. In the past, it was assumed that human RPE melanin exclusively consists of the dark-brown/black eumelanin, but at least for Caucasian donors it was shown that RPE melanin also

contains small amounts of pheomelanin, a red-coloured melanin type [29]. Ocular melanin has a variety of functions, including scavenging of extra light and reactive oxygen species [18, 22, 30], and its anti-oxidative properties are well documented [31-34]. However, once melanin ages, its former anti-oxidative character switches to pro-oxidative [35-37].

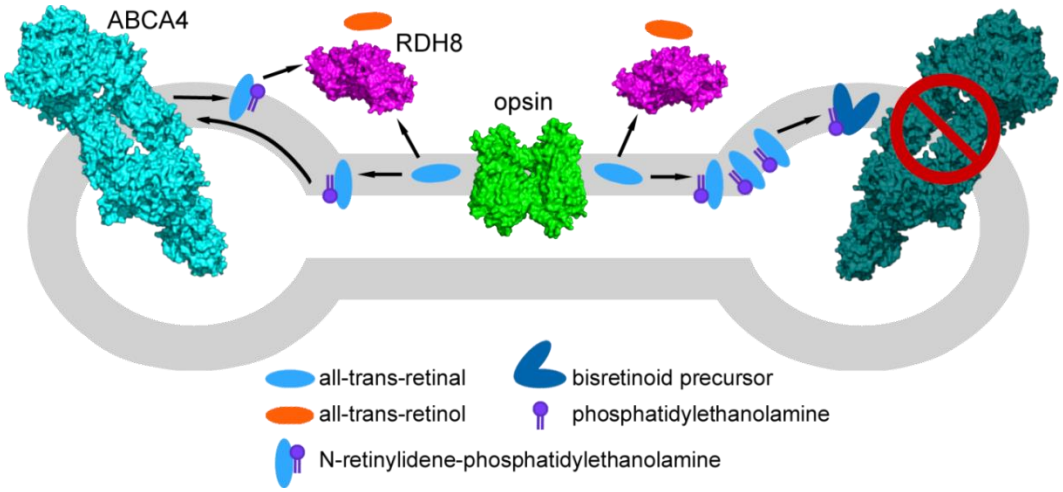

Figure 4: Scheme of proposed bisretinoid synthesis in the photoreceptor disc. All-*trans*-retinal (atRAL, light blue) is released from opsin (green) into the disc membrane of the photoreceptor. atRAL can either go to the cytoplasmic leaflet, where it is reduced by retinol dehydrogenase 8 (RDH8, magenta) to all-*trans*-retinol (atROL, orange) or it can go to the luminal leaflet where it binds to phosphatidylethanolamine (purple) forming N-retinylidene-phosphatidylethanolamine (NretPE) via Schiff-base formation. In the presence of functioning ATP-binding cassette A4 (ABCA4, cyan), NretPE is flipped to the cytoplasmic leaflet and atRAL can dissociate and is reduced by RDH8 to atROL. When no functioning ABCA4 is present, NretPE accumulates and can spontaneously react with atRAL to form a bisretinoid precursor molecule (dark blue). Modified from [38].

During life, an additional pigment, the so-called age-pigment lipofuscin accumulates within the RPE. In general, lipofuscin is considered to be a complex mixture of undegradable proteins and lipids that accumulates within the lysosomes of post-mitotic cells such as heart muscle cells and neurons [39]. It is characterised by its yellow-brown colour and a typical golden-orange autofluorescence. However, RPE lipofuscin was shown to contain only minimal amounts of protein and instead consisting mostly of lipids [40]. The major lipid components are bisretinoids, a family of undegradable molecules derived from retinal, emerging from side-reactions of the visual cycle in the outer segment discs [41] (Fig. 4). The newly formed bisretinoids reach the RPE by the daily occurring phagocytosis of shed outer segment tips. An essential role in the formation of bisretinoids plays the enzyme ATP-binding cassette A4 (ABCA4), a flippase located in the rims of photore-

ceptor outer segments discs. The role of this protein in inherited retinal disease will be discussed in section 1.4.2.

Apart from the universally accepted mechanism illustrated in Fig. 4, other pathways of lipofuscin biosynthesis have been proposed: A 2012 study found that *Abca4*$^{-/-}$ mice reared in total darkness accumulate levels of bisretinoids similar to those in *Abca4*$^{-/-}$ mice reared in cyclic light, suggesting that lipofuscin is also derived from free 11-cis-retinal [42]. Furthermore, a recent study found that ABCA4 is also located in the lysosomal compartment of the RPE [43]. Interestingly, mice expressing ABCA4 in the RPE but not in the photoreceptors (*RPE-Abca4-Tg/Abca4*$^{-/-}$ mice*)* have lower levels of bisretinoids and RPE autofluorescence than littermates expressing no ABCA4 at all [43], suggesting that RPE-localised ABCA4 is also involved in lipofuscin formation, but the mechanism still has to be elucidated.

Lipofuscin is often considered to be a cytotoxic compound since lipofuscin can inhibit photoreceptor phagocytosis [44] and cause photo-oxidative damage [45]. RPE lipofuscin can also fuse to melanin, creating a melanolipofuscin granule consisting of a melanin core and a lipofuscin shell. Analytical electron microscopy and nano-secondary ion mass spectrometry analyses of human RPE pigments confirmed that the elemental composition of melanin and melanin in melanolipofuscin, as well as of lipofuscin and lipofuscin in melanolipofuscin, are extremely similar, respectively [46, 47]. However, the melanin in melanolipofuscin has significantly elevated phosphorus levels (usually considered to be a marker for lipid content) compared to melanosomes, while the lipofuscin in melanolipofuscin has significantly elevated nitrogen levels (usually considered to be a marker for protein content) compared to lipofuscin granules [46, 47]. A2E (N-retinylidene-N-retinylethanolamin), the best studied bisretinoid compound of lipofuscin, has detergent-like effects on biomembranes [48, 49], disturbs the mitochondrial ATP-synthesis [50], reduces lysosomal activity in the RPE [51, 52], and has pro-apoptotic [53] as well as pro-angiogenic [54, 55] properties. After illumination of A2E-laden cells with blue light, DNA damage [56], changed expression of genes related to stress and immune response as well as apoptosis [57], and finally cell death [58-60] were documented. While noxious characteristics of lipofuscin and its constituent A2E have been extensively described [44, 45, 48-60], lipofuscin autofluorescence topography does not correlate to age-related photoreceptor loss

in the human [61]. Therefore, the relevancy of lipofuscin and melanolipofuscin for the development of age-related changes in the retina has recently been debated.

RPE pigments are increasingly used as a marker for the state of the RPE in medical patient care by monitoring pigment autofluorescence (AF) in the back of the eye (fundus autofluorescence). Lipofuscin can be excited with short-wavelength light (SW; excitation wavelength: 488 nm, emission wavelength: > 500 nm) [62], while near infrared (NIR)-AF is thought to present melanin (excitation wavelength: 787 nm, emission wavelength: > 800 nm) [63, 64]. SW-AF is routinely used not only to monitor the accumulation and distribution of lipofuscin in the RPE, but also as a substitute marker for the whole RPE. Thereby, SW-AF finds use in a broad spectrum of retinal disorders to judge the state of RPE, including but not limited to drug toxicity, tissue defects as well as inherited and acquired retinal dystrophies [65]. NIR-AF as a marker for melanin is a relatively new modality and while it has been established that not only RPE melanin, but also choroidal melanin can add to the signal, the exact ratio, as well as other potential contributors to the signal are still under discussion [66]. Nevertheless, NIR-AF has proven to show characteristic changes in a variety of retinal diseases that oftentimes precede changes in SW-AF patterns [67-72]. Two of these diseases, namely age-related macular degeneration and Stargardt disease, are in the focus of this thesis and will be introduced in section 1.4. The question whether NIR-AF is in fact only derived from melanin will be answered in section 3.2.

1.3 High-resolution central vision in the primate — the macula

A histologically distinct area of the primate retina that is not present in the eyes of other mammals is the macula (reviewed in [73]). It has its name from the high concentration of the carotenoids lutein, zeaxanthin and meso-zeaxanthin which give this area a yellowish colour; thus the name “yellow spot” or in Latin *macula lutea*.

In the macula’s centre, the inner neuroretinal layers up to the outer plexiform layer are radially displaced, resulting in the formation of a pit (Fig. 5). The bottom of the pit, the *foveola*, is made up of densely packed cones and Müller cells and is the region of high-resolution central colour vision. Outer and inner segments are elongated in the foveola and the resulting curve is referred to as *foveola externa*. The *foveola* is surrounded by the *fovea* that contains the foveal slope which en-

compasses all retinal layers. In this area, the ganglion and outer plexiform layers are very thick and the first rods appear. The *fovea* is enclosed by the *parafovea* with the thickest ganglion cell layer and increasing numbers of rods. The outermost area of the macula is the *perifovea* in which the ganglion cell layer decreases to a thickness of one cell layer and where rods outnumber cones.

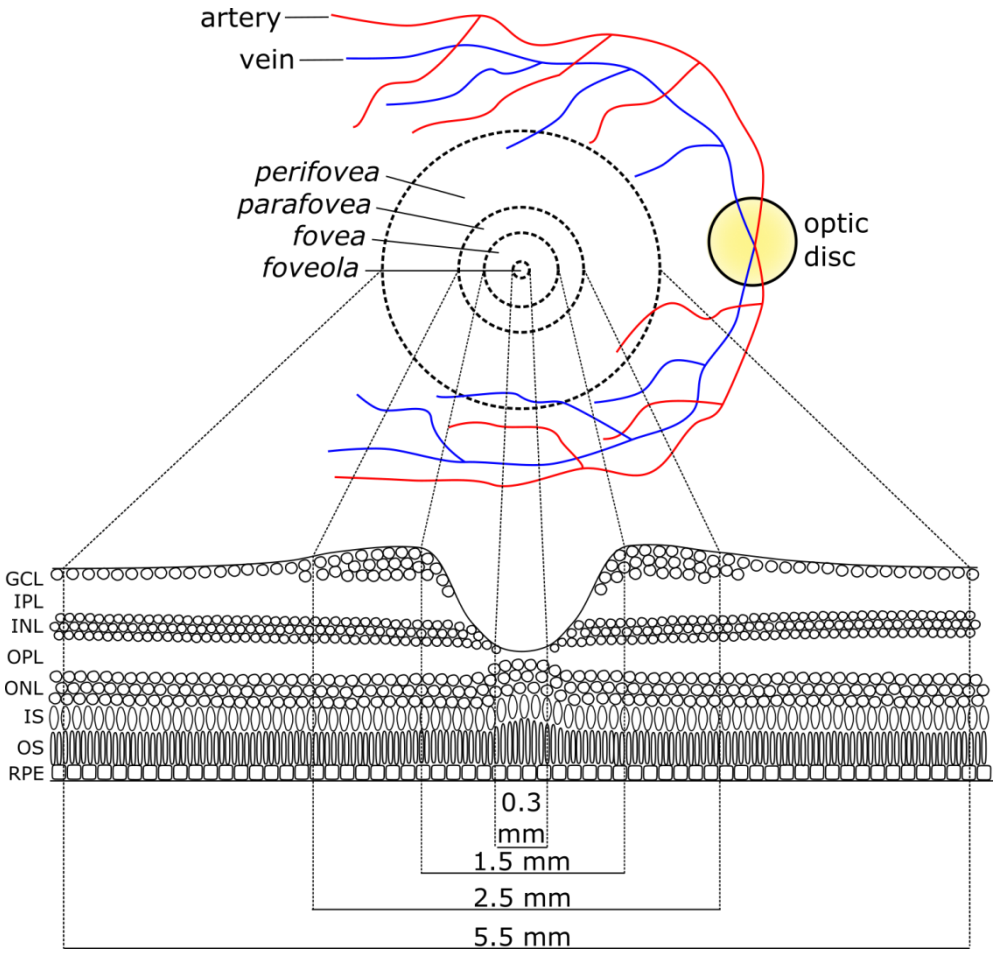

Figure 5: Schematic view of the primate macula (not to scale). Top: Schematic view of the fundus of a right eye. The centre of the anatomic macula comprises the *perifovea*, *parafovea*, *fovea* and *foveola* that are organised in concentric circles. The *foveola* is located approximately 4 mm temporal from the centre of the optic disc, the point where ganglion cell axons leave the eye and start forming the optic nerve. The superior and inferior temporal branches of the central retinal artery and vein surround the macula. Bottom: Schematic transversal view of the macula with approximate dimensions. GCL: ganglion cell layer, IPL: inner plexiform layer, INL: inner nuclear layer, OPL: outer plexiform layer, ONL: outer nuclear layer, IS: inner segments, OS: outer segments, RPE: retinal pigment epithelium. Own work based on data published in [73].

By the radial displacement of overlaying cell layers, any light scattering effects of these cell portions are prevented. Not only the organization of the retinal layers is shifted in the macula, but also the retinal vasculature is diminished; only capillar-

ies can be found in the macula, while the big retinal vessels surround the macula (Fig. 5). The *fovea* however, is completely avascular (foveal avascular zone), making the foveal cells fully dependent on the choriocapillaris for oxygen and nutrition supply.

The diminishment of potential light scattering elements in combination with the high density of cones and a low ratio of cones to ganglion cells (which means that signals from several cones do not converge to one ganglion cell, but rather each cone is connected to two to three ganglion cells [74]) allows the achievement of high visual acuity.

The human macula has a diameter of about 5.5 mm, while the *foveola* has a diameter of about 0.35 mm. Although very small in size, this tissue is crucial for everyday visual tasks relying on high-resolution and high-acuity, such as reading and face recognition. This is also reflected in the fact that the *fovea* occupies only 0.02% of the total retinal area, while it contains 25% of ganglion cells [73]. If the macula is damaged, central vision is heavily impaired. A group of diseases that damage the macula are summarised under the term macular degeneration.

1.4 Macular degeneration

Macular degeneration is an umbrella term that comprises several different diseases with different aetiology. The most common one is the acquired age-related macular degeneration (AMD), a multifactorial disease that is the major cause for legal blindness in the elderly in industrialised nations [75]. Much rarer are the inherited juvenile macular degenerations that are associated with mutations in certain genes and typically present during childhood, such as Stargardt disease, X-linked juvenile retinoschisis, and Best vitelliform macular dystrophy [76]. Other causes for macular degeneration are for instance pathologic myopia [77], drug toxicity [78] and presumed ocular histoplasmosis syndrome [79].

Since AMD and the subtype 1 of Stargardt disease (STGD1) share certain characteristics, both diseases are in the focus of this thesis. An examination of the disease progression in both AMD and STGD1 will be performed in section 3.1.

1.4.1 Age-related macular degeneration (AMD)

AMD has a global prevalence of 8.7% in individuals aged 45 to 85 years [80]. It is estimated that in the year 2040 288 million people will be affected [80]. There are

several risk factors for the development and progression for AMD being discussed. A 2010 meta-analysis suggested that advanced age, smoking, previous cataract surgery and a familial history of AMD are strong and consistent risk factors for AMD, while a high body mass index, a history of cardiovascular disease, hypertension and plasma fibrinogen were identified as moderate risk factors [81]. However, a randomised clinical trial found no link between cataract surgery and the progression from early to advanced AMD [82]. On the other hand, a prospective population-based cohort study found that a diet with high amounts of vegetables, fruit and fish significantly reduces the risk of developing AMD [83]. Genes involved in predisposition to AMD encode for proteins involved in the complement system (e.g. *CFH*, *C3*, *CFI*, C2/*CFB*), cholesterol and fat metabolism (e.g. *APOE*, *CETP*, *LIPC*), extracellular matrix (e.g. *TIMP3*) and yet unknown functions (*ARMS2*, *HTRA1*) [84-87].

AMD can be divided into an early, an intermediate and a late stage (Fig. 6, reviewed in [75]). In early AMD, the characteristic hallmark is the formation of medium-sized drusen, extensive basal linear deposits beneath the RPE, in both eyes (section 1.1). However, few small drusen in a single eye are not considered to be AMD, since drusen formation in itself is considered to be a part of normal aging [14]. Intermediate AMD is defined by the presence of at least one large druse and several medium sized drusen [75]. Late stage AMD can have two distinctive forms, either dry (non-neovascular, non-exudative) or wet (neovascular, exudative). Dry AMD is characterised by a local degeneration of choriocapillaris, RPE and photoreceptor cells (geographic atrophy, GA), while the most common form of wet AMD in western countries is the formation of choroidal neovascularisation (CNV) that causes oedema and bleeding [75]. In Asia, a subtype termed polypoidal choroidal vasculopathy, characterised by haemorrhagic and/or serous detachments of the RPE, represents a larger share of wet AMD cases [88, 89]. Even though wet AMD accounts for the minority of all AMD cases, this form is devastating since it can lead to fast progressing vision loss. Dry AMD advances slower and thus high acuity vision can be retained longer. Prevalence for AMD in Germany was estimated as 11.4 – 11.9% for the early and 0.2% for the late form [90, 91]. Hereafter, the term wet AMD will be used to exclusively refer to the CNV-form that is prevalent in Europe.

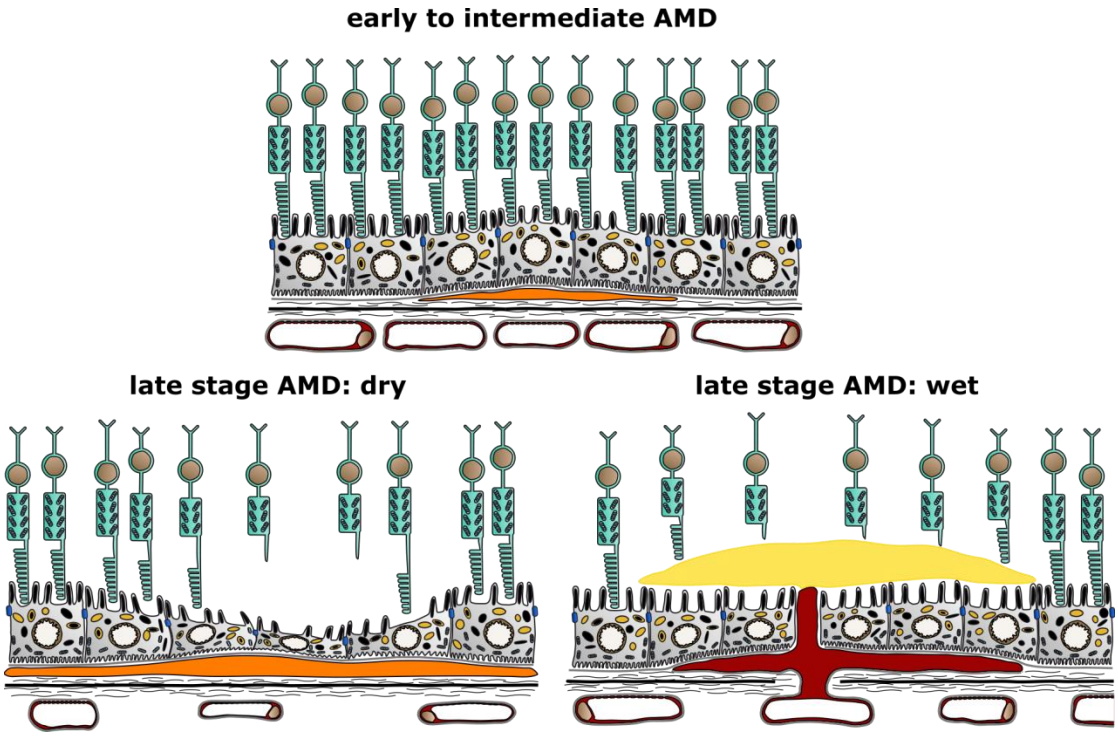

Figure 6: Schematic depiction of AMD stages (not to scale). In early to intermediate AMD, formation of drusen is characteristic. The stage of disease is only defined by number and size of drusen per eye. The overlaying RPE and retina are not injured in this state. In late stage dry AMD, drusen become larger or even confluent and RPE and photoreceptor cells are lost (geographic atrophy, GA). In late stage wet AMD, neovessels grow from the choriocapillaris through Bruch's membrane (choroidal neovascularisation, CNV) and can either remain below the RPE (occult CNV) or break through the RPE into the subretinal space (classic CNV, shown in image). Neovessels are malformed and can leak blood and plasma fluid, resulting in oedema (yellow material in subretinal space). Own work.

As aforementioned, AMD is considered to be a multifactorial disease with advanced age being one of the main risk factors [81]. One of the ultrastructural hallmarks of the aged retina is the accumulation of the age pigments lipofuscin and melanolipofuscin in the RPE (discussed in section 1.2) throughout life. An early onset of accumulation of these age pigments can be found in young individuals with certain genetic mutations, leading to Stargardt disease.

1.4.2 Stargardt disease (STGD1)

One of the most common hereditary diseases that lead to macular degeneration is Stargardt disease 1 (STGD1, OMIM #248200), affecting approximately 1 in 10,000 individuals [92]. The name refers to the German ophthalmologist Karl Bruno Stargardt, who described 7 patients from two families affected by the disorder in 1909 [93]. The autosomal recessive disease is caused by mutations in the *ABCA4* gene

[94] which encodes a flippase located in the rims of the photoreceptor discs that is part of the visual cycle (Fig. 4). A lack of functional ABCA4 protein leads to formation of bisretinoids that are the main constituents of the age pigment lipofuscin (section 1.2). It is thought that the early accumulation of extensive lipofuscin and the resulting potential cytotoxic burden early in life leads to the retinal degeneration.

To date, over 1200 disease-causing and disease-associated mutations have been identified in the *ABCA4* gene [95]. Most of these mutations are related to STGD1, but some are also found in cone-rod dystrophy, retinitis pigmentosa and AMD [96-100]. A genotype-phenotype model, linking the severity of the mutations in *ABCA4* to the extent of the retinal damage and thus the resulting disease, has been proposed [96, 101, 102].

Since there is such a huge genetic variety in STGD1 patients, it is plausible that there is also a huge phenotypic variety. Onset varies from early-onset (during childhood) to late-onset (later adulthood, historically also referred to as fundus flavimaculatus [103]), with a generally better prognosis associated with later onset. Typical features include yellow-white flecks in the fundus, atrophic lesions in the macula and progressive loss of visual acuity. Drusen, as they are common in AMD, are not described in STGD1. Since the clinical presentation of late-onset STGD1 and dry AMD can be extremely similar, it is suspected that a considerable amount of late-onset STGD1 patients is misdiagnosed with dry AMD [104, 105].

Even though this thesis is focused on Stargardt disease 1, two additional subclassifications of Stargardt disease, which are much rarer and both inherited in an autosomal dominant manner, will be briefly described for the sake of completeness: Stargardt disease 3 (OMIM #600110) is caused by mutations in *ELOVL4* (Elongation of very long chain fatty acids-like 4), a gene important for the formation of very long polyunsaturated fatty acids with 28 and more carbon atoms that are incorporated into photoreceptor membranes (reviewed in [106]). Stargardt disease 4 (OMIM #603786) is caused by mutations in *PROM1* (Prominin-1) [107] which encodes a protein crucial in the photoreceptor disc morphogenesis [108] and involved in regulating autophagosome maturation and trafficking in the RPE [109]. Another classification, Stargardt disease 2, was found to be in error and was therefore abolished.

Both Stargardt disease 3 and 4 are caused by mutations in genes relevant for the photoreceptor outer segment formation; thus, the mutations themselves directly induce retinal degeneration since the daily outer segment renewal is hampered in their presence. Stargardt disease 1 differs in the sense that the underlying mutations do not affect the upkeep of the retinal structure, but instead provoke increased accumulation of lipofuscin in the RPE, which can be interpreted as accelerated aging. This underlines the similarity to particularly the dry form of AMD, since both diseases are characterised by formation of geographic atrophy secondary to lipofuscin accumulation.

1.5 AMD and STGD1 intervention

1.5.1 Current treatment options for AMD and STGD1

For patients with dry AMD or STGD1, there is currently no treatment available. Patients with intermediate AMD can benefit from nutritional supplements containing antioxidants and zinc, which can slow the progression from intermediate to advanced AMD [110]. For STGD1 patients, light protection is discussed to be an option to reduce disease progression [111]. However, a whole range of different approaches, including but not limited to gene therapy, stem-cell transplantation and visual cycle inhibitors are under pre-clinical and early clinical investigation for both diseases (extensively reviewed in [112]).

To date, there is no cure for wet AMD, but symptoms may be alleviated. In the past, approaches like laser photocoagulation, photodynamic therapy, surgical removal of CNV membranes and others were used, but with limited success since the progression of vision loss could at most be reduced but not halted, let alone reversed (reviewed in [113] and [114]). Today, to stop the growth and exudation of the CNV, current standard treatment is the repeated intravitreal application of anti-vascular endothelial growth factor (anti-VEGF) therapeutics (reviewed in [115] and [116]). With these drugs, acute deterioration in vision due to oedema can be reversed and disease progression can be reduced. However, since this approach does not resolve the underlying cause of the disease, treatment has to be continued for years with oftentimes monthly or bi-monthly intravitreal injections. This does not only result in a high treatment burden for the patient, but some studies suggest that long-term anti-VEGF treatment can lead to the development of yet untreatable geographic atrophy [117-119].

The first approved anti-VEGF drug for treatment of wet AMD was pegaptanib (Macugen®, OSI Pharmaceutical/Pfizer, FDA approval in 2004, EMA approval in 2006). Pegaptanib is a PEGylated aptamer that binds specifically to VEGF-A_{165}. Since newer drugs are more potent, it is hardly used in wet AMD management anymore.

Ranibizumab (Lucentis®, Genentech/Novartis) was the next drug approved in 2006 and 2007 by the FDA and EMA, respectively. Ranibizumab is a 48.3 kDa Fab fragment of a humanised monoclonal antibody that binds to all isoforms of VEGF-A (Fig. 7).

In 2011/2012, aflibercept (Eylea®, Regeneron/Bayer) was approved by the FDA and EMA, respectively. Aflibercept is a recombinant fusion protein consisting of the VEGF-binding portions of human VEGF receptor 1 and 2 and a human Immunoglobulin G (IgG) backbone with a molecular weight of 115 kDa (Fig. 7). This molecule binds to VEGF-A, VEGF-B and placental growth factor with high affinity. Due to the higher potency, a better treatment response was expected.

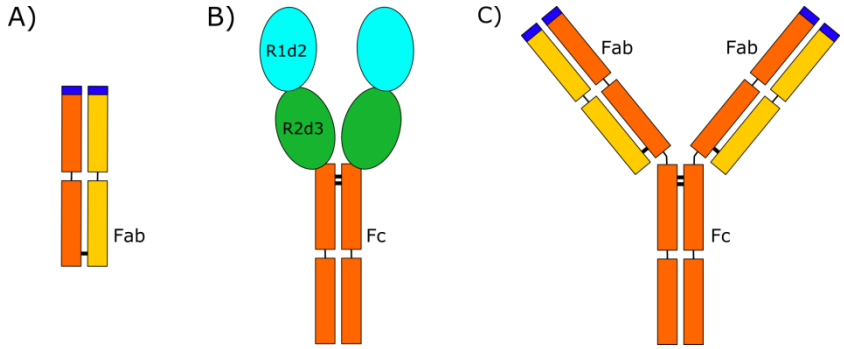

Figure 7: Schematic structures of the most commonly used anti-VEGF drugs ranibizumab (A), aflibercept (B) and bevacizumab (C). Domains of heavy chains are depicted in orange, while domains of light chains are painted in yellow. Inter-chain disulphide bridges are shown as black bars. Antigen binding domains are shown in dark blue. Aflibercept is a fusion protein that is composed of an IgG Fc backbone and domain 3 of VEGF receptor 2 (R2d3) and domain 2 of VEGF receptor 1 (R1d2). Own work.

Another frequently used drug, though off-label, is bevacizumab (Avastin®, Roche), a 149 kDa recombinant, humanised monoclonal antibody targeted towards all isoforms of VEGF-A (Fig. 7). Bevacizumab is only approved for the treatment of certain types of metastatic cancer, but since the individual intravitreal dose is very cheap (for instance, ranibizumab is 20x to 50x more expensive than bevacizumab,

depending on the country [120]), it is frequently used for several ocular diseases and was in fact used even before approval of ranibizumab [121].

An additional drug called conbercept (Lumitin®, Chengdu Kanghong Biotech), a 143 kDa fusion protein similar to aflibercept, was approved for the treatment of wet AMD in China in 2013, but is not used in the rest of the world [122].

Ranibizumab, aflibercept and bevacizumab show similar clinical outcome and all three are routinely used for wet AMD management [123, 124]. In fact, if a patient does not respond to a certain anti-VEGF drug, switching to another one is worth considering [125-130]. Instead, the question which treatment scheme (for instance monthly, as needed (*pro re nata*), treat-and-extent or observe-and-plan) is the most beneficial one has come into focus (reviewed in [131-133]).

Ophthalmologic use of anti-VEGF compounds is not limited to the treatment of wet AMD, but also includes other vascular and oedema-related diseases like diabetic macular oedema, retinal vein occlusion, retinopathy of prematurity and others [134-140].

Novel anti-VEGF drugs for wet AMD are currently under clinical investigation. The most advanced ones are brolucizumab (Novartis), a 26.3 kDa single-chain variable fragment (scFv) and abicipar pegol (Allergan), a 34 kDa designed ankyrin repeat protein (DARPin, both agents reviewed in [141]). The low molecular weight of both substances allows higher molar concentrations to be prepared in a single intravitreal injection, which may allow elongated intervals between injections and thus reduce treatment burden for the patients. Brolucizumab was non-inferior to aflibercept in two double-masked randomized phase III trials and over 50% of brolucizumab-treated eyes could be maintained on an every-12-weeks dosing interval without reactivation of the disease [142]. The compound is currently under FDA review and if approved, market launch is expected by the end of 2019 [143]. Abicipar pegol has reached study completion status in two phase III trials (ClinicalTrials.gov Identifiers: NCT02462486, NCT02462928).

Since VEGF is not the only growth factor involved in CNV formation, other therapeutic routes are also being pursued. One drug under clinical investigation is the bispecific antibody faricimab (Roche) that is designed for intraocular use against both VEGF and angiopoietin 2 (Ang-2), a growth factor involved in vascular destabilization (reviewed in [144]). The compound consists of two Fab fragments tar-

geted against VEGF-A and Ang-2, respectively, and an engineered Fc fragment, reducing systemic availability and inflammatory potential [145]. Phase II results of faricimab for diabetic macular oedema have recently been published [146], phase II results for wet AMD are still awaited (ClinicalTrials.gov Identifier: NCT03038880). Nevertheless, phase III studies for wet AMD have started in early 2019 (ClinicalTrials.gov Identifiers: NCT03823287, NCT03823300).

1.5.2 Adverse events after intravitreal anti-VEGF for wet AMD

Several types of ocular adverse events have been reported after intravitreal anti-VEGF application, including transient elevation of the intraocular pressure [124, 147], subconjunctival haemorrhage [148], rhegmatogenous retinal detachment [147] and endophthalmitis [124], but incidence was generally low. It should be noted that these types of adverse events are common after intravitreal injections, so distinguishing between events due to the procedure and due to the applied compound is challenging. However, in animal studies involving *Macaca fascicularis* (cynomolgus monkey) that were intravitreally injected with bevacizumab, ultrastructural analysis revealed that thrombotic microangiopathy, degranulation of platelets and neutrophils, blood flow alterations, signs of haemolysis and immune complex formation were present [149-152].

Systemic adverse events after intravenous application of bevacizumab include hypertension, fatigue, infections, thrombosis, bleeding, gastrointestinal events including bowel perforation, proteinuria, delayed wound healing, fistula formation and others [153]. To potentially cause systemic adverse events after intravitreal injection, anti-VEGF drugs must leave the eye and reach systemic circulation. In AMD patients, bevacizumab, aflibercept and ranibizumab can all be found in blood plasma and also reduce free VEGF levels after a single intravitreal application [154]. The reductive effect was highest for aflibercept and minimal compared to baseline for ranibizumab [154]. Furthermore, both bevacizumab and aflibercept accumulate in the blood plasma after repeated intravitreal injection and lead to a more pronounced reduction of free VEGF levels, while ranibizumab does not have this effect [154]. Similar results were found in patients treated for diabetic macular oedema [155]. So not only ocular, but potentially also systemic adverse events can arise after intravitreal application of anti-VEGF drugs.

A 2014 Cochrane review found no differences concerning deaths and serious systemic adverse events within the first two years of intravitreal treatment between ranibizumab and bevacizumab, except for gastrointestinal disorders, for which there was a higher risk after bevacizumab [156]. Systematic reviews of long-term safety data for aflibercept are not yet available, since the drug was only approved in 2011/2012. However, recent studies indicate that the intravitreal injection of bevacizumab leads to higher mortality of patients with a history of stroke or transient ischemic attack [157] and is also associated with myocardial infarct within 2 months after injection, independent of indication for bevacizumab treatment [158].

Adverse events after intravitreal anti-VEGF are rare, but potentially severe since they encompass cardiovascular events like thrombotic events, stroke, myocardial infarct and others. It is important to note that due to demographic change, the prevalence of AMD is expected to rise [159] and that the elderly often show comorbidity with diabetes, hypertension and a history of cardiovascular events putting them at a higher risk. Since anti-VEGF treatment due to wet AMD has to be continued for years, medications with a favourable safety-profile confirmed by long-term safety data exceeding 2 years are indispensable.

An investigation of ultrastructural ocular adverse events after the application of aflibercept and ranibizumab in comparison to previous results from bevacizumab and an investigation of the role of the Fc fragment in adverse events will be described in section 3.3.

2 Objectives

This thesis aims to elucidate the disease progression of the blinding diseases AMD and STGD1 (section 3.1), specifying the subcellular origin of NIR-AF that is thought to primarily emerge from RPE melanin (section 3.2) and to investigate the mechanism behind adverse events of certain frequently used anti-VEGF drugs for the management of wet AMD (section 3.3).

In the first part of this thesis, the disease progressions of AMD and STGD1 are described (section 3.1). The natural progression of retinal degeneration was investigated in human donor eye tissue with and without AMD in order to answer the long asked question whether RPE or choriocapillaris degeneration is the initial step in retinal degeneration due to AMD [1] (section 3.1.1). Since STGD1 is a rare disease and thus human donor tissue of affected individuals is scarce, three frequently used STGD1 mouse models and a single human STGD1 eye were employed for immunohistochemical and light, fluorescence and electron microscopic investigation of pathologic processes [5] (section 3.1.2).

The second part of this thesis deals with a histological approach to identify the subcellular origin of NIR-AF seen in fundus autofluorescence [6] (section 3.2). While it was already established that the majority of NIR-AF originates from the RPE melanin, the extent of contribution of choroidal melanin and potential yet unidentified fluorophores was still unclear. Especially the contribution of lipofuscin to the NIR-AF was suggested, but not confirmed. Correlation of fluorescence and electron microscopy of murine and human tissue, as well as isolated porcine ocular melanosomes was therefore used to address this question.

The third part of this thesis is concerned with adverse events after intravitreal anti-VEGF treatment (section 3.3). To better characterise the adverse event profiles of the frequently used anti-VEGF drugs aflibercept and ranibizumab, eyes of intravitreally injected monkeys were investigated by immunohistochemistry and light and electron microscopy [2, 3]. Pathologic changes in the retina/choroid [2] (section 3.3.1) and the iris/ciliary body [3] (section 3.3.2) were investigated. Since these two works found that aflibercept induces more ocular adverse events than ranibizumab and earlier studies revealed similar adverse events after treatment with bevacizumab [150-152], a study to investigate the effect of isolated Fc fragment (that is part of the IgG backbone in aflibercept and bevacizumab, but lacks in

ranibizumab) injected intravitreally into the rat eye was conducted [4] (section 3.3.3).

In sum, the present thesis highlights key events in the course of AMD and STGD1 that might give rise to a better understanding of these diseases and also investigates medical interventions and disease monitoring approaches to advance patient diagnostics and treatment.

3 Results and discussion

3.1 Disease progression in AMD and STGD1

Understanding the cellular and molecular changes in disease is crucial for developing new therapeutic options. It is well established that photoreceptors, RPE, Bruch's membrane and choriocapillaris form an interdependent complex, which means that damage/loss of one tissue results in damage/loss of the other tissues (reviewed in [16]).

Loss of RPE and choriocapillaris has been identified as first step in retinal degeneration in AMD in the past, but it has been unclear which of the two tissues is the first one to perish [160, 161]. Yet knowing the exact order of tissue degeneration would give crucial information about possible underlying mechanistic causes. Therefore, a correlated light and electron microscopic study was performed, investigating tissue of 12 eyes diagnosed with AMD (8 eyes wet AMD, 4 eyes dry AMD; ages 71 to 100 years, mean age 82 ± 15 years) and 9 age-matched control eyes without known eye disease (ages 57 to 85 years, mean age 75 ± 10 years) [1] (section 3.1.1).

In light microscopic sections, the tissue was graded according to its degradation state using a five–stage model, in order to identify transition sites which were later-on investigated in depth. The focus was put on the transition sites, since there, within < 50 µm distance, very abrupt switches between degradation stages occurred. The grading model can be summarised as: healthy (stage I), normal age-related early changes (stage II), occult CNV, i.e. growth of new vessels beneath the RPE but not within the subretinal space (stage III), GA, i.e. loss of outer and inner segments of photoreceptors and RPE (stage IV), and classic CNV, i.e. growth of new vessels into the neuroretina (stage V). The tissue was investigated for presence of photoreceptors, RPE cells, deposits between RPE and Bruch's membrane, choriocapillaris vessels, as well as area size of choriocapillaris vessels and choriocapillaris fenestration among others.

Two approaches were taken: 1) Investigation of whole sections of AMD eyes compared to control eyes, independent of degeneration grading, to obtain overall information of differences between healthy and diseased tissue. 2) Comparison of stages identified at transition sites to gain insight into the disease progress.

Analysis of whole sections revealed a loss of photoreceptors, RPE, choriocapillaris vessel area and choriocapillaris fenestration, as well as a pronounced formation of basal deposits within Bruch's membrane in AMD tissue compared to control. For transition sites, data for each single stage were pooled, independent of the transition partner stage, giving information about histological changes with AMD progression. Choriocapillaris was found to be reduced even when RPE was still completely present, in fact, even control tissue from age-matched donors already showed a slight reduction of choriocapillaris. Interestingly, stages I and II of AMD donors already had loss of choriocapillaris vessels compared to age-matched healthy control tissue that was also graded as stage I and II. When stage II in transition to stage IV (border zone of GA) was compared to stage II in transition to stage V (border zone of CNV), it became evident that stage II in transition to stage IV (GA) has a more pronounced loss of RPE and choriocapillaris than stage II in transition to stage V (CNV). This suggests that the type of subsequent degeneration is already foreshadowed in stage II areas that by definition only show early degenerative changes. However, it is yet unknown whether the border regions really depict spatiotemporal preliminary stages, but it seems likely.

This work confirms that the loss of choriocapillaris is the very first step in retinal degeneration due to AMD before subsequent loss of RPE and photoreceptors. This work also confirms that even healthy aged tissue shows a slight reduction in choriocapillaris, as was also described before [161, 162]. This involvement of choriocapillaris in both the dry and wet form of AMD supports the idea that AMD can be considered to be a vascular disease, as has previously been suggested [163-165].

One interesting finding in two investigated sections was the survival of isolated photoreceptor-RPE interfaces in the midst of scar tissue due to CNV formation: in these areas, photoreceptors with underlying continuous RPE layer were situated above intact CNV vessels (healthy endothelial cells, presence of pericytes), whereas in the immediate surroundings, photoreceptors and RPE were absent and CNV vessels were damaged (dead endothelial cells, loss of cell contacts between endothelial cells). This observation highlights the natural function of CNV formation as a response to hypoxic conditions in AMD [166]. And indeed, subclinical CNV without exudation and stable visual acuity has been repeatedly found in patients with unilateral wet AMD and has been shown to often remain stable for years [167, 168].

A difficulty in the investigation of the natural disease process in STGD1 is the scarcity of donor tissue from affected individuals. Before the start of the present thesis, histological characterisations of eyes from only three individual STGD1 donors have been published [169-171]. Therefore, a different approach was chosen: three STGD1 mouse models frequently used in pre-clinical research, namely pigmented *Abca4*$^{-/-}$, albino *Abca4*$^{-/-}$ and pigmented *Abca4*$^{-/-}$.*Rdh8*$^{-/-}$ mice [172-174], were longitudinally investigated by light, fluorescence, and electron microscopic methods up to an age of 25 months [5] (section 3.1.2). In addition, a single human donor STGD1 eye was included, which unfortunately had a very long death-to-fixation time of 48 hours, so only a limited set of meaningful analysis was possible.

None of the currently existing STGD1 mouse models fully reflect the situation in human STGD1 patients (Table 1). The three different STGD1 mouse models were described to vary in their phenotype: although all three strains show the typical increased accumulation of lipofuscin compared to their respective wildtype [172, 175, 176], only the albino *Abca4*$^{-/-}$ and pigmented *Abca4*$^{-/-}$.*Rdh8*$^{-/-}$ mice were described to show overall retinal degeneration with 7 and 3 months, respectively [172, 177]. Pigmented *Abca4*$^{-/-}$ mice lack any signs of retinal degeneration [174, 175].

However, in our hands, the pigmented *Abca4*$^{-/-}$.*Rdh8*$^{-/-}$ mice did not present the published retinal rosette formation with 6 weeks and overall retinal degeneration with 3 months [174], but instead showed a later onset of degeneration, comparable to albino *Abca4*$^{-/-}$ mice.

A longitudinal analysis revealed the earliest retinal changes, indicative of retinal degeneration, in albino *Abca4*$^{-/-}$ mice as young as 4 months. These changes included ruptured photoreceptor inner segments, disorganised and shortened photoreceptor outer segments, RPE cell-cell contact weakening, and cell detachment. Photoreceptor outer segment disorganisation and shortening, as well as RPE detachment first became apparent in 6-month-old pigmented *Abca4*$^{-/-}$.*Rdh8*$^{-/-}$ mice and never appeared in pigmented *Abca4*$^{-/-}$ mice. Ruptured inner segments and RPE cell-cell contact did not appear in pigmented mice. Pigmented *Abca4*$^{-/-}$.*Rdh8*$^{-/-}$ mice additionally had hypertrophic RPE and the highest levels of lipofuscin, quantified as percentage of the RPE cytoplasm occupied by lipofuscin and the lipofuscin-moiety of melanolipofuscin. Most of the encountered retinal changes in STGD1 mice were previously described in models of oxidative stress of

the RPE [178-181] and in fact oxidative stress levels were highest in albino *Abca4*$^{-/-}$ and pigmented *Abca4*$^{-/-}$.*Rdh8*$^{-/-}$ mice.

Table 1: Overview of characteristics of STGD1 patients and published STGD1 mouse models

	STGD1 patient	**pigmented *Abca4*$^{-/-}$**	**albino *Abca4*$^{-/-}$**	**pigmented *Abca4*$^{-/-}$.*Rdh8*$^{-/-}$**	**pigmented *Abca4*$^{PV/PV}$ [1]**
Abca4 null mutations in both alleles	no[2]	yes	yes	yes	no
Additional mutated genes	no	no	no	yes[3]	no
Accumulation of lipofuscin	yes	yes	yes	yes	yes
Retinal degeneration	yes	no	yes	yes	no
Presence of ocular melanin	yes	yes	no	yes	yes

1 The pigmented *Abca4*$^{PV/PV}$ model [182] has a homozygous knock-in of the L541P;A1038V mutation that leads to early-onset STGD1 in humans [98]. Phenotypically, this model does not differ from the pigmented *Abca4*$^{-/-}$ model, probably due to degradation of the mutated ABCA4 protein [182]. To my knowledge, this model has not been used in the literature besides the initial description and was therefore not included in the present work even though it was published prior to the start of my study.

2 Both alleles affected by *ABCA4* null mutations were only found in patients diagnosed with autosomal recessive retinitis pigmentosa; STGD1 patients have one allele with a null mutation in *ABCA4* at most [96, 97, 101, 183, 184].

3 Mutations in *RDH8* are not known to be involved in human diseases (OMIM *608575).

The fact that signs for retinal degeneration were earliest identifiable in albino *Abca4*$^{-/-}$ mice was somewhat surprising, since pigmented *Abca4*$^{-/-}$.*Rdh8*$^{-/-}$ mice were described to have a rather prominent retinal degeneration [174] and their genetically induced elevated levels of all-*trans*-retinal were shown to be highly toxic [185, 186]. Melanin is a known anti-oxidative agent [31, 32] that also fulfils a cytoprotective function against oxidative stress in RPE cells [33]. The striking evidence for oxidative stress and early onset of oxidative stress related pathologies in albino *Abca4*$^{-/-}$ mice supports the hypothesis of RPE melanin being a key factor in retinal health. However, an important limitation of the study is the differing genetic background of the STGD1 model strains. Since the main goal of this study was an ultrastructural comparison of existing and utilised STGD1 mouse models, the *Abca4* and *Rdh8* mutations were not moved onto coisogenic pigmented and albino strains. For instance, BALB/c mice (background of albino *Abca4*$^{-/-}$ mice) were shown to have a lower resistance to light-induced retinal damage that is independ-

ent of pigmentation, compared to 129 mice (background of pigmented *Abca4*$^{-/-}$ mice) [187]. To verify the protective role of RPE melanin against retinal degeneration, further research is therefore needed.

To conclude, the two publications discussed in this section identify the loss of choriocapillaris as the initial step in retinal degeneration in both wet and dry AMD [1] (section 3.1.1) and emphasize on the relevance of melanin for retinal health [5] (section 3.1.2).

3.1.1 Choriocapillaris breakdown precedes retinal degeneration in age-related macular degeneration

Authors: Biesemeier A., Taubitz T., Julien S., Yoeruek E., & Schraermeyer U.

Published in *Neurobiology of aging* in 2014
DOI: 10.1016/j.neurobiolaging.2014.05.003

This work was conducted as a student research assistant and is included since it presents groundwork to the later publications.

Declaration of own contributions:

Planning, writing and revision of the manuscript was done by PD Dr. Antje Biesemeier. Data acquisition and interpretation was done by PD Dr. Antje Biesemeier and me, I prepared part of the high resolution panoramic pictures and performed part of the quantification and statistical analyses of choriocapillaris area and fenestration. Prof. Dr. Efdal Yörük provided part of the human donor eyes. I and the other authors proof read the manuscript.

Neurobiology of Aging 35 (2014) 2562–2573

Contents lists available at ScienceDirect

Neurobiology of Aging

journal homepage: www.elsevier.com/locate/neuaging

Choriocapillaris breakdown precedes retinal degeneration in age-related macular degeneration☆

Antje Biesemeier[a,*], Tatjana Taubitz[a], Sylvie Julien[a], Efdal Yoeruek[b], Ulrich Schraermeyer[a]

[a] Section for Experimental Vitreoretinal Surgery, Center for Ophthalmology, University of Tuebingen, Tuebingen, Germany
[b] Cornea Bank, Center for Ophthalmology, University of Tuebingen, Tuebingen, Germany

ARTICLE INFO

Article history:
Received 16 September 2013
Received in revised form 23 April 2014
Accepted 2 May 2014
Available online 10 May 2014

Keywords:
Age related macular degeneration
Choriocapillaris
Retinal pigment epithelium
Transition between healthy and atrophied areas
Whole-section panorama images

ABSTRACT

This work presents a combined light and electron microscopical approach to investigate the initial breakdown of the retinal pigment epithelium (RPE) and choriocapillaris (CC) in age-related macular degeneration (AMD). Perimacular sections of 12 dry and wet AMD eyes (82 ± 15 years) and 7 age-matched controls (75 ± 10 years) without retinal pathology were investigated. Disease progression was classified into 5 stages of retinal degeneration to investigate the concurrent CC breakdown. Special emphasis was laid on transitions where intact CC–RPE–retina complexes went over into highly atrophied areas. AMD sections showed elevated loss of photoreceptors, RPE and CC ($p < 0.01$), and thickened Bruch's membrane with increased basal laminar and linear deposits compared with controls. Up to 27% of the CC was lost in controls although RPE and retina were still intact. This primary loss of CC further increased with AMD (up to 100%). The data implicate that CC breakdown already occurs during normal aging and precedes degeneration of the RPE and retina with AMD, defining AMD as a vascular disease. Particular attention should be given to the investigation of early AMD stages and transitional stages to the late stage that reveal a possible sequence of degenerative steps with aging and AMD.
© 2014 The Authors. Published by Elsevier Inc. All rights reserved.

1. Introduction

Age-related macular degeneration (AMD) is the major cause of vision loss in the elderly individuals of the western world (Kocur and Resnikoff, 2002; Prokofyeva and Zrenner, 2011). It is a multifactorial late-onset disease (Herrmann et al., 2013), the main factors being smoking, obesity, and genetic predisposition (Liu et al., 2012), but primarily aging. AMD is characterized by changes in the retinal pigment epithelium (RPE), Bruch's membrane (BM), and choriocapillaris (CC), which together facilitate retinal degeneration predominantly in the macular region of the eye.

The RPE and CC share a mutualistic relationship, if one is compromised, the other will follow and thus both may degenerate within a short time of each other (Bhutto and Lutty, 2012). Many research and review articles have addressed the factors for onset and progression of AMD in the last 10 years, however, the actual order of degeneration in the choroid–RPE–retina interface is still not fully understood (Bhutto and Lutty, 2012; Lutty et al., 1999).

Actually, also in the brain, loss of microvascular density and basement membrane thickening with aging precede cerebrovascular dysfunction and successive age-related neurodegeneration, for example, in vascular dementia and Alzheimer's disease (Brown and Thore, 2010). Smoking, obesity, and hypertension contribute to both Alzheimer's disease (Sierra, 2012) and AMD, and both diseases are associated with amyloid and heavy metal deposition. These examples already reflect the obvious, but until now rarely studied communalities within these and other age-related neurodegenerative disorders. The present work aimed to investigate different stages of AMD in human donor eye tissue by light and electron microscopy to find out whether CC breakdown precedes RPE degeneration with age and AMD. In addition, high-resolution overview images of AMD histology are presented, which show sites of the degenerating retina which are directly facing other areas with surviving photoreceptors (Supplementary Figs. 1–3).

2. Methods

2.1. Donor eyes

Perimacular regions (about 7 mm from the foveal center) of 12 AMD donor eyes (8 wet AMD; 4 dry AMD) and 23 controls without known ophthalmic pathology were excised and fixed for electron

☆ This is an open access article under the CC BY-NC-ND license (http://creativecommons.org/licenses/by-nc-nd/3.0/).
* Corresponding author at: Section for Experimental Vitreoretinal Surgery, Center for Ophthalmology, University of Tuebingen, Schleichstr.12/1, 72076 Tuebingen, Germany. Tel.: +49 7071 2984774; fax: +49 7071 4554.
E-mail address: antje.biesemeier@med.uni-tuebingen.de (A. Biesemeier).

0197-4580/$ – see front matter © 2014 The Authors. Published by Elsevier Inc. All rights reserved.
http://dx.doi.org/10.1016/j.neurobiolaging.2014.05.003

Table 1
Donor demographics and overview of measured stages I–V

Donor number	Age (y)	Sex	AMD type	Postmortem time (h)	Cause of death	Stages investigated
A1	71	M	Wet	7	Unknown	II, II–IV, IV
A2	72	F	Dry	48	Cerebral vascular infarction	II, II–IV, IV
A3	74	F	Wet	10	Liver cancer	II, II–IV, IV
A4	75	F	Wet	9	Septic shock secondary to urinary tract infection	II, II–III, III
A5	76	M	Wet	9.5	Respiratory failure, COPD	III, III–V, V II, II–V, V
A6	80	M	Wet	6.5	Pneumonia	V, V, V
A7	83	F	Wet	13	Unknown	II, II–IV, IV
A8	84	M	Dry	7.5	COPD, seizure	II, II, II
A9	90	F	Dry	11	Colicystitis, presented to ER	II, II–IV, IV
A10	91	F	Wet	23.5	CAD-MI	II, II–IV, IV–V, V
A11	93	F	Dry	7	Congestive heart failure	II, II–IV, IV
A12	100	F	Wet	7	Leukemia	I, I–II, II–V, V

Key: AMD, age-related macular degeneration; CAD-MI, coronary artery disease-myocardial infarcation; COPD, chronic obstructive pulmonary disease; F, female; M, male.

microscopy (EM). If possible, the samples were excised right at the border between atrophied and healthier regions (only in AMD eyes) to facilitate investigation of the transition areas.

2.1.1. AMD eyes

Glutaraldehyde-fixed tissue samples of the perimacular central region of 12 AMD donor eyes (age 71–100 years; mean 82 ± 15 years; Table 1) were obtained from the Cole Eye Institute of the Cleveland Clinic Foundation (USA). The death to fixation time was 13 ± 12 hours. The eyes were investigated by experienced ophthalmologists who stated the AMD type of both eyes including the different types of lesions found in each eye. The pathology reports also stated the cause of death and further diseases. Written informed consent of the donors for use in medical research and additional approval of the Institutional Review Board of the University of Tuebingen were obtained. The experiments were performed in adherence to the tenets of the Declaration of Helsinki.

2.1.2. Control eyes

Healthy donor eyes without known ophthalmic diseases were sectioned and investigated histologically. All eyes showing increased age-related lesions like RPE detachment or outer segment loss, or even geographic atrophy (GA) or choroidal neovascularization (CNV) and thus, resembling clinically unrecognized AMD or another pathology were excluded from the cohort of control eyes. Finally, 9 age-matched eyes aged 57–85 years (mean age 75 ± 10 years; death to fixation time 19 ± 10 hours; not significant [NS] to AMD) were integrated in this study and served as healthy controls (Table 2).

The eyes were obtained from the Institute of Anatomy and the Eye Hospital Tuebingen with informed consent of the donors and approval of the Institutional Review Board of the University of Tuebingen. They were opened with a circular slit at the limbus and fixed overnight at 4 °C in 4% glutaraldehyde in 0.1 M cacodylate buffer (pH 7.4). Then the iris and vitreous were removed and the perimacular region was excised according to the AMD samples and further prepared for EM as follows.

2.2. Embedding

Small pieces (1.5 mm^3) of already fixed perimacular tissue samples were washed 3 times in 0.1 M cacodylate buffer, postfixed in 1% osmium tetroxide, stained with uranyl acetate and dehydrated in a graded series of ethanol and propylenoxide and embedded in Epon. All EM reagents were purchased from FLUKA (Sigma-Aldrich, St. Louis, MO, USA) and PLANO (Wetzlar, Germany).

2.3. Correlative light and electron microscopy

For each eye, one representative 2–3 mm long semithin perimacular section of the retina–choroid complex was stained with toluidin blue and completely photographed with 600× magnification by light microscopy. The images were rearranged with the photomerge function of Adobe Photoshop CS3 or the Microsoft ICE tool yielding a panorama overview containing up to 200 single images (examples in Figs. 1–6 and the Supplementary Figs. 1–3, with about 50 single images each). By zooming into this panorama, different topics were addressed individually and in context with the surrounding tissue. For example, the presence or absence of photoreceptors, RPE, basal deposits, and CC were quantified in whole semithin sections (about 2–3 mm length of BM), within central areas of the single stages and, if apparent, directly at the transitions (investigated over a length of 200 μm of BM; frames in Fig. 1A).

Three subsequent ultrathin sections were investigated by EM yielding subcellular information of the same area, for example,

Table 2
Control donor demographics. All donors showed foremost stage II

Donor number	Age (y)	Sex	AMD type	Postmortem time (h)	Cause of death	Stages investigated
C1	57	M	No AMD	16	Hemorrhagic shock	I, I, I
C2	67	F	No AMD	21	Respiratory failure	I, I–II, II
C3	68	F	No AMD	6	Massive hemorrhage	II, II, II
C4	75	M	No AMD	38	Cerebral edema	II, II, II
C5	78	M	No AMD	21	Circulatory failure	I, I–II, II
C6	80	M	No AMD	22	Aspiration and/or laryngeal cancer	II, II, II
C7	80	M	No AMD	26	Circulatory failure	II, II, II
C8	81	M	No AMD	8	Cardiac failure	II, II, II
C9	85	F	No AMD	Unknown	Unknown	II, II, II

Key: AMD, age-related macular degeneration; F, female; M, male.

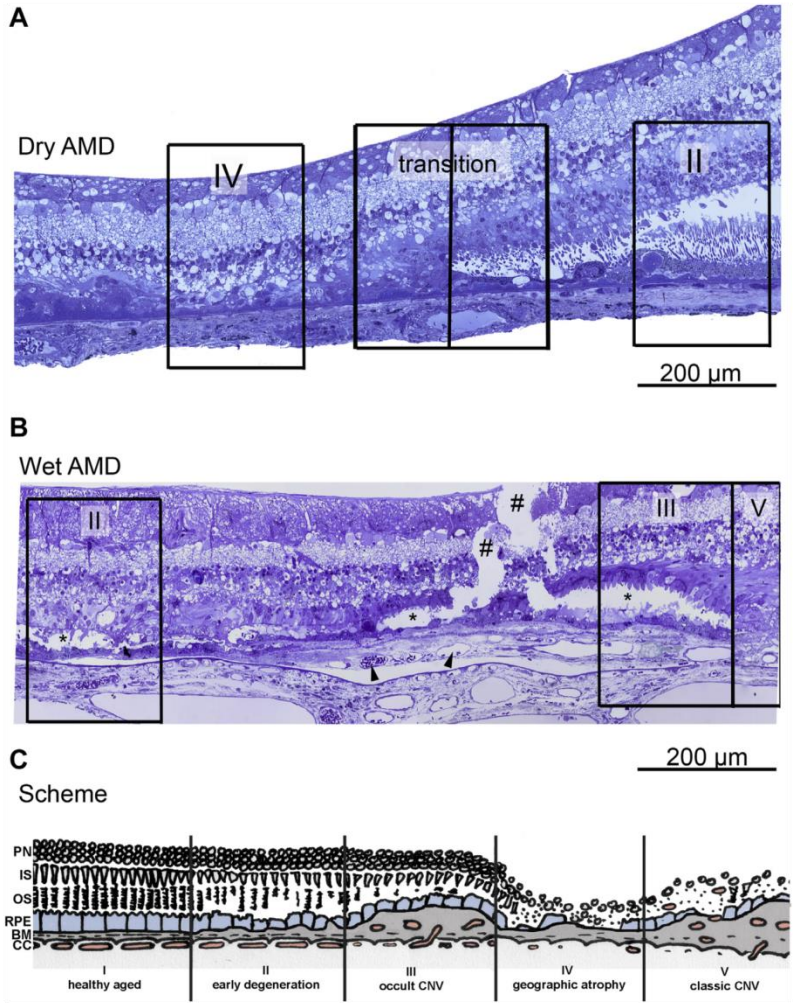

Fig. 1. The 5 stages of degeneration in AMD. (A) Light microscopical panorama image of a section from a dry AMD donor: shown is a transition between a highly atrophied region on the left (photoreceptors, RPE, and CC lumina are completely absent) and a histologically complete area on the right (complete photoreceptors, confluent RPE, open capillaries, basal deposits begin to detach the RPE from the BM). According to the scheme in (C) they were defined as stages IV and II, respectively. (B) Light microscopical panorama image of a section from a wet AMD donor: on the left, the RPE is still in contact with the Bruch's membrane and is separated from the photoreceptors by a subretinal space (*, stage II). This area goes over into an area with occult CNV as the RPE layer is separated from the Bruch's membrane by a CNV sheet with newly formed blood vessels (arrowheads). In the center region of stage III, some photoreceptor inner segments are still recognizable. On the right, stage III goes over into stage V, where the RPE and photoreceptor layer have completely disappeared leaving behind the CNV vessels and a retinal scar. The choroid shows highly enlarged deeper blood vessels and only a few melanocytes. # Breaks are sectioning artefacts. (C) Diagram showing the 5 histologic stages categorized for this work. They are based on RPE and photoreceptor ultrastructure and used for follow-up investigation of CC loss. A relation to inner retinal layers was not intended and thus of the retinal layers only the photoreceptors are shown. Stage I: control histology showing complete photoreceptors, an even RPE monolayer and regular CC vessels; basal deposits if apparent are few in number or very thin. Stage II: age-related changes shown by lost outer segments, RPE detachment or hypertrophy, basal deposits, enlarged Bruch's membrane or loss or shrinkage of CC vessels. Stage III: occult CNV with newly-formed capillaries between CC and RPE. Stage IV: geographic atrophy with loss of photoreceptor inner and outer segments, RPE, and CC vessels. If basal deposits are present, this stage is also associated with remnant basal deposits (as shown in (A). Stage V: classic CNV with newly formed blood vessels growing into the retina through the, not always present, RPE layer (see digital version for color images). High-resolution whole section panorama images of the tissues illustrated in A and B are provided in the Supplementary Figs. 1 and 2, respectively. Abbreviations: AMD, age-related macular degeneration; BM, Bruch's membrane; CC choriocapillaris; CNV, choroidal neovascularization; IS, inner segments; OS, outer segments; PN, photoreceptor nuclei; RPE, retinal pigment epithelium.

integrity of the endothelium and number of fenestrations. If a panorama overview was also needed for the EM investigations, for example, for proper investigation of vessels and photoreceptors within the same image, it was made using the multiple image alignment function of the iTEM 5.0 (Olympus) software (Fig. 6B). Of each one representative semi and ultrathin section per donor, semiquantitative evaluations were performed as follows (2.4–2.7).

2.4. Grading of histologic stages

After a first examination of both AMD and control panorama overviews, 3 independent areas of 200 µm length were selected per section, and each graded in 1 of 5 stages of retinal and RPE degeneration by 2 independent researchers. The stages were defined as follows:

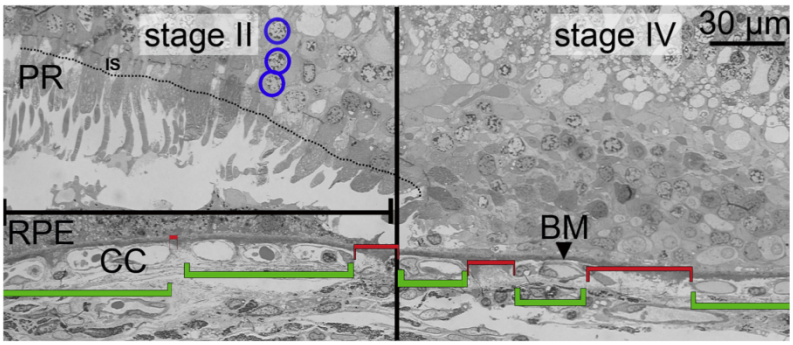

Fig. 2. Light microscopic image of how CC and RPE layer presence were measured: almost 100% of Bruch's membrane (arrowhead) is covered with RPE cells in the stage II area, whereas the RPE is missing completely in the stage IV area. The choriocapillaris was measured as follows: the green brackets (⌊⌋) include the vessel lumina plus the endothelium and typical pillars with a width of less than 10 µm. The red brackets (⌐¬) illustrate the areas of degenerated (no endothelium) or shrunken capillaries, which can be empty or contain extracellular matrix or alien cells. In stage II, about 90% of the CC is present, whereas in stage IV about 40% of the CC has disappeared. Photoreceptors (PR) were measured as follows: nuclei were counted in rows (filled circles), inner segments per µm BM, (dotted line) and outer segments per µm BM (as the inner segments, not shown) (see digital version for color and magnified images). The whole section panorama image of this donor tissue is presented in Supplementary Fig. 3). Abbreviations: BM, Bruch's membrane; CC choriocapillaris; RPE, retinal pigment epithelium.

Stage I: healthy (photoreceptors contain clearly distinguishable inner and outer segments, the RPE builds a continuous monolayer, no, or few deposits between the RPE and Bruch's membrane).

Stage II: normal age-related early retinal and RPE damage, that is, either changes in the structure of photoreceptors (shortened outer segments, first loss of photoreceptors foremost at transitions of AMD sections) or an irregular or hyperplastic but still confluent RPE monolayer or thickened BM.

All control sections used in this study were selected to fit in one of the first 2 stages I and II. Samples of control donors, which showed any AMD-related pathology like RPE or retinal degeneration were excluded from the examination.

Stage III: occult CNV (or type 1 neovascularization [Freund et al., 2010]), that is, blood vessel outgrowth through a thickened BM, with vessels close to the RPE but not infiltrating the subretinal space. Photoreceptors already impaired, but present.

Stage IV: GA, that is photoreceptor outer segments, inner segments, and the RPE are completely absent and degenerated leaving behind only single cells if any. The subretinal space is more or less abolished when the outer nuclear layer is touching Bruch's membrane.

Stage V: classic CNV (or type 2 neovascularization [Freund et al., 2010]), that is, the outgrowth of blood vessels through the not always present RPE layer into a highly damaged retina.

These 5 stages were put into a scheme, which is illustrated in Fig. 1c. This scheme is adapted from Sarks (1976) and shows the progression of the disease as a function of RPE and retinal destruction.

Seven sections of 7 different AMD donors were investigated more thoroughly, yielding changes in the RPE and choriocapillaris directly at transitions between different stages (Fig. 2). Transitions from stages II–IV were most common (5 donors), followed by stage II–V (2 donors). Transitions from I to II, IV to V and III to V occurred only once.

The following questions were addressed:

1) CC breakdown was investigated in relation to the RPE or retinal presence to answer the question whether the RPE or CC dies first with AMD progression.
2) The same stage of AMD progression was investigated and compared with samples of different donors, for example, differences in stage II of donors with dry or wet AMD help to explain the progression in the given direction.

2.5. Quantification of photoreceptors, RPE, BM, and CC

Fig. 2 shows how transition stages between healthier and more damaged areas, here stage II to stage IV, were analyzed. The spaces covered by photoreceptors, RPE, basal deposits, or CC were investigated and correlated to each other using the common unit "percent of BM length". This nomenclature gives no information about the morphology or quality of tissue, but it indicates whether a certain tissue layer is present or absent in this area. Using this approach, the "kinetics" of degeneration, for example, whether the RPE or CC fades away first were investigated histologically.

2.5.1. Measurement of photoreceptors

The area covered by outer and inner segments was measured per µm length of BM in semithin sections. Photoreceptor nuclei were counted in nuclei per row.

2.5.2. Bruch's membrane and basal depositions

The thickness of BM was measured in the semithin sections at 3 positions per section yielding the distance between the CC basal membrane and the RPE basal membrane. If BM was thickened, that area was investigated on a semiquantitative basis as performed in Curcio et al. (1998) and van der Schaft et al. (1992): that is, (0) no deposit, (1) patchy deposit <125 µm length, (2) thin continuous with >125 µm length and <2 µm height, (3) thick continuous with >2 µm height. The type of deposit (linear, laminar) was addressed at 20,000× magnification in the EM. Basal linear deposits (lin) were defined as being between the RPE basal lamina and the inner collagenous layer of BM (Green and Enger, 1993). Basal laminar deposit was defined as being between the RPE basal lamina and the RPE cell membrane (Loffler and Lee, 1986).

2.5.3. Measurements in the CC

The areas of the lumina of the CC capillaries were measured ($\mu m^2/\mu m$ BM). Additionally, 2 markers for CC integrity, fenestration and length of CC layer present were addressed as follows.

The number of fenestrations per µm of CC endothelium was counted in 30 images with 50,000× magnification. Only fenestrations facing the RPE side were counted, also if further fenestrations were visible on the choroid-faced side.

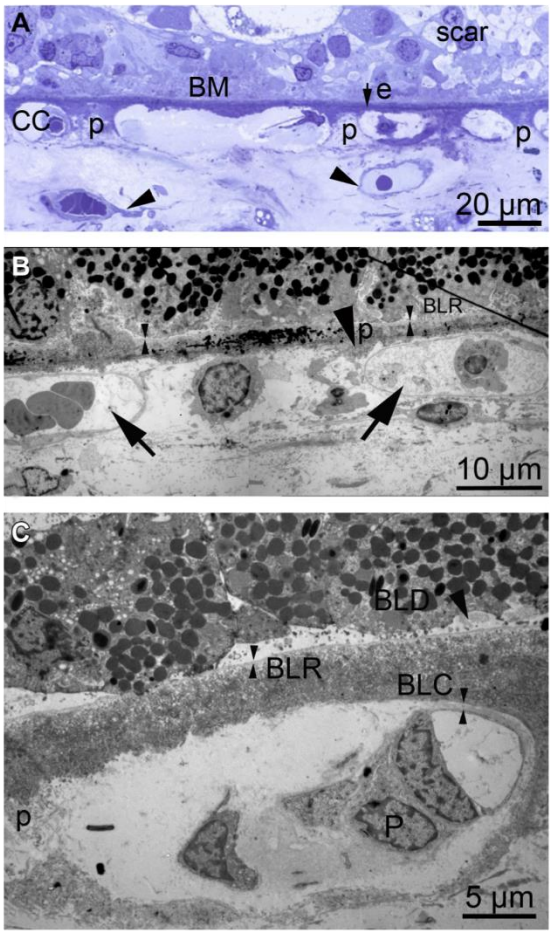

Fig. 3. Loss of choriocapillaris vessels. (A) Light microscopical image of geographic atrophy in AMD. Photoreceptors and the RPE are completely lost, leaving a scar. The CC is highly impaired, only one shrunken capillary (resembling that shown in (C) remains on the left side), whereas the CC is completely absent in the rest of the image showing foremost ghost vessels with loss of endothelia. The arrowheads point to deeper choroidal vessels with intact endothelia. Nevertheless, typical pillars (p) can be recognized showing where the vessels were originally situated. Using LM, the elastica of Bruch's membrane (BM) can be clearly recognized (e). (B) EM image of an AMD section where 1 capillary is entirely lost between 2 complete capillaries (black arrows). The space left is filled with macrophage-like cells. The arrowhead points to a pillar (p). By EM, BM can further be investigated: the elastic layer is calcified, basal laminae of RPE (BLR) and CC are not always discernible and fuse with the collagenous material. (C) EM image of another AMD eye, where a choriocapillaris lumen has shrunk to about 1/4 of its original size. Its basal membrane (BLC) surrounds only the small remaining capillary. The space between the remaining vessel and the original flanking pillar (p) is not yet filled with extracellular material. BM is slightly thickened, only the basal membrane of the RPE (BLR) is still completely discernible. Basal laminar deposits (BLD-arrowhead) are present. Abbreviations: AMD, age-related macular degeneration; CC choriocapillaris; EM, electron microscopy; LM, light microscopy; RPE, retinal pigment epithelium.

The whole length of the capillary layer including endothelial cell bodies and pillars was quantified (Fig. 2). CC was defined as being present when the capillaries were covered by a light microscopically visible endothelium and filling the whole space between 2 pillars of Bruch's membrane (green brackets in Fig. 2 ⌊⌋). If a capillary was shrunken, that is, a space appeared between pillar and endothelial wall, or a vessel was completely absent (no capillary on a length of more than 10 µm between neighboring capillaries) then this area was defined as lacking CC (red brackets in Fig. 2 ⌐¬). If unclear, this was controlled by EM. Examples of such absent or shrunken capillaries in higher magnification are illustrated in Fig. 3. In comparison to measuring only the area of CC vessel lumina, this approach yields additional information on the overall composition and integrity of the whole CC layer and thus more accurately describes CC density. It is also less vulnerable for postmortem artefacts like capillary collapse. Percent coverage of CC length can also more easily be compared with RPE length as it is used in the analyses for Figs. 7–9, where local degradation of either RPE and/or CC is investigated.

2.6. Statistical analysis

Statistics were performed using either Student *t* test for parametric analyses or the Wilcoxon–Mann–Whitney test for nonparametric data sets. The null hypothesis was that the AMD affected samples were histologically not different from the control samples. All *p*-values <0.05 were stated significantly different (error probability 5%). Linear regression analyses yielded the interdependency of RPE and CC survival in the different stages.

3. Results

3.1. Whole section analysis

Histologic changes in AMD compared with healthy control were addressed in whole perimacular sections of 12 AMD donor eyes and 9 control eyes.

All control sections did fit in one of the 2 first stages I and II. They showed a complete retina and RPE over section length (each about 100%), basal deposits were not present or few in number and area, leading to a mean thickness of BM of 3 ± 1 µm.

Compared with controls, AMD sections showed areas with loss of photoreceptors (nuclei, inner, and outer segments, all $p < 0.01$), RPE ($p = 0.009$), and CC ($p < 0.0001$). Bruch's membrane was thickened and basal deposits were more pronounced in AMD sections ($p = 0.006$ to controls).

In 7 of the 12 AMD sections such degenerative areas were directly facing other areas with intact retina–choroid complexes. These transitions are described in detail in Section 3.2.

3.1.1. Choriocapillaris

Loss of choriocapillaris density was identified as empty spaces beside shrunken capillaries or enlarged pillars (Fig. 3). With AMD, the areas covered by CC lumina were halved in value compared with controls ($p < 0.0001$, Fig. 4A and B). Also the number of fenestrations in the remaining vessel endothelia was greatly decreased ($p < 0.0001$, Fig. 4C and D). A detailed analysis of CC breakdown in relation to the RPE is presented in Section 3.2 (Figs. 8 and 9).

3.1.2. Bruch's membrane and basal deposits

Semithin sections revealed the thickness of Bruch's membrane and the abundance of basal deposits, whereas EM sections clarified whether basal laminar or linear deposits were accumulating (Fig. 5). In Table 3, the results per donor are presented. Healthy control sections showed foremost small amounts of deposit formation, which were predominantly composed of basal laminar material. The AMD samples showed higher amounts of deposit formation, which were often continuously spread over the whole section length. All contained laminar deposits.

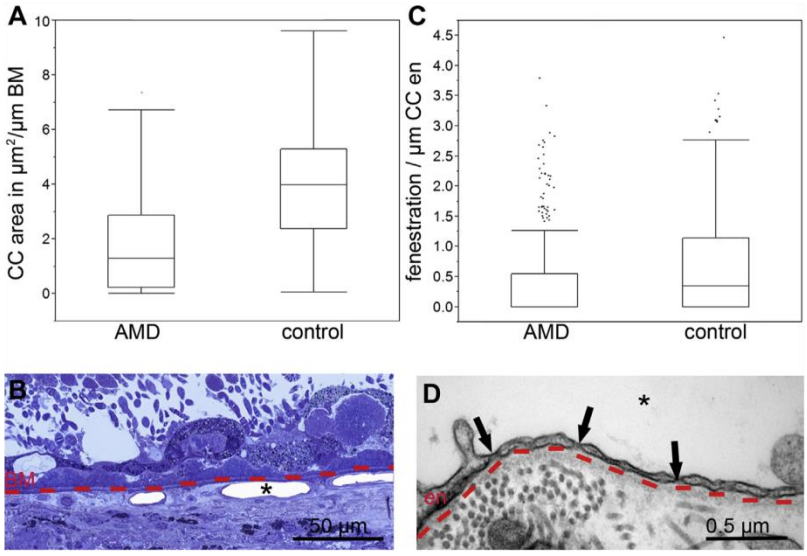

Fig. 4. Changes in the choriocapillaris. (A, B) Light microscopical analysis of CC area in $\mu m^2/\mu m$ BM (dashed line), $p < 0.0001$. CC lumina are shaded white and marked with an asterisk. (C, D) Electron microscopical analysis of CC fenestration (arrows) per µm length of the CC endothelium (dashed line, en). The asterisk marks the CC lumen, $p < 0.0001$. (see digital version for color images). Abbreviations: BM, Bruch's membrane; CC choriocapillaris.

3.1.3. Retinal pigment epithelium

The RPE was present in controls and early AMD but completely lost in areas of severe degeneration (97% ± 7% present in control; 63.7% ± 27% present in AMD sections; $p = 0.009$ to control).

In the earlier AMD stages, the RPE showed more morphologic changes rather than the absence of cells. The cells were often hypertrophic, microvilli clumped together or completely absent. Heavy deposition of basal waste was often associated with basal detachment of single, hypertrophic cells into the subretinal space. However, areas where the photoreceptors were already completely degenerated and the nuclei of the remnant retinal cells did reach to the underlying tissue were also free of the RPE in most cases. In these areas, the subretinal space had completely collapsed. On the other hand, when the subretinal space was still separating the degenerating photoreceptors from the underlying tissue, the RPE was also still present (Figs. 1 and 6, Supplementary Fig. 2).

3.1.4. Photoreceptor layer

The photoreceptors of AMD donors were highly degenerated as compared with those in controls (Table 4). When investigating photoreceptor loss, it was obvious that outer segments were the first to be lost with AMD. Already in stage II, first lesions could be observed, but mainly at the transitions going over into more damaged areas (stage II, 64% ± 42% of BM; stage IV, 0%). The inner segments were much more robust but absent with late stage AMD (stage II 76% ± 33% BM; stage IV 10% ± 22% BM). Photoreceptor nuclei were also lost with late stage AMD (6 ± 2 rows of nuclei in controls; IV 2.8 ± 3 rows of nuclei; V 0 rows;). Statistics showed significances between stages I or II as compared with stages IV and V, respectively (all $p < 0.001$).

In the late stage CNV, surviving photoreceptors, where just the outer segments were missing, were only observed at 3 small areas (80–500 µm; Fig. 1B, Fig. 6A and B, and Supplementary Fig. 2). Here, the RPE cells were also still present forming a continuous layer and were separated from the photoreceptors by a clearly recognizable subretinal space. However, up to 50-µm thick CNV sheets separated them from the remnant CC vessels. These comparatively healthy areas were surrounded by otherwise highly degenerated neovascularization scars. In the morphologically more intact areas, functional CNV vessels (defined as containing an intact endothelium, an open lumen and pericytes, and optionally with red blood cells; vessels 2–4 in Fig. 6A–C) were also observed more frequently than in scar tissue, where CNV vessels were often degenerating and showed leaky endothelia as judged by either loss of cell connections or death of whole endothelial cells (Fig. 6D and E, and Supplementary Fig. 2). CNV vessel morphology resembled mostly that of capillaries of the CC, but often they also displayed very large lumina and endothelial walls of different thickness. In addition, artery-like and venule-like vessels were observed. Typical pericytes such as that shown in Fig. 6C were seldom seen, but fibroblast-like cells were often found accompanying the endothelial membrane of CNV vessels (Fig. 6D and E).

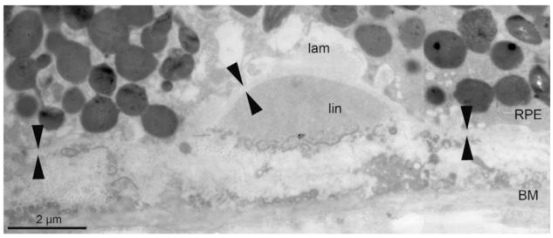

Fig. 5. EM micrograph of an AMD eye showing basal deposits: basal laminar deposits (lam) are located between the basal membrane of the RPE (arrows) and the RPE labyrinth. Basal linear deposits (lin) reside between the basal membrane of the RPE and the inner collagenous layer of Bruch's membrane (BM).

3.2. Analysis of transitional stages

3.2.1. Combined analysis of choriocapillaris and RPE in transition stages

Outside of transitions, areas where either the RPE or CC was missing whereas the other survived were equally abundant, thus a primary destruction of either tissue was hard to identify. Thus, the

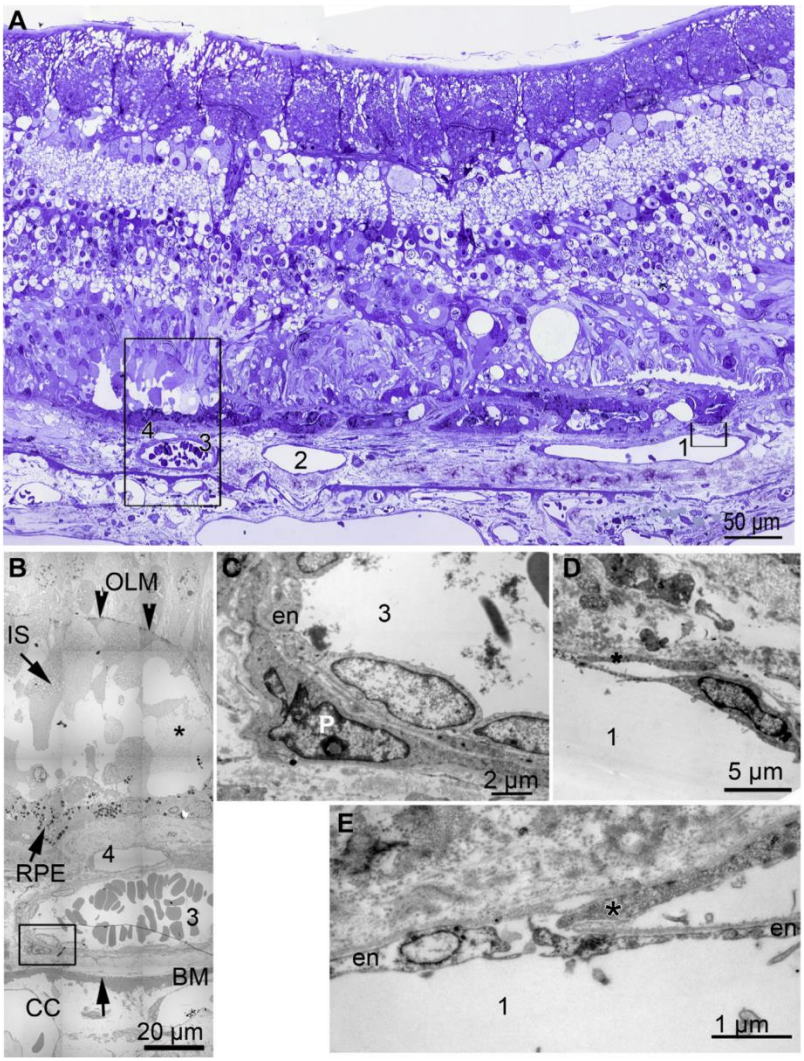

Fig. 6. Choroidal neovascularization can support retinal survival in certain areas. (A) Light microscopical panorama image showing an area where photoreceptors with inner segments and RPE can survive, functional CNV vessels (2, 3, 4), one of them with erythrocytes, can be observed (box magnification in B and C). This area is surrounded on both sides by highly atrophied tissue. CNV vessels 1 (and 5, 6, 7, 8 in the Supplementary Fig. 2) show endothelial lesions (magnification in D, E). Note also the broken elastic layer of BM close to vessel 1. (B) Electron microscopical panorama image showing the surviving area in higher magnification. Photoreceptors show an outer limiting membrane (OLM), nuclei, and inner segments (IS) of the photoreceptor cells. Remnants of the outer segments formed reticular drusen (subretinal drusenoid deposit, Curcio et al., 2012) in the subretinal space (*). Between the RPE and the elastic layer of Bruch's membrane (BM) functional CNV vessels can be observed. CC choriocapillaris (C) Higher magnification of the box in B showing CNV vessel 3 with the typical architecture of an intact and functional vessel: it has a thicker endothelial wall (en) compared with the other CNV vessels. The lumen is open and wide and contains red blood cells. On the left border, a pericyte (P) can be observed. It is separated from the vessel and covered by the same basal membrane. (D) CNV vessel 1 shows an intact endothelium in about 75% of the vessel area. However, some cells appear abnormal, for example, a fibroblastic cell of unknown origin (*) is connected to the endothelial cells of the vessel wall and they are covered by the same basal membrane. (E) With higher magnification it can be observed that the endothelial cells lack cell connections and are thus leaky. In addition, the left endothelial cell is disintegrating. Abbreviations: CNV, choroidal neovascularization; RPE, retinal pigment epithelium.

changes with AMD progression were investigated at transitions between 2 stages. Seven AMD donors showed such transitions (Table 1). As an example, the mean values for transitions between stage II and IV and transitions between stage II and V are illustrated in Fig. 7. RPE and CC loss from stage II to stage IV are significant. The data indicate also that the CC is always more damaged in stage II compared with the RPE (NS) suggesting first loss of CC followed by RPE. It also shows that the RPE in stage II of donors with GA is already more damaged compared with the RPE in stage II of CNV.

In Fig. 8A, the transition data were resorted according to the single stages (independent of their transition partner stage) yielding changes to the RPE and CC with AMD progression.

The data confirm the results of Fig. 7 and additionally prove that even control sections could suffer from initial loss of intact vessels with an otherwise intact RPE layer. This is also illustrated in the

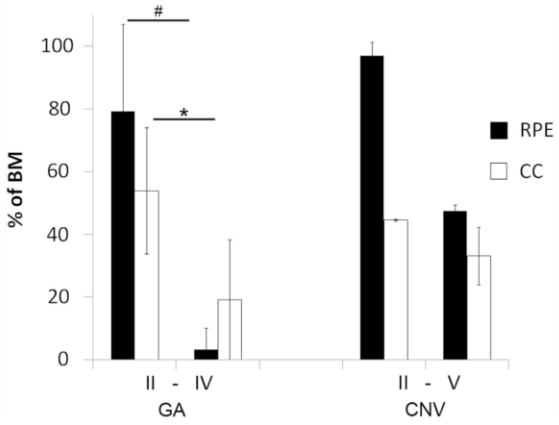

Fig. 7. The presence of CC and RPE in transitions between stage II and stage IV in the case of GA (n = 5 donors) and stage II and stage V in the case of CNV (n = 2 donors), respectively. Only those donors were included that show exactly one of the 2 types of transitions. Presented are mean values and standard deviations. * $p = 0.04$ for CC stage II–IV; # $p = 0.01$ for RPE stage II–IV; the CC and RPE loss in GA (II–IV) were positively correlated according to linear regression analysis of the single values ($R^2 = 0.57$). *p*-values for transitions between stage II and V were not statistically significant because of the small sample number. Abbreviations: CC choriocapillaris; CNV, choroidal neovascularization; GA, geographic atrophy; RPE, retinal pigment epithelium.

corresponding correlation diagram (Fig. 8B), which also shows the high interdependency of the RPE and CC values ($R^2 = 0.89$ for mean values of the stages; $R^2 = 0.57$ for their original data). For further correlation of CC with RPE loss within or between the individual stages, Tables 5–7.

To investigate whether the RPE or CC was surviving whereas the other one had already disappeared, those areas were measured where either the RPE or the CC, both or none of these layers were lost. For better understanding refer to Fig. 9A. Fig. 9B–C illustrates the relation of the present and lost RPE and CC for the different stages of destruction in dry and wet AMD and for control sections. Again, sections which appeared normal at first sight already contained areas where the CC area was decreased (control and stage I [0%–30%]). This can only be investigated using detailed analyses as performed in Fig. 9. In early AMD (stage II) of both wet and dry AMD donors, RPE cells also showed first lesions but CC area loss was still more prominent. In wet AMD (Stage III, V), the CC was affected more severely compared with the RPE, which was counterbalanced by blood vessel outgrowth.

4. Discussion

The main focus of the present work was to find out whether RPE or CC loss precedes retinal degeneration with AMD, independent of the AMD type. Already in the late 60s, scientists were discussing whether the CC (Duke-Elder, 1966) or BM and RPE (Hogan, 1967, 1972) were the initiators of AMD (Sarks, 1976). However, this question still remains to be solved as the RPE and CC share a mutualistic relationship (Bhutto and Lutty, 2012).

Early AMD is described as affecting primarily the RPE and Bruch's membrane. Changes in the RPE are thought to lead to oxidative stress and deposition of undegradable material between the RPE and Bruch's membrane, where it can build basal deposits and large drusen. However, drusen formation can also occur as a result of normal physiological outflow stopped by a barrier yielding particle fusion and formation of lipoprotein-derived debris, which does not have to be oxidized. This "response-to-retention" model reflects the likely source of soft drusen and basal linear deposits more accurately (Curcio et al., 2011).

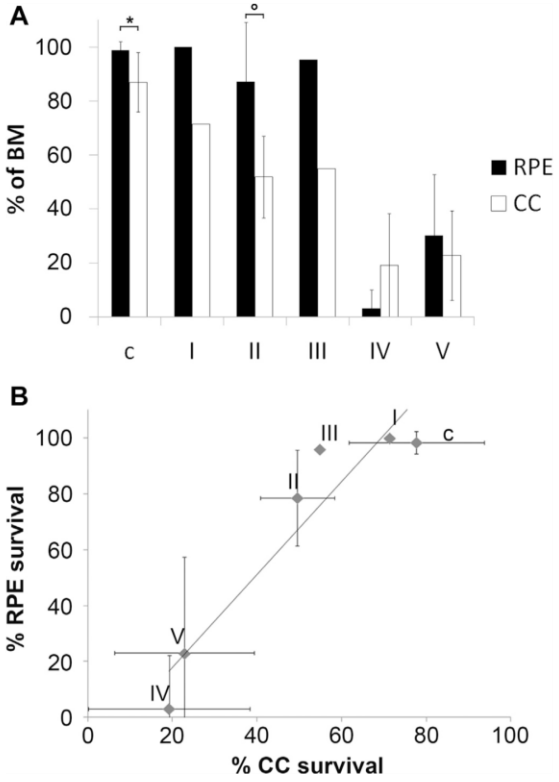

Fig. 8. The presence of CC and RPE in relation to the length of BM sorted by stage. (A) Controls (c) already show a slightly decreased CC compared with RPE (* $p = 0.01$). In the AMD stages I–III, this effect is even more obvious (e.g., stage II ° $p = 0.007$). Stage IV GA shows lower values for RPE, respectively (NS). Note, that data are only taken from transition stages, that is, for control n = 10 areas of 5 donors (10/5); stage I n = 1/1, stage II n = 9/7, stage III n = 1/1, stage IV n = 5/5, and stage V n = 4/3. Statistics for transitions from II to IV, II to V, and IV to V are shown in Table 6. (B) Positive correlation of the survival of RPE and CC in the different AMD stages and controls ($R^2 = 0.89$). Abbreviations: AMD, age-related macular degeneration; BM, Bruch's membrane; CC choriocapillaris; GA, geographic atrophy; RPE, retinal pigment epithelium.

Together with increasing thickness of BM with age, these deposits are responsible for diminished transport of nutrients and metabolites through the blood-retinal barrier leading to more oxidative stress in the retina-choroid complex. Finally, these cumulative reactions may result in (dry) AMD. In this scenario, the main initiator is supposed to be the RPE, but meanwhile the occurrence of deposits and drusen was also correlated to the capillary layer of the choroid, the choriocapillaris. It was found that deposits often form at the pillars between single CC vessels (Kochounian et al., 2009; Lengyel et al., 2004; Sarks, 1999), where a rapid removal of the material by the bloodstream is inhibited. A concurrent thinning (Margolis and Spaide, 2009) and loss of capillaries with age is discussed controversially (Jonas et al., 2014), but would further lead to impaired blood perfusion (Grunwald et al., 1998) and probably also to additional waste accumulation in BM. This impaired blood perfusion is further increased with AMD (Machalinska et al., 2011; Metelitsina et al., 2008; Mullins et al., 2011). Others found elevated levels of circulating endothelial cells as a marker of chronical vascular dysfunction in both wet and dry AMD patients (Machalinska et al., 2011).

In our opinion, in wet AMD, the loss of the CC is counteracted by the formation and growth of new blood vessels into the

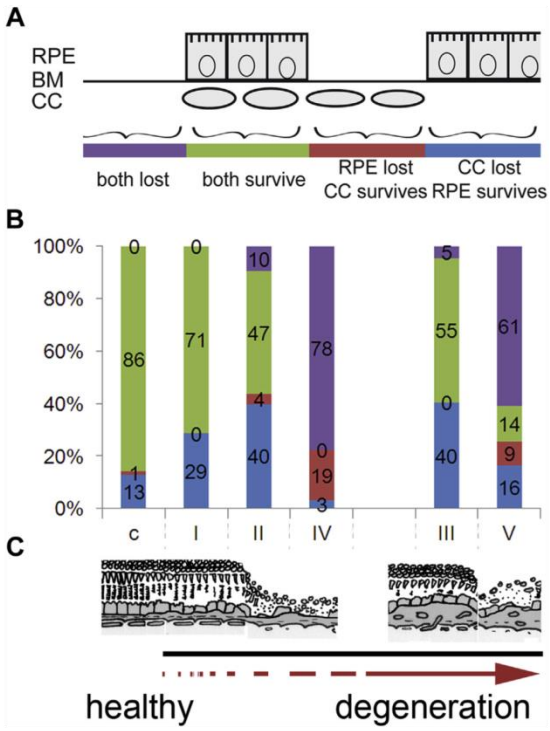

Fig. 9. The order of CC and RPE loss. (A) The presence ("survival") of RPE and CC per µm of BM was measured. Areas where both layers were lost were labeled violet in the diagram in part (B). Areas where both layers were present were labeled green. Areas where only the RPE was lost whereas the underlying CC was still there were labeled red. Vice versa, areas where the RPE was still there but the underlying CC lost were stained blue. (B) The diagram shows the mean values of the previously mentioned 4 situations per stage. Controls and stage I sections thus show both the surviving RPE and CC in over 70% of the area investigated. There are no areas where both layers were missing; however, in about 13% (control) and 29% (Stage I) the CC was missing although the RPE was still there. Also stage III, the initial stage of wet AMD still showed a high amount of viable RPE and CC (over 50%), but the CC was already highly impaired (40% + 5% where both layers are already completely lost). In the late stages of AMD (IV, V), most of the areas investigated had completely degenerated (violet). Depending on the AMD type either the RPE (dry AMD; IV) or the CC (wet AMD; V) was additionally affected more severely. Control (c) n = 10 areas of 5 donors (10/5); I, n = 1/1; II, n = 9/7; III, n = 1/1; IV, n = 5/5; and V, n = 4/3. (C) The scheme of degenerative stages is presented below the diagram to illustrate the given order of stages for better understanding (see digital version for color images). Statistics are given in Table 7. Abbreviations: AMD, age-related macular degeneration; BM, Bruch's membrane; CC choriocapillaris; RPE, retinal pigment epithelium.

subretinal space where they should substitute the CC function, probably leading to longer survival of the RPE and retina, as indicated in Fig. 6 and Supplementary Fig. 2. Unfortunately, these newly formed blood vessels are often stunted and unfunctional and instead of restoring the transport of metabolites to and from the retina, they promote blood leakage, accumulation of extracellular matrix and the invasion of macrophages and finally lead to scar formation and vision loss (Fig. 6, Supplementary Fig. 2). Our suggestions concerning the extended survival of retinal layers with early CNV are only based on 2 sections investigated in this work and will thus not be discussed further. However, they are in line with the excellent previous work that showed that CNV is a stereotypic and nonspecific wound healing response to a specific stimulus, here AMD (reviewed in Grossniklaus and Green, 2004).

Table 3
Type and frequency of basal deposits

Donor number	Semi	EM	Grade[a]
C1	None	—	0
C2	Patchy-continuous	LAM	1–2
C4	None	—	0
C5	None-patchy	—	0–1
C7	Patchy-continuous	LAM	1–2
C8	Patchy	LIN + LAM	1
C9	None-patchy	—	0–1
A1	Thin-thick continuous	LIN < LAM	2–3
A2	Patchy-thick continuous	NI	1–3
A3	Thick continuous	NI	3
A4	Thick continuous	LIN > LAM	3
A5	Thick continuous	CNV, LIN?	3
A6	Patchy-continuous	LAM	1–2
A7	Thick continuous	LAM	3
A8	Patchy-continuous	LIN < LAM	1–2
A9	Thick continuous	LIN > LAM	3
A10	Thick continuous	CNV, LIN + LAM	3
A11	Thick continuous	LAM	3
A12	Thin-thick continuous	LIN < LAM	2–3

No deposit is indicated by (0), Patchy deposit <125 µm length is indicated by (1), Thin continuous with >125 µm length and <2 µm height is indicated by (2), thick continuous with >2 µm height is indicated by (3).
Key: CNV, choroidal neovascularization; EM, electron microscopy; LAM, laminar; LIN, linear; NI, not investigated.
[a] Grading according to data presented by experts in the field (Curcio et al., 1998; van der Schaft et al., 1992).

4.1. The scheme of degenerative stages

We graded the different eye samples from control and AMD donors according to a scheme, which was adapted from the groundbreaking work of Sarks (1976). She used sections stained for different BM markers to investigate the influence of basal deposits on retinal degeneration. Accordingly, her scheme of 6 degeneration stages included (I) no deposit, (II) patchy deposits, (III) thin continuous deposits, first clumping of pigment, (IV) thick continuous deposits with occult CNV, (V) basal deposits with loss of the overlying RPE (GA), and finally (VI) disciform degeneration in classic CNV. This scheme has been adapted by different groups before, yielding comparable data sets acquired by different methods (Rudolf et al., 2013; Vogt et al., 2011).

The progression of degeneration in this work was graded in 5 stages and as a function of the RPE and retinal damage rather than deposit formation. Nevertheless, the progression of stages was intriguingly similar.

Note that the terms "occult" and "classic" CNV are derived from a fluorescein angiography-based classification system. They were originally defined as areas with "poorly-defined" or "well-demarcated choroidal hyperfluorescent" margins, respectively (as defined by the Macular Photocoagulation Study Group [1991, 1996]). Meanwhile, histologic data and multimodal imaging devices, such

Table 4
Loss of photoreceptors with AMD, whereas controls show complete photoreceptors all over the section lengths, AMD sections showed increasing loss of nuclei < inner < outer segments compared with controls

	Mean ± SD control	Mean ± SD AMD	*p*-value
Photoreceptor nuclei present (>7 rows)	87 ± 19	38 ± 30	**<0.0001**
Inner segments present (% per BM length)	100 ± 0	41 ± 43	**<0.0001**
Outer segments present (% per BM length)	100 ± 0	30 ± 44	**0.0001**

Key: AMD, age-related macular degeneration; BM, Bruch's membrane; SD, standard deviation.

Table 5
Correlation of CC and RPE within single stages

Stage	Correlation	R^2
Stage 2	$y = 0.18x + 38$	0.18
Stage 4	$y = -0.45x + 21$	0.03
Stage 5	$y = 0.36x + 15$	0.55

Key: CC, choriocapillaris; RPE, retinal pigment epithelium.

as spectral domain optical coherence tomography (SD-OCT), show more clearly the lesion composition with wet AMD. Thus, a new classification system has been proposed by Freund et al. (2010) and should be adapted regularly according to the newly emerging criteria. This classification system is based on 3 different types of CNV: (1) Type 1, vessels confined to the sub-RPE space; (2) vessels proliferating through the RPE into the subretinal space; and (3) intraretinal neovascularization. Although we used the definitions used by Sarks (1976), we also included the new nomenclature in the hope that it will spread when used regularly.

4.2. The impact of capillary loss

Loss of CC vessels was observed in all investigated stages, but was more pronounced with late AMD. It was unexpected that control donors also showed loss of capillaries in about 13% of the investigation area. However, increasing variability of CC density, including up to 50% loss in CC in the 10th decade of life (Ramrattan et al., 1994) has also been observed before and would suggest that loss of capillaries with age may be an initiating factor of AMD, thus also making dry AMD a vascular disease (Friedman, 1997; Machalinska et al., 2011; Verhoeff and Grossman, 1937). Also McLeod et al. (2009) investigated the border regions of macular degeneration in comparison with healthy controls and likewise found loss of a viable CC in alkaline phosphatase stained eyes with GA but even more with CNV. In Fig. 3 of McLeod et al. (2009) they also show initial loss of CC in controls. The same is true for Curcio et al., (2000) who investigated RPE and CC atrophy in peripapillary regions of non-AMD donor eyes. They also found preliminary but unsuspicious choriocapillaris loss in areas with an otherwise normal RPE.

Mullins et al. (2011) performed immunohistological investigations on cryosections of early AMD donors and found a decreasing CC density and increased accumulation of deposits with AMD compared with controls. By differentiation of viable (UEA-1 positive) and non-viable "ghost" vessels they also showed that drusen density was negatively correlated to healthy CC density but positively correlated to CC death. But whether drusen formation was the cause or consequence of CC death could not be answered by their studies. Our data are also in accordance with this excellent publication. Although we did not investigate the EEA-1 or alkaline-phosphatase status of our capillaries, we were able to judge CC health by endothelial cell ultrastructure and determined an increasing loss of viable capillaries with age and AMD by measuring significant changes in CC area, length, and fenestration, which is also in accordance with McLeod et al. (2002).

Table 6
Statistics given for data in Fig. 8 (*p*-values)

	CC (%)	RPE (%)
C-II	NS	<0.001
C-IV	<0.0001	<0.0001
C-V	<0.0001	<0.0001
AMD II–IV	0.004	<0.0001
AMD II–V	0.01	0.001
AMD IV–V	NS	0.04

Key: AMD, age-related macular degeneration; CC, choriocapillaris; NS, not significant; RPE, retinal pigment epithelium.

Table 7
Statistics given for data in Fig. 9 (*p*-values)

AMD stages	II–IV	II–V	IV–V
Only CC lost (%)	0.001	0.05	NS
Only RPE lost (%)	0.04	NS	NS
Both survive (%)	0.0001	0.008	NS
Both lost (%)	<0.0001	0.001	NS
Control-AMD	**C-II**	**C-IV**	**C-V**
Only CC lost (%)	0.02	NS	NS
Only RPE lost (%)	NS	0.01	0.02
Both survive (%)	0.001	<0.0001	<0.0001
Both lost (%)	0.1	<0.0001	<0.0001

Key: AMD, age-related macular degeneration; CC, choriocapillaris; NS, not significant; RPE, retinal pigment epithelium.

Although an intense correlation of basal depositions with AMD stages was not intended in this work, the presented data show that a continuous low layer of basal deposits could already be involved in CC loss and AMD onset, and huge drusen might only be a severe form of this condition. Thus, we suggest that CC loss is actually the cause, rather than the effect of drusen. This is also in accordance with the hypothesis that severe deposits grow close to pillars and already impaired CC vasculature. Further outstanding work on deposit formation, composition, and impact on RPE and CC loss in AMD can be obtained in previous publications, (Curcio and Millican, 1999; Lengyel et al., 2007; Russell et al., 2000; Sarks et al., 2007; Spaide and Curcio, 2010; Spraul et al., 1998).

Meanwhile, gene expression analyses demonstrated a clear decrease in the expression of endothelium-expressed genes in eyes of early AMD donors with concomitant increase in RPE-related genes (Whitmore et al., 2013). This work further suggests loss or dedifferentiation of choroidal endothelial cells before the loss of the RPE (Whitmore et al., 2013).

4.3. Impact of the RPE and the value of investigating transitions

As expected and in accordance with the literature, we found a longer survival of the RPE and predominant loss of the CC in CNV and RPE loss with surviving CC in GA. Interestingly, the RPE of stage II in GA donor eyes was more highly impaired compared with the RPE in stage II of CNV donors (Fig. 7) implicating that the progression in either direction, wet or dry, can already be foreshadowed in areas with early degeneration (stage II). Thus, investigation of transitions between early stages I or II to later stages III, IV, and/or V have to be analyzed more thoroughly to understand the regulatory events leading to either dry or wet AMD. However, the transitions were mostly very abrupt (<50 μm distance) and a clear transition zone between surviving photoreceptor and retinal scarring could hardly be observed. Such abrupt transitions with AMD-like changes in the retina–RPE–CC complex were also shown for age-related peripapillary chorioretinal atrophy of eyes without AMD (Curcio et al., 2000). Thus, the first 200 μm of each stage had to be investigated instead and correlated to each other but also to more central areas of each zone. And indeed, values taken at either side of the transitions did differ from values taken in the central parts of the different stages (e.g., the RPE loss was more severe in central parts of a stage compared with its border region to a healthier area, data not shown). The data show the importance of investigating early stages of AMD and their transitions to end stage degeneration, as it is only here that the possible reasons of the progression of the disease become visible. But note that it is only an assumption that the margins of the lesion represent a directional or temporal intermediate between health and disease, as this is not really known.

4.4. Strength and weaknesses of the study

Sample number: Although this study investigated only a small number of donor eyes, the data of the single donors were investigated with high accuracy using light and electron microscopy and they nicely represent a common behavior of degeneration in the RPE and CC of AMD donor eyes. However, statistics applied in this work should be handled with care because of sample size, extensive mixed statistical approaches accounting for dependencies, as those performed by Vogt et al. (2011) were not applicable. Instead, linear regression analyses account for CC and RPE dependency in the different stages.

Reproducibility: Nevertheless, the values for BM thickness and basal deposits (Ramrattan et al., 1994; Spraul et al., 1996), density of CC vessels (Mullins et al., 2011) and the correlation of RPE and CC loss (Bhutto and Lutty, 2012; McLeod et al., 2009) investigated here were very close to results published before by the experts in this field. This shows the high reproducibility of our work in comparison with other morphologic methodologies but also with clinical imaging techniques like optical coherence tomography (OCT) (Brown et al., 2009) or angiography (Curcio et al., 1998), which can also be applied to donor eyes. Thus, a correlation of different light, fluorescence, and electron microscopical work is of high value.

Postmortem effects: Note that postmortem times could affect ultrastructure especially that of blood vessels yielding collapsed lumina or invisibility of fenestrations. However, this would affect both controls and AMD donors, and it is not the case here, as shrunken vessels mostly show still intact margins like cell membranes, fenestration and a basal lamina, and appear thus morphologically viable (Fig. 3). In addition, they are facing neighboring intact vessels without damage. Besides, the approach used in this work is not solely based on vessel lumen area but addresses the whole CC layer integrity ("length/BM"), which would not be changed by postmortem artefacts. Both approaches show an about 60% loss CC in AMD compared with controls.

Correlative light and electron microscopy: The combination of light and electron microscopy in neighboring sections of the same tissue block is only possible in plastic sections (here epon) and was a great plus, as both the overview information and the ultrastructural resolution complement each other. They show per se an excellent contrast and ultrastructure compared with stained paraffin or frozen sections. Thus, ghost vessels can be recognized without further staining. However, other cell types, such as those present in BM, can only be fully addressed with antibody labeling which was not performed here. In addition, all histologic analyses represent only one stage in time, thus a progression over time cannot be addressed by either of the discussed methods.

Grading: Our grading primarily addressed the presence of cell layers rather than the viability and/or morphology of these cells. However, it is an estimate of where RPE cells in particular were still viable enough to remain at their destined position, and where organelles like the melanosomes could still participate in antioxidative defense and retinal survival.

Nevertheless, the work shows a practicable method for the investigation of AMD progression. It addresses the importance of investigating border areas between healthy and atrophied regions in AMD samples. With this approach, we showed that loss of choriocapillaris vessels with age occurs and could serve as an indicator and prevalence factor for AMD.

4.5. Summary

Initial CC breakdown is shown to precede RPE and retinal degeneration, as judged from the comparison of control and AMD sections in different stages of destruction. Thus, AMD is presumed to be a vascular disease as has already been postulated before (Friedman, 1997; Verhoeff and Grossman, 1937). Special emphasis should be laid on AMD sections where different stages of degeneration pass over into each other. By comparing these interfaces using the given approach, a possible sequence of degenerative steps with aging and AMD can be revealed.

Disclosure statement

The authors have no actual or potential conflicts of interest including financial, personal, or other relationships with other people or organizations within 3 years of beginning this work submitted that could inappropriately influence their work. Written informed consent of the eye donors for use in medical research and approval of the Institutional Review Board of the University of Tuebingen were obtained.

Acknowledgements

The authors thank Prof Dr Joe Hollyfield and Dr Vera Bonilha (Retinal Degeneration Histopathology Laboratory, Cole Eye Institute —The Cleveland Clinic Foundation) for their kind help in providing them with AMD donor eyes. They also thank the collegues of Dr Yoeruek, namely, Dr Max Warga, Johanna Hofmann, and Dr Barbara Wallenfels-Thilo of the Cornea Bank Tuebingen, and Dr Bernhard Hirt of the Department of Anatomy Tuebingen for providing them with the control eyes. They are indebted to the donors and their families for allowing the use of their eyes in reseach. They thank Sigrid Schultheiss for excellent technical assistance and Judith Birch for proof reading. This work was supported by the following grants: Deutsche Forschungsgemeinschaft BI 1551/2-1, fortuene 1957-0-0, and fortuene 2062-0-0.

Supplementary data

Supplementary data associated with this article can be found, in the online version, at http://dx.doi.org/10.1016/j.neurobiolaging.2014.05.003.

References

Bhutto, I., Lutty, G., 2012. Understanding age-related macular degeneration (AMD): relationships between the photoreceptor/retinal pigment epithelium/Bruch's membrane/choriocapillaris complex. Mol. Aspects Med. 33, 295–317.
Brown, N.H., Koreishi, A.F., McCall, M., Izatt, J.A., Rickman, C.B., Toth, C.A., 2009. Developing SDOCT to assess donor human eyes prior to tissue sectioning for research. Graefes Arch. Clin. Exp. Ophthalmol. 247, 1069–1080.
Brown, W.R., Thore, C.R., 2010. Review: cerebral microvascular pathology in ageing and neurodegeneration. Neuropathol. Appl. Neurobiol. 37, 56–74.
Curcio, C.A., Johnson, M., Rudolf, M., Huang, J.D., 2011. The oil spill in ageing Bruch membrane. Br. J. Ophthalmol. 95, 1638–1645.
Curcio, C.A., Medeiros, N.E., Millican, C.L., 1998. The Alabama age-related macular degeneration grading system for donor eyes. Invest Ophthalmol. Vis. Sci. 39, 1085–1096.
Curcio, C.A., Messinger, J.D., Sloan, K.R., McGwin, G., Medeiros, N.E., Spaide, R.F., 2012. Subretinal drusenoid deposits in non-neovascular age-related macular degeneration: morphology, prevalence, topography, and biogenesis model. Retina 33, 265–276.
Curcio, C.A., Millican, C.L., 1999. Basal linear deposit and large drusen are specific for early age-related maculopathy. Arch. Ophthalmol. 117, 329–339.
Curcio, C.A., Saunders, P.L., Younger, P.W., Malek, G., 2000. Peripapillary chorioretinal atrophy: Bruch's membrane changes and photoreceptor loss. Ophthalmology 107, 334–343.
Duke-Elder, S., 1966. System of Ophthalmology. Kimpton, London, p. 610.
Freund, K.B., Zweifel, S.A., Engelbert, M., 2010. Do we need a new classification for choroidal neovascularization in age-related macular degeneration? Retina 30, 1333–1349.
Friedman, E., 1997. A hemodynamic model of the pathogenesis of age-related macular degeneration. Am. J. Ophthalmol. 124, 677–682.
Green, W.R., Enger, C., 1993. Age-related macular degeneration histopathologic studies. The 1992 Lorenz E. Zimmerman Lecture. Ophthalmology 100, 1519–1535.

Grossniklaus, H.E., Green, W.R., 2004. Choroidal neovascularization. Am. J. Ophthalmol. 137, 496–503.
Grunwald, J.E., Hariprasad, S.M., DuPont, J., Maguire, M.G., Fine, S.L., Brucker, A.J., Maguire, A.M., Ho, A.C., 1998. Foveolar choroidal blood flow in age-related macular degeneration. Invest Ophthalmol. Vis. Sci. 39, 385–390.
Herrmann, P., Holz, F.G., Charbel Issa, P., 2013. Etiology and pathogenesis of age-related macular degeneration. Ophthalmologe 110, 377–387; quiz 388–9.
Hogan, M.J., 1967. Bruch's membrane and disease of the macula. Role of elastic tissue and collagen. Trans. Ophthalmol. Soc. U.K 87, 113–161.
Hogan, M.J., 1972. Role of the retinal pigment epithelium in macular disease. Trans. Am. Acad. Ophthalmol. Otolaryngol. 76, 64–80.
Jonas, J.B., Forster, T.M., Steinmetz, P., Schlichtenbrede, F.C., Harder, B.C., 2014. Choroidal thickness in age-related macular degeneration. Retina 34, 1149–1155.
Kochounian, H., Johnson, L.V., Fong, H.K., 2009. Accumulation of extracellular RGR-d in Bruch's membrane and close association with drusen at intercapillary regions. Exp. Eye Res. 88, 1129–1136.
Kocur, I., Resnikoff, S., 2002. Visual impairment and blindness in Europe and their prevention. Br. J. Ophthalmol. 86, 716–722.
Lengyel, I., Flinn, J.M., Peto, T., Linkous, D.H., Cano, K., Bird, A.C., Lanzirotti, A., Frederickson, C.J., van Kuijk, F.J., 2007. High concentration of zinc in sub-retinal pigment epithelial deposits. Exp. Eye Res. 84, 772–780.
Lengyel, I., Tufail, A., Hosaini, H.A., Luthert, P., Bird, A.C., Jeffery, G., 2004. Association of drusen deposition with choroidal intercapillary pillars in the aging human eye. Invest Ophthalmol. Vis. Sci. 45, 2886–2892.
Liu, M.M., Chan, C.C., Tuo, J., 2012. Genetic mechanisms and age-related macular degeneration: common variants, rare variants, copy number variations, epigenetics, and mitochondrial genetics. Hum. Genomics 6, 13.
Loffler, K.U., Lee, W.R., 1986. Basal linear deposit in the human macula. Graefes Arch. Clin. Exp. Ophthalmol. 224, 493–501.
Lutty, G., Grunwald, J., Majji, A.B., Uyama, M., Yoneya, S., 1999. Changes in choriocapillaris and retinal pigment epithelium in age-related macular degeneration. Mol. Vis. 5, 35.
Machalinska, A., Safranow, K., Sylwestrzak, Z., Szmatloch, K., Kuprjanowicz, L., Karczewicz, D., 2011. Elevated level of circulating endothelial cells as an exponent of chronic vascular dysfunction in the course of AMD. Klin Oczna 113, 228–232.
Macular Photocoagulation Study Group, 1991. Laser photocoagulation of subfoveal neovascular lesions in age-related macular degeneration. Results of a randomized clinical trial. Arch. Ophthalmol. 109, 1220–1231.
Macular Photocoagulation Study Group, 1996. Occult choroidal neovascularization. Influence on visual outcome in patients with age-related macular degeneration. Arch. Ophthalmol. 114, 400–412.
Margolis, R., Spaide, R.F., 2009. A pilot study of enhanced depth imaging optical coherence tomography of the choroid in normal eyes. Am. J. Ophthalmol. 147, 811–815.
McLeod, D.S., Grebe, R., Bhutto, I., Merges, C., Baba, T., Lutty, G.A., 2009. Relationship between RPE and choriocapillaris in age-related macular degeneration. Invest Ophthalmol. Vis. Sci. 50, 4982–4991.
McLeod, D.S., Taomoto, M., Otsuji, T., Green, W.R., Sunness, J.S., Lutty, G.A., 2002. Quantifying changes in RPE and choroidal vasculature in eyes with age-related macular degeneration. Invest Ophthalmol. Vis. Sci. 43, 1986–1993.
Metelitsina, T.I., Grunwald, J.E., DuPont, J.C., Ying, G.S., Brucker, A.J., Dunaief, J.L., 2008. Foveolar choroidal circulation and choroidal neovascularization in age-related macular degeneration. Invest Ophthalmol. Vis. Sci. 49, 358–363.
Mullins, R.F., Johnson, M.N., Faidley, E.A., Skeie, J.M., Huang, J., 2011. Choriocapillaris vascular dropout related to density of drusen in human eyes with early age-related macular degeneration. Invest Ophthalmol. Vis. Sci. 52, 1606–1612.
Prokofyeva, E., Zrenner, E., 2011. Epidemiology of major eye diseases leading to blindness in Europe: a literature review. Ophthalmic Res. 47, 171–188.
Ramrattan, R.S., van der Schaft, T.L., Mooy, C.M., de Bruijn, W.C., Mulder, P.G., de Jong, P.T., 1994. Morphometric analysis of Bruch's membrane, the choriocapillaris, and the choroid in aging. Invest Ophthalmol. Vis. Sci. 35, 2857–2864.
Rudolf, M., Vogt, S.D., Curcio, C.A., Huisingh, C., McGwin Jr., G., Wagner, A., Grisanti, S., Read, R.W., 2013. Histologic basis of variations in retinal pigment epithelium autofluorescence in eyes with geographic atrophy. Ophthalmology 120, 821–828.
Russell, S.R., Mullins, R.F., Schneider, B.L., Hageman, G.S., 2000. Location, substructure, and composition of basal laminar drusen compared with drusen associated with aging and age-related macular degeneration. Am. J. Ophthalmol. 129, 205–214.
Sarks, S., Cherepanoff, S., Killingsworth, M., Sarks, J., 2007. Relationship of Basal laminar deposit and membranous debris to the clinical presentation of early age-related macular degeneration. Invest Ophthalmol. Vis. Sci. 48, 968–977.
Sarks, S.H., 1976. Ageing and degeneration in the macular region: a clinico-pathological study. Br. J. Ophthalmol. 60, 324–341.
Sarks, S.H., A, J.J., Killingsworth, M.C., Sarks, J.P., 1999. Early drusen formation in the normal and aging eye and their relation to age related maculopathy: a clinicopathological study. Br. J. Ophthalmol. 83, 358–368.
Sierra, C., 2012. Cerebral small vessel disease, cognitive impairment and vascular dementia. Panminerva Med. 54, 179–188.
Spaide, R.F., Curcio, C.A., 2010. Drusen characterization with multimodal imaging. Retina 30, 1441–1454.
Spraul, C.W., Lang, G.E., Grossniklaus, H.E., 1996. Morphometric analysis of the choroid, Bruch's membrane, and retinal pigment epithelium in eyes with age-related macular degeneration. Invest Ophthalmol. Vis. Sci. 37, 2724–2735.
Spraul, C.W., Lang, G.E., Grossniklaus, H.E., Lang, G.K., 1998. Characteristics of drusen and changes in Bruch's membrane in eyes with age-related macular degeneration. Histological study. Ophthalmologe 95, 73–79.
van der Schaft, T.L., Mooy, C.M., de Bruijn, W.C., Oron, F.G., Mulder, P.G., de Jong, P.T., 1992. Histologic features of the early stages of age-related macular degeneration. A statistical analysis. Ophthalmology 99, 278–286.
Verhoeff, F.H., Grossman, H.P., 1937. The pathogenesis of disciform degeneration of the macula. Trans. Am. Ophthalmol. Soc. 35, 262–294.
Vogt, S.D., Curcio, C.A., Wang, L., Li, C.M., McGwin Jr., G., Medeiros, N.E., Philp, N.J., Kimble, J.A., Read, R.W., 2011. Retinal pigment epithelial expression of complement regulator CD46 is altered early in the course of geographic atrophy. Exp. Eye Res. 93, 413–423.
Whitmore, S.S., Braun, T.A., Skeie, J.M., Haas, C.M., Sohn, E.H., Stone, E.M., Scheetz, T.E., Mullins, R.F., 2013. Altered gene expression in dry age-related macular degeneration suggests early loss of choroidal endothelial cells. Mol. Vis. 19, 2274–2297.

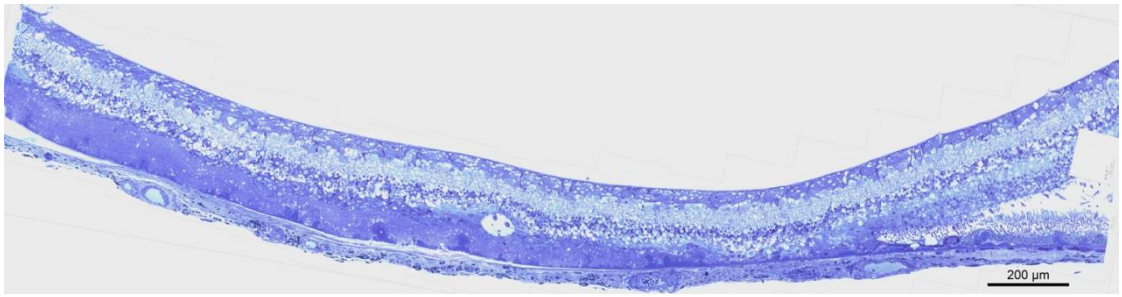

Supplementary Fig. 1. Dry AMD: whole section light microscopical panorama image of a dry AMD donor, female, 93-year-old. The right part of the image is exemplarily shown in Fig. 1A. Abbreviation: AMD, age-related macular degeneration.

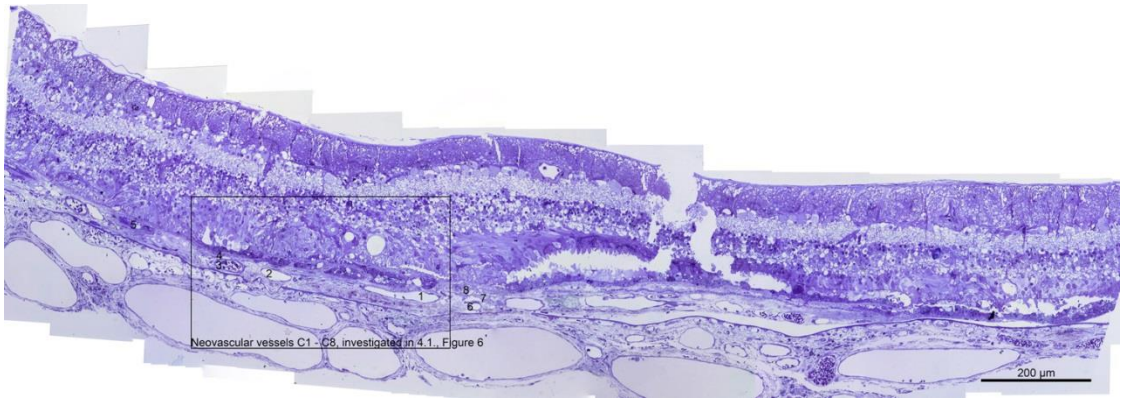

Supplementary Fig. 2. Wet AMD: whole section light microscopical panorama image of a wet AMD donor, male, 76-year-old. The middle part of the image is exemplarily shown in Fig. 1B. The box with the numbered CNV vessels refers to the vessels investigated for Fig. 6 in the text. CNV 1, 5, 6, 7, and 8 show endothelial lesions when investigated with EM. CNV vessels 2, 3, and 4 are intact. Abbreviations: AMD, age-related macular degeneration; CNV, choroidal neovascularization; EM, electron microscopy.

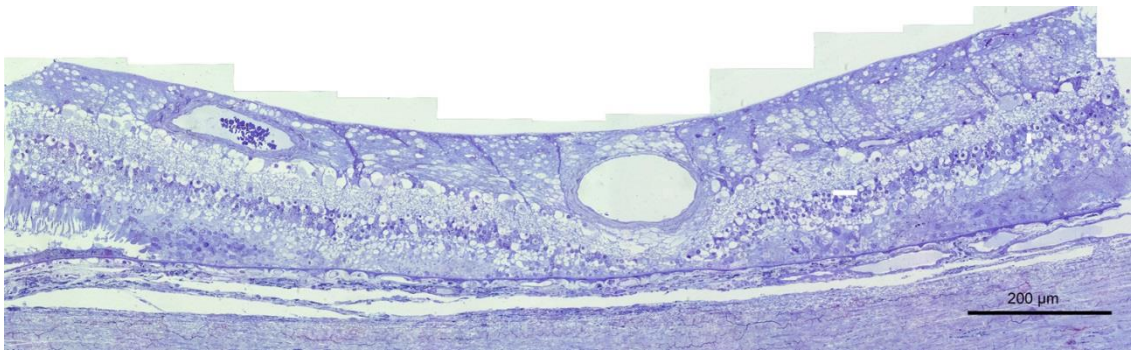

Supplementary Fig. 3. Wet AMD: whole section light microscopical panorama image of a wet AMD donor, male, 71-year-old. The left part of the image is exemplarily shown in Fig. 2. Abbreviation: AMD, age-related macular degeneration.

3.1.2 Ultrastructural alterations in the retinal pigment epithelium and photoreceptors of a Stargardt patient and three Stargardt mouse models: indication for the central role of RPE melanin in oxidative stress

Authors: Taubitz T., Tschulakow A. V., Tikhonovich M., Illing B., Fang Y. Biesemeier A., Julien-Schraermeyer S., Schraermeyer U.

Published in *PeerJ* in 2018

DOI: 10.7717/peerj.5215

Declaration of own contributions:

Planning of the manuscript was done by me in consultation with Prof. Dr. Schraermeyer. Sample preparation (tissue preparation, embedding, sectioning) was done by me, Barbara Illing and Yuan Fang. Machine-learning based quantification of lipofuscin in the RPE cytoplasm was established and performed by Dr. Alexander Tschulakow. Quantification of nuclei in the outer nuclear layer was done by Marina Tikhonovich. All remaining experiments, data acquisition and analyses were performed by me. Interpretation of the data was done by me with input from PD Dr. Antje Biesemeier, PD Dr. Sylvie Julien-Schraermeyer and Prof. Dr. Schraermeyer. Manuscript writing, figure preparation, literature research and revision was done by me, proof reading was done by all co-authors.

PeerJ

Ultrastructural alterations in the retinal pigment epithelium and photoreceptors of a Stargardt patient and three Stargardt mouse models: indication for the central role of RPE melanin in oxidative stress

Tatjana Taubitz, Alexander V. Tschulakow, Marina Tikhonovich, Barbara Illing, Yuan Fang, Antje Biesemeier, Sylvie Julien-Schraermeyer and Ulrich Schraermeyer

Division of Experimental Vitreoretinal Surgery, Centre for Ophthalmology, University of Tuebingen, Tuebingen, Germany

ABSTRACT

Background. Stargardt disease (SD) is characterized by the accumulation of the age-pigment lipofuscin in the retinal pigment epithelium (RPE) and subsequent neuroretinal degeneration. The disease leads to vision loss early in life. Here, we investigate age-dependent ultrastructural changes in three SD mouse models: albino *Abca4*$^{-/-}$ and pigmented *Abca4*$^{-/-}$ and *Abca4*$^{-/-}$.*Rdh8*$^{-/-}$ mice. Since we found indications for oxidative stress primarily in albino SD mice, we tested RPE melanin for its antioxidative capabilities.

Methods. SD mouse eyes were investigated by light, fluorescence and electron microscopy and were compared to the respective albino and pigmented wild type mice and to a human donor SD eye. To confirm the role of RPE melanin in scavenging oxidative stress, melanin from *S. officinalis* as a standard and porcine RPE were tested for their capability to quench superoxide anions.

Results. Histological alterations indicative of oxidative stress and/or lysosomal dysfunction were present in albino *Abca4*$^{-/-}$ and *Abca4*$^{-/-}$.*Rdh8*$^{-/-}$ mice. Retinal damage, such as inner segment rupture and pyknotic or free photoreceptor nuclei in the subretinal space and RPE vacuolization were exclusively found in albino *Abca4*$^{-/-}$ mice. Shortened and disorganized photoreceptor outer segments and dead RPE cells were found in albino *Abca4*$^{-/-}$ and *Abca4*$^{-/-}$.*Rdh8*$^{-/-}$ mice, with earlier onset in albino *Abca4*$^{-/-}$ mice. Undegraded phagosomes and lipofuscin accumulation were present in the RPE of all three SD strains, but numbers were highest in *Abca4*$^{-/-}$.*Rdh8*$^{-/-}$ mice. Lipofuscin morphology differed between SD strains: (melano-)lipofuscin granules in pigmented *Abca4*$^{-/-}$ mice had a homogenous electron density and sharp demarcations, while lipofuscin in albino *Abca4*$^{-/-}$ mice had a flocculent electron density and often lacked a surrounding membrane, indicating loss of lysosomal integrity. Young *Abca4*$^{-/-}$.*Rdh8*$^{-/-}$ mice showed (melano-)lipofuscin granules with homogenous electron density, while in aged animals granules with flocculent electron density predominated. Both strains of pigmented SD mice had melanolipofuscin clusters as found in the human SD eye. Like melanin from *S. officinalis*, porcine RPE melanin can also quench superoxide anions.

Submitted 10 March 2018
Accepted 19 June 2018
Published 19 July 2018

Corresponding author
Tatjana Taubitz,
tatjana.taubitz@med.uni-tuebingen.de

Academic editor
Juan Riesgo-Escovar

Additional Information and Declarations can be found on page 26

DOI **10.7717/peerj.5215**

Copyright
2018 Taubitz et al.

Distributed under
Creative Commons CC-BY 4.0

OPEN ACCESS

How to cite this article Taubitz et al. (2018), Ultrastructural alterations in the retinal pigment epithelium and photoreceptors of a Stargardt patient and three Stargardt mouse models: indication for the central role of RPE melanin in oxidative stress. **PeerJ 6:e5215; DOI 10.7717/peerj.5215**

PeerJ

Discussion. The presented pathologies in albino *Abca4*$^{-/-}$ and *Abca4*$^{-/-}$.*Rdh8*$^{-/-}$ mice suggest oxidative stress and/or lysosomal dysfunction within the RPE. Since albino *Abca4*$^{-/-}$ mice have the earliest onset and severest damage and as absence of melanin and also melanin turnover with age are known to diminish RPEs anti-oxidative properties, we assume that RPE melanin plays a role in SD related damages. A lack of pathology in pigmented *Abca4*$^{-/-}$ mice due to lower stress levels as compared to the *Abca4*$^{-/-}$.*Rdh8*$^{-/-}$ mice underlines this hypothesis. It is also supported by the finding that RPE melanin can quench superoxide anions. We therefore suppose that RPE melanin is important in retinal health and we discuss its role as an oxidative stress scavenger.

Subjects Cell Biology, Neuroscience, Ophthalmology, Pathology, Histology
Keywords Lipofuscin, Melanolipofuscin, Stargardt disease, Lysosomes, Oxidative stress, Melanin, Retinal degeneration

INTRODUCTION

Stargardt disease (STGD1, OMIM #248200) is one of the most frequent inherited macular dystrophies in humans and affects 1 in 8,000–10,000 individuals (*Blacharski, 1988*). It is caused by mutations in the ATP-binding cassette A4 (*ABCA4*) gene, which encodes for a transmembrane protein located in the rim of photoreceptor disks (*Allikmets et al., 1997*; *Molday, Zhong & Quazi, 2009*). The ABCA4 protein is involved in all-trans retinal transport through the photoreceptor disk membrane and is thus part of the visual cycle. Disrupted ABCA4 function leads to accumulation of all-trans retinal within the disk and facilitates formation of N-retinylidene-N-retinylethanolamine (A2E) and other bisretinoids (*Sparrow et al., 2012*). These substances are major components of lipofuscin, a cytotoxic age pigment that accumulates in the retinal pigment epithelium (RPE) and leads to RPE dysfunction and subsequent RPE and photoreceptor degeneration (*Sparrow et al., 2012*). Owing to the burden of cytotoxic lipofuscin accumulation early in life, Stargardt patients suffer from early onset macular degeneration, resulting in progressive bilateral vision loss.

The first animal model generated for Stargardt disease was the pigmented *Abca4*$^{-/-}$ mouse (*Weng et al., 1999*). This model shows several typical pathological changes related to Stargardt disease, including accumulation of lipofuscin granules in the RPE, elevated levels of A2E and other bisretinoid fluorophores and delayed dark adaption (*Charbel Issa et al., 2013*). Since this mouse strain lacks retinal degeneration (*Charbel Issa et al., 2013*; *Weng et al., 1999*), it is considered as a model for the early stage of Stargardt disease.

A second *Abca4*$^{-/-}$ mouse strain, the albino *Abca4*$^{-/-}$ mouse, was generated by crossbreeding pigmented *Abca4*$^{-/-}$ mice with Balb/c mice (*Radu et al., 2004*). This albino *Abca4*$^{-/-}$ mouse model differs from the pigmented *Abca4*$^{-/-}$ mouse model in several aspects. Albino *Abca4*$^{-/-}$ mice have lower levels of the lipofuscin component A2E, but higher levels of A2E oxidation products, so called A2E oxiranes than pigmented *Abca4*$^{-/-}$ mice (*Radu et al., 2004*). It was previously shown that lipofuscin can generate reactive oxygen species, including singlet oxygen, after exposure to blue light (*Rozanowska et al., 1995*) and that A2E is oxidized by singlet oxygen to A2E oxiranes *in vitro*

(*Ben-Shabat et al., 2002*). As a consequence, A2E can auto-oxidize to A2E oxiranes in the presence of light. Since A2E oxiranes are highly reactive and can cause DNA fragmentation (*Sparrow et al., 2003a*; *Sparrow, Zhou & Cai, 2003b*), this might be an important mechanism of A2E cytotoxicity. In contrast to pigmented *Abca4*$^{-/-}$ mice, albino *Abca4*$^{-/-}$ mice show a mild retinal degeneration, starting at an age of 7 months (*Radu et al., 2011*) and leading to a loss of approximately 30 to 40% of photoreceptor nuclei at the age of 11 months compared to WT (*Radu et al., 2008*; *Wu, Nagasaki & Sparrow, 2010*). Furthermore, albino *Abca4*$^{-/-}$ mice show a range of signs of chronic inflammation in the RPE including upregulated expression of oxidative stress genes, elevated levels of the oxidative stress markers malondialdehyde and 4-hydroxynonenal, activation of complement, downregulation of complement regulatory proteins and monocyte chemoattractant protein-1, increased C-reactive protein immunoreactivity and thickening of Bruch's Membrane (*Radu et al., 2011*).

A third Stargardt disease mouse model is the pigmented *Abca4*$^{-/-}$.*Rdh8*$^{-/-}$ mouse strain, generated by crossbreeding *Abca4*$^{-/-}$ mice with *Rdh8*$^{-/-}$ mice (*Maeda et al., 2008*). *Abca4*$^{-/-}$.*Rdh8*$^{-/-}$ mice are described to have reduced all-trans retinal clearance and higher amounts of A2E, A2E-precursors and retinal dimer conjugates than WT and pigmented *Abca4*$^{-/-}$ mice (*Maeda et al., 2008*). Regional retinal degeneration and rosette formation is observed by as early as 6 weeks of age and leads to advanced retinal degeneration by the age of 3 months (*Maeda et al., 2008*). Furthermore, drusen formation and thickening of Bruch's membrane in 3-month-old animals and choroidal neovascularization in 10-month-old animals are described (*Maeda et al., 2008*).

So far, ultrastructural changes were not investigated in detail in all three mentioned Stargardt disease mouse models, although they are widely used in the search of therapy options for SD. In this study, we conducted light and fluorescence microscopic as well as ultrastructural analysis of age-related retinal and RPE changes in these mouse strains. For comparison, we investigated tissue of the respective WT mouse strains and a single eye of a human donor with Stargardt disease. So far, electron microscopic examinations of human Stargardt eyes are scarce (*Birnbach et al., 1994*; *Bonilha et al., 2016*; *Eagle Jr et al., 1980*).

We found early onset of histologic alterations typical for oxidative stress and lysosomal impairment in albino *Abca4*$^{-/-}$ mice. Similar alterations were found with later onset and less severity in pigmented *Abca4*$^{-/-}$.*Rdh8*$^{-/-}$ mice and were lacking in pigmented *Abca4*$^{-/-}$ mice. Since both the absence of melanin and melanin ageing are known to diminish the antioxidative properties of the RPE, these finding underline the importance of RPE melanin for retinal health and disease.

MATERIALS AND METHODS

Animals

Pigmented *Abca4*$^{-/-}$ mice (129S4/SvJae-Abca4^{tm1Ght}) were kindly donated by P. Charbel Issa (University of Oxford, Oxford, England). Albino *Abca4*$^{-/-}$ mice (BALB/c-Abca4 ^{tm1Ght}) were kindly donated by G. Travis and R. Radu (University of California, Los Angeles, CA). Double knock-out *Abca4*$^{-/-}$.*Rdh8*$^{-/-}$ (129S4/SvJae- Abca4^{tm1Ght}*C57BL/6J-Rdh8^{tm1Kpal}) mice were kindly donated by K. Palczewski (Case Western Reserve University,

Cleveland, Ohio). Control albino WT mice (Balb/c) were purchased from Charles River (Sulzfeld, Germany) and control pigmented WT mice (129S2) were purchased from Harlan Laboratories (Hillcrest, UK). The knock-out mouse strains were bred in our in-house facility. Light cycling was 12 h light (approximately 50 lux in cages)/12 h dark, food and water were available *ad libitum*. All procedures involving animals were in accordance with the German laws governing the use of experimental animals and were previously approved by the local agency for animal welfare (Einrichtung für Tierschutz, Tierärztlichen Dienst und Labortierkunde der Eberhard Karls Universität Tübingen, Tuebingen, Germany) and the local authorities (Regierungspräsidium Tübingen, Tuebingen, Germany).

Sample preparation and light, fluorescence and electron microscopy

Animals were sacrificed by carbon dioxide inhalation and subsequent cervical dislocation and the eyes were immediately enucleated.

For light and electron microscopy, eyes were fixed overnight at 4 °C in 5% glutaraldehyde in 0.1 M cacodylate buffer (pH 7.4). After washing in cacodylate buffer, the cornea and lens were removed and eye cups were hemisected. Halves were post-fixed in 1% osmium tetroxide in 0.1 M cacodylate buffer and bloc-stained with uranyl acetate. Samples were dehydrated in a graded series of ethanol and propylene oxide and embedded in Epon. Reagents were purchased from AppliChem (Darmstadt, Germany), Merck (Darmstadt, Germany) and Serva (Heidelberg, Germany). Light microscopy on toluidine blue stained semi-thin sections (500 nm) was performed with a Zeiss Axioskop (Zeiss, Jena, Germany). Ultrathin sections (70 nm) were mounted on copper slot grids (Plano, Wetzlar, Germany) and stained with lead citrate and examined with a Zeiss 900 electron microscope (Zeiss, Jena, Germany).

For fluorescence microscopy and immunohistochemistry, eyes were fixed in 4.5% formaldehyde (Carl Roth, Karlsruhe, Germany) and embedded in paraffin wax, cut into 5 µm thick sections for fluorescence microscopy and 4 µm thick sections for immunohistochemistry. Samples for fluorescence microscopy were deparaffinized according to standard procedures, cover-slipped with FluorSave (Calbiochem, La Jolla, CA, USA) and were investigated with a Zeiss Axioplan2 imaging microscope (Zeiss, Jena, Germany). Lipofuscin autofluorescence was visualized with a custom lipofuscin filter set (excitation 360 nm, emission 540 nm).

Immunohistochemistry

Sections were deparaffinized, rehydrated and subjected to heat induced antigen retrieval in a pressure cooker for 2 min in either citrate buffer at pH 6 (anti-HNE, anti-MDA) or Tris buffer at pH 9 (anti-NITT). Sections were incubated overnight at 4 °C with either rabbit anti-HNE (4-hydroxy-2-noneal, HNE11-S, alpha diagnostic international; major product of endogenous lipid peroxidation, 1:3,500), rabbit anti-MDA (malondialdehyde, MDA11-S, alpha diagnostic international; byproduct of endogenous lipid peroxidation, 1:2,000) or rabbit anti-NITT (nitrotyrosine, NITT12-A, alpha diagnostic international; peroxynitrite-induced nitration of tyrosine residues in proteins, 1:1,000). Dilution of primary antibodies was done with antibody diluent with background-reducing components

(Dako S3022; Agilent, Santa Clara, CA, USA). The primary antibodies were detected with the Dako REAL™ Detection System, Alkaline Phosphatase/RED, Rabbit/Mouse according to the manufacturer's instructions. In brief, sections were incubated with biotinylated goat anti-mouse and anti-rabbit immunoglobulins for 15 min at room temperature with subsequent incubation with streptavidin conjugated to alkaline phosphatase for 15 min at room temperature. Reaction products were visualized with freshly prepared substrate working solution supplemented with levamisole to block endogenous peroxidases. Sections were counterstained with hematoxylin solution modified according to Gill III (Merck, Darmstadt, Germany). To control for non-specific binding, control sections were prepared without incubation with primary antibodies. Sections were investigated using a Zeiss Axioskop (Zeiss, Jena, Germany).

Quantification of photoreceptor nuclei and outer segment length by light microscopy

Semi-thin sections of whole eye cups (up to 400 µm from the optic nerve head) were photographed using a 63× oil objective. Areas adjacent to the optic nerve and to the ora serrata were excluded from analysis due to the physiological thinning of the retina.

Photoreceptor nuclei were counted semi-automatically in an average of 11 digital images per section in on average three eyes per age group using Fiji software (*Schindelin et al., 2012*). In each image, a region of interest with a width of 100 µm along the outer nuclear layer was defined and total photoreceptor nuclei within the region of interest were counted as number of photoreceptor nuclei per 100 µm width of retina. The total numbers of eyes investigated by light microscopy and used for photoreceptor nuclei quantification per strain were 34 eyes (albino *Abca4*$^{-/-}$ mice), 30 eyes (pigmented *Abca4*$^{-/-}$ mice) and 47 eyes (*Abca4*$^{-/-}$.*Rdh8*$^{-/-}$ mice).

Outer segment layer length was measured manually in 11–16 positions per section in an average of two eyes per age group using Fiji software.

Electron microscopic investigation

Whole sections of mouse eyes were thoroughly investigated by electron microscopy. Total numbers of eyes investigated by electron microscopy for the different strains were 12 eyes (pigmented *Abca4*$^{-/-}$), 16 eyes (albino *Abca4*$^{-/-}$), 16 eyes (*Abca4*$^{-/-}$.*Rdh8*$^{-/-}$), six eyes (albino WT) and three eyes (pigmented WT). Sections were examined for changes in photoreceptor, RPE and Bruch's membrane structure. Lipid droplets in RPE cells were counted and their diameter measured in whole sections. Thickness of Bruch's membrane was measured in 15 consecutive images. All measurements were performed with iTEM 5.0 Software (Olympus Soft Imaging Solutions, Muenster; Germany).

Quantification of the area in RPE cytoplasm occupied by lipofuscin-like material

Lipofuscin-like material (derived from both lipofuscin and melanolipofuscin granules, hereafter referred to as lipofuscin) was quantified in young (aged 4 to 6 months) and old (aged 12 months) Stargardt mice in an average of 5 eyes per group. Thirty electron micrographs of the RPE (magnification× 20.000) per eye were taken in a way so only

cytoplasm and no nuclei, microvilli and basal labyrinth were visible. To compensate for vignetting, only an oval region of interest in the image center was analyzed. The Trainable Weka Segmentation (*Arganda-Carreras et al., 2017*) plugin for Fiji software, a machine learning tool, was used to determine the area of lipofuscin per image. A representative subset of images was used to train the tool to specifically recognize lipofuscin, so melanin was excluded from the analysis. A combination of the mean, median, maximum, minimum, variance and the anisotropic diffusion-, entropy- and neighbor algorithms was used. Segmentation calculations were performed on a 16 virtual central processing units system with 64 GB working memory (de.NBI Cloud Tübingen, https://denbi.uni-tuebingen.de).

Human tissue

Glutaraldehyde-fixed perimacular tissue of a 72-year-old donor with clinically diagnosed Stargardt disease was obtained through Foundation Fighting Blindness (Columbia, MD, USA). Post mortem time until fixation was 48 h. Written informed consent of the donor for use in medical research and approval of the Institutional Review Board of the University of Tuebingen (Ethik-Kommission an der Medizinischen Fakultät der Eberhard-Karls-Universität und am Universitätsklinikum Tübingen, Tuebingen, Germany, approval number 462/2009BO2) were obtained. The experiments were performed in adherence to the tenets of the Declaration of Helsinki. Human tissue was embedded for standard electron microscopy as described above. For investigation of lipofuscin autofluorescence in semi-thin sections, heavy-metal treatment during embedding (osmium tetroxide, uranyl acetate) was omitted.

Isolation of porcine RPE melanin

RPE melanin from pig eyes was isolated as described by (*Boulton & Marshall, 1985*) with modifications (*Zareba et al., 2006*). In brief, pig eyes were opened close to the ora serrata and the anterior segment and vitreous were discarded. The retina was removed with forceps and the eye cup washed with PBS (Gibco, Carlsbad, CA, USA). Eye cups were filled with trypsin/EDTA (Gibco, Carlsbad, CA, USA) and incubated for 10 min at 37 °C. RPE cells were isolated by pipetting jet streams onto the cell layer and collected in DMEM supplemented with 10% fetal bovine serum (Gibco, Carlsbad, CA, USA) to stop the enzymatic reaction. RPE cell pellets were homogenized using a tissue grinder. Cell debris were removed by centrifugation for 7 min at 60 g and the obtained supernatant was centrifuged for 10 min at 6,000 g to pellet all pigment granules. The pellet was collected in 0.3 M sucrose, loaded on a two-step sucrose gradient (1 M and 2 M) and centrifuged for 1 h at 103.000 g. Isolated RPE melanin granules were washed in PBS and the final granule concentration was determined using a hemocytometer.

Quenching of superoxide in an NBT assay

Quenching capability of melanin was investigated with the photochemical nitroblue tetrazolium (NBT) assay (*Cheng et al., 2015*). In this assay, superoxide generated by illumination of riboflavin reduces pale-yellow NBT to blue-violet formazan. The reaction mixture had a final concentration of 0.1 mM EDTA, 13 μM methionine, 75 μM NBT and 4 mM riboflavin in PBS pH 7.4. EDTA, methionine, NBT and riboflavin were purchased

from Sigma-Aldrich (St. Louis, MO, USA). The reaction mixture was illuminated for 15 min with blue light from an LED lamp at 2.5 mW/cm^2 (450 nm, SunaEco 1500 Ocean Blue XP, Tropic Marin, Wartenberg, Germany). Uniform illumination of the samples was ensured by placing the samples on a horizontally aligned rotator. The formazan was quantified at 560 nm (Synergy HT, BioTek, Winooski, VT, USA).

Controls included positive controls (all reagents, no melanin, illuminated), negative controls (all reagents, no melanin, kept in the dark) and blanks (no riboflavin, melanin, illuminated) to compensate for melanin absorption at readout.

Statistical analysis

Statistical analysis was performed with JMP 13 (SAS, Cary, NC, USA). All data sets were tested for normal distribution to decide on using parametric or non-parametric testing. Since all data sets were not normally distributed and contained several groups, we used the Steel-Dwass All Pairs test, a multiple non-parametrical test with alpha correction. The null hypothesis was that the groups were not significantly different. Values are given as mean ±standard deviation, $p < 0.05$ was considered statistically significant.

RESULTS

Photoreceptors

Light microscopic investigation of tissue of 12-month-old animals (Fig. 1A) showed overall typical histology in pigmented *Abca4*$^{-/-}$ mice compared to pigmented WT as already published in (*Charbel Issa et al., 2013*) (not shown). Albino *Abca4*$^{-/-}$ mice had shortened outer segments whereas *Abca4*$^{-/-}$.*Rdh8*$^{-/-}$ showed a hypertrophy of the RPE (Fig. 1A, Fig. S1).

Outer segment length was measured in light microscopy. Compared to age-matched albino WT animals, albino *Abca4*$^{-/-}$ mice aged 4 months showed a significant reduction in outer segment length (albino *Abca4*$^{-/-}$ 4 months 22.3 ± 3.2 µm, albino WT 4 months 26.2 ± 2.5 µm, $p < 0.001$, Fig. 1B). In *Abca4*$^{-/-}$.*Rdh8*$^{-/-}$ mice, outer segment shortening had later onset: no difference was found for 3-month-old animals, whereas 6-month-old animals had shortened outer segments (*Abca4*$^{-/-}$.*Rdh8*$^{-/-}$ 3-month-old 32.1 ± 2.7 µm, pigmented WT 3-month-old 32.6 ± 1.6 µm, not significant; *Abca4*$^{-/-}$.*Rdh8*$^{-/-}$ 6-month-old 27.7 ± 2.0 µm, pigmented WT 12-month-old 33.9 ± 2.0 µm, $p < 0.0001$, Fig. 1B). Pigmented *Abca4*$^{-/-}$ had no outer segment shortening compared to pigmented WT.

A detailed analysis of the age-dependent reduction of photoreceptor nuclei numbers of the three different Stargardt mouse strains revealed similar retinal degeneration courses for both albino *Abca4*$^{-/-}$ and *Abca4*$^{-/-}$.*Rdh8*$^{-/-}$ mice (Fig. 1C) as compared to the pigmented *Abca4*$^{-/-}$ mice for which it is known that they do not present signs of retinal degeneration (*Charbel Issa et al., 2013*; *Weng et al., 1999*). We quantified total photoreceptor nuclei numbers, as opposed to the more commonly used outer nuclear layer thickness, to account for nuclei disorganization and gaps between nuclei that occurred in albino *Abca4*$^{-/-}$ and, to a lesser extent, in *Abca4*$^{-/-}$.*Rdh8*$^{-/-}$ mice.

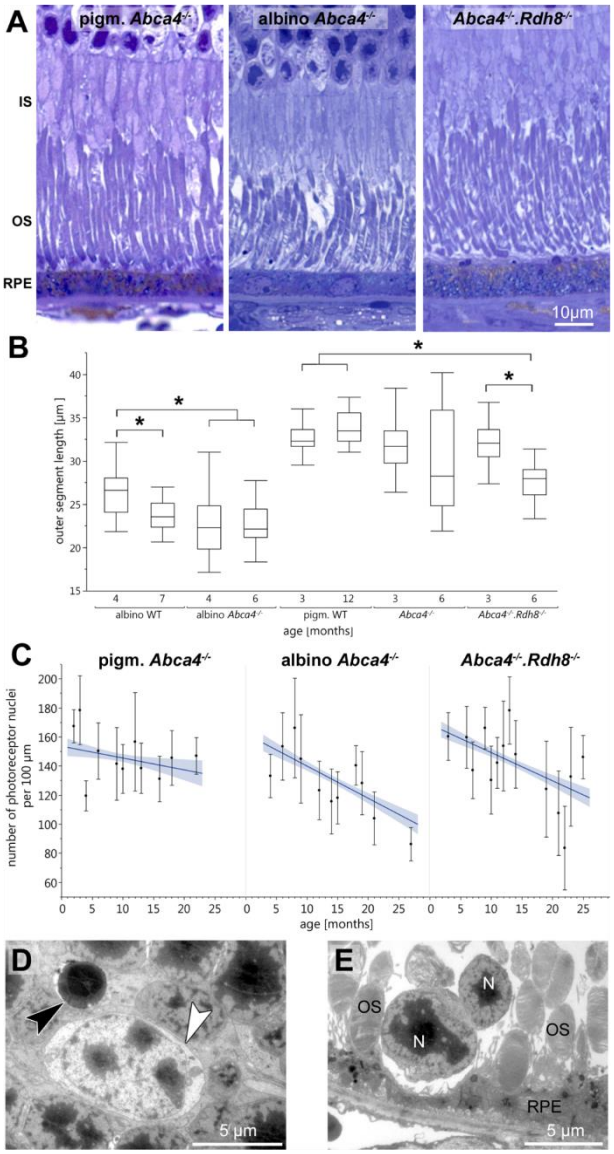

Figure 1 Retinal degeneration in Stargardt mice. (A) Representative light micrographs of 12-month-old pigmented and albino *Abca4*$^{-/-}$ and *Abca4*$^{-/-}$.*Rdh8*$^{-/-}$ mice. Albino *Abca4*$^{-/-}$ mice have shorter outer segments whereas *Abca4*$^{-/-}$.*Rdh8*$^{-/-}$ mice have hypertrophic RPE. (B) Quantification of outer segment length in Stargardt mice compared to WT animals. In albino *Abca4*$^{-/-}$ mice, outer segment length is already reduced in 4-month-old animals, compared to albino WT. (continued on next page…)

Full-size DOI: 10.7717/peerj.5215/fig-1

Figure 1 (…continued)
Abca4$^{-/-}$.*Rdh8*$^{-/-}$ mice show a significant reduction of outer segment length between 3 and 6 months (n = on average 2 eyes/age group, $*p \leq 0.001$, Steel-Dwass All Pairs test). (C) Quantification of numbers of photoreceptor nuclei per 100 µm width of retina. Linear regression and 95% confidence interval are shown (n = on average 3 eyes/age group). (D) A pyknotic nucleus is present (black arrowhead) next to a cone nucleus (white arrowhead) (albino *Abca4*$^{-/-}$, 4 months). (E) Photoreceptor nuclei are located next to unusually thinned RPE cells (albino *Abca4*$^{-/-}$, 4 months). IS, inner segments; OS, outer segments; RPE, retinal pigment epithelium; N, nucleus.

On the ultrastructural level, shrunken, electron dense nuclei, resembling pyknosis, were only found in albino *Abca4*$^{-/-}$ animals (Fig. 1D). Furthermore, isolated photoreceptor nuclei were present in the subretinal space next to unusually thinned RPE cells, even in young albino *Abca4*$^{-/-}$ animals (Fig. 1E). In our colony of *Abca4*$^{-/-}$.*Rdh8*$^{-/-}$mice, we could not find the previously described rosette formation at 3 weeks and the rather prominent retinal degeneration beginning at 3 months (*Maeda et al., 2008*). Rosette formation was only seen in a single 12-month-old animal. Instead, RPE hypertrophy was regularly seen in *Abca4*$^{-/-}$.*Rdh8*$^{-/-}$animals (Fig. 1A, Fig. S1).

Genotype and age-dependent alterations of the disc membrane stacking were apparent on the ultrastructural level (Fig. 2A, Table 1). Those alterations seemed to start at the outer segment tips (next to the RPE) and spread towards the base of the outer segment. Alterations in outer segment tip organization were never seen in pigmented WT and pigmented *Abca4*$^{-/-}$ mice. In albino WT and *Abca4*$^{-/-}$.*Rdh8*$^{-/-}$ animals, it was not seen in the youngest animals investigated (3–4 months), but in animals aged 6–7 months and older. In albino *Abca4*$^{-/-}$ mice, outer segment tip disorganization was already present in 4-month-old animals, the youngest group investigated in this strain.

In albino *Abca4*$^{-/-}$ and *Abca4*$^{-/-}$.*Rdh8*$^{-/-}$ animals, alterations in overall disc membrane stacking were observed starting with 6 months but were lacking in pigmented and albino WT and pigmented *Abca4*$^{-/-}$ animals.

Inner segments of photoreceptors appeared swollen and/or ruptured in albino *Abca4*$^{-/-}$ mice (Fig. 2B). In pigmented *Abca4*$^{-/-}$ mice and *Abca4*$^{-/-}$.*Rdh8*$^{-/-}$ mice, inner segment damages were only occasionally observed (Table 1).

In albino *Abca4*$^{-/-}$ mice, agglomerated electron dense material was occasionally present between inner segment and outer segment (Fig. 2C) and disk membrane renewal seemed to be somewhat disturbed as disk membrane swirls were sporadically present at the nascent part of the outer segment (Fig. 2D). These changes were not present in albino WT and pigmented Stargardt mice. Outer segment tips were in contact to RPE microvilli in all mouse strains and age groups.

Vacuole-like structures within the RPE

In semi-thin sections of albino *Abca4*$^{-/-}$ mice, vacuole-like structures within the RPE monolayer were apparent in animals as young as 6 months (Fig. 3A). Electron microscopic investigation revealed that the vacuole-like structures were an enlargement of the intercellular space between RPE cells and were apically limited by the junctional complex (Fig. 3B). Sometimes vacuole-like structures were also seen within the cytoplasm, usually in proximity to the lateral plasma membrane and probably also of intercellular

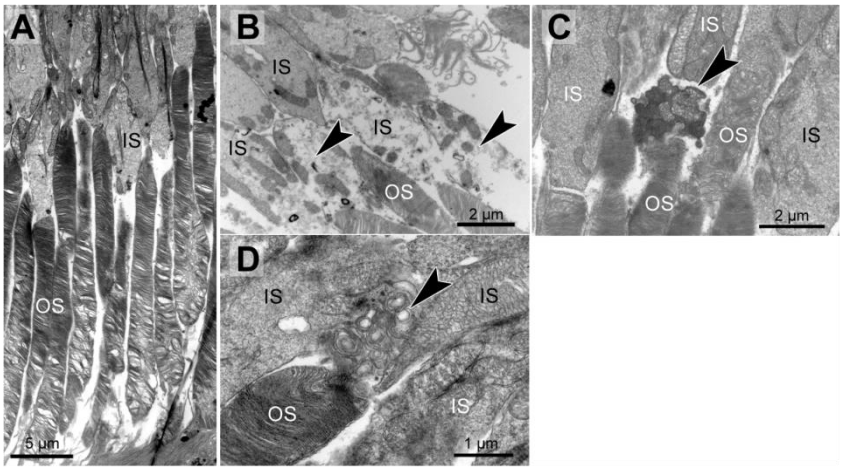

Figure 2 Morphological changes in inner and outer segments of albino *Abca4*$^{-/-}$ mice. (A) Disc membrane stacking in outer segments gets more disorganized towards the RPE (albino *Abca4*$^{-/-}$, 6 months). (B) Inner segments are ruptured (arrowheads) (albino *Abca4*$^{-/-}$, 4 months). (C) Electron dense agglomerations (arrowhead) are seen between inner and outer segment (albino *Abca4*$^{-/-}$, 6 months). (D) Newly synthesized disk membranes are disorganized and accumulate outside of the outer segment (arrowhead) (albino *Abca4*$^{-/-}$, 9 months). IS, inner segments; OS, outer segments.

Full-size DOI: 10.7717/peerj.5215/fig-2

space origin. The contents of the vacuole-like structures varied between empty (not shown), filled with membranous material (Fig. 3B) and filled with a variety of fibrillous, granular, lamellar and amorphous materials (Fig. 3C). Different types of contents were often seen within the same eye. Ultrastructurally, vacuole-like structures were apparent in albino *Abca4*$^{-/-}$ mice of all age groups, but were barely present in pigmented *Abca4*$^{-/-}$ and *Abca4*$^{-/-}$.*Rdh8*$^{-/-}$ mice (Fig. 3D). The number of vacuole-like structures increased with age, though there was a considerable variance between eyes of the same age. Vacuole-like structures were considerably fewer in albino WT mice.

Lipofuscin

To compare the lipofuscin autofluorescence between the different Stargardt mouse strains, paraffin sections of 12-month-old animals were investigated by fluorescence microscopy (Fig. 4A). In pigmented *Abca4*$^{-/-}$ sections, the lipofuscin autofluorescence was clearly defined, indicating the presence of granules with well-defined borders. In albino *Abca4*$^{-/-}$ sections, the lipofuscin autofluorescence was predominantly blurry. In *Abca4*$^{-/-}$.*Rdh8*$^{-/-}$ sections, both clearly defined and blurry lipofuscin autofluorescence were present. Autofluorescence in albino *Abca4*$^{-/-}$ and *Abca4*$^{-/-}$.*Rdh8*$^{-/-}$ tissue was elevated compared to pigmented *Abca4*$^{-/-}$ tissue.

The morphological appearance of lipofuscin granules in the different Stargardt mouse strains was investigated by electron microscopy. Typical morphological appearances are

Table 1 **Ultrastructural observations in WT and Stargardt mice.**

	albino WT		albino *Abca4*$^{-/-}$							pigm. WT		pigm. *Abca4*$^{-/-}$								*Abca4*$^{-/-}$.*Rdh8*$^{-/-}$							
Age [months]	**4**	**7**	**4**	**6**	**9**	**12**	**15**	**18**	**21**	**3**	**12**	**2**	**4**	**6**	**9**	**12**	**16**	**18**	**22**	**3**	**6**	**9**	**12**	**14**	**19**	**23**	**25**
OS tips disarranged	–	+/–	+/–	+	+	+	+	+	+	–	–	–	–	–	–	–	–	–	–	–	+/–	+/–	+	+/–	+/–	+/–	+/–
OS on full length disarranged	–	–	–	+/–	+	+	+	+	+	–	–	–	–	–	–	–	–	–	–	–	+/–	+/–	+	+	+	+	+
Swollen/ ruptured IS	–	–	+	+	+	+	+	+	+	–	–	–	–	–	+/–	–	–	–	–	–	–	–	+/–	–	–	–	–
Lipofuscin:																											
– homogenous	+/–	+/–	+	+	+/–	+	+	+	+	+/–	+	+	++	++	++ +	++ ++	++ ++	++ +	++ +	+	++	+	++ ++	++ +	++ +	+	++
– flocculent	+/–	+/–	+	++	++ +	++ +	++ +	++ +	++ +	+/–	+/–	–	–	–	–	–	–	–	–	–	–	–	+/–	++ +	++	++	++
Lipid droplets:																											
– apical	++	++	+/–	–	–	–	+/–	–	–	+	++	+/–	–	–	–	–	–	–	–	–	–	–	–	–	–	–	–
– basal	–	++	+	++	++	+	+	+	+/–	+	++	+	+/–	+/–	+	+/–	–	+/–	–	+/–	+	+/–	–	+/–	+/–	+/–	+/–
Detached RPE cells	+/–	+	+	+	+/–	+	+	+/–	+/–	–	–	–	–	–	–	–	-	+/–	–	–	–	–	–	+/–	+	+	+
Undegraded phagosomes	–	+	+	+/–	+	+	+	++	+	+/–	+	+	+	+	+/–	+	+	+	+	+	++	++ +	+	+	+	+	++
Lateral basal labyrinth expansions	+/–	+	+	+	+	+	+	+	+	–	–	–	–	–	–	–	–	–	–	–	–	–	–	–	–	+	–

Notes.

–, not or rarely observed; +/–, occasionally observed; +, regularly observed; ++, regularly observed in high amounts; +++, regularly observed in extreme amounts.

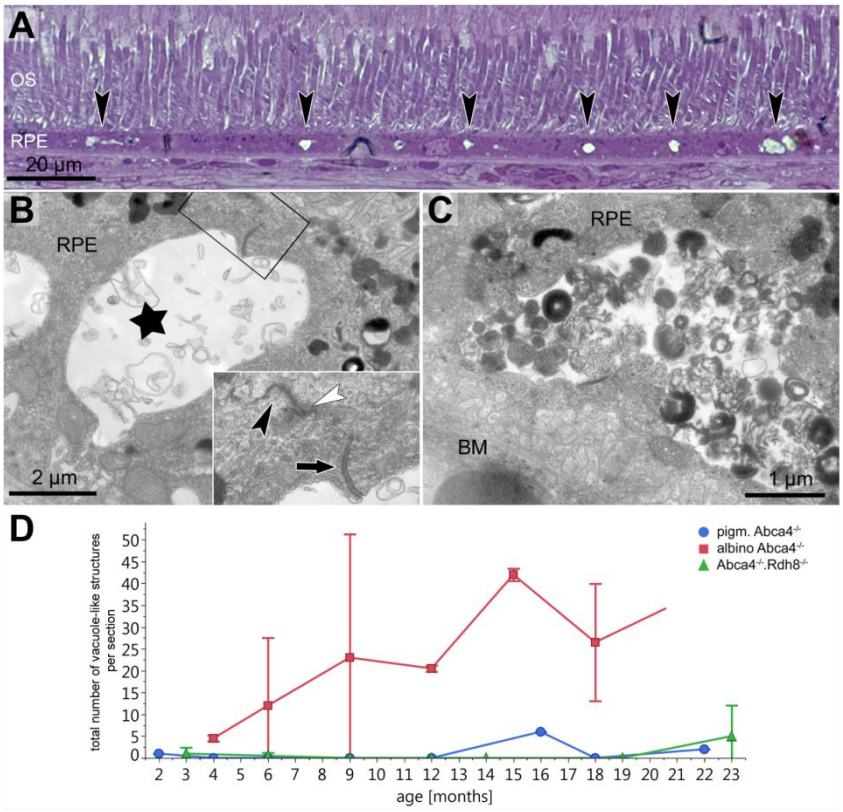

Figure 3 **Vacuole-like structures in RPE cells are most prominent in albino *Abca4*$^{-/-}$ mice.** (A) In light microscopic images, vacuole-like structures (black arrowheads) within the RPE layer are present in albino *Abca4*$^{-/}$ mice (6 months). (B) A vacuole-like structure (asterisk) turns out to be an enlargement of the intercellular space. Inset: apically, the vacuole-like structure is limited by a junctional complex consisting of a desmosome (arrow), zonula adherens (white arrowhead) and tight junction (black arrowhead) (albino *Abca4*$^{-/-}$, 9 months). (C) Vacuole-like structures are regularly filled with very heterogeneous types of material and are surrounded by a membrane (albino *Abca4*$^{-/-}$, 15 months). (D) Quantification in electron microscopy revealed that vacuole-like structures are barely present in pigmented *Abca4*$^{-/-}$ and *Abca4*$^{-/-}$.*Rdh8*$^{-/-}$ mice (n = on average 2 eyes/age group). OS, outer segments; RPE, retinal pigment epithelium; BM, Bruch's membrane.

Full-size DOI: 10.7717/peerj.5215/fig-3

illustrated in Fig. 4B and age-dependent quantification of the different identified lipofuscin subtypes can be found in Table 1.

In pigmented *Abca4*$^{-/-}$ mice, we found exclusively lipofuscin with homogenous electron density and clearly defined margins indicating an intact limiting membrane (Fig. 4B), as previously described (*Charbel Issa et al., 2013*). Most of the lipofuscin was fused to melanin and formed melanolipofuscin.

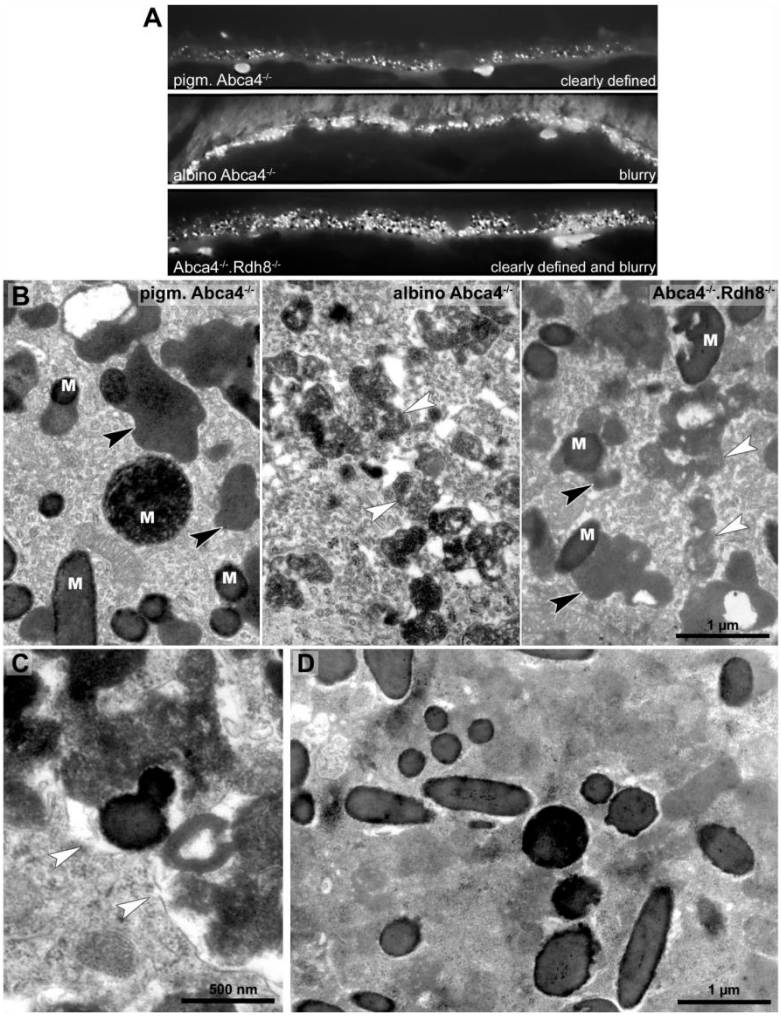

Figure 4 **Lipofuscin in Stargardt mice is highly variable in fluorescence and electron microscopy.** (A) Comparison of lipofuscin autofluorescence in paraffin-embedded sections of 12-month-old Stargardt mice. (B) Lipofuscin and melanolipofuscin have different morphologies in the different Stargardt mouse strains. In pigmented *Abca4*$^{-/-}$ mice, lipofuscin has a homogenous electron-density and sharp demarcations (black arrowheads), while in albino *Abca4*$^{-/-}$ mice, most lipofuscin granules have a flocculent electron-density with unclear demarcations (white arrowheads). While in young *Abca4*$^{-/-}$.*Rdh8*$^{-/-}$ mice, only granules with homogenous electron density can be found, both lipofuscin morphologies can be found in aged animals. M: melanin granules (pigmented and albino *Abca4*$^{-/-}$, 9 months, *Abca4*$^{-/-}$.*Rdh8* $^{-/-}$, 12 months). (C) Membranes surrounding lipofuscin and melanolipofuscin with flocculent electron density are often damaged (white arrowheads) (*Abca4*$^{-/-}$.*Rdh8*$^{-/-}$, 21 months). (D) In very old Stargardt mice, the RPE cytoplasm is abnormally electron dense. Borders of individual lipofuscin granules are barely visible (*Abca4*$^{-/-}$.*Rdh8* $^{-/-}$, 23 months).

Full-size DOI: 10.7717/peerj.5215/fig-4

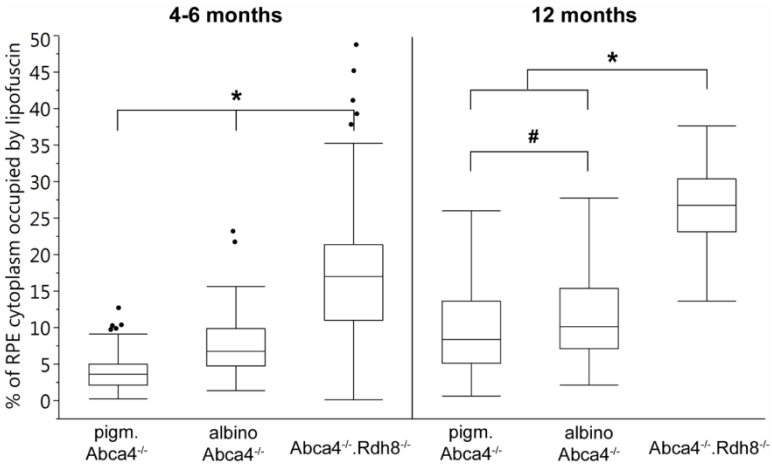

Figure 5 Quantification of the RPE area occupied by lipofuscin in young and old Stargardt mouse strains. Lipofuscin granules and lipofuscin moieties of melanolipofuscin granules were taken into account. ($n =$ on average 5 eyes/age group, # $p < 0.05$, * $p < 0.0001$, Steel-Dwass All Pairs test).
Full-size DOI: 10.7717/peerj.5215/fig-5

In albino *Abca4*$^{-/-}$ mice, lipofuscin with homogenous electron density was also seen. However, the majority of lipofuscin granules belonged to another type that had a flocculent electron density (Fig. 4B, Table 1). The margins of this type of lipofuscin were often not clearly defined, suggesting loss of the lysosomal membrane. As albino *Abca4*$^{-/-}$ mice accumulated lipofuscin with age, the amount of lipofuscin with flocculent electron density increased while the amount of lipofuscin with homogenous electron density seemed to stay constant (Table 1).

In *Abca4*$^{-/-}$.*Rdh8*$^{-/-}$ mice, the first type of lipofuscin with homogenous electron density had a considerable variability between age groups (Table 1). After the age of 12 months, the second type of lipofuscin with flocculent electron density was also present (Table 1). As in pigmented *Abca4*$^{-/-}$ mice, most of the lipofuscin was fused to melanin and formed melanolipofuscin.

Membranes enclosing lipofuscin of the flocculent electron density type were often damaged or absent (Fig. 4C). In very old animals (aged 23 months and older), the RPE cytoplasm was abnormally electron dense (Fig. 4D). Clear demarcations between lipofuscin granules and the cytoplasm were hardly visible.

The area of RPE cytoplasm occupied by lipofuscin (both derived from lipofuscin and melanolipofuscin granules) was quantified in electron micrographs of young (4–6 months) and old (12 months) Stargardt mice (Fig. 5). In both age groups, *Abca4*$^{-/-}$.*Rdh8*$^{-/-}$ mice had the highest levels of lipofuscin (young 16.9% ± 8.3%, old 26.9% ± 5.3%). In young animals, albino *Abca4*$^{-/-}$ mice had almost twice the levels of pigmented *Abca4*$^{-/-}$ mice (albino *Abca4*$^{-/-}$ 7.5% ± 3.9%, pigmented *Abca4*$^{-/-}$ 3.9% ± 2.7%, $p < 0.0001$). In 12-month-old animals, the difference of lipofuscin levels in albino and pigmented

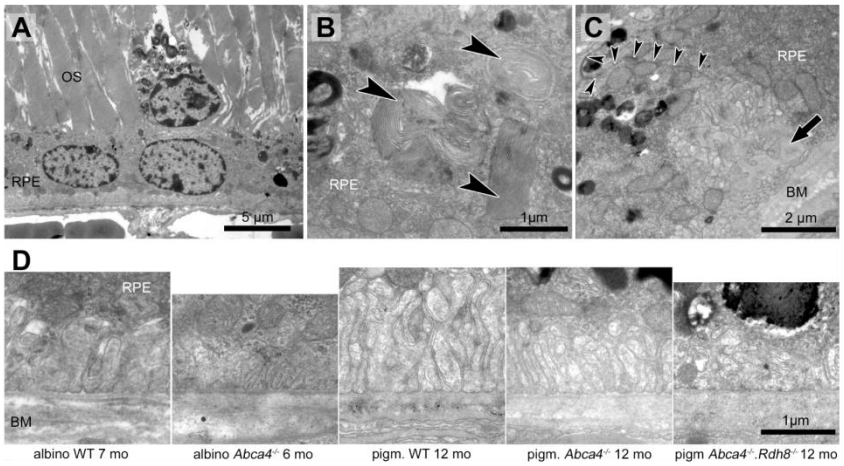

Figure 6 RPE integrity is compromised in albino *Abca4*$^{-/-}$ mice. (A) Detached and lysed RPE cell situated in the subretinal space (albino *Abca4*$^{-/-}$, 4 months). (B) RPE cells of all Stargardt mouse strains regularly contain undigested outer segments in the basal part. Few cells in albino *Abca4*$^{-/-}$ mice contain several large undigested outer segments (arrowheads) that claimed the majority of the cytoplasm (albino *Abca4*$^{-/-}$, 4 months). (C) Expansion of the basal labyrinth along the lateral cell borders is regularly seen in albino *Abca4*$^{-/-}$ animals (9 months). Arrowheads indicate the cell border. Basal infoldings were filled with a homogenous material (arrow). (D) Basal labyrinth expansion is reduced in the Stargardt mouse strains compared to the respective wild types. OS, outer segments; RPE, retinal pigment epithelium; BM, Bruch's membrane.

Full-size DOI: 10.7717/peerj.5215/fig-6

Abca4$^{-/-}$ mice was lower but nevertheless statistically significant (albino *Abca4*$^{-/-}$ 11.0% ± 5.5%, pigmented *Abca4*$^{-/-}$ 9.3% ± 5.5%, $p < 0.05$).

Lipid droplets

Lipid droplets were frequently seen in RPE cells of all investigated mouse strains, especially in albino *Abca4*$^{-/-}$ mice (Table 1). In pigmented and albino WT animals, lipid droplets were small (median diameter: albino WT 235 nm, pigmented WT 353 nm) and the majority of droplets was fused to lipofuscin (albino WT 59% and pigmented WT 82% of total lipid droplets, Fig. S2). They were found in both apical and basal parts of the RPE cells, with a tendency to be more often apically located (Table 1). In Stargardt mouse strains, lipid droplets were bigger (median diameter: pigmented *Abca4*$^{-/-}$ 555 nm, albino *Abca4*$^{-/-}$ 705 nm, *Abca4*$^{-/-}$.*Rdh8*$^{-/-}$ 687 nm) and only sporadically seen in the apical part of the RPE (Table 1, Fig. S2). Fusion with lipofuscin was rarely seen in albino *Abca4*$^{-/-}$ mice (3% of total lipid droplets) and absent in pigmented Stargardt mice.

RPE integrity and Bruch's membrane

Dead RPE cells were regularly encountered in eyes of albino *Abca4*$^{-/-}$ mice of all ages (Fig. 6A, Table 1). In contrast, dead RPE cells were only found in aged *Abca4*$^{-/-}$.*Rdh8*$^{-/-}$ mice (12 months and older). In pigmented *Abca4*$^{-/-}$ and young *Abca4*$^{-/-}$.*Rdh8*$^{-/-}$ mice,

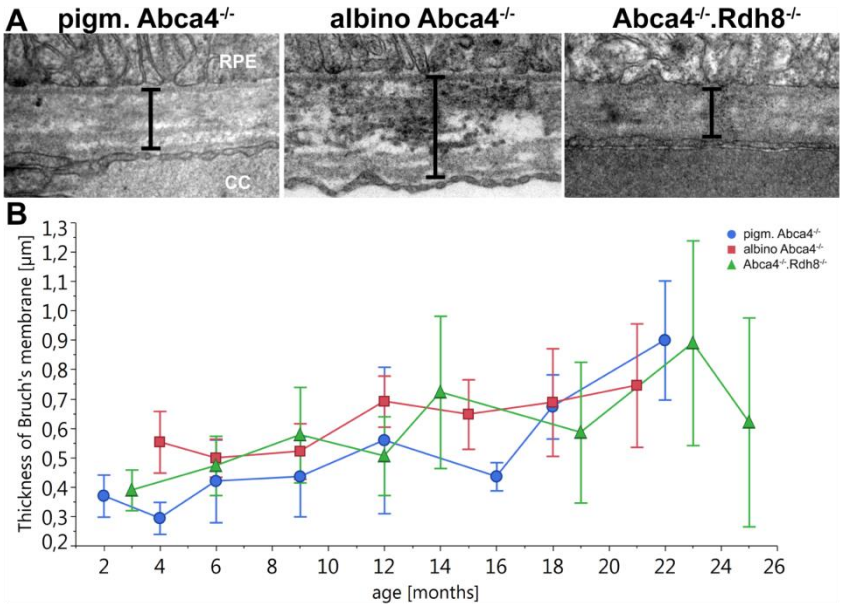

Figure 7 Thickening of Bruch's Membrane is comparable in all Stargardt mouse strains. (A) Representative electron microscopic images of Bruch's membrane in 12-month-old Stargardt mice. Thickness of Bruch's membrane was measured from the basement membrane of the RPE to the basement membrane of the endothelial cell of the choriocapillaris (indicated by bars). (B) Thickness of Bruch's membrane increases in all Stargardt mice to the same extent. There is no significant difference between the different Stargardt mouse strains. (n = on average 2 eyes/age group) RPE, retinal pigment epithelium; CC, choriocapillaris.

Full-size DOI: 10.7717/peerj.5215/fig-7

dead RPE cells were not found. Locally, RPE cells were unusually thin in albino *Abca4*$^{-/-}$ mice (Fig. 1E).

RPE cells regularly contained undegraded phagosomes in the basal area of the cytoplasm in all three Stargardt mouse strains (Table 1). RPE cells, whose cytoplasm was largely occupied by extensive undegraded phagosomes, were found in albino *Abca4*$^{-/-}$ and *Abca4*$^{-/-}$.*Rdh8*$^{-/-}$ mice (Fig. 6B). The highest numbers of undegraded phagosomes were found in *Abca4*$^{-/-}$.*Rdh8*$^{-/-}$ mice (Table 1).

Irregularly shaped basal infoldings were frequently seen in albino *Abca4*$^{-/-}$ mice, but rarely in pigmented Stargardt mice (Table 1). The irregular shape was due to the basal infoldings expanding to the lateral side of the cells (Fig. 6C). In general, basal infoldings were reduced in number and expansion in all Stargardt mouse strains compared to wild types (Fig. 6D).

Bruch's membrane became thicker with age in all Stargardt mouse strains (Fig. 7). There was no significant difference between the different strains.

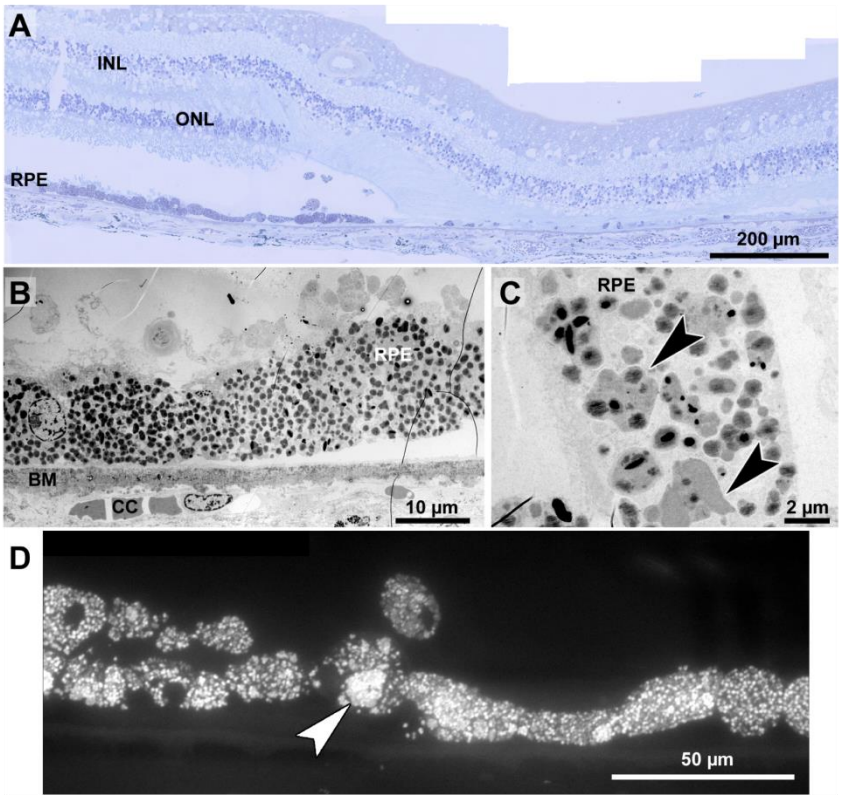

Figure 8 Histopathology and pigment changes in a human donor eye with late Stargardt disease. (A) Light microscopic panorama picture of a 72-year-old human donor Stargardt retina: The left area is histologically complete with photoreceptors and a confluent RPE layer. On the right, a typical geographic atrophy with lack of photoreceptors and RPE is present. (B) Electron microscopic overview of the RPE of a human donor eye with Stargardt disease. RPE is completely filled with pigment granules. Microvilli and basal infoldings are missing and Bruch's membrane is unorganized and contains electron dense deposits. (C) Big clusters of melanolipofuscin (arrowheads). (D) Fluorescence micrograph of a semi-thin section also shows abundant lipofuscin autofluorescence and cluster formation (arrowhead). INL, inner nuclear layer; ONL, outer nuclear layer; RPE, retinal pigment epithelium; BM, Bruch's membrane; CC, choriocapillaris.

Full-size DOI: 10.7717/peerj.5215/fig-8

Histopathology and pigment changes in late Stargardt disease

For comparison, we also investigated a single eye of a 72-year-old Stargardt patient (Fig. 8). In this late stage of the disease, photoreceptors were almost completely degenerated resulting in geographic atrophy as is typical for Stargardt patients (Fig. 8A). A reliable quantification of neuroretinal changes was not possible due to the long death-to-fixation time of the donor, but pigments can still be investigated under these conditions. RPE cells were nearly completely filled with pigment granules (Fig. 8B), mostly lipofuscin and

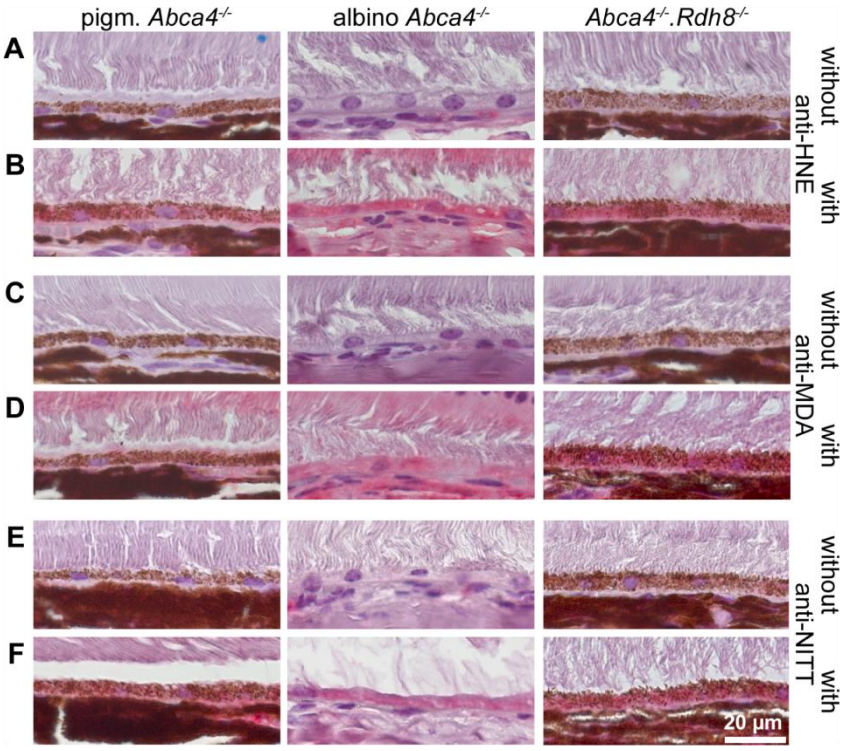

Figure 9 HNE, MDA and NITT adducts are present in RPE cells of 12-month-old Stargardt mice indicating oxidative stress. Immunohistochemical stainings show that (A, B) HNE, (C, D) MDA and (E, F) NITT adducts (*red*) can be found in the RPE of pigmented *Abca4*$^{-/-}$, albino *Abca4*$^{-/-}$, and *Abca4*$^{-/-}$.*Rdh8*$^{-/-}$ mice with levels being lowest in pigmented *Abca4*$^{-/-}$ mice. (A, C) and (E) show negative controls (primary antibody was omitted) for each antibody; (B, D) and (F) show the respective antibody stain for each primary antibody.

Full-size DOI: 10.7717/peerj.5215/fig-9

melanolipofuscin, melanin granules were barely present. Microvilli and basal infoldings were absent, while Bruch's membrane was unorganized and contained electron dense deposits (Fig. 8B). Melanolipofuscin formed clusters (Figs. 8C, and 8D), as they were also found in pigmented *Abca4*$^{-/-}$ and *Abca4*$^{-/-}$.*Rdh8*$^{-/-}$ mice.

Oxidative stress markers are present in Stargardt mice

Since ultrastructural changes in the RPE of Stargardt mice were indicative of oxidative stress, we tested for oxidative stress markers in 12-month-old mice by immunohistochemistry. We found HNE, MDA and NITT adducts in the RPE cells of pigmented and albino *Abca4*$^{-/-}$ and *Abca4*$^{-/-}$.*Rdh8*$^{-/-}$ mice with signals being generally lowest in pigmented *Abca4*$^{-/-}$ mice (Fig. 9). HNE, MDA and NITT signals were also present in the neuroretina, reaching from the inner limiting membrane to the inner segments, in all Stargardt strains and were

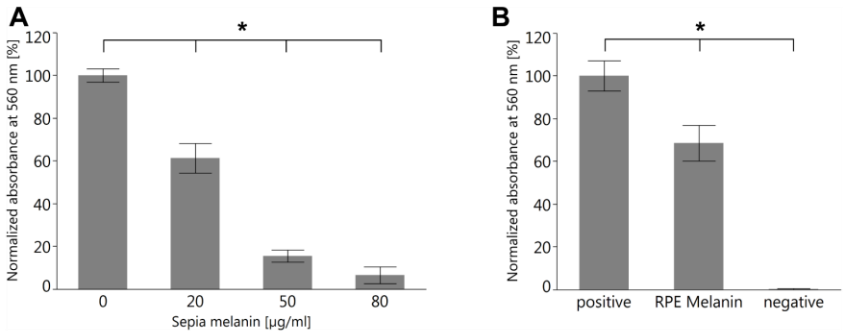

Figure 10 Both melanin from *S. officinalis* and porcine RPE melanin can quench superoxide radicals in an NBT assay. (A) Sepia melanin shows a dose dependent capability to quench superoxide anions produced by light-illuminated riboflavine. ($n = 8$ per group, two independent experiments, $^{*}p < 0.05$, Steel-Dwass All Pairs test). (B) Porcine RPE melanin (concentration 3×10^4 granules/ml) quenches superoxide anions. Negative control contained all reagents but no melanin and was kept in the dark so no superoxide was produced ($n = 12$ per group, three independent experiments, $^{*}p < 0.05$, Steel-Dwass All Pairs test).
Full-size DOI: 10.7717/peerj.5215/fig-10

highest in $Abca4^{-/-}.Rdh8^{-/-}$ mice in the case of HNE and MDA or at similar levels in the three strains in case of NITT (Fig. S3).

RPE melanin can quench superoxide

To investigate the capability of RPE melanin to quench superoxide, we employed the colorimetric NBT assay (*Cheng et al., 2015*). We first tested melanin from *S. officinalis* as a melanin standard for its quenching capabilities and found a dose–response relationship (Fig. 10A). Subsequently, we investigated RPE melanin isolated from pig eyes and found an approximately 30% reduction of detectable superoxide for 3×10^4 RPE melanin granules utilized in the assay (Fig. 10B).

DISCUSSION

The goal of this study was a comparison of the age-dependent ultrastructural changes in three frequently used mouse models for Stargardt disease in order to better understand these models. The three strains differ in their genetic background: pigmented $Abca4^{-/-}$ mice are bred on a 129 background, albino $Abca4^{-/-}$ mice have a BALB/c background and pigmented $Abca4^{-/-}.Rdh8^{-/-}$ mice have a mixed 129.B6 background.

Both the 129 and BALB/c strains have the Leu450 variant of RPE65, while the B6 strain has the Met450 variant, resulting in a lower visual cycle turnover and reduced light damage susceptibility in this strain. Since the pigmented $Abca4^{-/-}.Rdh8^{-/-}$ strain is on a mixed 129.B6 background, both alleles of RPE65 are present in this strain. Retinal degeneration was reported to be more common in $Abca4^{-/-}.Rdh8^{-/-}$ mice carrying the Leu450 variant (97.5% of investigated eyes) than animals carrying the Met450 variant (43.8% of investigated eyes) (*Maeda et al., 2008*). We did not genotype our animals for RPE65.

There is a growing body of evidence that different WT mouse strains show varied susceptibility to light-induced damage that is brought on by so far unidentified genetic modulators. For instance, even though BALB/c and 129 mice both have the LEU450 variant of RPE65, resulting in a high visual cycle turnover, BALB/c mice show a lower resistance to light-induced retinal damage that is independent of pigmentation (*Danciger et al., 2004*). Instead, two significant and two suggestive quantitative trait loci were identified that might be the reason for the greater sensitivity to light damage in BALB/c mice (*Danciger et al., 2004*). These findings were gained from experiments using intense, short-term light exposure, but their relevance for moderate, long-term light exposure as employed in animal husbandry is currently unknown. Nevertheless, care must be taken when comparing the results from the three different Stargardt mouse models concerning their predisposition to retinal degeneration.

Among Stargardt mice, albino *Abca4*$^{-/-}$ mice show the earliest onset and most varied retinal damages

It was previously described that albino *Abca4*$^{-/-}$ mice show a mild retinal degeneration that is not present in albino WT mice (*Sparrow et al., 2013*; *Wu, Nagasaki & Sparrow, 2010*). We found that absolute photoreceptor nuclei numbers decrease with age, resulting in a steeper decline of photoreceptor nuclei counts compared to pigmented *Abca4*$^{-/-}$ mice (Fig. 1C). By contrast, *Abca4*$^{-/-}$.*Rdh8*$^{-/-}$ mice are described to have regional retinal degeneration and rosette formation as early as 6 weeks of age and advanced retinal degeneration by 3 months (*Maeda et al., 2008*). We were unable to reproduce the published results with our colony of *Abca4*$^{-/-}$.*Rdh8*$^{-/-}$ mice. Our animals had a similar rate of retinal degeneration than the albino *Abca4*$^{-/-}$ mice (Fig. 1C) and rosette formation was only found in one 12-month-old animal from a total of 25 *Abca4*$^{-/-}$.*Rdh8*$^{-/-}$ animals examined light-microscopically up to an age of 25 months.

In addition to the photoreceptor loss, albino *Abca4*$^{-/-}$ mice show outer segment shortening (Fig. 1B), disordered disk membranes (Fig. 2A), damaged inner segments (Fig. 2B), and morphological changes at the base of the outer segments (Figs. 2C and 3D). These damages were not seen in pigmented *Abca4*$^{-/-}$ and to a much lesser extent in *Abca4*$^{-/-}$.*Rdh8*$^{-/-}$ mice (Table 1). Shortening and disorganization of outer and inner segments was also described after conditional knockout of superoxide dismutase in the RPE, resulting in oxidative stress (*Mao et al., 2014*).

In Stargardt patients, the junction between the inner and outer segments was described to be unorganized and/or lost on SD-OCT (*Gomes et al., 2009*). Furthermore, photoreceptor anomalies were found in patients that did not display equivalent fundus autofluorescence anomalies (*Gomes et al., 2009*). Damaged inner segments and defective outer segment synthesis in albino *Abca4*$^{-/-}$ mice (Figs. 2B–2D), but not in pigmented Stargardt mouse strains, might be histological representations of the SD-OCT findings in Stargardt patients and needs further investigation.

Outer segment renewal starts at the base of the outer segment, so the disks at the tips are the oldest disks in a photoreceptor and are affected the longest by any disturbance, e.g., accumulation of retinoids due to lack of ABCA4. Loss of fundamental outer segment

proteins like rhodopsin (*Lem et al., 1999*) or GARP (*Huttl et al., 2005*) leads to a severe outer segment damage starting early in life (reviewed by (*Goldberg, Moritz & Williams, 2016*)). ABCA4 is located in the rims of disk membranes (*Papermaster et al., 1978*) and does not form stable interactions with the peripherin-2·GARP complex (*Poetsch, Molday & Molday, 2001*), which is essential for linking disk rims to the outer segment plasma membrane and disk-disk stacking (*Kaupp & Seifert, 2002*). These findings, together with the lack of outer segment disk pathology in pigmented *Abca4*$^{-/-}$ mice (Table 1) (*Charbel Issa et al., 2013*), indicate that ABCA4 is not needed for proper disk formation, orientation and stability. Whether RPE malfunction is responsible for the presented outer segment defects in albino *Abca4*$^{-/-}$ and to a lesser extent *Abca4*$^{-/-}$.*Rdh8*$^{-/-}$ mice needs to be elucidated.

Indications for lysosomal dysfunction and oxidative stress in albino *Abca4*$^{-/-}$ mice

Formation of vacuole-like structures in the RPE as seen in albino *Abca4*$^{-/-}$ mice (Fig. 3) has been described after lysosomal integrity has been compromised and after oxidative stress. Increasing the lysosomal pH with chloroquine (*Peters et al., 2006*), inhibiting lysosomal cysteine proteases (*Okubo et al., 2000*) and a lack of functional βA3/A1-crystallin (*Valapala et al., 2014*; *Zigler Jr et al., 2011*) all lead to formation of vacuole-like structures within the RPE cell layer. Lysosomal pH was shown to be increased after treatment of RPE cells with the lipofuscin compound A2E *in vitro* (*Holz et al., 1999*; *Liu et al., 2008*) and in primary RPE cells isolated from pigmented *Abca4*$^{-/-}$ mice (*Liu et al., 2008*). Since the melanosome is a specialized lysosome (*Orlow, 1995*) that contains many lysosomal enzymes (*Diment et al., 1995*) and can fuse with phagosomes (*Schraermeyer & Heimann, 1999*), it is possible that albinism itself adds to the lysosomal dysfunction seen in albino *Abca4*$^{-/-}$ mice due to lack of melanosomes.

Similar pathologies were also described after oxidative stress. Changes in RPE morphology, such as vacuolization and loss of basal labyrinth, and deposit formation were seen after a lack of superoxide dismutase (*Mao et al., 2014*; *Seo et al., 2012*), knockout of Nrf2, a transcription factor that regulates genes involved in the cellular oxidative stress response (*Zhao et al., 2011*), and after chronic exposure to cigarette smoke (*Fujihara et al., 2008*). In some models, thinning of the outer nuclear layer (*Mao et al., 2014*; *Seo et al., 2012*) and shortening and disorganization of inner and outer segments (*Mao et al., 2014*) or RPE hyper- and hypopigmentation and choroidal neovascularization (*Zhao et al., 2011*) were also described. Besides the high oxygen partial pressure and the presence of light, other sources for oxidative stress in the RPE are phagocytosis of photoreceptor outer segments (*Miceli, Liles & Newsome, 1994*) and lipofuscin (*Rozanowska et al., 1995*).

Previous studies investigating oxidative stress in Stargardt mice found that albino *Abca4*$^{-/-}$ mice have higher levels of MDA and HNE adducts than age-matched albino WT and pigmented *Abca4*$^{-/-}$ mice (*Radu et al., 2011*) and that 6-month-old *Abca4*$^{-/-}$.*Rdh8*$^{-/-}$ mice have higher levels of 8-OHdG than 4-week-old *Abca4*$^{-/-}$.*Rdh8*$^{-/-}$ mice and age-matched WT mice (*Sawada et al., 2014*). We found similar results indicating that pigmented *Abca4*$^{-/-}$ mice have the lowest oxidative stress levels (Fig. 9).

Interestingly, *Abca4*$^{-/-}$.*Rdh8*$^{-/-}$ mice had higher numbers of undegraded phagocytosed outer segments than albino *Abca4*$^{-/-}$mice (Table 1), but albino *Abca4*$^{-/-}$ mice had higher numbers of vacuole-like structures (Fig. 3D). One reason might be higher oxidative stress levels in albino *Abca4*$^{-/-}$ mice. Melanin was shown to be a scavenger of superoxide anion and singlet oxygen (*Bustamante et al., 1993*; *Tada, Kohno & Niwano, 2010*) and protects human RPE cells from oxidative stress *in vitro* (*Burke et al., 2011*). Intravitreal application of paraquat, a superoxide anion generator, leads to higher superoxide levels and more pronounced lipid oxidation and retinal degeneration in albino compared to pigmented mice (*Cingolani et al., 2006*).

Additionally, changes of RPE morphology in albino animals might play a role in RPE vacuolization: embryonic RPE from albino mice was found to have an irregular morphology, compared to pigmented littermates (*Iwai-Takekoshi et al., 2016*). Furthermore, an altered distribution of the junctional protein P-cadherin was found in albino RPE and it was hypothesized that this might lead to defects in cell–cell adhesion (*Iwai-Takekoshi et al., 2016*). It is reasonable that a combination of weakened cell–cell contacts, impaired lysosomal function and elevated oxidative stress as described above might lead to the defects found in albino *Abca4*$^{-/-}$ mice.

Lipofuscin varies considerably between Stargardt mouse strains

Morphological appearance of lipofuscin granules differs in the three different Stargardt mouse strains. It has been described that the chemical composition of lipofuscin in pigmented and albino WT mice differs in terms of the amounts of the different types of bisretinoids that can be found (*Ueda et al., 2016*). It is hypothesized that the higher intraocular light levels in albino animals lead to photooxidation and photodegradation of A2E and other bisretinoids (*Ueda et al., 2016*), which is in accordance with earlier publications that demonstrated lower A2E and higher A2E oxirane levels in albino *Abca4*$^{-/-}$ mice compared to pigmented *Abca4*$^{-/-}$ mice (*Radu et al., 2004*). In *Abca4*$^{-/-}$.*Rdh8*$^{-/-}$ mice, higher amounts of all-trans retinal dimer can be found than in *Abca4*$^{-/-}$ mice (*Maeda et al., 2008*). Our results show that in addition to the difference in the chemical composition of lipofuscin between the three strains, there is also a considerable histological difference.

Strikingly, lipofuscin levels in 12-month-old animals seem to be elevated in albino *Abca4*$^{-/-}$compared to pigmented *Abca4*$^{-/-}$mice, when investigated by lipofuscin autofluorescence (Fig. 4A), while quantification of RPE cytoplasm occupied by lipofuscin granules shows similar lipofuscin levels in 12-month-old pigmented and albino *Abca4*$^{-/-}$mice (Fig. 5). Both quenching effects of the melanin and differences in nature and amount of present fluorophores, as described above, are possible explanations for this seeming contradiction.

The Met450 variant of RPE65 was described to be associated with lower levels of the lipofuscin fluorophores A2E and iso-A2E in *Abca4*$^{-/-}$.*Rdh8*$^{-/-}$ mice (*Kim et al., 2004*). Since pigmented and albino *Abca4*$^{-/-}$ mice carry the Leu450 variant of RPE65 and we did not genotype the *Abca4*$^{-/-}$.*Rdh8*$^{-/-}$ mice for RPE65, lipofuscin levels in Figs. 4 and 5 in *Abca4*$^{-/-}$.*Rdh8*$^{-/-}$ mice might be underreported.

The bisretinoid A2E was shown to have surfactant-like properties and to be able to compromise lysosomal and cellular membranes (*Schutt et al., 2002*; *Sparrow et al., 1999*). In fact, we found that lipofuscin granules often lacked membranes (Fig. 4C). Furthermore, in very old animals (aged 23 months and older), we found abnormally electron dense RPE cytoplasm (Fig. 4D), making distinguishing between lipofuscin granules and cytoplasm very difficult. Whether the RPE cytoplasm gained electron density due to free lipofuscin components that leaked from lipofuscin granules after losing their membranes is unclear but appears likely.

Bruch's membrane thickness does not vary between Stargardt mouse strains

For all three Stargardt mouse strains, a thickening of Bruch's membrane compared to WT was described (*Maeda et al., 2008*; *Radu et al., 2011*; *Weng et al., 1999*). Compared to each other, the three strains show comparable thickening of Bruch's membrane with age (Fig. 7). An increase in the thickness of Bruch's membrane is also typical in Stargardt patients (*Bonilha et al., 2016*).

The significance of RPE melanin and its role as a scavenger of oxidative stress

The role of reactive oxygen species in retinal health was extensively investigated (*Becquet et al., 1994*; *Cingolani et al., 2006*; *Mao et al., 2014*; *Seo et al., 2012*; *Zhao et al., 2011*) and melanin was identified as a potential scavenger of reactive oxygen species (*Bustamante et al., 1993*; *Tada, Kohno & Niwano, 2010*). However, RPE melanin differs from other melanin species in several aspects. For instance, while melanocytes continuously synthesize new melanin, it is still under debate whether melanin turnover in the RPE occurs and if so, to what extent (*Schraermeyer, 1993*). Furthermore, RPE melanin can react differently than melanin in the melanocytes of the choroid (*Schraermeyer & Heimann, 1999*). Therefore, we analyzed isolated RPE melanin granules to corroborate that also this melanin species is capable to quench superoxide radicals and in fact can play a role in protection against oxidative stress in the RPE (Fig. 10). Anti-oxidative properties of RPE melanin have also been confirmed in cell culture experiments (*Burke et al., 2011*).

Certain photoreceptor and RPE-damages typical for oxidative stress and/or lysosomal impairment were exclusively found in albino *Abca4*$^{-/-}$ mice (Figs. 1D, 2B–2D, 3, 6C), while others were found in albino *Abca4*$^{-/-}$ and *Abca4*$^{-/-}$.*Rdh8*$^{-/-}$ mice, but onset was earlier in albino *Abca4*$^{-/-}$ mice (Figs. 1A–1B, 2A, 6A & 6D). Notably, even though *Abca4*$^{-/-}$.*Rdh8*$^{-/-}$ mice have a more severe disease-causing genotype compared to albino *Abca4*$^{-/-}$ mice, they only show a more pathologic phenotype regarding RPE hypertrophy (Fig. 1A, Fig. S1), the number of undegraded phagosomes (Table 1) and the percentage of RPE cytoplasm occupied by lipofuscin (Fig. 5).

RPE melanin affects the accumulation of lipofuscin, a major hallmark of Stargardt disease

Melanin in the RPE plays a crucial role as scavenger for excess light and reactive oxygen species (*Hu, Simon & Sarna, 2008*). Lack of melanin has been associated with higher levels

of lipofuscin in primary RPE cells *in vitro* (*Sundelin, Nilsson & Brunk, 2001*) and a decrease of A2E with simultaneous increase of A2E oxiranes in albino compared to pigmented *Abca4*$^{-/-}$ mice (*Radu et al., 2004*). We show that albino *Abca4*$^{-/-}$ mice have higher levels of lipofuscin than pigmented *Abca4*$^{-/-}$ mice (Fig. 5).

We identified different morphologies of lipofuscin in the three different Stargardt mouse strains. In young age, pigmented *Abca4*$^{-/-}$ and *Abca4*$^{-/-}$.*Rdh8*$^{-/-}$ mice show exclusively lipofuscin with homogenous electron density (Table 1). After 12 months of age, *Abca4*$^{-/-}$.*Rdh8*$^{-/-}$ mice also have lipofuscin with flocculent electron density. Contrary, albino *Abca4*$^{-/-}$ mice have little lipofuscin with homogenous electron density, while lipofuscin with flocculent electron density is present even in young animals (Table 1).

Aged melanin becomes pro-oxidative and might be involved in Stargardt pathology

Melanin granules probably play an essential role in the detoxification of lipofuscin due to their anti-oxidative properties (*Burke et al., 2011*). With age, melanin granules switch from expressing anti-oxidative to pro-oxidative properties after illumination (*Biesemeier et al., 2008*; *Dontsov, Glickman & Ostrovsky, 1999*; *Rozanowski et al., 2008*). This might be due to degradative modifications of melanin that occur after long-term interaction of iron-containing melanin with lipid hydroperoxides, as it happens in melanolipofuscin (*Zadlo et al., 2017*). Nevertheless, formation of melanolipofuscin might be a protective process, since radicals formed by degradation of bisretinoids (*Wu et al., 2011*) can be absorbed by the melanin moiety of melanolipofuscin and thereby protect the lysosomal membrane from damage.

In fact, alterations in near-infrared-autofluorescence, which is a marker for melanin, were identified as the earliest detectable retinal change in patients with *ABCA4*-related retinal dystrophies and can be used for predicting the further disease progress (*Cideciyan et al., 2015*). Changes in near-infrared-autofluorescence were also found in pigmented *Abca4*$^{-/-}$ mice compared to wild type (*Charbel Issa et al., 2013*). Since *Abca4*$^{-/-}$.*Rdh8*$^{-/-}$ mice have higher loads of the pro-oxidative substances lipofuscin (*Rozanowska et al., 1995*) and all-*trans*-retinal (*Zhu et al., 2016*) than pigmented *Abca4*$^{-/-}$ mice, their melanin granules might age more rapidly and switch to the pro-oxidative state earlier. This might explain the presence of lipofuscin with flocculent electron density in aged *Abca4*$^{-/-}$.*Rdh8*$^{-/-}$ mice.

RPE melanin and its link to outer segment phagocytosis and ingestion of bisretinoids

Phagocytosis of outer segments was shown to be an oxidative stressor for the RPE (*Miceli, Liles & Newsome, 1994*). Since undegradable material from phagocytosed outer segments is transported to melanin granules in primary RPE cells (*Schraermeyer et al., 1999*; *Schraermeyer & Stieve, 1994*) and melanosomes can bind and store many toxic components (*Mecklenburg & Schraermeyer, 2007*), melanin granules might play a role in lowering phagocytosis-related oxidative or toxic stress. When post-confluent differentiated ARPE-19 cells are treated with low micromolar amounts of A2E for several weeks and then challenged with outer segments, melanin synthesis is induced (*Poliakov et al., 2014*). Poliakov et al. even proposed that A2E-induced alkalization of lysosomes could have a

physiological role in maintaining melanin pigmentation in RPE cells, since neutral pH favors eumelanogenesis (*Fuller, Spaulding & Smith, 2001*; *Ito et al., 2013*).

There is still much to be learned

Taken together, all these observations point to RPE melanin being an essential factor for retinal function. Complete lack of RPE melanin granules in albino *Abca4*$^{-/-}$ mice leads to extensive retinal damage that cannot be found in pigmented tissue, even in *Abca4*$^{-/-}$.*Rdh8*$^{-/-}$ mice that have an increased amount of toxic visual cycle byproducts like all-trans retinal dimer and higher levels of lipofuscin due to their genetic burden. We cannot rule out that the lack of melanin in the iris and the choroid is an additional reinforcing factor in albino animals, but there is overwhelming data supporting the essential role of RPE melanin. Furthermore, yet unidentified differences in the genetic background of the different mouse strains might skew the presented data.

Ocular pigmentation was shown to be correlated to the incidence of uveal melanoma (*Weis et al., 2006*) and age-related macular degeneration (*Chakravarthy et al., 2010*) and tyrosinase, the key enzyme for melanin biogenesis, was found to be a potential factor for developing early stages of age-related macular degeneration (*Holliday et al., 2013*).

CONCLUSION

In this work, we present a detailed ultrastructural comparison of the disease development of three frequently used Stargardt mouse models. As currently no animal model exists that reflects all aspects of the human disease, this will help researchers in the process of identifying which model is best suited for their research.

We found that albino *Abca4*$^{-/-}$ and *Abca4*$^{-/-}$.*Rdh8*$^{-/-}$ mice show typical histopathological signs of oxidative stress and/or lysosomal dysfunction, the earliest onset and severest changes being present in albino *Abca4*$^{-/-}$ mice. Since melanin in general is known to have anti-oxidative properties and age-dependent turnover of melanin is known to diminish the anti-oxidative properties of the RPE, we hypothesize that RPE melanin plays a crucial role in preventing Stargardt-related changes. The lack of pathology in pigmented *Abca4*$^{-/-}$ mice and the finding that also RPE melanin can quench superoxide anions support this hypothesis.

The protective role of melanin due to its antioxidative properties might be an explanation for the relatively late-onset of Stargardt disease with mild to moderate disease causing mutations (*Van Huet et al., 2014*): as long as melanin is capable of alleviating toxic effects of lipofuscin accumulation, RPE health is maintained. Once melanin is aged and lost its protective function, deleterious effects of lipofuscin accumulation can take over. This is strongly supported by the fact that changes in melanin-based near-infrared-autofluorescence temporally and spatially precede the progression of retinal degeneration in Stargardt disease (*Cideciyan et al., 2015*). Since RPE damage is a fundamental feature of Stargardt disease and age-related macular degeneration, RPE melanin should be strongly considered as a key factor in retinal health.

ACKNOWLEDGEMENTS

The authors thank Peter Charbel Issa, Gabriel H. Travis, Roxana Radu and Krzysztof Palczewski for providing them with the Stargardt mouse strains. Special thanks are due to Foundation Fighting Blindness, Vera Bonilha and Joe Hollyfield for collecting and providing the human Stargardt tissue. In this work, the segmentation calculations were performed using Fiji on the de.NBI Cloud Tübingen (https://denbi.uni-tuebingen.de). The authors thank Jens Krüger, Maximilian Hanussek and Felix Bartusch of the High Performance and Cloud Computing Group at the Zentrum für Datenverarbeitung of the University of Tuebingen. The authors also thank Monika Rittgarn and Sigrid Schultheiss for technical assistance and Daniel Dehncke for helpful discussions.

ADDITIONAL INFORMATION AND DECLARATIONS

Funding

This work was supported by Bundesministerium für Bildung und Forschung (grant numbers 01GQ1422B and 031A535A). There was no additional external funding received for this study. The funders had no role in study design, data collection and analysis, decision to publish, or preparation of the manuscript.

Grant Disclosures

The following grant information was disclosed by the authors:
Bundesministerium für Bildung und Forschung: 01GQ1422B, 031A535A.

Competing Interests

The authors declare there are no competing interests.

Author Contributions

- Tatjana Taubitz conceived and designed the experiments, performed the experiments, analyzed the data, prepared figures and/or tables, authored or reviewed drafts of the paper, approved the final draft.
- Alexander V. Tschulakow, Marina Tikhonovich, Antje Biesemeier and Sylvie Julien-Schraermeyer analyzed the data, authored or reviewed drafts of the paper, approved the final draft.
- Barbara Illing and Yuan Fang performed the experiments, authored or reviewed drafts of the paper, approved the final draft.
- Ulrich Schraermeyer conceived and designed the experiments, authored or reviewed drafts of the paper, approved the final draft.

Human Ethics

The following information was supplied relating to ethical approvals (i.e., approving body and any reference numbers):

Ethik-Kommission an der Medizinischen Fakultät der Eberhard-Karls-Universität und am Universitätsklinikum Tübingen granted Ethical approval (approval number 462/2009BO2).

Animal Ethics

The following information was supplied relating to ethical approvals (i.e., approving body and any reference numbers):

Einrichtung für Tierschutz, Tierärztlichen Dienst und Labortierkunde der Eberhard Karls Universität Tübingen (local agency for animal welfare) and the Regierungspräsidium Tübingen (local authorities) approved the research and all protocols involving animal handling and euthanasia.

Data Availability

The following information was supplied regarding data availability:

The raw data are provided in the Supplemental File.

Supplemental Information

Supplemental information for this article can be found online at http://dx.doi.org/10.7717/peerj.5215#supplemental-information.

REFERENCES

Allikmets R, Singh N, Sun H, Shroyer NF, Hutchinson A, Chidambaram A, Gerrard B, Baird L, Stauffer D, Peiffer A, Rattner A, Smallwood P, Li Y, Anderson KL, Lewis RA, Nathans J, Leppert M, Dean M, Lupski JR. 1997. A photoreceptor cell-specific ATP-binding transporter gene (ABCR) is mutated in recessive Stargardt macular dystrophy. *Nature Genetics* **15**:236–246 DOI 10.1038/ng0397-236.

Arganda-Carreras I, Kaynig V, Rueden C, Eliceiri KW, Schindelin J, Cardona A, Sebastian Seung H. 2017. Trainable weka segmentation: a machine learning tool for microscopy pixel classification. *Bioinformatics* **33**:2424–2426 DOI 10.1093/bioinformatics/btx180.

Becquet F, Goureau O, Soubrane G, Coscas G, Courtois Y, Hicks D. 1994. Superoxide inhibits proliferation and phagocytic internalization of photoreceptor outer segments by bovine retinal pigment epithelium in vitro. *Experimental Cell Research* **212**:374–382 DOI 10.1006/excr.1994.1157.

Ben-Shabat S, Itagaki Y, Jockusch S, Sparrow JR, Turro NJ, Nakanishi K. 2002. Formation of a nonaoxirane from A2E, a lipofuscin fluorophore related to macular degeneration, and evidence of singlet oxygen involvement. *Angewandte Chemie International Edition in English* **41**:814–817 DOI 10.1002/1521-3773(20020301)41:5%3C814::AID-ANIE814%3E3.0.CO;2-2.

Biesemeier A, Kokkinou D, Julien S, Heiduschka P, Berneburg M, Bartz-Schmidt KU, Schraermeyer U. 2008. UV-A induced oxidative stress is more prominent in naturally pigmented aged human RPE cells compared to non-pigmented human RPE cells independent of zinc treatment. *Journal of Photochemistry and Photobiology. B, Biology* **90**:113–120 DOI 10.1016/j.jphotobiol.2007.11.005.

Birnbach CD, Jarvelainen M, Possin DE, Milam AH. 1994. Histopathology and immunocytochemistry of the neurosensory retina in fundus flavimaculatus. *Ophthalmology* **101**:1211–1219.

Blacharski P. 1988. Fundus flavimaculatus. In: Newsome DA, ed. *Retinal dystrophies and degenerations*. New York: Raven Press, 135–159.

Bonilha VL, Rayborn ME, Bell BA, Marino MJ, Fishman GA, Hollyfield JG. 2016. Retinal histopathology in eyes from a patient with stargardt disease caused by compound heterozygous ABCA4 mutations. *Ophthalmic Genet* **37**:150–160 DOI 10.3109/13816810.2014.958861.

Boulton M, Marshall J. 1985. Repigmentation of human retinal pigment epithelial cells in vitro. *Experimental Eye Research* **41**:209–218 DOI 10.1016/0014-4835(85)90026-0.

Burke JM, Kaczara P, Skumatz CM, Zareba M, Raciti MW, Sarna T. 2011. Dynamic analyses reveal cytoprotection by RPE melanosomes against non-photic stress. *Molecular Vision* **17**:2864–2877.

Bustamante J, Bredeston L, Malanga G, Mordoh J. 1993. Role of melanin as a scavenger of active oxygen species. *Pigment Cell Research* **6**:348–353 DOI 10.1111/j.1600-0749.1993.tb00612.x.

Chakravarthy U, Wong TY, Fletcher A, Piault E, Evans C, Zlateva G, Buggage R, Pleil A, Mitchell P. 2010. Clinical risk factors for age-related macular degeneration: a systematic review and meta-analysis. *BMC Ophthalmology* **10**:31 DOI 10.1186/1471-2415-10-31.

Charbel Issa P, Barnard AR, Singh MS, Carter E, Jiang Z, Radu RA, Schraermeyer U, MacLaren RE. 2013. Fundus autofluorescence in the Abca4(-/-) mouse model of Stargardt disease—correlation with accumulation of A2E, retinal function, and histology. *Investigative Ophthalmology and Visual Science* **54**:5602–5612 DOI 10.1167/iovs.13-11688.

Cheng CW, Chen LY, Chou CW, Liang JY. 2015. Investigations of riboflavin photolysis via coloured light in the nitro blue tetrazolium assay for superoxide dismutase activity. *Journal of Photochemistry and Photobiology B: Biology* **148**:262–267 DOI 10.1016/j.jphotobiol.2015.04.028.

Cideciyan AV, Swider M, Schwartz SB, Stone EM, Jacobson SG. 2015. Predicting progression of ABCA4-associated retinal degenerations based on longitudinal measurements of the leading disease front. *Investigative Ophthalmology and Visual Science* **56**:5946–5955 DOI 10.1167/iovs.15-17698.

Cingolani C, Rogers B, Lu L, Kachi S, Shen J, Campochiaro PA. 2006. Retinal degeneration from oxidative damage. *Free Radical Biology and Medicine* **40**:660–669 DOI 10.1016/j.freeradbiomed.2005.09.032.

Danciger M, Lyon J, Worrill D, Hoffman S, Lem J, Reme CE, Wenzel A, Grimm C. 2004. New retinal light damage QTL in mice with the light-sensitive RPE65 LEU variant. *Mammalian Genome* **15**:277–283 DOI 10.1007/s00335-003-2336-2.

Diment S, Eidelman M, Rodriguez GM, Orlow SJ. 1995. Lysosomal hydrolases are present in melanosomes and are elevated in melanizing cells. *Journal of Biological Chemistry* **270**:4213–4215.

Dontsov AE, Glickman RD, Ostrovsky MA. 1999. Retinal pigment epithelium pigment granules stimulate the photo-oxidation of unsaturated fatty acids. *Free Radical Biology and Medicine* **26**:1436–1446 DOI 10.1016/S0891-5849(99)00003-9.

Eagle Jr RC, Lucier AC, Bernardino Jr VB, Yanoff M. 1980. Retinal pigment epithelial abnormalities in fundus flavimaculatus: a light and electron microscopic study. *Ophthalmology* **87**:1189–1200 DOI 10.1016/S0161-6420(80)35106-3.

Fujihara M, Nagai N, Sussan TE, Biswal S, Handa JT. 2008. Chronic cigarette smoke causes oxidative damage and apoptosis to retinal pigmented epithelial cells in mice. *PLOS ONE* **3**:e3119 DOI 10.1371/journal.pone.0003119.

Fuller BB, Spaulding DT, Smith DR. 2001. Regulation of the catalytic activity of preexisting tyrosinase in black and Caucasian human melanocyte cell cultures. *Experimental Cell Research* **262**:197–208 DOI 10.1006/excr.2000.5092.

Goldberg AF, Moritz OL, Williams DS. 2016. Molecular basis for photoreceptor outer segment architecture. *Progress in Retina and Eye Research* **55**:52–81 DOI 10.1016/j.preteyeres.2016.05.003.

Gomes NL, Greenstein VC, Carlson JN, Tsang SH, Smith RT, Carr RE, Hood DC, Chang S. 2009. A comparison of fundus autofluorescence and retinal structure in patients with Stargardt disease. *Investigative Ophthalmology and Visual Science* **50**:3953–3959 DOI 10.1167/iovs.08-2657.

Holliday EG, Smith AV, Cornes BK, Buitendijk GH, Jensen RA, Sim X, Aspelund T, Aung T, Baird PN, Boerwinkle E, Cheng CY, Van Duijn CM, Eiriksdottir G, Gudnason V, Harris T, Hewitt AW, Inouye M, Jonasson F, Klein BE, Launer L, Li X, Liew G, Lumley T, McElduff P, McKnight B, Mitchell P, Psaty BM, Rochtchina E, Rotter JI, Scott RJ, Tay W, Taylor K, Teo YY, Uitterlinden AG, Viswanathan A, Xie S, Wellcome Trust Case Control C, Vingerling JR, Klaver CC, Tai ES, Siscovick D, Klein R, Cotch MF, Wong TY, Attia J, Wang JJ. 2013. Insights into the genetic architecture of early stage age-related macular degeneration: a genome-wide association study meta-analysis. *PLOS ONE* **8**:e53830 DOI 10.1371/journal.pone.0053830.

Holz FG, Schutt F, Kopitz J, Eldred GE, Kruse FE, Volcker HE, Cantz M. 1999. Inhibition of lysosomal degradative functions in RPE cells by a retinoid component of lipofuscin. *Investigative Ophthalmology and Visual Science* **40**:737–743.

Hu DN, Simon JD, Sarna T. 2008. Role of ocular melanin in ophthalmic physiology and pathology. *Photochemistry and Photobiology* **84**:639–644 DOI 10.1111/j.1751-1097.2008.00316.x.

Huttl S, Michalakis S, Seeliger M, Luo DG, Acar N, Geiger H, Hudl K, Mader R, Haverkamp S, Moser M, Pfeifer A, Gerstner A, Yau KW, Biel M. 2005. Impaired channel targeting and retinal degeneration in mice lacking the cyclic nucleotide-gated channel subunit CNGB1. *Journal of Neuroscience* **25**:130–138 DOI 10.1523/JNEUROSCI.3764-04.2005.

Ito S, Suzuki N, Takebayashi S, Commo S, Wakamatsu K. 2013. Neutral pH and copper ions promote eumelanogenesis after the dopachrome stage. *Pigment Cell & Melanoma Research* **26**:817–825 DOI 10.1111/pcmr.12137.

Iwai-Takekoshi L, Ramos A, Schaler A, Weinreb S, Blazeski R, Mason C. 2016. Retinal pigment epithelial integrity is compromised in the developing albino mouse retina. *Journal of Comparative Neurology* **524**:3696–3716 DOI 10.1002/cne.24025.

Kaupp UB, Seifert R. 2002. Cyclic nucleotide-gated ion channels. *Physiological Reviews* **82**:769–824 DOI 10.1152/physrev.00008.2002.

Kim SR, Fishkin N, Kong J, Nakanishi K, Allikmets R, Sparrow JR. 2004. Rpe65 Leu450Met variant is associated with reduced levels of the retinal pigment epithelium lipofuscin fluorophores A2E and iso-A2E. *Proceedings of the National Academy of Sciences of the United States of America* **101**:11668–11672 DOI 10.1073/pnas.0403499101.

Lem J, Krasnoperova NV, Calvert PD, Kosaras B, Cameron DA, Nicolo M, Makino CL, Sidman RL. 1999. Morphological, physiological, and biochemical changes in rhodopsin knockout mice. *Proceedings of the National Academy of Sciences of the United States of America* **96**:736–741 DOI 10.1073/pnas.96.2.736.

Liu J, Lu W, Reigada D, Nguyen J, Laties AM, Mitchell CH. 2008. Restoration of lysosomal pH in RPE cells from cultured human and ABCA4(-/-) mice: pharmacologic approaches and functional recovery. *Investigative Ophthalmology and Visual Science* **49**:772–780 DOI 10.1167/iovs.07-0675.

Maeda A, Maeda T, Golczak M, Palczewski K. 2008. Retinopathy in mice induced by disrupted all-trans-retinal clearance. *Journal of Biological Chemistry* **283**:26684–26693 DOI 10.1074/jbc.M804505200.

Mao H, Seo SJ, Biswal MR, Li H, Conners M, Nandyala A, Jones K, Le YZ, Lewin AS. 2014. Mitochondrial oxidative stress in the retinal pigment epithelium leads to localized retinal degeneration. *Investigative Ophthalmology and Visual Science* **55**:4613–4627 DOI 10.1167/iovs.14-14633.

Mecklenburg L, Schraermeyer U. 2007. An overview on the toxic morphological changes in the retinal pigment epithelium after systemic compound administration. *Toxicologic Pathology* **35**:252–267 DOI 10.1080/01926230601178199.

Miceli MV, Liles MR, Newsome DA. 1994. Evaluation of oxidative processes in human pigment epithelial cells associated with retinal outer segment phagocytosis. *Experimental Cell Research* **214**:242–249 DOI 10.1006/excr.1994.1254.

Molday RS, Zhong M, Quazi F. 2009. The role of the photoreceptor ABC transporter ABCA4 in lipid transport and Stargardt macular degeneration. *Biochimica et Biophysica Acta/General Subjects* **1791**:573–583 DOI 10.1016/j.bbalip.2009.02.004.

Okubo A, Sameshima M, Unoki K, Uehara F, Bird AC. 2000. Ultrastructural changes associated with accumulation of inclusion bodies in rat retinal pigment epithelium. *Investigative Ophthalmology and Visual Science* **41**:4305–4312.

Orlow SJ. 1995. Melanosomes are specialized members of the lysosomal lineage of organelles. *Journal of Investigative Dermatology* **105**:3–7.

Papermaster DS, Schneider BG, Zorn MA, Kraehenbuhl JP. 1978. Immunocytochemical localization of a large intrinsic membrane protein to the incisures and margins of frog rod outer segment disks. *Journal of Cell Biology* **78**:415–425 DOI 10.1083/jcb.78.2.415.

Peters S, Reinthal E, Blitgen-Heinecke P, Bartz-Schmidt KU, Schraermeyer U. 2006. Inhibition of lysosomal degradation in retinal pigment epithelium cells induces

exocytosis of phagocytic residual material at the basolateral plasma membrane. *Ophthalmic Research* **38**:83–88 DOI 10.1159/000090268.

Poetsch A, Molday LL, Molday RS. 2001. The cGMP-gated channel and related glutamic acid-rich proteins interact with peripherin-2 at the rim region of rod photoreceptor disc membranes. *Journal of Biological Chemistry* **276**:48009–48016 DOI 10.1074/jbc.M108941200.

Poliakov E, Strunnikova NV, Jiang JK, Martinez B, Parikh T, Lakkaraju A, Thomas C, Brooks BP, Redmond TM. 2014. Multiple A2E treatments lead to melanization of rod outer segment-challenged ARPE-19 cells. *Molecular Vision* **20**:285–300.

Radu RA, Hu J, Yuan Q, Welch DL, Makshanoff J, Lloyd M, McMullen S, Travis GH, Bok D. 2011. Complement system dysregulation and inflammation in the retinal pigment epithelium of a mouse model for Stargardt macular degeneration. *Journal of Biological Chemistry* **286**:18593–18601 DOI 10.1074/jbc.M110.191866.

Radu RA, Mata NL, Bagla A, Travis GH. 2004. Light exposure stimulates formation of A2E oxiranes in a mouse model of Stargardt's macular degeneration. *Proceedings of the National Academy of Sciences of the United States of America* **101**:5928–5933 DOI 10.1073/pnas.0308302101.

Radu RA, Yuan Q, Hu J, Peng JH, Lloyd M, Nusinowitz S, Bok D, Travis GH. 2008. Accelerated accumulation of lipofuscin pigments in the RPE of a mouse model for ABCA4-mediated retinal dystrophies following Vitamin A supplementation. *Investigative Ophthalmology and Visual Science* **49**:3821–3829 DOI 10.1167/iovs.07-1470.

Rozanowska M, Jarvis-Evans J, Korytowski W, Boulton ME, Burke JM, Sarna T. 1995. Blue light-induced reactivity of retinal age pigment. In vitro generation of oxygen-reactive species. *Journal of Biological Chemistry* **270**:18825–18830.

Rozanowski B, Cuenco J, Davies S, Shamsi FA, Zadlo A, Dayhaw-Barker P, Rozanowska M, Sarna T, Boulton ME. 2008. The phototoxicity of aged human retinal melanosomes. *Photochemistry and Photobiology* **84**:650–657 DOI 10.1111/j.1751-1097.2007.00259.x.

Sawada O, Perusek L, Kohno H, Howell SJ, Maeda A, Matsuyama S, Maeda T. 2014. All-trans-retinal induces Bax activation via DNA damage to mediate retinal cell apoptosis. *Experimental Eye Research* **123**:27–36 DOI 10.1016/j.exer.2014.04.003.

Schindelin J, Arganda-Carreras I, Frise E, Kaynig V, Longair M, Pietzsch T, Preibisch S, Rueden C, Saalfeld S, Schmid B, Tinevez JY, White DJ, Hartenstein V, Eliceiri K, Tomancak P, Cardona A. 2012. Fiji: an open-source platform for biological-image analysis. *Nature Methods* **9**:676–682 DOI 10.1038/nmeth.2019.

Schraermeyer U. 1993. Does melanin turnover occur in the eyes of adult vertebrates? *Pigment Cell Research* **6**:193–204.

Schraermeyer U, Heimann K. 1999. Current understanding on the role of retinal pigment epithelium and its pigmentation. *Pigment Cell Research* **12**:219–236 DOI 10.1111/j.1600-0749.1999.tb00755.x.

Schraermeyer U, Peters S, Thumann G, Kociok N, Heimann K. 1999. Melanin granules of retinal pigment epithelium are connected with the lysosomal degradation pathway. *Experimental Eye Research* **68**:237–245 DOI 10.1006/exer.1998.0596.

Schraermeyer U, Stieve H. 1994. A newly discovered pathway of melanin formation in cultured retinal pigment epithelium of cattle. *Cell and Tissue Research* **276**:273–279.

Schutt F, Bergmann M, Holz FG, Kopitz J. 2002. Isolation of intact lysosomes from human RPE cells and effects of A2-E on the integrity of the lysosomal and other cellular membranes. *Graefes Archive for Clinical and Experimental Ophthalmology* **240**:983–988 DOI 10.1007/s00417-002-0558-8.

Seo SJ, Krebs MP, Mao H, Jones K, Conners M, Lewin AS. 2012. Pathological consequences of long-term mitochondrial oxidative stress in the mouse retinal pigment epithelium. *Experimental Eye Research* **101**:60–71 DOI 10.1016/j.exer.2012.05.013.

Sparrow JR, Blonska A, Flynn E, Duncker T, Greenberg JP, Secondi R, Ueda K, Delori FC. 2013. Quantitative fundus autofluorescence in mice: correlation with HPLC quantitation of RPE lipofuscin and measurement of retina outer nuclear layer thickness. *Investigative Ophthalmology and Visual Science* **54**:2812–2820 DOI 10.1167/iovs.12-11490.

Sparrow JR, Gregory-Roberts E, Yamamoto K, Blonska A, Ghosh SK, Ueda K, Zhou J. 2012. The bisretinoids of retinal pigment epithelium. *Progress in Retina and Eye Research* **31**:121–135 DOI 10.1016/j.preteyeres.2011.12.001.

Sparrow JR, Parish CA, Hashimoto M, Nakanishi K. 1999. A2E, a lipofuscin fluorophore, in human retinal pigmented epithelial cells in culture. *Investigative Ophthalmology and Visual Science* **40**:2988–2995.

Sparrow JR, Vollmer-Snarr HR, Zhou J, Jang YP, Jockusch S, Itagaki Y, Nakanishi K. 2003a. A2E-epoxides damage DNA in retinal pigment epithelial cells. Vitamin E and other antioxidants inhibit A2E-epoxide formation. *Journal of Biological Chemistry* **278**:18207–18213 DOI 10.1074/jbc.M300457200.

Sparrow JR, Zhou J, Cai B. 2003b. DNA is a target of the photodynamic effects elicited in A2E-laden RPE by blue-light illumination. *Investigative Ophthalmology and Visual Science* **44**:2245–2251 DOI 10.1167/iovs.02-0746.

Sundelin SP, Nilsson SE, Brunk UT. 2001. Lipofuscin-formation in cultured retinal pigment epithelial cells is related to their melanin content. *Free Radical Biology and Medicine* **30**:74–81 DOI 10.1016/S0891-5849(00)00444-5.

Tada M, Kohno M, Niwano Y. 2010. Scavenging or quenching effect of melanin on superoxide anion and singlet oxygen. *Journal of Clinical Biochemistry and Nutrition* **46**:224–228
DOI 10.3164/jcbn.09-84.

Ueda K, Zhao J, Kim HJ, Sparrow JR. 2016. Photodegradation of retinal bisretinoids in mouse models and implications for macular degeneration. *Proceedings of the National Academy of Sciences of the United States of America* **113**:6904–6909
DOI 10.1073/pnas.1524774113.

Valapala M, Wilson C, Hose S, Bhutto IA, Grebe R, Dong A, Greenbaum S, Gu L, Sengupta S, Cano M, Hackett S, Xu G, Lutty GA, Dong L, Sergeev Y, Handa JT, Campochiaro P, Wawrousek E, Zigler Jr JS, Sinha D. 2014. Lysosomal-mediated waste clearance in retinal pigment epithelial cells is regulated by

CRYBA1/betaA3/A1-crystallin via V-ATPase-MTORC1 signaling. *Autophagy* **10**:480–496 DOI 10.4161/auto.27292.

Van Huet RA, Bax NM, Westeneng-Van Haaften SC, Muhamad M, Zonneveld-Vrieling MN, Hoefsloot LH, Cremers FP, Boon CJ, Klevering BJ, Hoyng CB. 2014. Foveal sparing in Stargardt disease. *Investigative Ophthalmology and Visual Science* **55**:7467–7478 DOI 10.1167/iovs.13-13825.

Weis E, Shah CP, Lajous M, Shields JA, Shields CL. 2006. The association between host susceptibility factors and uveal melanoma: a meta-analysis. *Archives of Ophthalmology* **124**:54–60 DOI 10.1001/archopht.124.1.54.

Weng J, Mata NL, Azarian SM, Tzekov RT, Birch DG, Travis GH. 1999. Insights into the function of Rim protein in photoreceptors and etiology of Stargardt's disease from the phenotype in abcr knockout mice. *Cell* **98**:13–23 DOI 10.1016/S0092-8674(00)80602-9.

Wu L, Nagasaki T, Sparrow JR. 2010. Photoreceptor cell degeneration in Abcr (-/-) mice. *Advances in Experimental Medicine and Biology* **664**:533–539 DOI 10.1007/978-1-4419-1399-9_61.

Wu Y, Zhou J, Fishkin N, Rittmann BE, Sparrow JR. 2011. Enzymatic degradation of A2E, a retinal pigment epithelial lipofuscin bisretinoid. *Journal of the American Chemical Society* **133**:849–857 DOI 10.1021/ja107195u.

Zadlo A, Pilat A, Sarna M, Pawlak A, Sarna T. 2017. Redox active transition metal ions make melanin susceptible to chemical degradation induced by organic peroxide. *Cell Biochemistry and Biophysics* DOI 10.1007/s12013-017-0793-6.

Zareba M, Szewczyk G, Sarna T, Hong L, Simon JD, Henry MM, Burke JM. 2006. Effects of photodegradation on the physical and antioxidant properties of melanosomes isolated from retinal pigment epithelium. *Photochemistry and Photobiology* **82**:1024–1029.

Zhao Z, Chen Y, Wang J, Sternberg P, Freeman ML, Grossniklaus HE, Cai J. 2011. Age-related retinopathy in NRF2-deficient mice. *PLOS ONE* **6**:e19456 DOI 10.1371/journal.pone.0019456.

Zhu X, Wang K, Zhang K, Zhou F, Zhu L. 2016. Induction of oxidative and nitrosative stresses in human retinal pigment epithelial cells by all-trans-retinal. *Experimental Cell Research* **348**:87–94 DOI 10.1016/j.yexcr.2016.09.002.

Zigler Jr JS, Zhang C, Grebe R, Sehrawat G, Hackler Jr L, Adhya S, Hose S, McLeod DS, Bhutto I, Barbour W, Parthasarathy G, Zack DJ, Sergeev Y, Lutty GA, Handa JT, Sinha D. 2011. Mutation in the betaA3/A1-crystallin gene impairs phagosome degradation in the retinal pigmented epithelium of the rat. *Journal of Cell Science* **124**:523–531 DOI 10.1242/jcs.078790.

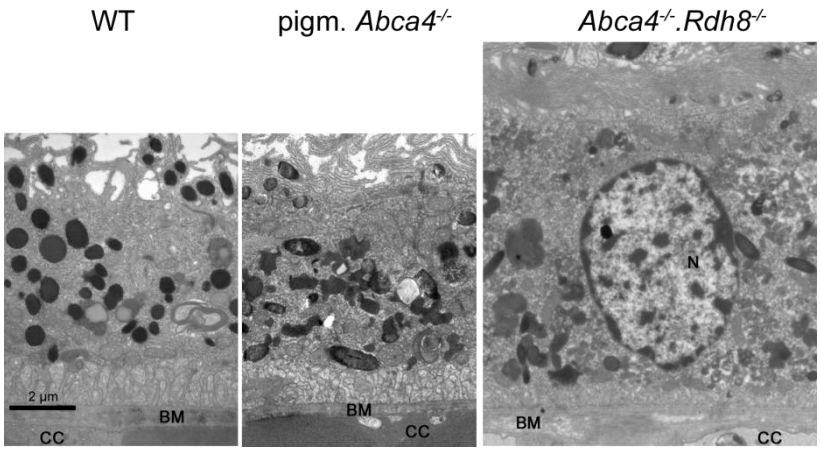

Supplemental Figure 1. Retinal pigment epithelium in 12-month-old pigmented WT and Stargardt mice. There is no apparent difference in cell size between pigmented WT and *Abca4*$^{-/-}$, but RPE in *Abca4*$^{-/-}$.*Rdh8*$^{-/-}$ mice is hypertrophic. DOI: 10.7717/peerj.5215/supp-1

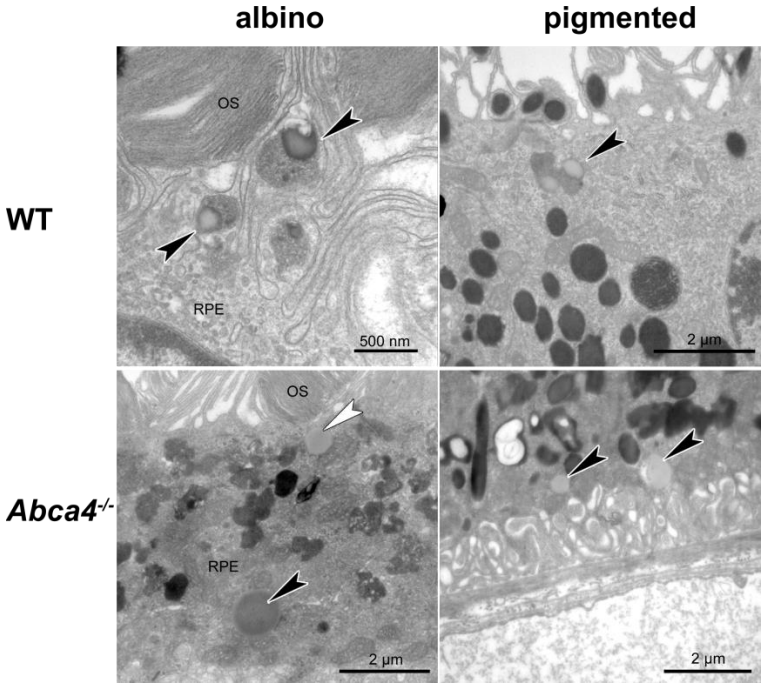

Supplemental Figure 2. Lipid droplets in WT and *Abca4*$^{-/-}$ animals. (Top) In WT animals, lipid droplets (black arrowheads) often fused with lipofuscin and were regularly located in the apical part of the RPE (left: albino WT, 4 months; right: pigm. WT, 12 months). (Bottom) Lipid droplets were regularly seen close to the basal labyrinth (black arrowheads) in albino *Abca4*$^{-/-}$ mice and occasionally in pigmented *Abca4*$^{-/-}$ mice. Rarely, lipid droplets were also seen apically close to the microvilli in albino *Abca4*$^{-/-}$ mice (white arrowhead) (left: albino *Abca4*$^{-/-}$, 15 months; right: pigm. *Abca4*$^{-/-}$, 18 months). DOI: 10.7717/peerj.5215/supp-2

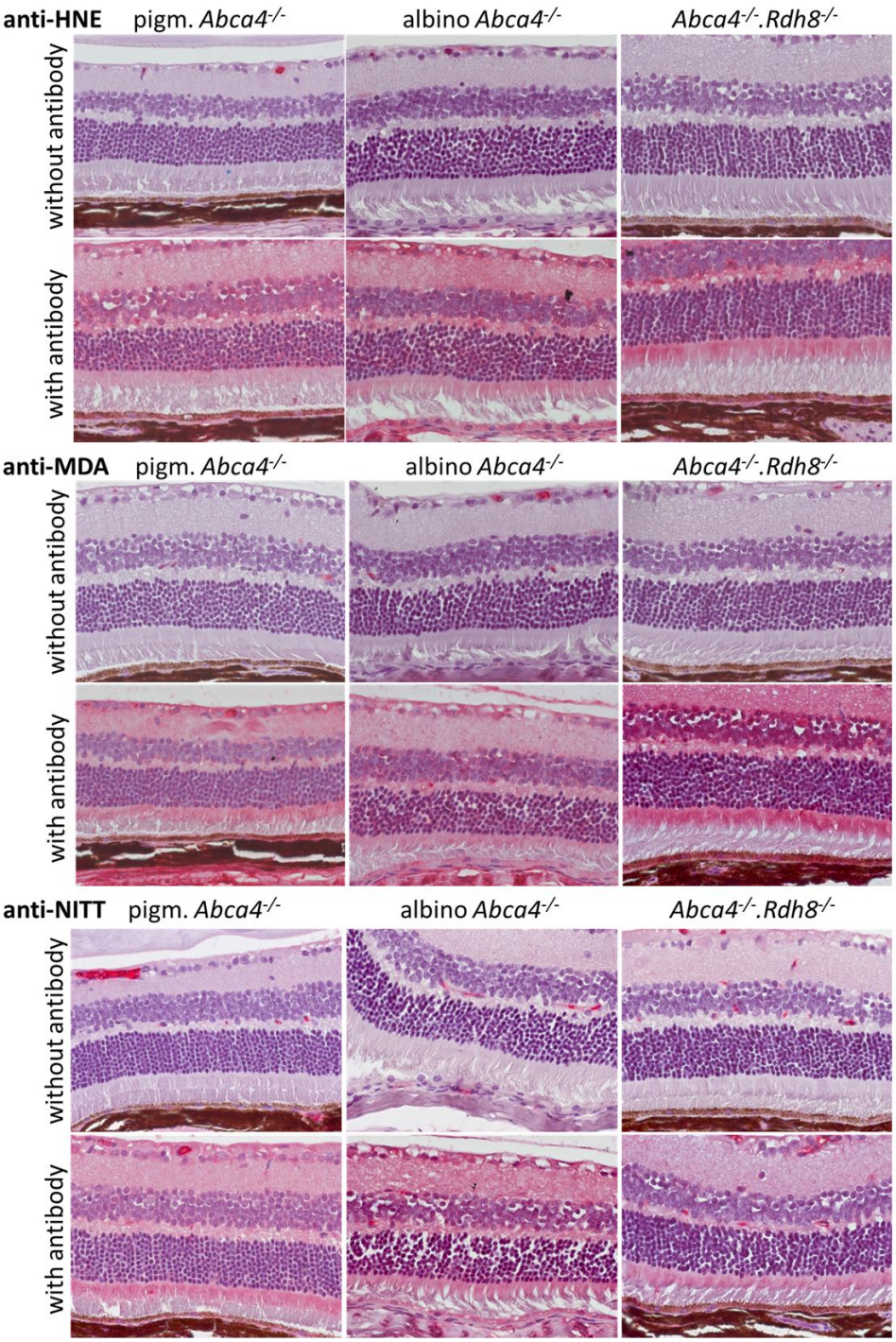

Supplemental Figure 3. Immunohistochemical staining of Stargardt mouse retinas of 12-month-old animals with anti-HNE, anti-MDA and anti-NITT. Upper panels for each primary antibody show negative controls (primary antibody was omitted); bottom panels for each primary antibody show the respective antibody stain (*red*).

DOI: 10.7717/peerj.5215/supp-3

3.2 Identifying the source of fundus near-infrared autofluorescence

A major non-invasive examination technique used for disease diagnostics and monitoring in ophthalmology is fundus autofluorescence that is based on the visualisation of autofluorophores in the back of the eye. Conventional fundus autofluorescence uses SW-AF (excitation 488 nm), which is an established marker for lipofuscin in the RPE [62]. Therefore, SW-AF can be used to either monitor the accumulation and distribution of lipofuscin or instead as a substitute marker for the whole RPE. SW-AF is applicable in a wide range of retinal disorders, including but not limited to drug toxicity, tissue defects (such as macular hole and RPE tears) as well as inherited and acquired retinal dystrophies such as STGD1 and AMD (reviewed in [65]). NIR-AF (excitation 787 nm) on the other hand is a more recent development and of high interest as an early disease marker and as potential endpoint in patient studies, since NIR-AF changes occur in many retinal diseases and oftentimes precede changes in SW-AF patterns [67-72]. However, the origin of NIR-AF is still being discussed: melanin in both the RPE and choroid has been identified as the main source [63, 64, 66], while involvement of lipofuscin is disputed [66, 69].

Since the spatial resolution of fundus autofluorescence is limited, a histological approach combining light, fluorescence and electron microscopy was chosen to identify the subcellular origin of NIR-AF [6] (section 3.2.1).

Melanosome-derived NIR-AF intensity in the RPE and the choroid increased with age in both WT and *Abca4*$^{-/-}$ mice. But NIR-AF intensity varied between melanosomes: In the choroid, some melanosomes appeared indistinguishable in bright field, but differed vastly in their NIR-AF intensity. In RPE cells of young mice, the spindle-shaped melanosomes had very weak NIR-AF that did not span the whole granule profile, while spherical melanosomes showed a high variety in NIR-AF intensity. In RPE cells of aged mice, almost all melanosomes showed high NIR-AF intensity over the whole profile.

In aged WT (18 months) and young *Abca4*$^{-/-}$ mice (7 months) that have comparable levels of lipofuscin, some areas exhibiting SW-AF also showed NIR-AF. Since these areas with superimposed SW- and NIR-AF were in close proximity to bright field-confirmed melanosomes, it is plausible to assume that these areas are the lipofuscin moiety of melanolipofuscin. In aged *Abca4*$^{-/-}$ mice (13 months) however,

also SW-AF positive areas that were spatially separated from bright field-confirmed melanosomes showed NIR-AF, suggesting that in these animals also true lipofuscin granules emit NIR-AF.

In albino *Abca4*$^{-/-}$ mice however, no specific NIR-AF signals co-localizing with SW-AF signals were found; only very weak NIR-AF signals, comparable to background intensity, were detectable when using prolonged acquisition times. It is plausible that these weak NIR-AF signals in albino *Abca4*$^{-/-}$ mice have a differing molecular origin. Most likely the signal is fluorescence spillover due to the broad range of emitted wavelengths of the variety of fluorophores in lipofuscin.

To corroborate the findings from mice, eye tissue of two human donors (68 and 80 years) without known ophthalmic diseases was investigated. Correlative fluorescence and electron microscopy on single tissue sections was used to clearly attribute the two types of autofluorescences to the different RPE pigment types: virtually all lipofuscin granules identified by EM showed strong signals in SW-AF and additional signals in NIR-AF. Melanolipofuscin granules showed a NIR-AF-positive but SW-AF-negative melanin core and a NIR- and SW-AF-positive shell of lipofuscin. Melanosomes showed only NIR-AF, but never SW-AF. This confirmed that also in aged human donor eyes without ocular disease, NIR-AF is not only emitted from melanin, but also from lipofuscin and the lipofuscin moiety of melanolipofuscin.

AF of melanin was previously described after photic and oxidative stress [188-192], so it was investigated whether NIR-AF can also be induced by these noxious factors. Porcine melanosomes isolated from choroid and RPE were exposed to either white light or hydrogen peroxide, respectively. RPE melanosomes showed an increase of NIR-AF after both treatments, while choroidal melanosomes only showed a significant increase after 6 hours of hydrogen peroxide treatment. This verifies that melanin NIR-AF increases with both photic and oxidative stress, although the two granule types react to a different extent. Nevertheless, this can serve as an explanation of the observed age-dependent increase of melanosome-derived NIR-AF in WT and pigmented *Abca4*$^{-/-}$ mice. Furthermore, an *in vivo* phototoxicity model of advanced STGD1 was used, in which pigmented *Abca4*$^{-/-}$ mice are illuminated with blue light to induce a light-depended RPE and retinal changes similar to the situation in patients with advanced STGD1 [193]. In this *in*

vivo model, melanosomes and lipofuscin granules in the RPE showed higher NIR-AF in illuminated eyes than in unilluminated ones, confirming the *in vitro* results.

But how can melanosome-based NIR-AF that can be induced by photic or oxidative stress be reconciled with lipofuscin-based NIR-AF? It was shown that oxidation of eumelanin (which is the main type of melanin in both the RPE and choroid) results in the formation of degradation products that are highly autofluorescent [191]. The biological fate of these degradation products is not known to date. However, elemental analysis of human RPE pigments found that the lipofuscin moiety of melanolipofuscin has significantly elevated nitrogen levels compared to lipofuscin granules [46, 47]. Generally, nitrogen is considered to be a marker for protein, but also melanin and the aforementioned autofluorescent melanin degradation products contain nitrogen [191]. It is conceivable that autofluorescent melanin degradation products accumulate in the lipofuscin moiety of melanolipofuscin granules, which could explain the finding of co-localized SW- and NIR-AF in close association to bright field-confirmed melanosomes in mice. Melanosomes and lipofuscin granules, and therefore also melanolipofuscin granules, belong to the lysosomal compartment [19, 41]. Melanosomes were shown to be able to fuse with phagosomes [194] and dynamic processes involving lipofuscin granules, such as fusion of lipofuscin with primary and secondary lysosomes, have been suggested before [195]. By such dynamic and exchange processes, NIR-AF positive melanin degradation products might amass in lipofuscin granules. Lipofuscin-derived NIR-AF being caused by melanin degradation products would also explain why individual lipofuscin granules in albino *Abca4*$^{-/-}$ mice show no NIR-AF exceeding background NIR-AF.

However, trafficking between melanosomes and lipofuscin granules has not been described to date. Also, molecular confirmation of presence of melanin degradation products in lipofuscin is yet lacking. This is in part due to most chemical analysis of lipofuscin composition being based on Folch extraction which only allows the analysis of chloroform soluble lipids.

Nevertheless, this study shows that NIR-AF is not an intrinsic property of melanosomes and can under certain conditions also arise from lipofuscin granules. This is not only relevant for refined diagnostics of patient NIR-AF data, but also opens the possibility to gain deeper insights into pathomechanisms in melanin and lipofuscin-derived diseases.

3.2.1 Age, lipofuscin and melanin oxidation affect fundus near-infrared autofluorescence

Authors: Taubitz T., Fang Y., Biesemeier A., Julien-Schraermeyer S., Schraermeyer U.

Published in *EBioMedicine* in 2019.

DOI: 10.1016/j.ebiom.2019.09.048

Declaration of own contributions:

Planning of the manuscript was done by me in consultation with Prof. Dr. Schraermeyer and Sylvie Julien-Schraermeyer. Yuan Fang and I performed the blue light damage experiments in mice, while data acquisition from the blue light treated mice was done by Yuan Fang. PD Dr. Antje Biesemeier performed part of the fluorescence microscopical investigation from human tissue samples and performed the energy-dispersive X-ray measurements, and helped me with the analysis of this data. All remaining experiments, data acquisition and analyses were performed by me. Data interpretation was done by me with input from all co-authors. Manuscript writing, figure preparation, literature research and revision was done by me, proof reading was done by all co-authors.

EBioMedicine 48 (2019) 592–604

Contents lists available at ScienceDirect

EBioMedicine

journal homepage: www.elsevier.com/locate/ebiom

EBioMedicine
Published by THE LANCET

Age, lipofuscin and melanin oxidation affect fundus near-infrared autofluorescence

Tatjana Taubitz[a,*], Yuan Fang[a], Antje Biesemeier[a,b], Sylvie Julien-Schraermeyer[a], Ulrich Schraermeyer[a,c]

[a] Division of Experimental Vitreoretinal Surgery, Centre for Ophthalmology, University of Tübingen, Schleichstrasse 12/1, 72076 Tübingen, Germany
[b] NMI Natural and Medical Sciences Institute at the University of Tübingen, Reutlingen, Germany
[c] STZ OcuTox Preclinical Drug Assessment, Hechingen, Germany

ARTICLE INFO

Article history:
Received 23 July 2019
Revised 16 September 2019
Accepted 17 September 2019
Available online 21 October 2019

Keywords:
Melanin
Lipofuscin
Melanolipofuscin
Oxidative stress
Aging

ABSTRACT

Background: Fundus autofluorescence is a non-invasive imaging technique in ophthalmology. Conventionally, short-wavelength autofluorescence (SW-AF) is used for detection of lipofuscin, a byproduct of the visual cycle which accumulates with age or disease in the retinal pigment epithelium (RPE). Furthermore, near-infrared autofluorescence (NIR-AF) is used as a marker for RPE and choroidal melanin, but contribution of lipofuscin to the NIR-AF signal is unclear.
Methods: We employed fluorescence microscopy to investigate NIR-AF properties of melanosomes, lipofuscin and melanolipofuscin granules in histologic sections of wildtype and *Abca4*$^{-/-}$ mouse eyes, the latter having increased lipofuscin, as well as aged human donor eyes. Differentiation between these pigments was verified by analytical electron microscopy. To investigate the influence of oxidative and photic stress we used an *in vitro* model with isolated ocular melanosomes and an *in vivo* phototoxicity mouse model.
Findings: We show that NIR-AF is not an intrinsic property of melanin, but rather increases with age and after photic or oxidative stress in mice and isolated melanosomes. Furthermore, when lipofuscin levels are high, lipofuscin granules also show NIR-AF, as confirmed by correlative fluorescence and electron microscopy in human tissue. However, lipofuscin in albino *Abca4*$^{-/-}$ mice lacks NIR-AF signals.
Interpretation: We suggest that NIR-AF is derived from melanin degradation products that accumulate with time in lipofuscin granules. These findings can help to improve the interpretation of patient fundus autofluorescence data.
Funding: This work was supported by Bundesministerium für Bildung und Forschung, Deutsche Forschungsgemeinschaft and Chinese Scholarship Council. Major instrumentation used in this work was supported by Deutsche Forschungsgemeinschaft, the European Fund for Regional Development and the state of Baden-Württemberg.

© 2019 The Authors. Published by Elsevier B.V.
This is an open access article under the CC BY-NC-ND license.
(http://creativecommons.org/licenses/by-nc-nd/4.0/)

Research in context

Evidence before this study

Conventional fundus autofluorescence using short-wavelength light for excitation is routinely used for disease monitoring and diagnosis in ophthalmology and its origin from lipofuscin, a pigment in the retinal pigment epithelium, is well established. A further fundus autofluorescence modality employing near-infrared light for excitation is becoming more established in clinical practice, however, the subcellular origin of this signal is not completely understood yet. While it has been established that melanin, both from the retinal pigment epithelium and the choroid, adds to the near-infrared autofluorescence signal, the contribution of lipofuscin to this signal is still disputed.

Added value of this study

With this proof-of-concept study we present two major findings: 1) Near infrared autofluorescence of individual melanosomes increases with age and due to photic and oxidative stress. This im-

* Corresponding author.
E-mail address: tatjana.taubitz@med.uni-tuebingen.de (T. Taubitz).

https://doi.org/10.1016/j.ebiom.2019.09.048
2352-3964/© 2019 The Authors. Published by Elsevier B.V. This is an open access article under the CC BY-NC-ND license. (http://creativecommons.org/licenses/by-nc-nd/4.0/)

plies that near infrared autofluorescence is not an intrinsic property of melanin but is rather caused by autofluorescent melanin degradation products. 2) Near-infrared autofluorescence can be emitted from individual lipofuscin granules. However, this phenomenon was prevalent in aged tissue with high amounts of lipofuscin granules while it was mostly absent in younger tissue with low amounts of lipofuscin granules.

Implications of all the available evidence

So far, patient near-infrared fundus autofluorescence data were often directly equated with melanin content. Both major findings, near-infrared autofluorescence from melanin increasing with age and oxidative status, as well as lipofuscin being a source of near-infrared autofluorescence under certain circumstances, can help to refine the interpretation of patient near-infrared fundus autofluorescence data. This offers the possibility to gain deeper insights into pathologic processes and refinement of diagnostics for a variety of retinal diseases.

1. Introduction

Melanin is a known anti-oxidant and its cell-protective properties against photic and oxidative injury in the eye are well investigated (reviewed in [1]). However, when melanin ages, the anti-oxidative capability is diminished and is replaced by a pro-oxidative character [2–4]. This transformation is particularly relevant for the retinal pigment epithelium (RPE), a post-mitotic cell layer in the back of the eye. While other pigmented cells in the body, such as skin and choroidal melanocytes, continuously express tyrosinase, the canonical key enzyme of melanogenesis, and therefore are capable to renew their melanin-bearing melanosomes, it is still unknown whether this is also the case for RPE cells (reviewed in [5]). Tyrosinase-independent melanin synthesis in RPE cells was seen *in vitro* [6], but it is unclear whether a substantial melanin-turnover in the RPE exists *in vivo*, making the RPE potentially vulnerable to detrimental effects of aged melanin.

Aging of melanin has been attributed to photodegradation that results in structural modifications such as oxidative cleavage and cross-linking (reviewed in [7]) and is considered to be at least partly responsible for the progression from anti- to pro-oxidative behaviour [8]. During photodegradation of eumelanin, a brown to black type of melanin that is the dominant melanin type in ocular melanosomes, a diaryl ketone product is formed that is highly autofluorescent [9]. Indeed, increased autofluorescence (AF) of biological melanin was found after treatment with light [10–12], hydrogen peroxide [11], superoxide [13], but also as a function of age [14].

Another fluorophore in the RPE is lipofuscin whose key constituent is a class of non-degradable lipids called bisretinoids that emerge as a byproduct of the visual cycle [15]. Due to the (photo-)oxidative properties of some of its components, the accumulation of lipofuscin with age or disease is thought to be associated with RPE dysfunction and subsequent RPE and photoreceptor degeneration [15], but this theory is controversial [16].

In the clinical practice, the importance of investigating fundus AF for the diagnosis and monitoring of retinal disease has increased in recent years. The most common modality is the use of short wavelength AF (SW-AF, excitation 488 nm, emission > 500 nm) to monitor lipofuscin [17]. SW-AF is used in a broad spectrum of retinal diseases, including drug toxicity, inherited retinal dystrophies (such as Stargardt disease, Best macular dystrophy, and retinitis pigmentosa), and age-related macular degeneration [18]. A recent development is the use of near-infrared AF (NIR-AF, excitation 787 nm, emission > 800 nm) that is thought to allow the investigation of ocular melanin [19,20]. NIR-AF investigation has proven to be useful for clinical application, since various ocular diseases, such as age-related macular degeneration [21], Stargardt disease [22], retinitis pigmentosa [23], and others [24] have characteristic changes in NIR-AF patterns that oftentimes precede changes in SW-AF patterns. However, there is still uncertainty whether melanin is the only contributor to NIR-AF, especially lipofuscin is discussed to add to the NIR-AF signal [25].

In this work, we use light, fluorescence and electron microscopy to examine NIR- and SW-AF properties of RPE and choroidal pigment granules of mice, pigs, and humans. Thereby, precise analysis of the contribution of the different pigment types to NIR- and SW-AF signals is facilitated. Furthermore, we investigate whether photic and oxidative damage alters the NIR-AF signal of isolated RPE and choroidal melanosomes, which helps understanding the biological origin and implication of NIR-AF.

2. Materials and methods

2.1. Animals

Pigmented WT mice (129S2), pigmented *Abca4*$^{-/-}$ mice (129S4/SvJae-Abca4^{tm1Ght}) and albino *Abca4*$^{-/-}$ mice (BALB/c-Abca4^{tm1Ght}) were used in this work. WT mice were purchased from Harlan Laboratories (Hillcrest, UK), the knock-out strains were bred in our in-house facility. Light cycling was 12 h light (approximately 50 lx in cages)/12 h dark, food and water were available *ad libitum*. All procedures involving animals were in accordance with the German laws governing the use of experimental animals and were previously approved by the local agency for animal welfare and the local authorities.

2.2. Human donor tissue

Eye globes without known ophthalmic disease were obtained from the cornea bank Tübingen. Written informed consent of the donors for use in medical research and approval of the Institutional Review Board of the University of Tuebingen were obtained. The experiments were performed in adherence to the tenets of the Declaration of Helsinki.

2.3. Blue light damage in mice

Light exposure was performed according to published methods [26] with small modifications. In brief, animals were anesthetized by i.p. injection of a mix of fentanyl (0•05 mg/kg body weight), midazolam (5•0 mg/kg body weight) and medetomidine (0•50 mg/kg body weight). Pupils were dilated with tropicamide drops. Methocel 2% (Omnivision, Puchheim, Germany) was applied to the corneas to prevent them from drying out. Animals were placed on a heating mat and additionally covered with a tissue paper to avoid hypothermia. Light was delivered from a Lumencor Sola light engine (Beaverton, OR, USA) light source equipped with a light conductor and a custom-made blue light filter (430 nm). Light intensity was measured with a RM-12 radiometer (Opsytec, Ettlingen, Germany) with a VISBG sensor (400 to 570 nm). For illumination, a cover slide was placed on the cornea to eliminate light scatter. Illumination took place with an intensity of 50 mW/cm² for 15 min. The non-illuminated eye was shielded from stray light by carefully covering it with aluminium foil. Care was taken so the light beam entered the eye along the optical axis. After light exposure, narcosis was antagonized by s.c. injection of an antidote (naloxone 1•2 mg/kg body weight, flumazenil 0•5 mg/kg body weight, atipamezole 2•5 mg/kg body weight) and animals were kept in a dark room for 7 days before sacrifice. This setup results

in reproducible light damage around the optic nerve head, as corroborated by SLO/OCT and histology (Fang et al., manuscript submitted). Non-illuminated eyes served as control.

2.4. Isolation of RPE and choroidal granules

RPE granules were isolated from human donor eyes (12 eyes, mean age 70•2 years ± 14•7 years standard deviation; range 46 to 91 years) and pig eyes, obtained from a local slaughter house, according to published methods [27]. Choroidal melanosomes were additionally isolated from pig eyes. In brief, eyes were opened close to the ora serrata and the anterior segment and vitreous were discarded. The retina was removed with forceps and the eyecups washed with PBS pH 7•4 (Gibco, Carlsbad, CA, USA). Eyecups were filled with trypsin/EDTA (Gibco, Carlsbad, CA, USA) and incubated for 10 min at 37 °C. RPE cells were washed from Bruch's membrane by repeatedly pipetting the trypsin solution and collected in DMEM supplemented with 10% foetal bovine serum (Gibco, Carlsbad, CA, USA) to stop the enzymatic reaction. Porcine choroid was collected by gently removing it from the sclera with forceps. RPE cells and choroidal tissue were pelleted by centrifugation and homogenized using a tissue grinder. Cell debris was removed by centrifugation for 7 min at 60 g and the obtained supernatant was centrifuged for 10 min at 6000 g to pellet all pigment granules. The pellets were collected in 0·3 M sucrose, loaded on a discontinuous sucrose gradient (2 M to 1 M in 8 steps for human granules [27] and in 2 steps for porcine granules [8]) and centrifuged for 1 h at 103,000 g. Bands containing lipofuscin granules were identified by their yellow-orange tinge and were collected by carefully removing them with a thin pipette. Melanosomes adhered to the centrifugation tube walls and were washed off after removing the sucrose gradient. Isolated granules were washed in PBS and counted with a haemocytometer. Granules were stored at −20 °C until further use.

2.5. Oxidative stress in isolated melanosomes

Isolated porcine melanosomes were suspended in PBS pH 7•4 to yield a final concentration of 30,000 granules/µl. To induce photic stress, melanosome suspensions were illuminated with 45,000 lx white light (measured with a Colormaster 3 F, Gossen, Nuremberg, Germany) delivered by an LED lamp (SunaEco 1500 Ocean Blue XP, Tropic Marin, Wartenberg, Germany). For oxidative stress, melanosomes were incubated with freshly prepared hydrogen peroxide solution (0•3% in PBS, Sigma-Aldrich, St. Louis, MO, USA) in the dark. Incubation times were up to 6 h. Melanosomes incubated in PBS in the dark served as control. Melanosomes were washed twice with demineralized water and prepared for fluorescence or electron microscopy as described below.

2.6. Sample preparation for fluorescence and electron microscopy

Donor and mouse eyes were fixed, embedded in epon resin and sectioned according to standard procedures [28,29]. For fluorescence analysis, post-fixation and staining with heavy metals was omitted. Semi-thin sections (500 nm) were prepared and coverslipped with Dako fluorescent mounting medium. For electron microscopy, ultra-thin sections (70 nm) were collected on formvar-coated slot grids stained with lead citrate and investigated on a Zeiss 900 electron microscope (Zeiss, Jena, Germany). For fluorescence microscopy of isolated granules, the granule suspension was pipetted onto glass slides and let sit to dry at room temperature in the dark. Samples were cover-slipped with Dako fluorescent mounting medium. For electron microscopy, isolated granules were fixed in 2% glutaraldehyde and encased in 3% NuSieve GTG low melting agarose (Lonza, Rockland, ME, USA) and subjected to embedding and sectioning as described above.

2.7. Fluorescence microscopy

Specimens were investigated with a Zeiss Axioplan 2 microscope (Zeiss, Jena, Germany) equipped with a Lumencor Sola SE II NIR (Beaverton, OR, USA) light source and using a x63 objective. Filter sets were a custom made lipofuscin filter set (excitation 370/36 nm, emission 575/15, 400 nm beam splitter) for SW-AF and a commercial Cy7 filter set (excitation 708/75 nm, emission 809/81 nm, 757 nm beam splitter) for NIR-AF, respectively. The lipofuscin filter set is designed to fit the reported excitation and emission maximums for lipofuscin [30]. Binning x2 was applied for all images and acquisition times, as well as microscope and software settings were held constant for any set of samples to allow comparison of fluorescence intensities. If indicated in the figure legends, images with low AF intensities were post-processed with the Auto adjust colours function of the IrfanView software to allow the localization of weak AF signals. This function enhances the contrast by redefining the darkest pixel as pure black and the brightest pixel as pure white in the histogram on a channel-by-channel basis.

2.8. Semi-quantitative analysis of fluorescence intensities

Fluorescence intensities were determined using Fiji software. Regions of interest were determined in fluorescence and BF images using the default threshold, and area and integrated optical density (IOD) of the region of interest were measured. To correct for varied amounts of pigment granules displayed in each image, fluorescence IOD values were normalized to the area of pigment thresholded in corresponding BF images.

2.9. Correlative fluorescence and electron microscopy

To accommodate the requirements of both fluorescence and electron microscopy, ultra-thin sections with a thickness of 150 nm were used. This allows improved detection of fluorophores compared to standard 70 nm ultra-thin sections (as routinely used for electron microscopy), while still being thin enough to allow electron microscopic investigation (as opposed to 500 nm semi-thin sections that would be too thick to be penetrated by the electron beam). Non-osmicated sections were collected on formvar-coated mesh grids. Grids were placed on glass slides in a drop of water, coverslipped, and investigated with light and fluorescence microscopy as described before. Acquisition times had to be prolonged compared to 500 nm thick sections and additionally the auto-contrast function of the camera capture software was used. Signal-to-noise ratio was rather low due to the limited section thickness, so five pictures per channel were averaged using Photoshop CS2. Since sections tend to adhere to the coverslips, grids had to be carefully manipulated off the coverslips with forceps to not destroy the sections. Nevertheless, sections are stressed by being coverslipped and easily damaged, therefore post-staining with uranyl acetate and lead citrate was ultimately omitted, since this often resulted in complete loss of the sections. Grids were air dried and investigated by electron microscopy as described before. The lack of any heavy-metal staining results in low contrast, but melanosomes and lipofuscin granules are still reliably identifiable.

2.10. Energy-dispersive X-ray - scanning transmission electron microscopy analysis

Energy-dispersive X-ray (EDX) analyses were performed on a scanning transmission electron microscope (STEM; Jeol ARM 200F)

equipped with two JEOL EDX detectors at an acceleration voltage of 200 kV. Images were obtained at a size of 512×512 pixels. The obtained elemental maps were 4 × 4 binned using Fiji software.

2.11. Statistical analysis

JMP 13 software (SAS, Cary, NC, USA) was used for statistical analysis. The null hypothesis was that the groups were not statistically different. Dunnett's test, a multiple parametrical test with alpha correction, was used and $p < 0{\bullet}05$ was considered statistically significant.

3. Results

3.1. Differentiating factors between RPE pigment granules in microscopy

In order to be able to investigate the NIR-AF properties of the different RPE pigment types by microscopy, these pigments need to be clearly distinguished from one another. Fig. 1 illustrates how RPE pigments can be identified by light and electron microscopy. In routine transmission electron microscopy, melanin presents as either spherical or spindle-shaped electron-dense structures [31] (Fig. 1a), while lipofuscin either forms evenly shaped granules (for instance in human or monkey RPE [31,32]) or irregularly shaped granules (for instance in *Abca4*$^{-/-}$ mice [29,33], Fig. 1a). Melanolipofuscin is a complex granule that in healthy aged humans consists of a melanin core and a lipofuscin shell or protrusions [31,32], while in *Abca4*$^{-/-}$ mice, several melanosomes can fuse with one lipofuscin granule [29,33] (Fig. 1a). Analytical electron microscopy approaches, such as EDX mapping, can be used to corroborate the identity of the granules based on their elemental composition (Fig. 1b – d). Nitrogen and sulphur serve as markers for melanin, while phosphorus serves as marker for lipofuscin [32].

In this work, we performed all investigations on tissue that was embedded for electron microscopy in epon resin, but heavy metal-staining steps were omitted since they inhibit autofluorescence. The routine staining procedure for light microscopic investigation of epon-embedded sections involves Toluidine blue that yields a medium blue colour in lipofuscin and lets melanosomes appear dark blue to black (Fig. 1e). However, Toluidine blue inhibits autofluorescence as well, preventing NIR-AF investigation in stained sections. Alternatively, melanin can be readily identified in unstained sections by its inherent colour in bright field (BF), while lipofuscin can be identified in the same section by its characteristic SW-AF (Fig. 1e). Therefore, a combination of BF and SW-AF investigation gives similar information concerning melanosome and lipofuscin distribution than Toluidine staining and also allows the investigation of NIR-AF. Moreover, since the SW-AF is confined to the lipofuscin moiety of melanolipofuscin, melanolipofuscin granules in human samples can easily be identified by a gap in a given SW-AF signal that co-localizes with a bright field-identified melanosome (Fig. 1e). However, this does not apply to mouse samples, since their melanolipofuscin is highly irregular in shape and BF contrast. Therefore, distinguishing between true melanolipofuscin on the one hand, and closely situated melanosomes and lipofuscin granules on the other hand, is difficult using only light and fluorescence microscopy in mouse samples.

3.2. NIR-AF intensity in the RPE and choroid increases with age in pigmented WT mice

To investigate whether NIR-AF intensity and distribution change with age, we compared 3-, 12- and 18-month-old WT mice. We found that overall NIR-AF intensity of BF-confirmed melanosomes in the RPE and choroid increases with age (Fig. 2a, b). To allow the identification of areas with NIR-AF in images with low intensity, images were post-processed as described in the methods section. Post-processing revealed that even at 3 months of age and with very weak intensity, NIR-AF signals are present in both RPE and choroid, just as in 18-month-old samples (Fig. 2c, d). Therefore, post-processing is used throughout the manuscript for images with low AF intensities to allow the detection of weak AF signals. In BF images, choroidal cells with brighter granules than neighbouring melanocytes were evident in all age-groups but appeared to increase in number with age (Fig. 2a). These macrophage-like cells were often round and showed higher NIR-AF intensities compared to the surrounding melanocytes in all age-groups (Fig. 2b-d). Electron microscopic investigation of these cells showed that several melanosomes were clustered and surrounded by a common membrane, while this was not the case in typical melanocytes where each melanosome is surrounded by its own membrane (Fig. 2e). Semi-quantitative analysis of total NIR-AF signals derived from RPE and choroid revealed an approx. 3-fold and 9-fold increase in 12-month-old and 18-month-old animals compared to 3-month-old animals, respectively (SI S1). Melanosomes from 12- and 18-month-old animals appear brighter in BF images than those of 3-month-old animals, especially in the choroid (Fig. 2a, SI S1).

3.3. NIR-AF intensity varies between individual melanosomes and can co-localize with WT mice

In the choroid, some melanosomes were prominent in BF images as they appeared darker and larger in size. However, these melanosomes varied considerably in their NIR-AF intensities: while most of them had pronounced NIR-AF, some only showed very weak NIR-AF (SI S2).

At closer inspection of individual RPE melanosomes, we found that in 3-month-old animals, spindle-shaped RPE melanosomes did not show NIR-AF over their whole profile and AF intensities of these granules were very weak compared to neighbouring spherical melanosomes (Fig. 3). In contrast, spherical RPE melanosomes showed inter-granular variability in their NIR-AF intensity; both very weak and very high intensities were observed (Fig. 3). In 18-month-old animals, spindle-shaped melanosomes had mildly higher NIR-AF intensities compared to neighbouring spherical melanosomes. Most spherical melanosomes in this age-group showed a dark margin and a bright centre in BF images; this characteristic in internal morphology was also evident in NIR-AF as the darker margin had higher NIR-AF intensity compared to the brighter granule centre (Fig. 3).

Since it was suggested that lipofuscin contributes to NIR-AF signals [25], we investigated whether this was also evident in histologic sections of WT animals. In 3-month-old animals, lipofuscin, as identified by SW-AF, was scarce and NIR-AF signals from these granules were not evident (Fig. 3). However, in 18-month-old animals, co-localization of NIR- and SW-AF was readily seen, but not present in all granules (Fig. 3). Photoreceptor outer segments also presented SW-AF that increased with age (Fig. 3), probably due to presence of fluorescent bisretinoid precursors [15,34].

3.4. Co-localization of NIR- and SW-AF in the lipofuscin moiety of melanolipofuscin and in lipofuscin in pigmented WT and Abca4$^{-/-}$ mice

We asked the question whether co-localization of NIR- and SW-AF in lipofuscin was a sign of the lipofuscin at hand being a moiety of melanolipofuscin. Since aged WT mice have moderate levels of lipofuscin, we additionally investigated pigmented *Abca4*$^{-/-}$ mice that accumulate high levels of lipofuscin and melanolipofuscin early in life, with the melanolipofuscin appearing as a fusion of melanosomes and irregularly shaped lipofuscin granules [29,33].

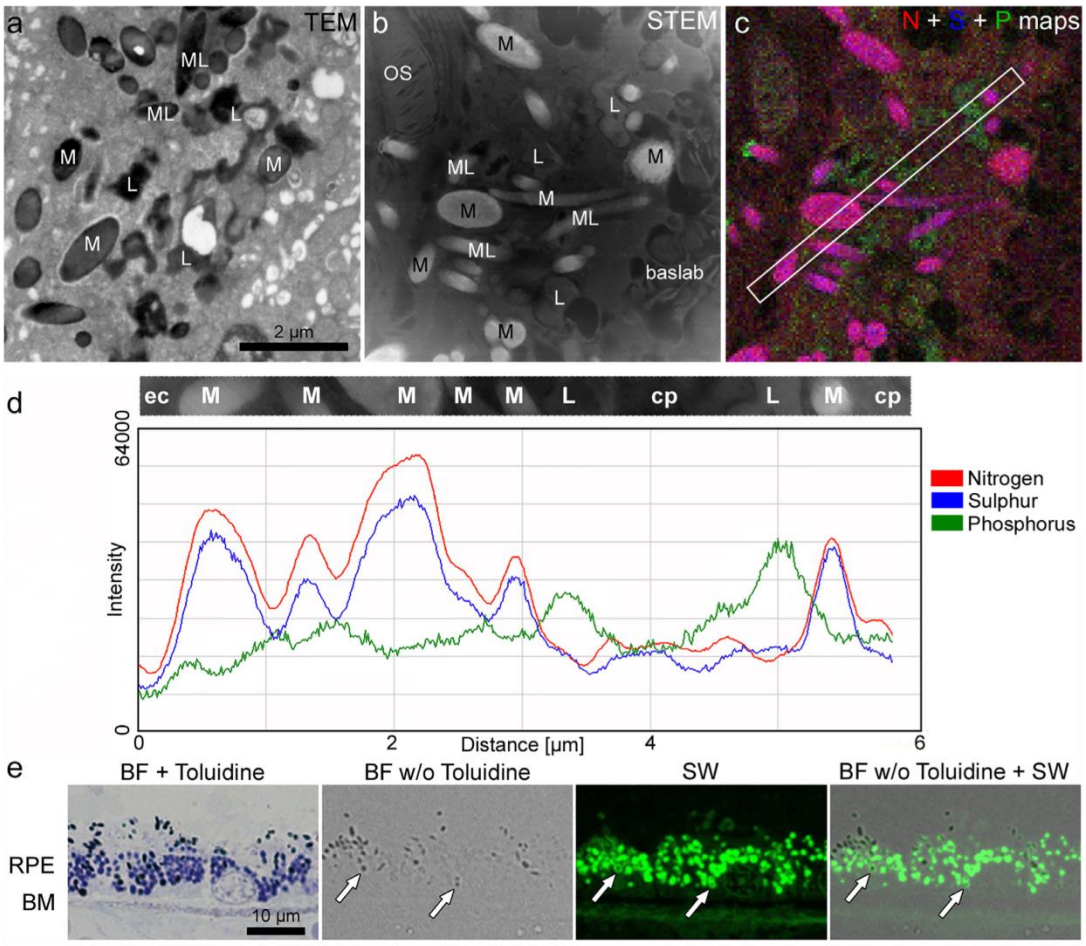

Fig. 1. Distinction between melanosomes, lipofuscin and melanolipofuscin granules in microscopy. a-d) Ultrastructural and elemental identification of pigment granules in an 18-month-old *Abca4*$^{-/-}$ mouse RPE cell. a) Routine transmission electron microscopic image of the RPE showing melanosomes, lipofuscin and melanolipofuscin granules. b) Scanning transmission electron microscopic image of an unstained section of the same eye. c) Superimposition of the 4 × 4 binned EDX maps for nitrogen (N), sulphur (S) (both a marker for melanin) and phosphorus (P) (a marker for lipofuscin) maps of the same area as shown in (b). The box marks a region of interest that crosses several melanosomes and lipofuscin granules. d) Intensity profile of the region of interest shown in (c) highlighting the differing elemental composition of the respective pigment granules. e) Light and fluorescence microscopical identification of RPE pigment granules in a 68-year-old human donor eye. Staining with Toluidine blue yields dark blue to black melanosomes and blue lipofuscin granules. Without Toluidine blue staining, only melanosomes are readily visible in bright field images, however, lipofuscin can be identified in the same section by its characteristic SW-AF. Since SW-AF is confined to the lipofuscin moiety of melanolipofuscin, also regularly shaped melanolipofuscin granules can be identified (arrows). baslab: basal labyrinth; BF: bright field; BM: Bruch's membrane; cp: cytoplasm; ec: extra cellular; M: melanosome; ML: melanolipofuscin; L: lipofuscin; OS: outer segment; RPE: retinal pigment epithelium; STEM: scanning transmission electron microscopy; TEM: transmission electron microscope; SW: short wavelength.

While in 18-month-old WT mice, co-localization of NIR- and SW-AF was exclusively seen adjacent to BF verified melanosomes, 13-month-old *Abca4*$^{-/-}$ mice, with higher lipofuscin levels showed co-localization of NIR- and SW-AF additionally in granules that were spatially separated from melanosomes (Fig. 4). This suggests that in these animals, also lipofuscin granules can emit NIR-AF.

When comparing young (7 months) to aged (13 months) pigmented *Abca4*$^{-/-}$ mice, an overall increase of the NIR-AF signal and brightening of melanosomes in BF images, the latter predominantly in the choroid, similar to the results in WT mice, was evident (SI S3).

Furthermore, in 7-month-old *Abca4*$^{-/-}$ mice, NIR-AF derived from lipofuscin granules was rare, resulting in predominantly green lipofuscin granules in NIR-AF/SW-AF overlay images as opposed to the majority of lipofuscin granules in 13-month-old *Abca4*$^{-/-}$ mice that appeared yellow in NIR-AF/SW-AF overlay images (Fig. 4, SI S3). This suggests that, in these animals, lipofuscin granules can also emit NIR-AF (Fig. 4, SI S3).

3.5. Lipofuscin in albino Abca4$^{-/-}$ *mice does not show specific NIR-AF signals*

Histologic differences between lipofuscin from pigmented and albino *Abca4*$^{-/-}$ mice were described before [29]. Furthermore, RPE cells of pigmented and albino *Abca4*$^{-/-}$ mice show varying SW-AF patterns which might be due to the differences in lipofuscin morphology [29]. Therefore, we compared NIR-AF properties of 12–13 months old pigmented and albino *Abca4*$^{-/-}$ mice to age-matched

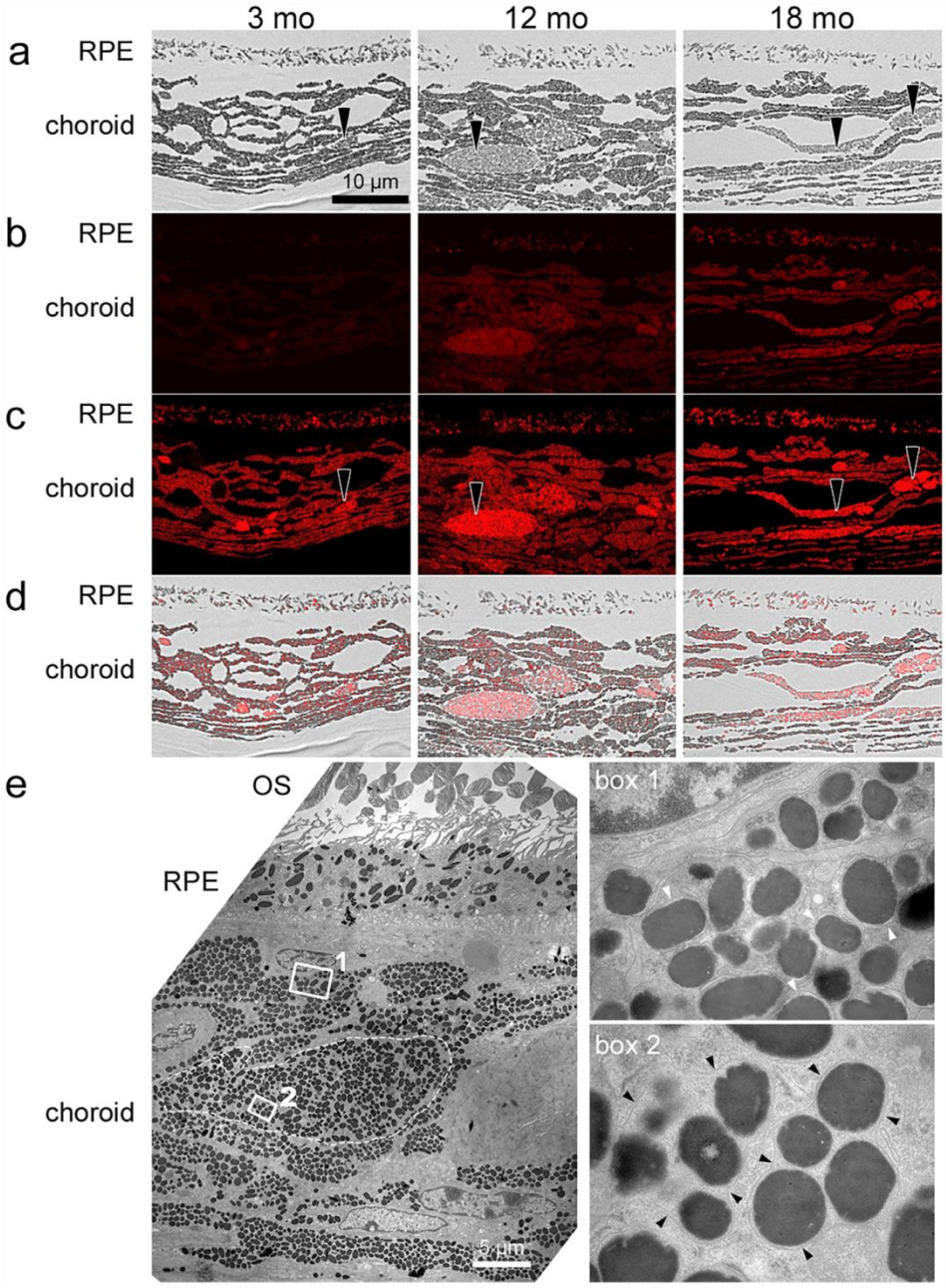

Fig. 2. NIR-AF in the RPE and choroid increases with age in pigmented WT mice. a) BF images of samples from 3-, 12- and 18-month-old mice. Since staining with toluidine blue would have resulted in loss of AF signal, only melanosomes can be identified. Arrowheads point to choroidal cells with brighter granules than typical choroidal melanocytes. b) Corresponding NIR-AF images taken under identical conditions. c) Same images as shown in (b), but post-processed to allow the localization of weak signals. Arrowheads show that choroidal cells with bright granules (as shown in (a)) have a higher NIR-AF intensity compared to the surrounding melanocytes, independent of age. d) Overlay of BF (a) and post-processed NIR-AF (c) images. $N = 1–2$ animals/group. e) Electron microscopic image of a macrophage-like cell (marked with a dashed line) in a 12-month-old pigmented WT mouse. The boxed areas of a typical melanocyte and the macrophage-like cell are shown in higher magnification on the right side. In choroidal melanocytes, individual melanosomes are surrounded by their respective membranes that are in close contact to the granule in young animals, but are often detached in aged animals (box 1, white arrowheads). In macrophage-like cells, several melanosomes form clusters that are surrounded by a continuous membrane (box 2, black arrowheads). OS: outer segments; RPE: retinal pigment epithelium.

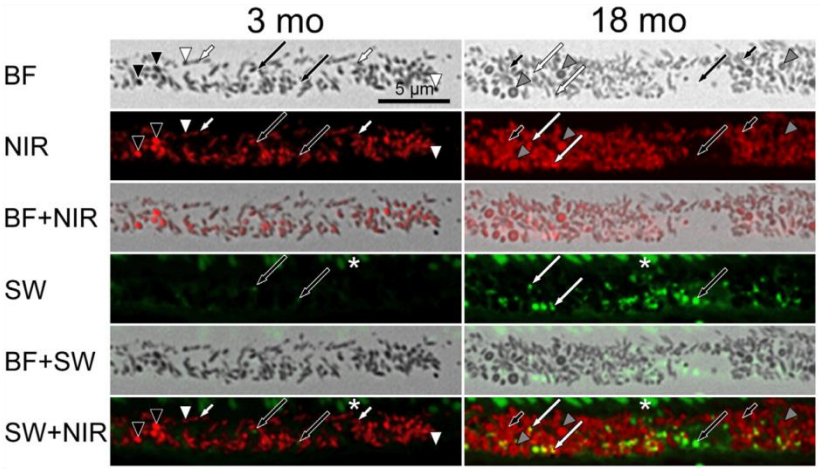

Fig. 3. RPE melanosomes vary in their NIR-AF properties and lipofuscin granules can add to the total NIR-AF signal. Comparison of NIR-AF (red) and SW-AF (green) in 3 and 18-month-old WT mice. AF images were post-processed to allow the localization of weak signals. In young mice, most spindle-shaped melanosomes show weak NIR-AF (short white arrows), while in old mice, most spindle-shaped melanosomes show strong NIR-AF (short black arrows) relative to neighbouring spherical melanosomes. Spherical, dark melanosomes vary between weak NIR-AF (white arrowheads) and very intense NIR-AF (black arrowheads). In old animals, spherical melanosomes with dark margin were evident in BF (grey arrowheads). The dark margin had higher NIR-AF intensity than the bright centre. Areas with high SW-AF sometimes also showed additional NIR-AF (overlay of red and green, yielding yellow; long white arrows), while in other instances and in young animals did not (long black arrows). Asterisks mark autofluorescent outer segments. $N = 1–2$ animals/group. BF: bright field; NIR: near-infrared; SW: short wavelength.

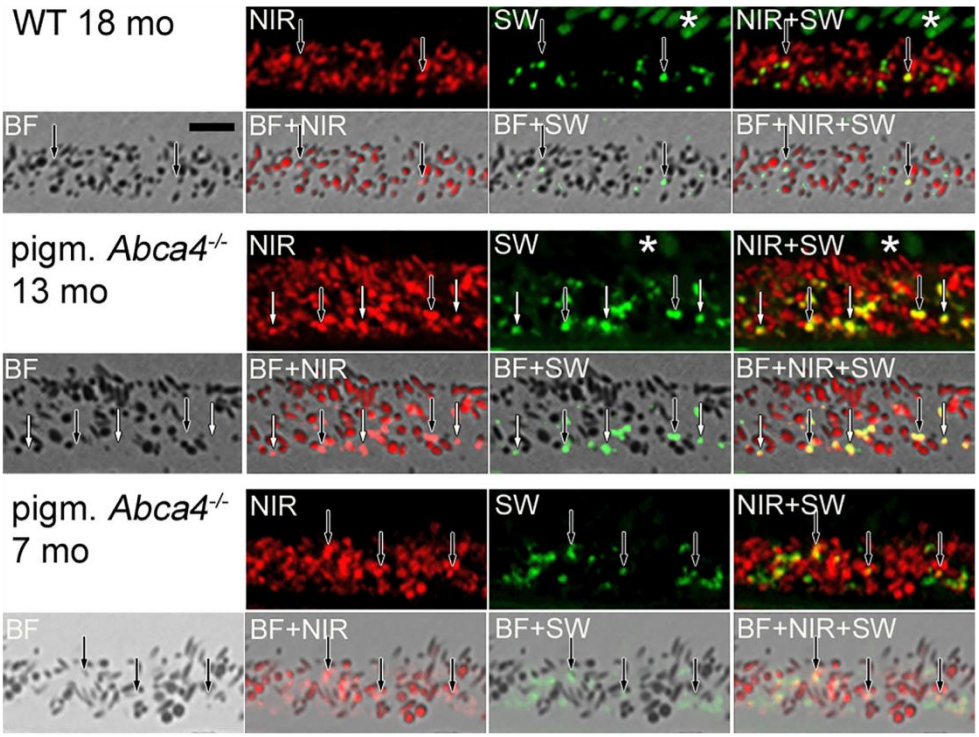

Fig. 4. Co-localization of NIR-AF and SW-AF in the RPE of WT and pigmented *Abca4*$^{-/-}$ mice. NIR-AF is shown in red while SW-AF is shown in green, yielding yellow when superimposed. Black arrows point to co-localization of NIR-AF and SW-AF in direct contact to BF-identified melanosomes, while white arrows point to co-localization of NIR-AF and SW-AF spatially separated from melanosomes. Asterisks mark autofluorescent outer segments. Scale bar: 2 µm. $N = 1–2$ animals per group. BF: bright field; NIR: near-infrared; SW: short wavelength.

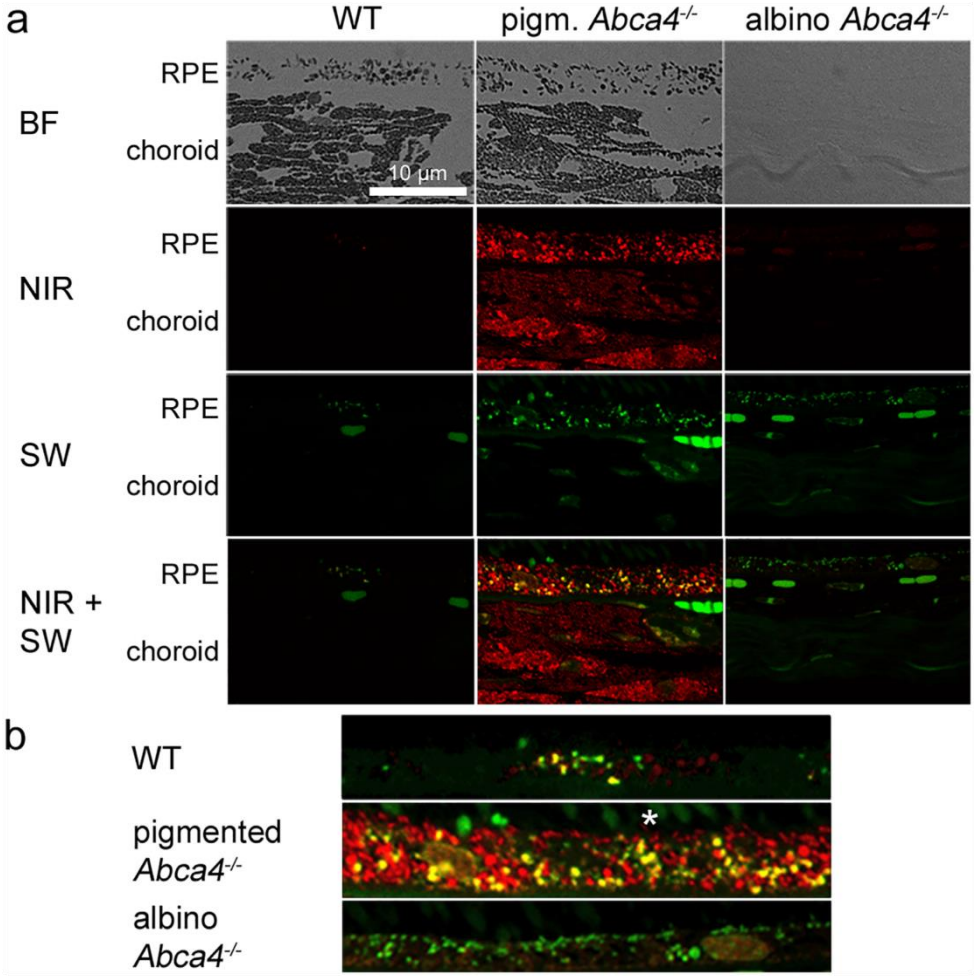

Fig. 5. Comparison of NIR-AF and SW-AF in 12 to 13 months old WT and pigmented and albino *Abca4*$^{-/-}$ mice. NIR-AF (red) and SW-AF (green) images of the different strains were taken under identical conditions. Yellow colour shows areas where NIR-AF and SW-AF superimpose. a) Overview of RPE and choroidal BF, NIR-AF and SW-AF. Note that there are no tissue structures visible in the BF image of the albino mouse, due to lack of melanin and lack of additional staining. AF Images are not post-processed to allow comparison of AF intensities. b) Magnified overlay of NIR-AF and SW-AF images of the RPE areas shown in (a). AF Images are post-processed to allow the localization of weak signals. An asterisk marks autofluorescent outer segments. $N = 1–2$ animals per group. BF: bright field; NIR: near-infrared; SW: short wavelength.

pigmented WT. In pigmented *Abca4*$^{-/-}$ mice, melanosomes of the RPE and choroid gave higher NIR-AF signals than in age-matched WT mice (Fig. 5a). In albino *Abca4*$^{-/-}$ mice, choroidal and RPE melanosomes are lacking and consequently no melanosome-derived NIR-AF signals were found.

Correlation of NIR- and SW-AF showed that in WT mice, some, but not all lipofuscin granules present NIR-AF (Fig. 5b). In pigmented *Abca4*$^{-/-}$ mice, most areas with SW-AF also showed NIR-AF (Fig. 5b), independent of whether they were in close contact to BF-identified melanosomes or being spatially separate from melanosomes. Only very small lipofuscin granules did not exhibit NIR-AF. In albino *Abca4*$^{-/-}$ mice however, no specific NIR-AF signals co-localizing with SW-AF were present (Fig. 5b). When we used prolonged acquisition times, very weak NIR-AF signals co-localizing with SW-AF were found in albino *Abca4*$^{-/-}$ mice, however, the signal intensity was comparable to background signal (SI S4).

3.6. NIR- AF signals in aged human RPE originate from melanosomes, melanolipofuscin and lipofuscin granules

To verify the findings from mouse tissue, we investigated tissue of two aged human donors (68 and 80 years) without known ophthalmic diseases. Virtually all of the SW-AF co-localized with NIR-AF, some of it being in direct contact to BF-identified melanosomes, suggesting melanolipofuscin (SI S5). Melanosomes and lipofuscin granules show similar intensity of NIR-AF and the NIR-AF signal is present in the whole lipofuscin granule profile, resulting in a bright yellow colour in the overlay image. Lipofuscin granules showing SW-AF, but not NIR-AF, were scarce and small in diameter. Routine electron microscopy confirmed overall localization and morphology of granules identified by fluorescence microscopy; just as in fluorescence images, melanolipofuscin consisted of a melanin core with a shell or protrusions of lipofuscin-

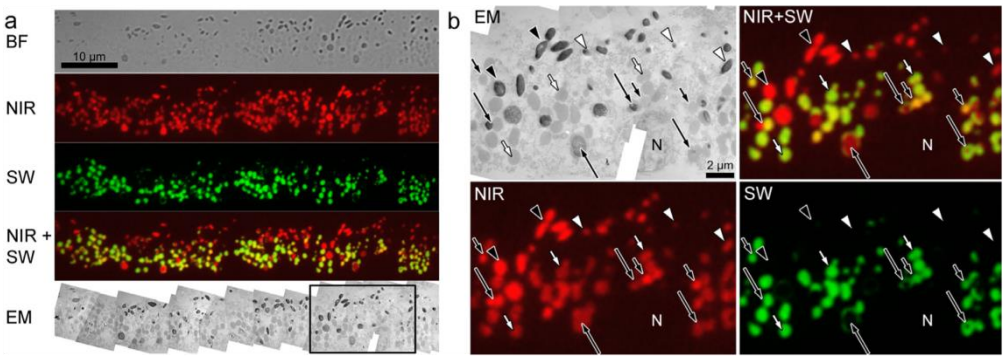

Fig. 6. Correlative fluorescence and electron microscopy of the RPE of an 80-year-old human donor. a) A 150 nm thick section was first investigated by BF and for NIR-AF (red) and SW-AF (green) and subsequently investigated by electron microscopy. To compensate for low signal to noise ratio, 5 individual images of BF, NIR-AF and SW-AF were averaged, respectively. In the NIR-/SW-AF overlay image, lipofuscin granules appear yellow due to the presence of both NIR- and SW-AF. The EM image shown is a composite image of 20 individual images taken at x12,000 magnification. Contrast is low due to complete lack of heavy-metal staining, however, melanosomes and (melano-)lipofuscin granules are still readily identifiable (compare to SI S5 that shows a heavy-metal stained section from the same eye). Magnified EM and fluorescence pictures of the boxed area are shown in (b). The full resolution version of the EM composite image can be accessed under DOI:10.6084/m9.figshare.7951097. b) Melanosomes (arrowheads) show exclusively NIR-AF, but no SW-AF. However, NIR-AF intensity varies between high (black arrowheads) and low (white arrowheads). Lipofuscin granules (short arrows) appear ultrastructurally indistinguishable and show similar SW-AF intensities, but their NIR-AF intensities vary between high (short black arrows) and low (short white arrows). Virtually all lipofuscin granules present NIR-AF. Melanolipofuscin granules (long arrows) can be identified by their NIR-AF positive melanin core and a SW-AF and NIR-AF positive lipofuscin shell or protrusions. BF: bright field; EM: electron microscopy; N: nucleus; NIR: near-infrared; SW: short wavelength.

like material (SI S5). Lipofuscin granules had typical spherical morphology with a homogenous electron-opaque matrix (SI S5).

To corroborate that aged human lipofuscin has both NIR- and SW-AF, we investigated isolated human RPE granules that were separated by density gradient centrifugation into lipofuscin, melanolipofuscin and melanosome fractions (SI S6). In the lipofuscin fraction most granules showed both NIR- and SW-AF. Few granules showed only NIR-AF, but no SW-AF, pointing to minor contamination with melanosomes, as confirmed by electron microscopy. Granules showing only SW-AF, but no NIR-AF, were not present.

In a final step, we performed correlative fluorescence and electron microscopy on single tissue sections. For this, 150 nm thick sections were first investigated by fluorescence microscopy and the same sections were then examined by transmission electron microscopy. This allows unequivocal attribution of fluorescence signals to individual granules within the RPE. Fig. 6 shows that virtually all lipofuscin granules identified by EM showed both SW-AF and NIR-AF. Melanolipofuscin granules are clearly identified by their NIR-AF presenting melanin core and a shell or protrusions of lipofuscin that is positive for both SW- and NIR-AF. Melanosomes varied in their NIR-AF intensity (Fig. 6), but never showed SW-AF.

3.7. *Photic and oxidative stress intensify NIR-AF of melanosomes* in vitro

Since both light and oxidative stress have been found to increase melanin AF [10–12], we tested whether these stressors also increase NIR-AF of melanosomes. Therefore, isolated RPE and choroidal melanosomes from pig eyes were treated with either white light (45,000 lx) or 0•3% hydrogen peroxide at pH 7•4 for 3 or 6 h, respectively (Fig. 7, SI S7). NIR-AF intensity from RPE melanosomes increased significantly after 6 h of light treatment and already after 3 h of hydrogen peroxide treatment, respectively. For choroidal melanosomes, significant alterations of NIR-AF were only seen after 6 h of hydrogen peroxide treatment and not after the applied illumination conditions. Brightening was especially seen in choroidal melanosomes (SI S7). SW-AF was not found in either melanosome fraction in any of the investigated conditions. Ultrastructural analysis of control and treated granules found that light treated RPE melanosomes showed an increase in number and size of small holes close to the melanosome edge, whereas hydrogen peroxide treatment resulted in a less homogenous electron density of RPE melanosomes (SI S8). In choroidal melanosomes, ultrastructural changes were less obvious.

3.8. *NIR-AF of both melanosomes and lipofuscin granules increase in an* in vivo *phototoxicity model*

The pigmented *Abca4*$^{-/-}$ mouse strain is considered as a model for the early phase of Stargardt disease, since it mimics the accumulation of lipofuscin in the RPE but lacks the retinal degeneration encountered in Stargardt patients. Illumination with blue light can be used to induce retinal degeneration which can be considered as a model for the late stage of Stargardt disease. We used a slightly modified phototoxicity protocol based on that published by Wu et al. [26] (Fang et al., manuscript submitted).

We found that the NIR-AF intensity and the share of the melanosome profiles that exhibit NIR-AF in the RPE and to a lesser extent in the choroid increases after illumination of 9-month-old *Abca4*$^{-/-}$ mice (Fig. 8). Furthermore, also the share of lipofuscin granules with co-localizing SW- and NIR-AF increases. These findings resemble the previously described data from aged WT and pigmented *Abca4*$^{-/-}$ mice (Figs. 2–4, SI S3).

4. Discussion

Light exposure of melanin is known to result in extensive structural modifications such as oxidative cleavage and cross-linking [7]. Photodegradation of DHICA-melanin, a synthetic model for eumelanin that is the major melanin type in the eye, resulted in a 16-fold increase of AF intensity [9].

In the present work, we show that NIR-AF emerging from RPE and choroidal melanosomes increases with age (Figs. 2, 3, SI S3) and oxidative stress (Figs. 7, SI S7). Additionally, NIR-AF emerging from RPE melanosomes increases with light stress as well (Figs. 7, 8, S7). Furthermore, while melanosomes in the RPE and choroid of 12-month-old WT mice have very low NIR-AF intensity, melanosome-derived NIR-AF signals from age-matched pigmented *Abca4*$^{-/-}$ mice are greatly increased (Fig. 5). This might be due to

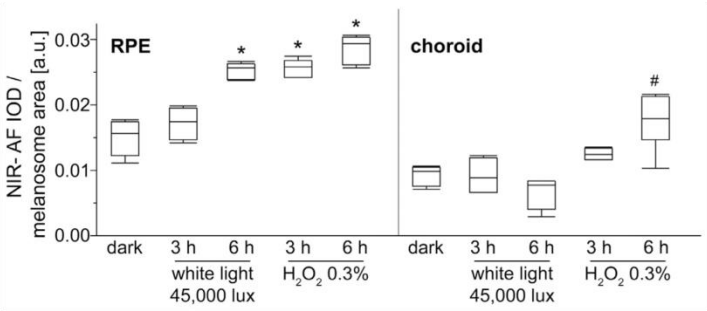

Fig. 7. Semi-quantitative analysis of NIR-AF intensities of RPE and choroidal melanosomes after photic and oxidative stress. Isolated porcine RPE and choroidal melanosomes were treated with either 45,000 lx white light or 0·3% hydrogen peroxide at pH 7•4 for 3 or 6 h, respectively ($N = 4$–6, # $p < 0$•01, * $p < 0$•0001, Dunnett's test). IOD: integrated optical density; NIR: near-infrared.

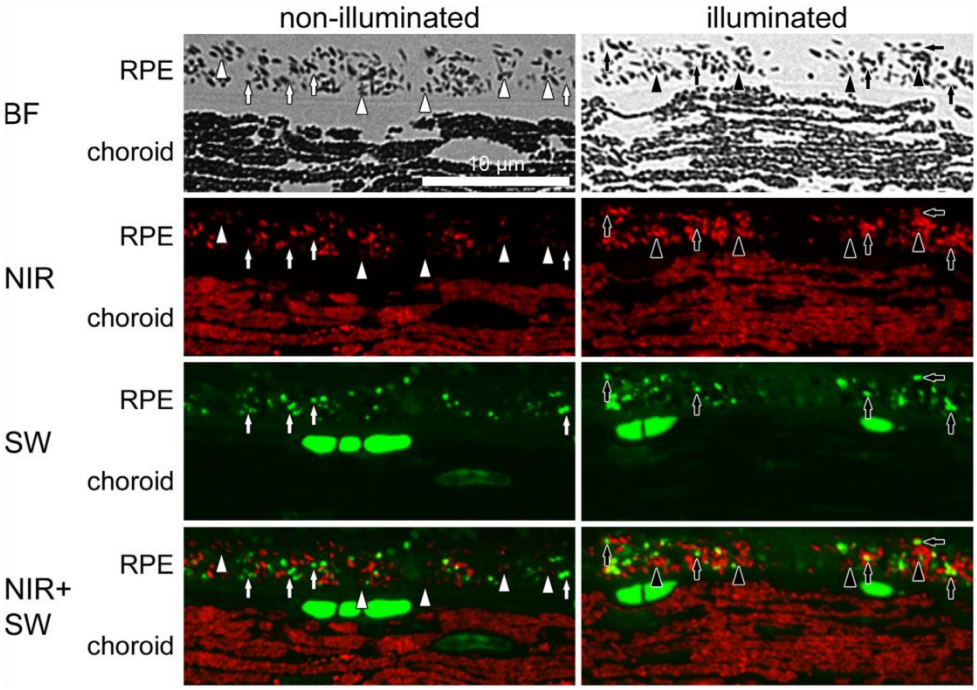

Fig. 8. Blue light stress increases NIR-AF signals in 9-month-old pigmented *Abca4*$^{-/-}$ mice. NIR-AF (red) and SW-AF (green) images of both groups were taken under identical conditions. In non-illuminated eyes, many melanosomes show only minimal or no NIR-AF (white arrowheads), while after blue light stress the overall number of melanosomes showing NIR-AF and the NIR-AF intensity increases (black arrowheads). In non-illuminated eyes, the majority of lipofuscin granules only show SW-AF (white arrows), while after illumination the number of lipofuscin granules showing co-localization of SW-AF and NIR-AF increases (black arrows). $N = 7$ animals per group. BF: bright field; NIR: near-infrared; SW: short wavelength.

melanin damage caused by elevated levels of oxidative stress in these animals. These findings question the common assumption that NIR-AF is an intrinsic property of melanin; it may be more appropriate to consider NIR-AF as a marker for aged or oxidized melanin.

In addition to an increase of NIR-AF intensity with age, we saw a simultaneous brightening of melanosomes in BF images in WT and *Abca4*$^{-/-}$ mice, especially in the choroid (Fig. 2, SI S1, SI S3). Melanosome bleaching is most likely due to melanin degradation, as bleaching also occurs after treatment with superoxide anions, known to degrade melanin [13]. This suggests that the observed increase of NIR-AF is linked to melanin degradation.

Melanosomes from RPE and choroidal melanocytes differ in their reaction to photic and oxidative damage: while RPE melanosomes exhibit more readily NIR-AF (Fig. 7), choroidal melanosomes react more readily with granule brightening (SI S7). Both melanosome types consist mostly of eumelanin with only little amounts of pheomelanin, however, choroidal melanin is suggested to have a higher 5,6-dihydroxyindole-2-carboxylic acid (DHICA) to 5,6-dihydroxyindole (DHI) ratio, with DHICA and DHI being the two proposed monomers of eumelanin [35]. A high DHICA:DHI ratio was suggested to be indicative of a high potential to quench reactive oxygen species [36]. This difference in chemical composition might at least partly explain the observed dif-

ference in reaction to photic and oxidative damage in RPE and choroidal melanosomes (Fig. 7, SI S7, SI S8). Acknowledging the different properties of RPE and choroidal melanin is of interest for fundus AF, since with current clinical imaging systems, both RPE and choroidal melanin add to the NIR-AF measurements [19,20]. However, new imaging techniques, such as adaptive optics scanning laser ophthalmoscopy, are being developed that allow the selective visualisation of RPE cells [37].

Furthermore, we found that there is a considerable variation in NIR-AF properties within both the RPE and the choroidal melanosome populations. In young RPE cells, ellipsoidal melanosomes have a uniform weak NIR-AF that does not cover the whole melanosome profile, whereas spherical melanosomes show a high inter-granule variability, with either very high or very low NIR-AF intensity (Fig. 3). In the choroid, melanosomes that seem uniform in light microscopy can differ vastly in their NIR-AF intensity (SI S2). It seemed that this variability was more prominent in 18-month-old animals, however, this might be due to overall weak NIR-AF intensities in young animals making it difficult to detect such variabilities in these specimens. Little is known about potential functional differences between ellipsoidal and spherical melanosomes of the RPE, however, both types of RPE melanosomes do not differ in their melanin composition, they mostly contain eumelanin. For choroidal melanosomes, even less is known about their function and properties. The inter-granule difference in NIR-AF intensities in a given tissue is a sign that individual melanosomes are not subjected to the same levels of noxious agents that can induce chemical alterations which finally result in NIR-AF intensity increase.

In the choroid, individual rounded cells were present that showed elevated NIR-AF intensities compared to the neighbouring, typically elongated melanocytes (Fig. 2, SI S2). Ultrastructural investigation revealed clusters of melanosomes in lysosome-like organelles in these cells (Fig. 2E). Our group previously identified choroidal cells with similar morphology as macrophages by immunohistochemistry [38].

The contribution of lipofuscin to the NIR-AF signal has long been under debate [25,39]. We found the first occurrences of co-localization of SW- and NIR-AF in areas adjacent to BF-identified melanosomes, suggesting that the lipofuscin moiety of melanolipofuscin is the first area to present both AF types (Figs. 3, 4, SI S3). With increased load of lipofuscin, also lipofuscin granules (indicated by spatial separation from BF-identified melanosomes) did readily contribute to the NIR-AF signal, although the proportion of NIR-AF-contributing lipofuscin granules varies (Figs. 3–6, SI S3, S5). When investigating isolated human RPE granules, the lipofuscin fraction showed both SW- and NIR-AF (SI S6). The possibility of misidentifying melanolipofuscin as lipofuscin granules, *e.g.* due to the melanin moiety not being visible in the section, was prevented by separating the granules by density centrifugation and investigating whole granules.

To our surprise, we did not detect specific lipofuscin NIR-AF signals from albino *Abca4*$^{-/-}$ mice (Fig. 5). With longer acquisition times, we found weak NIR-AF signals co-localizing with lipofuscin granules with high SW-AF intensities, however, these NIR-AF signals were merely as intense as background signals derived from nuclei (SI S4). We therefore suppose that these signals are fluorescence spillover from lipofuscin fluorophores and are not derived from the same molecular source as the high-intensity NIR-AF signals found in lipofuscin granules from pigmented animals and aged humans. So while lipofuscin in albino *Abca4*$^{-/-}$ mice lacks the high-intensity NIR-AF signal seen in pigmented samples, some NIR-AF background is present. This is in accordance with the results from a fundus AF-based study by Paavo et al. that found an increase of NIR-AF intensities in tandem with SW-AF intensities in albino *Abca4*$^{-/-}$ mice[25]: our data suggest that increasing amounts of lipofuscin result in increasing SW-AF and a mild parallel increase of NIR-AF due to presumed fluorescence spillover in these animals. Lipofuscin from pigmented and albino mice was shown to have different bisretinoid composition [40] and morphological properties [29], therefore a difference in NIR-AF properties due to molecular differences is conceivable. In histologic sections and isolated granules from aged human donors however, virtually all lipofuscin granules (and lipofuscin moieties of melanolipofuscin granules) exhibited co-localization of SW- and NIR-AF (Fig. 6, SI S5, SI S6).

How can we explain these observed differences in lipofuscin NIR-AF intensities? As outlined before, co-localization of SW- and NIR-AF first emerging in close association to bright-field-confirmed melanosomes is suggestive of the granule in question being melanolipofuscin. This suggests that the lipofuscin moiety in melanolipofuscin has certain properties that distinguish it from true lipofuscin granules. Analytical electron microscopy as well as nano-secondary ion mass spectrometry analyses of human RPE pigments found that the lipofuscin moiety of melanolipofuscin has significantly elevated nitrogen levels (usually considered a marker for protein content, but also a marker for melanin) compared to lipofuscin granules, while the melanin moiety of melanolipofuscin was found to have elevated phosphorus levels (considered a marker for lipid content) compared to true melanosomes [28,32]. This suggests that the lipofuscin and melanin moieties in melanolipofuscin have some sort of molecular exchange. It is possible that the elevated nitrogen levels found in melanolipofuscin are in fact not derived from proteins, but from melanin degradation products that also contain nitrogen atoms.

Assuming that melanin degradation products amass in melanolipofuscin, how can we explain their subsequent presence in lipofuscin granules? Melanosomes and lipofuscin granules - and consequently melanolipofuscin granules as well - are part of the lysosomal compartment [5,15]. It was shown that lysosomes can exchange contents [41] and it was hypothesized that this occurs by similar mechanisms, as they are established for lysosome-endosome exchange [42]. Moreover, lipofuscin granule dynamics and linkage to degradative processes of melanosomes have been suggested before [31]. To our knowledge, potential trafficking processes between RPE pigments have not been investigated to date. However, it was shown that phagocytosed material, including material associated to phagocytosed outer segments, is transported to melanosomes [43,44] which highly suggests an involvement of the melanosome in the lysosomal degradation pathway. By this means, bisretinoids are likely to be transported to the melanosome. Due to their oxidative properties, bisretinoids might therefore be involved in melanin degradation. Additionally, this process might be the gateway to melanolipofuscin formation. Indeed, we previously suggested the hypothesis that melanosomes can degrade ingested bisretinoids by radical processes and that an insufficient degradation of these ingested bisretinoids results in their accumulation within the melanosome, yielding melanolipofuscin (Schraermeyer U, et al. Invest Ophthalmol Vis Sci. 2019;60:ARVO E-Abstract 1912). The concept of melanin being able to degrade bisretinoids is supported by recent findings highlighting that human foetal RPE cells accumulate less lipofuscin-like material than unpigmented RPE cells *in vitro* [45]. Little is known about the biological fate of melanin degradation products. It is conceivable that fluorescent degradation products of melanin are incorporated into the lipofuscin moiety of melanolipofuscin granules and, with time, are distributed to lipofuscin granules by mechanisms similar to lysosome-lysosome exchange mechanisms. This would not only explain the increase of lipofuscin granules with co-localized SW- and NIR-AF with time, but also elegantly explain the observed lack of specific high-intensity NIR-AF, exceeding what we currently consider fluores-

cence spillover, in albino *Abca4*$^{-/-}$ lipofuscin. Furthermore, accumulation of melanin-degradation products in lipofuscin granules with time could also lead to a tipping point when lipofuscin granules have a greater contribution to overall NIR-AF than melanosomes, especially considering that melanosomes are lost from the RPE with age.

However, molecular confirmation of melanin degradation products accumulating in (melano-)lipofuscin is currently lacking. To date, most compositional analyses of lipofuscin are based on extracts obtained by Folch extraction, which only allows the investigation of chloroform-soluble lipids, therefore, new analytic approaches, going beyond Folch extraction, are needed.

A potential weakness of this study is that we had to resort to standard fluorescence microscopy, since even though the confocal laser scanning system at our disposal (Leica TCS SP8 STED) is equipped with multiple excitation lasers, excitation with 708 nm or longer is not available. We tested whether 635 nm (the longest excitation wavelength available in our system) can be used for excitation of NIR-AF but this resulted in no detectable signals from both melanosomes and lipofuscin granules in a range from 648 to 800 nm, as detected with a Leica prism-based tuneable multiband spectral detection system. However, since we limited section thickness to 500 nm, we were still able to achieve good resolution in standard fluorescence microscopy. Furthermore, *Abca4*$^{-/-}$ and WT mice belong to different substrains of the 129S strain, so we cannot rule out the presence of genetic differences that influence the presented results between these two mouse models. Another limitation is the low number of biological replicates. Nevertheless, the increase of melanin-derived NIR-AF with oxidative and photic stress was found in melanosomes from two species (mouse and pig) as was the presence of NIR-AF signals in lipofuscin (mouse and human). We therefore consider our results a proof-of-concept that requires further investigation. One important question is for instance the degree of influence increasing melanin-derived NIR-AF and additionally occurring lipofuscin-derived NIR-AF have on patient fundus autofluorescence data. Also the underlying mechanism and time frame of lipofuscin granules emitting NIR-AF is of high relevance as is its potential involvement in lipofuscin-related retinal disease, such as in age-related macular degeneration and Stargardt disease.

Strengths of this study are that the used NIR excitation and emission wavelengths are very similar to the wavelengths used in fundus AF examination in patients, so the NIR-AF findings in this study are transferable to patient findings. Furthermore, the microscopical approach employed allows identification of AF properties of individual granules, which is not yet possible with clinical fundus AF based techniques. However, new techniques, such as adaptive optics scanning laser ophthalmoscopy, have the potential to achieve subcellular resolution *in vivo* in the future [37]. Correlative fluorescence and electron microscopy showed unambiguously that both melanosomes and lipofuscin granules are sources of NIR-AF in aged human donor eyes.

In conclusion, our study suggests that NIR-AF is derived from melanin degradation products that emerge from either photic or oxidative stress. As a consequence, aged/damaged melanosomes emit higher NIR-AF signals than young/undamaged melanosomes. Therefore, melanin could be considered a “wear and tear” material that is meant to quench photic or oxidative stress at its own expense. This is indicated by elevated NIR-AF levels in the RPE and choroid of pigmented *Abca4*$^{-/-}$ mice that have more oxidative stress than age-matched WT mice. Pigmented *Abca4*$^{-/-}$ mice do not develop retinal degeneration even up to 22 months of age, while albino *Abca4*$^{-/-}$ mice show first signs of retinal damages as early as 4 months old [29]. Although pigmented and albino *Abca4*$^{-/-}$ mice differ in their genetic background (as discussed in [29]), the lack of melanin in the RPE and choroid of albino *Abca4*$^{-/-}$ mice can at least partly explain the differing susceptibility to retinal degeneration.

However, also the lipofuscin moiety of melanolipofuscin and subsequently lipofuscin granules can emit relevant levels of NIR-AF, potentially due to accumulation of melanin degradation products. The exact mechanism of how and when lipofuscin granules start to emit NIR-AF is however still unclear.

Both aspects, melanin NIR-AF increasing with age and oxidative status, as well as lipofuscin being a source of NIR-AF under certain circumstances, are of great importance for interpretation of clinical and research NIR-AF data. The common assumption that NIR-AF intensity equates melanin quantity cannot be supported with the present data. Elucidating the mechanisms behind changing AF properties of melanosomes and lipofuscin granules opens the possibility to gain deeper insights into pathologic processes and refinement of diagnostics.

5. Funding sources

This work was funded by a grant from Bundesministerium für Bildung und Forschung (01GQ1422B). YF was funded by a Chinese Scholarship Council. AB was funded by Deutsche Forschungsgemeinschaft (BI1551/3-1). The laser scanning microscope was funded by a grant from Deutsche Forschungsgemeinschaft (INST 2388/62-1). The STEM-EDX system was supported by funds of the European Fund for Regional Development (EFRE-FKZ: 712303), the state of Baden-Württemberg, and the NMI Reutlingen. The funders were not involved in study design, data collection, data analysis, data interpretation, decision to publish, or manuscript writing.

6. Declaration of Competing Interest

The authors declare that they have no competing interests.

7. Author contributions

Conceptualization: TT, SJS, US; Data curation: TT; Formal analysis: TT; Funding acquisition: US; Investigation: TT, YF, AB; Supervision: SJS, US; Visualization: TT; Writing - original draft: TT; Writing - review and editing: YF, AB, SJS, US

Acknowledgments

The authors thank Peter Charbel Issa, Gabriel H. Travis, and Roxana Radu for providing them with the knockout mouse strains. They also thank the Cornea Bank Tübingen for providing them with human eye tissue. Special thanks are due to the donors and their families. The authors also thank Timm Schubert for performing the confocal laser scanning microscopy analysis and Sigrid Schultheiss, Barbara Illing, and Antonina Burda for excellent technical assistance. We also thank Clementine Warres and Max Becker for their support in STEM handling.

Supplementary materials

Supplementary material associated with this article can be found, in the online version, at doi:10.1016/j.ebiom.2019.09.048.

References

[1] Hu DN, Simon JD, Sarna T. Role of ocular melanin in ophthalmic physiology and pathology. Photochem Photobiol 2008;84:639–44.
[2] Dontsov AE, Glickman RD, Ostrovsky MA. Retinal pigment epithelium pigment granules stimulate the photo-oxidation of unsaturated fatty acids. Free Radic Biol Med 1999;26:1436–46.

[3] Biesemeier A, Kokkinou D, Julien S, et al. UV-A induced oxidative stress is more prominent in naturally pigmented aged human RPE cells compared to non-pigmented human RPE cells independent of zinc treatment. J Photochem Photobio B Bio 2008;90:113–20.
[4] Rozanowski B, Cuenco J, Davies S, et al. The phototoxicity of aged human retinal melanosomes. Photochem Photobiol 2008;84:650–7.
[5] Schraermeyer U, Heimann K. Current understanding on the role of retinal pigment epithelium and its pigmentation. Pigment Cell Res 1999;12:219–36.
[6] Poliakov E, Strunnikova NV, Jiang JK, et al. Multiple A2E treatments lead to melanization of rod outer segment-challenged ARPE-19 cells. Mol Vis 2014;20:285–300.
[7] Ito S, Wakamatsu K, Sarna T. Photodegradation of eumelanin and pheomelanin and its pathophysiological implications. Photochem Photobiol 2018;94:409–20.
[8] Zareba M, Szewczyk G, Sarna T, et al. Effects of photodegradation on the physical and antioxidant properties of melanosomes isolated from retinal pigment epithelium. Photochem Photobiol 2006;82:1024–9.
[9] Wakamatsu K, Nakanishi Y, Miyazaki N, Kolbe L, Ito S. UVA-induced oxidative degradation of melanins: fission of indole moiety in eumelanin and conversion to benzothiazole moiety in pheomelanin. Pigment Cell Melanoma Res 2012;25:434–45.
[10] Elleder M, Borovansky J. Autofluorescence of melanins induced by ultraviolet radiation and near ultraviolet light. A histochemical and biochemical study. Histochem J 2001;33:273–81.
[11] Kayatz P, Thumann G, Luther TT, et al. Oxidation causes melanin fluorescence. Invest Ophthalmol Vis Sci 2001;42:241–6.
[12] Sarna T, Burke JM, Korytowski W, et al. Loss of melanin from human RPE with aging: possible role of melanin photooxidation. Exp Eye Res 2003;76:89–98.
[13] Dontsov AE, Sakina NL, Ostrovsky MA. Loss of melanin by eye retinal pigment epithelium cells is associated with its oxidative destruction in melanolipofuscin granules. Biochem Biokhimiia 2017;82:916–24.
[14] Docchio F, Boulton M, Cubeddu R, Ramponi R, Barker PD. Age-related changes in the fluorescence of melanin and lipofuscin granules of the retinal pigment epithelium: a time-resolved fluorescence spectroscopy study. Photochem Photobiol 1991;54:247–53.
[15] Sparrow JR, Gregory-Roberts E, Yamamoto K, et al. The bisretinoids of retinal pigment epithelium. Prog Retin Eye Res 2012;31:121–35.
[16] Ach T, Huisingh C, McGwin G Jr, et al. Quantitative autofluorescence and cell density maps of the human retinal pigment epithelium. Invest Ophthalmol Vis Sci 2014;55:4832–41.
[17] Schmitz-Valckenberg S, Holz FG, Bird AC, Spaide RF. Fundus autofluorescence imaging: review and perspectives. Retina 2008;28:385–409.
[18] Yung M, Klufas MA, Sarraf D. Clinical applications of fundus autofluorescence in retinal disease. Int J Retina Vitreous 2016;2:12.
[19] Keilhauer CN, Delori FC. Near-infrared autofluorescence imaging of the fundus: visualization of ocular melanin. Invest Ophthalmol Vis Sci 2006;47:3556–64.
[20] Weinberger AW, Lappas A, Kirschkamp T, et al. Fundus near infrared fluorescence correlates with fundus near infrared reflectance. Invest Ophthalmol Vis Sci 2006;47:3098–108.
[21] Pilotto E, Vujosevic S, Melis R, et al. Short wavelength fundus autofluorescence *versus* near-infrared fundus autofluorescence, with microperimetric correspondence, in patients with geographic atrophy due to age-related macular degeneration. Br J Ophthalmol 2011;95:1140–4.
[22] Cideciyan AV, Swider M, Schwartz SB, Stone EM, Jacobson SG. Predicting progression of ABCA4-Associated retinal degenerations based on longitudinal measurements of the leading disease front. Invest Ophthalmol Vis Sci 2015;56:5946–55.
[23] Duncker T, Tabacaru MR, Lee W, Tsang SH, Sparrow JR, Greenstein VC. Comparison of near-infrared and short-wavelength autofluorescence in retinitis pigmentosa. Invest Ophthalmol Vis Sci 2013;54:585–91.
[24] Skondra D, Papakostas TD, Hunter R, Vavvas DG. Near infrared autofluorescence imaging of retinal diseases. Semin Ophthalmol 2012;27:202–8.
[25] Paavo M, Zhao J, Kim HJ, et al. Mutations in GPR143/OA1 and ABCA4 inform interpretations of short-wavelength and near-infrared fundus autofluorescence. Invest Ophthalmol Vis Sci 2018;59:2459–69.
[26] Wu L, Ueda K, Nagasaki T, Sparrow JR. Light damage in Abca4 and Rpe65rd12 mice. Invest Ophthalmol Vis Sci 2014;55:1910–18.
[27] Boulton M, Marshall J. Repigmentation of human retinal pigment epithelial cells *in vitro*. Exp Eye Res 1985;41:209–18.
[28] Biesemeier A, Eibl O, Eswara S, Audinot JN, Wirtz T, Schraermeyer U. Transition metals and trace elements in the retinal pigment epithelium and choroid: correlative ultrastructural and chemical analysis by analytical electron microscopy and nano-secondary ion mass spectrometry. Metallomics 2018;10:296–308.
[29] Taubitz T, Tschulakow AV, Tikhonovich M, et al. Ultrastructural alterations in the retinal pigment epithelium and photoreceptors of a Stargardt patient and three Stargardt mouse models: indication for the central role of RPE melanin in oxidative stress. PeerJ 2018;6:e5215.
[30] Jung T. Hohn a and grune T. lipofuscin: detection and quantification by microscopic techniques. Methods Mol Biol 2010;594:173–93.
[31] Feeney L. Lipofuscin and melanin of human retinal pigment epithelium. Fluorescence, enzyme cytochemical, and ultrastructural studies. Invest Ophthalmol Vis Sci 1978;17:583–600.
[32] Biesemeier A, Schraermeyer U, Eibl O. Chemical composition of melanosomes, lipofuscin and melanolipofuscin granules of human RPE tissues. Exp Eye Res 2011;93:29–39.
[33] Charbel Issa P, Barnard AR, Singh MS, et al. Fundus autofluorescence in the Abca4(-/-) mouse model of Stargardt disease–correlation with accumulation of A2E, retinal function, and histology. Invest Ophthalmol Vis Sci 2013;54:5602–12.
[34] Paavo M, Lee W, Allikmets R, Tsang S, Sparrow JR. Photoreceptor cells as a source of fundus autofluorescence in recessive Stargardt disease. J Neurosci Res 2019;97:98–106.
[35] Liu Y, Hong L, Wakamatsu K, et al. Comparisons of the structural and chemical properties of melanosomes isolated from retinal pigment epithelium, iris and choroid of newborn and mature bovine eyes. Photochem Photobiol 2005;81:510–16.
[36] Sarangarajan R, Apte SP. Melanin aggregation and polymerization: possible implications in age-related macular degeneration. Ophthalmic Res 2005;37:136–41.
[37] Granger CE, Yang Q, Song H, et al. Human retinal pigment epithelium: in vivo cell morphometry, multispectral autofluorescence, and relationship to cone mosaic. Invest Ophthalmol Vis Sci 2018;59:5705–16.
[38] Julien S, Biesemeier A, Kokkinou D, Eibl O, Schraermeyer U. Zinc deficiency leads to lipofuscin accumulation in the retinal pigment epithelium of pigmented rats. PLoS ONE 2011;6:e29245.
[39] Gibbs D, Cideciyan AV, Jacobson SG, Williams DS. Retinal pigment epithelium defects in humans and mice with mutations in MYO7A: imaging melanosome-specific autofluorescence. Invest Ophthalmol Vis Sci 2009;50:4386–93.
[40] Ueda K, Zhao J, Kim HJ, Sparrow JR. Photodegradation of retinal bisretinoids in mouse models and implications for macular degeneration. Proc Natl Acad Sci USA 2016;113:6904–9.
[41] Ferris AL, Brown JC, Park RD, Storrie B. Chinese hamster ovary cell lysosomes rapidly exchange contents. J Cell Biol 1987;105:2703–12.
[42] Storrie B, Desjardins M. The biogenesis of lysosomes: is it a kiss and run, continuous fusion and fission process. Bioessays 1996;18:895–903.
[43] Schraermeyer U, Stieve H. A newly discovered pathway of melanin formation in cultured retinal pigment epithelium of cattle. Cell Tissue Res 1994;276:273–9.
[44] Schraermeyer U, Peters S, Thumann G, Kociok N, Heimann K. Melanin granules of retinal pigment epithelium are connected with the lysosomal degradation pathway. Exp Eye Res 1999;68:237–45.
[45] Zhang Q, Presswalla F, Calton M, et al. Highly differentiated human fetal RPE cultures are resistant to the accumulation and toxicity of lipofuscin-like material. Invest Ophthalmol Vis Sci 2019;60:3468–79.

Supplementary Information

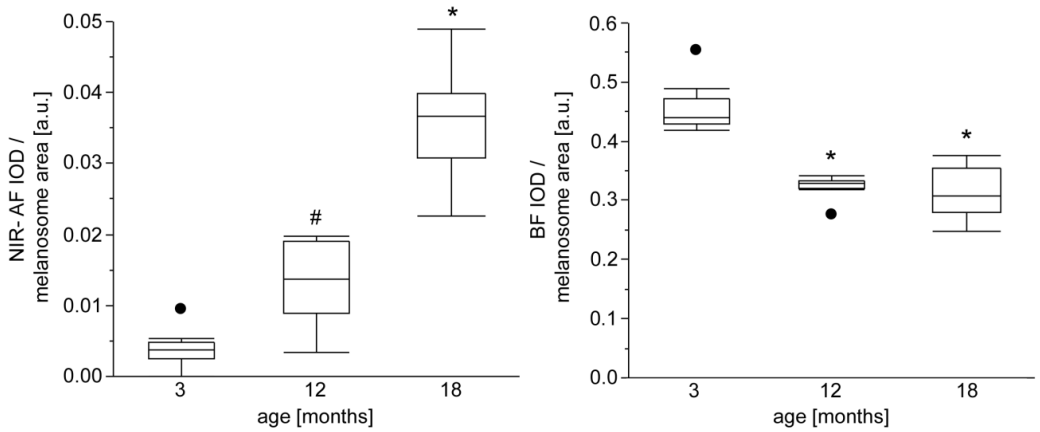

Figure S1. Semi-quantitative analysis of total NIR-AF (left) and BF (right) intensities derived from RPE and choroid of WT mice (N = 7-11 pictures per group, # p < 0·01, * p < 0·0001, Dunnett's test). AF: autofluorescence; BF: bright field; IOD: integrated optical density; NIR: near-infrared.

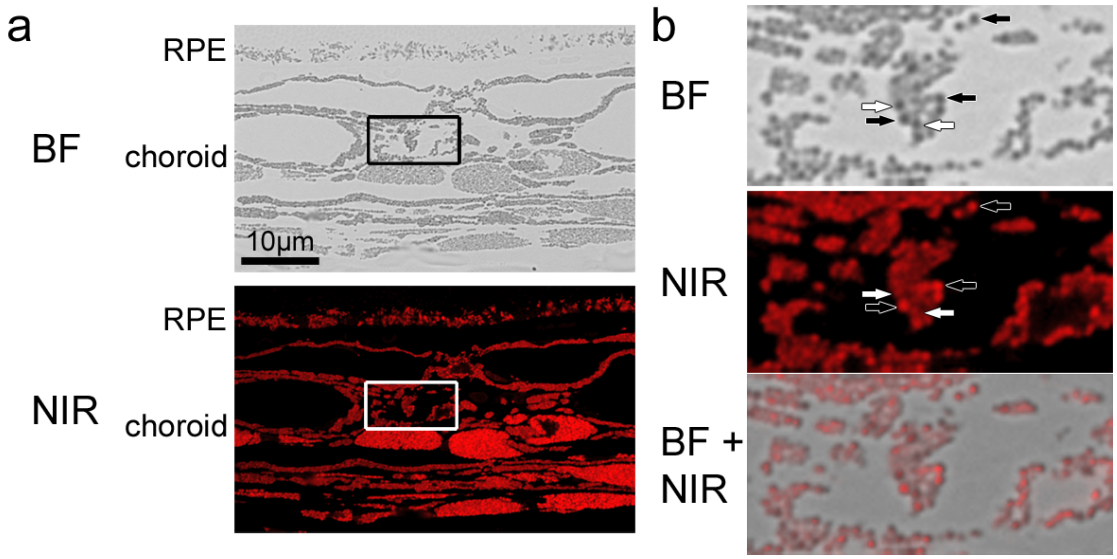

Figure S2. Choroidal melanosomes differ in their NIR-AF properties. Bright field and post-processed NIR-AF micrographs of an 18-month-old WT mouse. Boxed areas in a) are shown magnified in b). Even though melanosomes have similar size and density in bright field, they can show either very intense (black arrows) or very weak (white arrows) NIR-AF. Also note the large, roundish cells with high levels of NIR-AF in the choroid that are macrophage-like cells (compare with Fig. 2). BF: bright field; NIR: near-infrared.

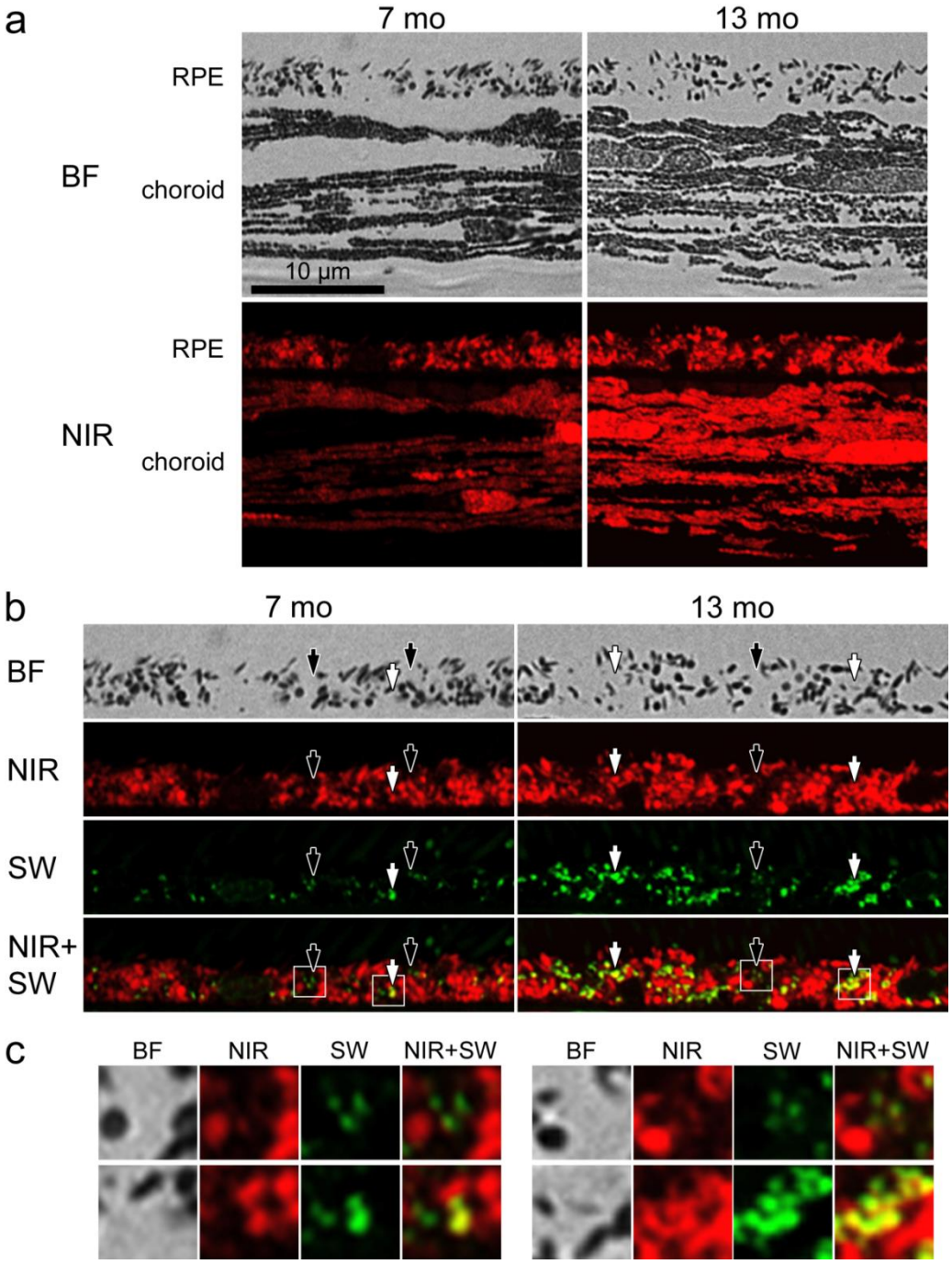

Figure S3. Comparison of 7- and 13-month-old pigmented *Abca4*$^{-/-}$ mice. a) Overview of RPE and choroidal NIR-AF (red) taken under identical conditions. Note the large, roundish cells with high levels of NIR-AF in the choroid of the 13-month-old animal that are macrophage-like cells (compare with Fig. 2). b) Magnified BF and NIR-AF (red) and SW-AF (green) images of the RPE areas shown in (a). AF images were post-processed to allow the localization of weak signals. White arrows point to lipofuscin with prominent NIR-AF signal, resulting in yellow colour in overlay images, while black arrows point to lipofuscin with no or limited NIR-AF signal, resulting in green colour in overlay images. Boxed areas are magnified in (c). c) Magnified images of the boxed areas in (b). Top row shows black arrow areas, bottom row shows white arrow areas. BF: bright field; NIR: near-infrared; SW: short wavelength.

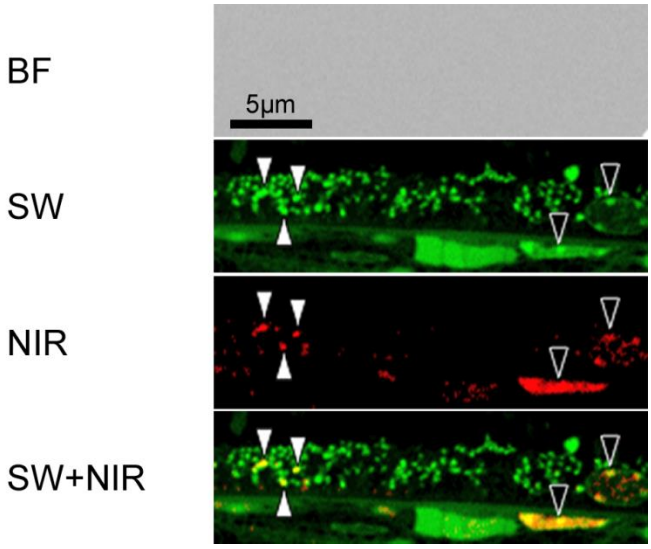

Figure S4. Autofluorescence in the RPE of a 12-month-old albino *Abca4*$^{-/-}$ mouse. The bright field image shows no tissue structures due to lack of melanin in albino animals and no additional staining. AF images were post-processed to allow the localization of weak signals. Areas exhibiting both AF modalities are yellow in the superimposed image. Few lipofuscin granules show NIR-AF signals (white arrowheads) that are not stronger than background signals derived from RPE and choroidal nuclei (black arrowheads). BF: bright field; NIR: near-infrared; SW: short wavelength.

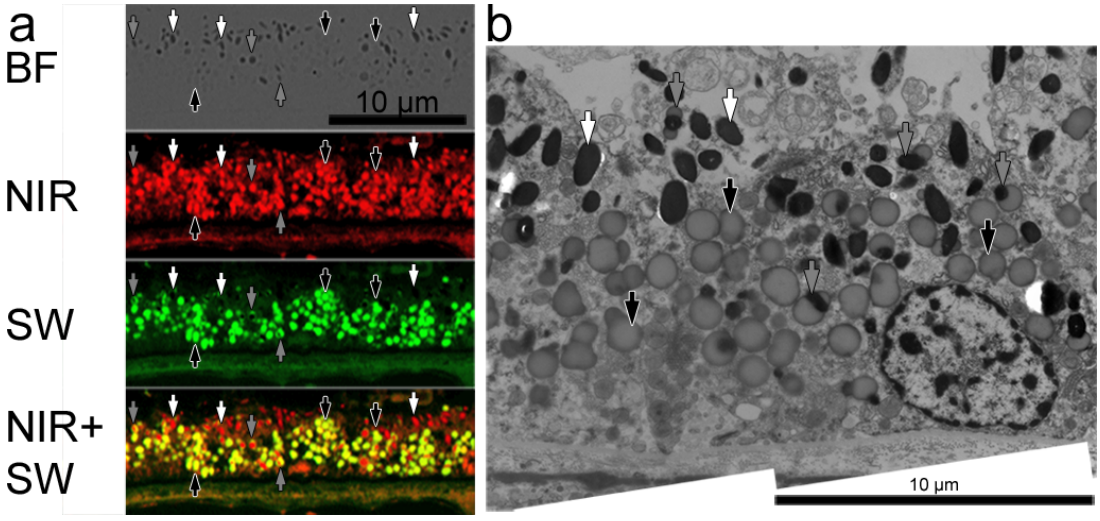

Figure S5. Autofluorescence and electron microscopy of the RPE of a 80-year-old human donor. a) NIR-AF (red) and SW-AF (green) images were post-processed to allow the localization of weak signals. Yellow colour shows areas where NIR-AF and SW-AF superimpose. In aged human RPE, melanosomes (white arrows) are reduced and mostly found apically. Many BF-identified melanosomes are surrounded by SW-AF identified lipofuscin, indicative of melanolipofuscin (grey arrows). Lipofuscin granules are marked with black arrows and predominantly show both NIR- and SW-AF. b) Routine ultrastructural image (post-fixed with osmium tetroxide, stained with uranyl acetate and lead citrate) from the same eye, pigment granules are labelled identical as in a). BF: bright field; NIR: near-infrared; SW: short wavelength.

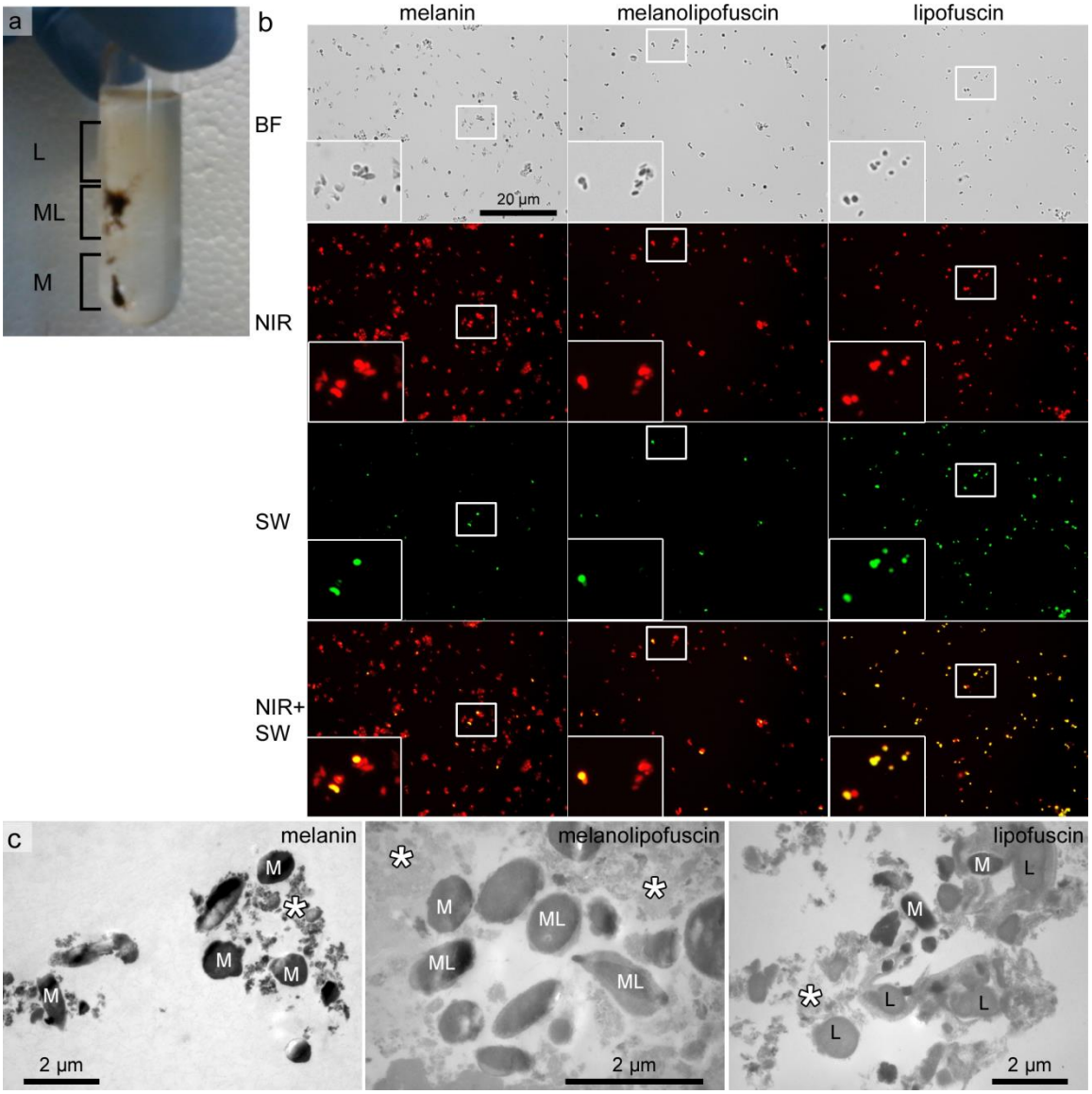

Figure S6. NIR-AF and SW-AF of isolated human RPE granules (46 – 91 years old, mean age 70·2 ± 14·7 years). a) RPE granules were separated by density gradient centrifugation into three fractions containing lipofuscin (L), melanolipofuscin (ML) and melanin (M), respectively. b) NIR-AF (red) and SW-AF (green) images of isolated granules were post-processed to allow the localization of weak signals. Yellow colour in NIR-/SW-AF overlay images shows areas where NIR-AF and SW-AF superimpose. Insets show magnifications of the boxed areas. c) Electron micrographs of granules from the three isolated fractions. Note that granules are surrounded by extragranular debris (asterisks), as has been described before[1]. BF: bright field; NIR: near-infrared; SW: short wavelength.

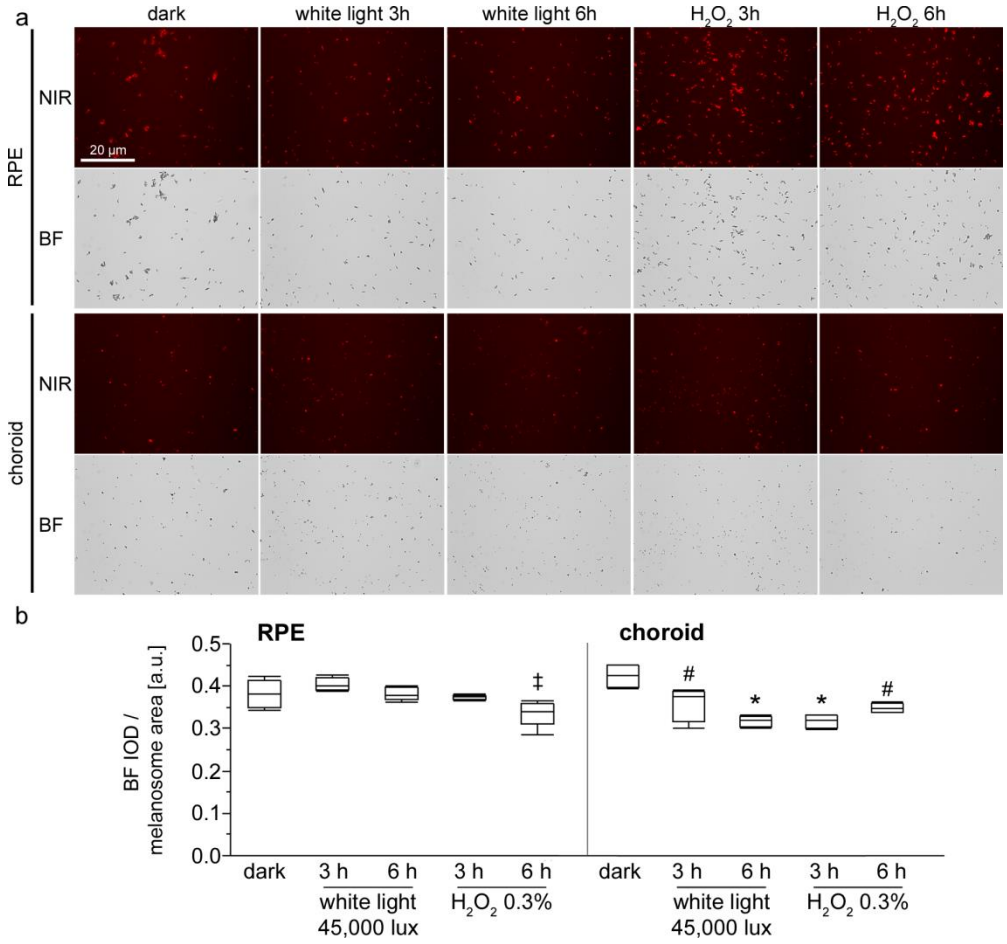

Figure S7. Porcine RPE and choroidal melanosomes after photic and oxidative stress. Isolated melanosomes were either kept in the dark (control) or treated with white light (45,000 lux) or with 0·3% hydrogen peroxide at pH 7·4 for 3 to 6 hours, respectively. a) Representative NIR-AF and BF images of the different groups. b) Semi-quantitative analysis of melanosome darkness in bright field images. Choroidal melanosomes react more readily with granule brightening than RPE melanosomes, while RPE melanosomes predominately react to photic and oxidative stress with presence of NIR-AF (see Fig. 7 in main text). (N = 4-6 images per group, ‡ $p < 0{\cdot}05$, # $p < 0{\cdot}01$, * $p < 0{\cdot}0001$, Dunnett's test). BF: bright field; IOD: integrated optical density; NIR: near-infrared.

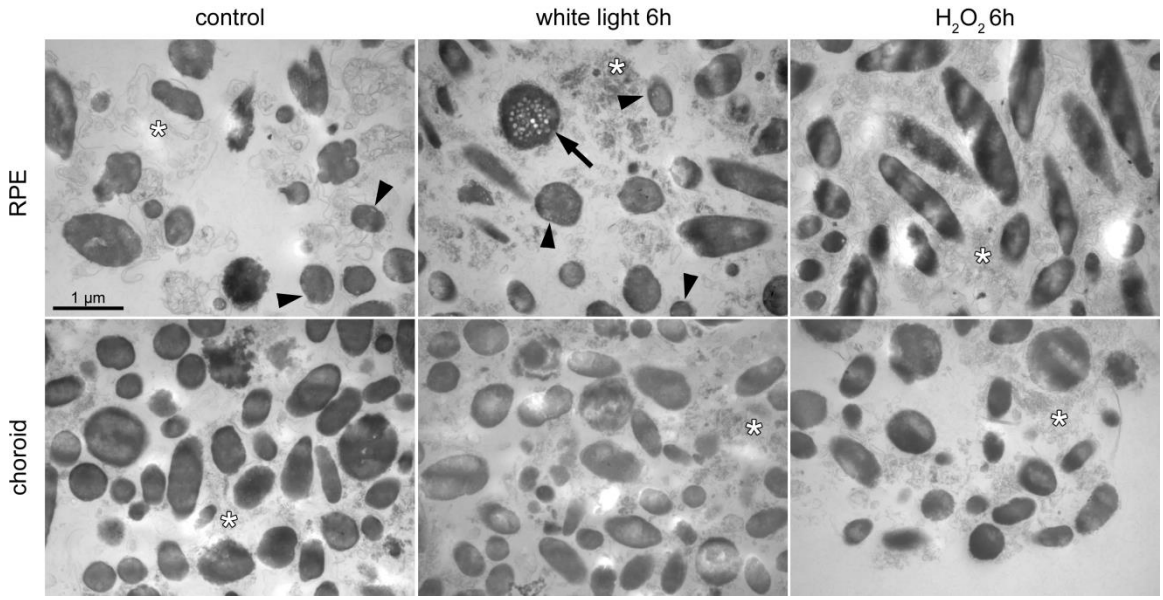

Figure S8. Ultrastructural changes of porcine RPE and choroidal melanosomes after photic and oxidative stress. Control RPE melanosomes have a relatively homogenous electron dense presence and occasionally show small holes close to the granule edge (arrowheads). After treatment with white light, these holes appear more often in RPE melanosomes and seem to increase in size. Individual melanosomes present with numerous big holes throughout the granule profile (arrow). In hydrogen peroxide treated RPE melanosomes, the holes are less prominent, but the formerly relative homogenous electron density appears striated. In choroidal melanosomes, ultrastructural changes are much less prominent. Note that granules are surrounded by extragranular debris (asterisks), as has been described before[1].

References

1. Ng KP, Gugiu B, Renganathan K, et al. Retinal pigment epithelium lipofuscin proteomics. *Molecular & cellular proteomics : MCP* 2008; **7**: 1397–405.

3.3 Treatment of wet AMD: the influence of the Fc fragment in anti-VEGF adverse events

In the past, the group of Prof. Dr. Schraermeyer extensively investigated the effects of intravitreal injection of bevacizumab in monkey eyes [149-152, 196-199]. Key findings were thrombotic microangiopathy, signs of haemolysis, formation of immune complexes, and blood flow alterations within one to 14 days after a single intravitreal injection of bevacizumab [149-152]. The formation of immune complexes by bevacizumab was first described to be a reaction between bevacizumab, VEGF-A_{165} and heparin involving the FcγRIIa receptor on thrombocytes [200] and was supposed to be the reason for the elevated risk of arterial thromboembolic events in patients with metastatic tumours treated with a combination of bevacizumab and chemotherapy [201]. However, bevacizumab, VEGF-A_{165} and heparin can also form immune complexes *in vitro* on endothelial cells, while ranibizumab, lacking an Fc fragment, does not [149].

The effects of a single intravitreal injection of ranibizumab and aflibercept into the monkey eye [2, 3] (sections 3.3.1 and 3.3.2) were investigated in a similar manner to bevacizumab [150-152, 196, 199, 202].

One day after a single injection, both ranibizumab and aflibercept were located in retinal and choroidal vessels. Ranibizumab permeated the neuroretina *via* intercellular clefts, while aflibercept was incorporated into ganglion cells. Ranibizumab and aflibercept were found to both reduce the lumen of the choriocapillaris one and seven days after a single intravitreal injection, as was previously found for bevacizumab [150]. This is in accordance with studies showing that free VEGF is essential for the upkeep of the choriocapillaris [203]. Choriocapillaris fenestration loss, microangiopathy and haemolysis were more pronounced after aflibercept than after ranibizumab. These findings were also previously observed after bevacizumab [150-152]. Hypertrophy and death of RPE, as well as the formation of protein complexes, representing as abundant fibrous material seemingly attaching erythrocytes to each other or to endothelial cells and thus reducing blood flow, were only evident after treatment with aflibercept and not after ranibizumab. The lack of abundant protein complexes after *in vivo* application of ranibizumab is consistent with the lack of immune complex formation *in vitro* [149].

One day after intravitreal injection, both ranibizumab and aflibercept were located in the walls of ciliary blood vessels, on the surface layer of the ciliary epithelium and in the connective tissue surrounding the vascular plexus, similar to the distribution pattern of bevacizumab in the ciliary body [199]. Both drugs induced a comparable reduction of free VEGF in the non-pigmented epithelium of the ciliary body and lead to a reduction of ciliary blood vessel fenestration. The reduction of free VEGF in the ciliary body epithelium by both drugs verifies the usefulness of anti-VEGF drugs in anterior segment pathologies, such as rubeosis iridis [140, 204]. However, exclusively in aflibercept-treated irides, vacuolisation of the interior iris pigment epithelium was evident after one and seven days after injection. The nature and relevance of these vacuoles remain to be elucidated.

In summary, studies involving monkeys showed that the most numerous and severe pathologies after intravitreal application of anti-VEGF compounds were encountered after bevacizumab and aflibercept. Notably microangiopathy, haemolysis and protein complex formation, which were exclusively found after bevacizumab [150-152] and aflibercept, are alarming outcomes, especially when one takes the systemic accumulation of these drugs after repeated intravitreal application into account [154].

It is unclear, whether aflibercept is actually able to induce immune complex formation by the mechanism described for bevacizumab [200], since it is not known how VEGF is bound by the fusion protein aflibercept and whether the heparin-binding site of VEGF needed for complex formation is still accessible. However, since treatment with ranibizumab resulted in fewer and less severe pathologies than treatment with aflibercept and bevacizumab, it suggested itself that the molecular structure of the drugs, i.e. the presence or lack of an Fc domain, might have an impact on the observed pathologies.

To investigate the effects of isolated Fc domains, rats were intravitreally injected with isolated rat Fc at a dose corresponding to the Fc fragment dose in anti-VEGF treatment in patients [4] (section 3.3.3). Thrombotic events, such as fibrin formation, as well as activation and loose aggregation of thrombocytes, were frequently observed at all time points after Fc fragment injection, but only infrequently in controls. These findings are in accordance with the aforementioned studies in monkeys, where treatment with both bevacizumab and aflibercept (both containing an Fc domain) resulted in a pronounced occurrence of thrombotic

events and stasis [2, 150, 151]. However, the most prominent finding after application of Fc fragments was the infiltration of immune cells in the vitreous-retina interface as early as one day after injection. The majority of cells in the vitreous were identified as macrophages by immunohistochemical analysis, but ultrastructurally, also granulocytes were identified. The observation of infiltrating cells was unexpected, since this was not seen in the earlier studies involving monkeys. However, a meta-study reported a significantly increased risk to develop a sterile endophthalmitis after intravitreal injection of bevacizumab compared to ranibizumab [205] which might be connected to these findings.

Fc cannot only directly be related to drug-induced pathologies, but also indirectly: IgG is known to be "recycled" and protected from catabolism by binding to the neonatal Fc receptor [206], elongating the serum half-live of the IgG. This process is utilised for therapeutic Fc-fusion proteins [207] and might also be the reason for the accumulation of bevacizumab and aflibercept in contrast to ranibizumab in patient serum [154]. However, since the vast majority of pathologies in the monkey studies were already present one day after injection, this process probably only plays a minor role in this context.

The present works [2, 3] (sections 3.3.1 and 3.3.2) show that after application of Fc-containing anti-VEGF drugs, more numerous and severe pathologies, such as microangiopathy, haemolysis and blood flow alterations, were present in monkey eyes, which was not the case after applying the Fc-less ranibizumab. Furthermore, even individual Fc fragments without any therapeutic effect induced thrombotic events and infiltration of immune cells into the vitreous-retina interface after a single intravitreal injection in a rat model [4] (section 3.3.3).

These data point to Fc-containing anti-VEGF drugs having an unfavourable safety profile, especially considering that AMD patients treated with anti-VEGF are elderly and often suffer from systemic diseases affecting cardiovascular health. Furthermore, since anti-VEGF intervention treats the symptoms, but not the underlying cause of wet AMD, treatment has to be continued for potentially years, which gives rise to possible long-term effects, particularly since Fc-containing anti-VEGF drugs were shown to accumulate after repeated intravitreal injection [154]. However, there is currently no consensus whether the established anti-VEGF drugs have different safety profiles [124, 147, 156, 208-210] and more research is needed.

3.3.1 Different effects of intravitreally injected ranibizumab and aflibercept on retinal and choroidal tissues of monkey eyes.

Authors: Julien S., Biesemeier A., Taubitz T., Schraermeyer U.

Published in *The British Journal of Ophthalmology* in 2014
DOI: 10.1136/bjophthalmol-2013-304019

This work was conducted as a student research assistant and is included since it presents groundwork to the later publications.

Declaration of own contributions:

Planning, writing and revision of the manuscript was done by PD Dr. Sylvie Julien-Schraermeyer. I performed part of the sample preparation (embedding, sectioning) as well as part of the light microscopic (quantification of choriocapillaris area and choriocapillaris area with free haemoglobin) and electron microscopic (quantification of choriocapillaris fenestrations and measurement of endothelial thickness) analyses. Data interpretation was done by PD Dr. Sylvie Julien-Schraermeyer, PD Dr. Antje Biesemeier and Prof. Dr. Ulrich Schraermeyer. I and the other authors proof-read the manuscript.

BJO Online First, published on March 17, 2014 as 10.1136/bjophthalmol-2013-304019
Laboratory science

Different effects of intravitreally injected ranibizumab and aflibercept on retinal and choroidal tissues of monkey eyes

Sylvie Julien,[1,2] Antje Biesemeier,[1] Tatjana Taubitz,[1,2] Ulrich Schraermeyer[1,2]

[1]Section of Experimental Vitreoretinal Surgery, Centre for Ophthalmology, Tuebingen, Germany
[2]Preclinical Drug Assessment, STZ OcuTox, Tübingen, Germany

Correspondence to
Dr Ulrich Schraermeyer, Section of Experimental Vitreoretinal Surgery, Centre for Ophthalmology, Schleichstrasse 12/1, Tuebingen 72076, Germany;
Ulrich.Schraermeyer@med.uni-tuebingen.de

Received 16 July 2013
Revised 20 December 2013
Accepted 23 December 2013

ABSTRACT

Background Since there is evidence that the Fc domain of antivascular endothelial growth factor drugs may cause unexpected consequences in retinal and choroidal vessels, the effects of intravitreal ranibizumab and aflibercept on monkey eyes were investigated.

Methods Four cynomolgus monkeys were intravitreally injected with 0.5 mg of ranibizumab and another four with 2 mg of aflibercept. Two untreated monkeys served as controls. Funduscopy, fluorescein angiography (FA), spectral-domain-optical coherence tomography (SD-OCT) and measurement of intraocular pressure (IOP) were performed. The eyes were inspected by light, fluorescence and electron microscopy. The diameter of the choriocapillaris (CC) was measured by morphometry, and the areas of the CC with free haemoglobin, CC fenestrations and endothelial thickness were quantified.

Results Analysis showed ranibizumab permeated the retina via intercellular clefts, whereas aflibercept was taken up by ganglion cells, cells of the inner and outer retinal layers and the retinal pigment epithelium (RPE). Stasis and haemolysis in the choriocapillaris and choroidal vessels were more frequent after aflibercept treatment, which caused hypertrophy and death of individual RPE cells. The area of the CC was significantly reduced after both drugs compared with controls, but the reduction of the CC endothelium thickness, number of fenestrations and the areas with haemolysis were more pronounced after aflibercept.

Conclusions Ranibizumab permeated the retina through intercellular spaces, whereas aflibercept was taken up by neuronal and RPE cells. Aflibercept induced protein complex formation and more haemolysis in the choriocapillaris, leading to individual RPE cell death. The clinical significance and relation of these findings to the Fc domain or to other characteristics of aflibercept remain to be investigated.

INTRODUCTION

Excessive angiogenesis is a major problem in many ocular diseases, particularly in such angioproliferative disorders as diabetic proliferative retinopathy and age-related macular degeneration (AMD) in adults, and retinopathy of prematurity in infants.

AMD is the leading cause of blindness in patients over the age of 65 years in developed countries with choroidal neovascularisation (CNV) being the main factor responsible for vision loss in AMD. It accounts for approximately 90% of AMD-related blindness[1] although neovascular AMD affects only 10–15% of AMD patients. CNV is characterised by the growth of new choroidal blood vessels through Bruch's membrane into the subretinal space, followed by leakage and accumulation of serum or blood beneath the retinal pigment epithelium (RPE), leading to an insult of the outer retina and RPE and finally to vision loss.[2]

Although the pathogenesis of AMD is not completely understood, several growth factors have been implicated in the disease process as they induce the development of blood vessels (ie, basic fibroblast growth factor, transforming growth factor β, insulin-like growth factor-1, epidermal growth factor, interleukins and vascular endothelial growth factor (VEGF)). However, only VEGF appears to be sufficient and essential for both physiological and pathological angiogenesis.[3] Oxidative stress and inflammation due to the accumulation of intracellular and extracellular waste material, including lipids in Bruch's membrane and drusen, stimulate VEGF synthesis. Indeed, an increase of VEGF in the RPE of maculae from patients with AMD[4] was observed, as well as an increase of VEGF expression in the laser model of CNV in monkeys[5] and rats.[6] Induction of CNV was also observed after ectopically delivered VEGF cDNAs to the RPE of rats[7–9] and non-human primates.[10]

In humans, the VEGF family consists of five related glycoproteins, VEGF-A, VEGF-B, VEGF-C, VEGF-D and placental growth factor (PlGF). VEGF-A is the most well-studied member of the VEGF family and is the major driver of pathological angiogenesis and vascular leakage in wet AMD.[11] Alternative splicing results in six VEGF-A isoforms of 121, 145, 165, 183, 189 and 206 amino acids, whose solubility is dependent on heparin-binding affinity. They can all bind the VEGFR1 (Flt-1) and VEGFR2 (KDR) receptors. VEGFR1 also binds VEGF-B and PlGF. In contrast to VEGF-A, neither VEGF-B nor PlGF is essential for vasculogenesis and angiogenesis, but they have been implicated in pathological vascular remodelling.[11] Growing evidence suggests that PlGF synergises with VEGF-A in promoting vascular pathology,[11] whereas the function of VEGF-B is still not clear.[12]

Since 2004, anti-VEGF therapy has become the standard treatment for wet AMD and has revolutionised the management of this disease. Between 2004 and 2006, three anti-VEGF drugs were introduced to ophthalmology after receiving regulatory approval for the treatment of AMD (pegaptanib, ranibizumab) or being used off-label (bevacizumab).[13] They exhibit important differences in their sites of activity, formulation methods, binding affinities and biological activities. Pegaptanib (Macugen,

To cite: Julien S, Biesemeier A, Taubitz T, *et al*. *Br J Ophthalmol* Published Online First: [*please include* Day Month Year] doi:10.1136/bjophthalmol-2013-304019

Julien S, *et al*. *Br J Ophthalmol* 2014;0:1–6. doi:10.1136/bjophthalmol-2013-304019 1
Copyright Article author (or their employer) 2014. Produced by BMJ Publishing Group Ltd under licence.

Eyetech/Pfizer) is an oligonucleotide aptamer that selectively binds to and neutralises the main pathological isoform of VEGF (VEGF-A^{165}) by attaching to its heparin-binding domain. Ranibizumab (Lucentis, Genentech/Novartis) is an affinity-matured, humanised, monoclonal antibody fragment (Fab), whereas bevacizumab (Avastin, Genentech/Roche) is a full-length, humanised, monoclonal antibody. Both work by blocking the receptor-binding domain of all isoforms of VEGF-A.[14] Aflibercept (VEGF Trap-Eye, Eylea, Regeneron/Bayer) is a new anti-VEGF agent recently approved by the Food and Drug Administration. It is a fully human, recombinant fusion protein composed of the second immunoglobulin (Ig)-binding domain of VEGFR1 and the third Ig-binding domain of VEGFR2 fused to the fragment crystallisable (Fc) region of human IgG1.[15] Aflibercept binds to all VEGF-A isoforms, VEGF-B and PlGF.[11]

Our group has extensively described the effects of intravitreally injected bevacizumab in the eyes of monkeys.[16–19] These included reductions in choriocapillaris fenestrations, photoreceptor damage, formation of immune complexes and thrombotic microangiopathy. A prevailing rationale for thrombosis after bevacizumab treatment was presented by Meyer and colleagues.[20] They found that bevacizumab can induce platelet aggregation, degranulation and thrombosis through complex formation with VEGF, heparin and activation of the platelet Fc gamma RIIa receptor. Moreover, other results have demonstrated effective binding of the Fc domain of bevacizumab to human RPE and human umbilical vascular endothelial cell membranes via Fc receptors or membrane-bound VEGF, activating the complement cascade and leading to cell death.[21] It is unclear whether there is a similar problem with aflibercept as it also contains the Fc domain of human IgG1. Furthermore, the IgG1 isotype is known to be very effective in the activation of the complement system through the classical pathway.[22] Indeed, the Fc portion of IgG1 has a high ability to bind C1q causing subsequent activation of the classical pathway.[22] In contrast, ranibizumab does not possess the Fc domain, avoiding activation of the complement cascade.

In this study, we investigated the influence of the Fc domain by comparing the effects on the retina and choroid of intravitreally injected ranibizumab versus aflibercept into monkey eyes. The monkey is the ideal model for this in vivo study since in contrast to rodents the interactions between the Fc domain and the Fc receptors mimic those present in humans.[23]

METHODS

Animals and study protocol

Ten healthy cynomolgus monkeys (*Macaca fascicularis*, aged 3–8 years) were raised at the Covance Laboratories (Muenster, Germany) under standard conditions. All animals were housed and handled in strict accordance with good animal practice under supervision of veterinarians and were monitored for evidence of disease and changes in attitude, appetite or behaviour suggestive of illness. Handling and housing of the animals at Covance Laboratories GmbH was done in accordance with the German Animal Welfare Act. Moreover, all animals underwent a range of ophthalmic examinations (described in 'Ophthalmic examinations') during the predose phase in order to detect possible ocular disorders that would have not been related to the injection of ranibizumab or aflibercept. Ranibizumab was intravitreally injected into both eyes of four animals, and aflibercept intravitreally into both eyes of another four animals. One and seven days after intravitreal injection, the animals were sacrificed under general anaesthesia and the eyes were enucleated (four eyes from two monkeys per time point). Two untreated monkeys served as controls. For each monkey, one eye was fixed for light and electron microscopy and the other eye for immunohistochemistry. For the notice of approval by the appropriate institutional animal care and use committee, please see Covance Studies 8260977 and 8274007.

Intravitreal injection of ranibizumab and aflibercept

In total, 50 µl of ranibizumab (10 mg/mL) and of aflibercept (40 mg/mL) were intravitreally injected. The animals were sedated by intramuscular injection of medetomidine (Domitor) and ketamine hydrochloride, the eyes having previously been examined for any signs of inflammation. Pupils were dilated (Mydriasis with 1% tropicamide) and anaesthetised (proxymetacaine; Proparakain-pos 0.5%; Ursapharm). The conjunctival and corneal surface was disinfected (povidone iodine 10%). After sterile coating and insertion of a lid speculum, 0.5 mg ranibizumab or 2 mg aflibercept were injected into the vitreous cavity using a 27-gauge canula. When removing the canula, the injection site was compressed with forceps to prevent reflux and a topical antibiotic (gentamicin) was administered. Animals were monitored for signs of inflammation until sacrificed.

Ophthalmic examinations

For all ophthalmic examinations, a mydriatic agent (tropicamide) and a local ophthalmic anaesthetic (proxymetacaine) were instilled in the eyes of the sedated animals before examination.

Macroscopic and slit lamp examinations, direct/indirect ophthalmoscopy

These examinations were performed during the predose phase on the day of dosing and on the day of necropsy. The surface of the eyes was macroscopically examined. Slit lamp examination consisted of anterior and medium segments with conjunctiva, cornea, anterior chamber, iris, lens and vitreous body, as well as fluorescein instillation, for epithelial staining. Direct and indirect ophthalmoscopy consisted of ocular fundus with macula lutea, papilla, ocular vessels and retina.

Funduscopy and fluorescein angiography (FA)

Fundus photographs and FA were obtained for all animals once during the predose phase and on the day of necropsy. For FA, an indwelling catheter was inserted and fluorescein was injected intravenously. A series of pictures was made immediately after injection and 10 min thereafter. The equipment used was a digital stationary fundus camera (TRC-50 ex; Topcon, Tokyo, Japan).

Spectral-domain-optical coherence tomography (SD-OCT)

SD-OCT was obtained for all animals once during the predose phase directly after injection (only for aflibercept) and on the day of necropsy. The equipment used was Spectralis HRA +OCT (Heidelberg Engineering, Heidelberg, Germany).

Intraocular pressure (IOP)

Measurement of IOP was performed in all animals once during the predose phase, before administration of the drugs, directly and 10 min after administration and on the day of necropsy by using TonoVet (Kruuse, Langeskov Denmark). Two readings were obtained per eye for each time point, and the mean IOP value was calculated and reported in millimetres of mercury (mm Hg).

Enucleation

On days 1 and 7 after intravitreal injection, the animals were sacrificed under general anaesthesia, that is, intramuscular injection of ketamine hydrochloride followed by an intravenous sodium pentobarbitone (Lethabarb, Virbac, Australia) overdose. The eyes were enucleated 5 min postmortem, cleaned of orbital tissue and were slit carefully at the limbus without damaging the ora serrata. Then 25 µL of the fixative were carefully injected into the vitreous before the eyes were fixed at 4°C by immersion into 5% glutaraldehyde in 0.1 M cacodylate buffer (pH 7.4, Sigma, St. Louis, Missouri, USA) overnight for electron microscopy or into formalin (Carl Roth, Karlsruhe, Germany) for immunohistochemistry. The eyes of two healthy monkeys without treatment were handled in the same manner.

Immunohistochemistry

Eyes were fixed in formalin, embedded in paraffin wax, cut into 5 µm sections and deparaffinised according to standard procedures. Ranibizumab and aflibercept were detected respectively using a goat antiserum to human Fab of IgG (GAHu/Fab/7S, dilution 1:250; Nordic Immunological Laboratories, Tilburg, The Netherlands) and a goat antihuman IgG-Fc antibody (NB7446, dilution 1:200, Novus Biologicals Europe, Cambridge, UK) with a cy3-rabbit antigoat antibody as a secondary antibody (305–167–003, dilution 1:400, Jackson ImmunoResearch Europe, Suffolk, UK). The following other antibodies were used for the detections of immune reactivity: a rabbit polyclonal anticow glial acidic fibrillary protein (GFAP) antibody for astrocytes and activated Mueller cells (Z0334, dilution 1:4000, Dako, Carpinteria, California, USA), with an anti-rabbit IgG labelled with FITC as secondary antibody (F0511, dilution 1:100; Sigma-Aldrich, St. Louis, Missouri, USA); a mouse monoclonal antivimentin antibody for Mueller cells (M7025, dilution 1:400; Dako), with goat antimouse IgG labelled with Alexa Fluor 488 (A11001, dilution 1:400; Invitrogen-Molecular Probes, Eugene, Oregon, USA) as a secondary antibody; a rabbit anti-ionised calcium-binding adaptor molecule 1 (Iba-1) antibody for macrophages and microglia (01–1974, dilution 1:100, Wako, Neuss, Germany), with a cy3-goat antirabbit antibody (111–166–045, dilution 1:300, Jackson ImmunoResearch); a mouse antihuman hypoxia-inducible factor-1α (HIF-1α) antibody as a marker for hypoxia (610 958, dilution 1:50, BD Transduction Laboratories, Franklin Lakes, USA) with a Alexa Fluor 488-goat antimouse IgG antibody (A11001, dilution 1:400, Invitrogen-Molecular Probes). Stained sections were embedded (FluorSave; Calbiochem, La Jolla, California, USA) and inspected with a fluorescence microscope (Axioplan2; Carl Zeiss, Oberkochen, Germany).

Light and electron microscopy

Specimens were postfixed with 1% OsO_4 at room temperature in 0.1 M cacodylate buffer (pH 7.4), stained with uranyl acetate and embedded in Epon after dehydration in a graded series of ethanol and propylenoxide. Semithin sections were stained with toluidine blue and examined by light microscopy (Zeiss Axioplan2 imaging, Zeiss, Jena, Germany). For electron microscopy, the sections were cut ultrathin and analysed with a Zeiss 902 A electron microscope (Zeiss, Jena, Germany). For every eye at each time point (days 1 to 7 and control), two different regions of interest were chosen. One piece of tissue was taken from the fovea, the second piece at 2 mm distance at the 3 o'clock position.

Quantification of the area occupied by the choriocapillaris and of free haemoglobin

Under the light microscope at a magnification of 600-fold, the capillaries directly facing the Bruch´s membrane were photographed in semithin sections and the quantification of the area occupied by the choriocapillaris was performed blinded as previously described.[19] Briefly, 20 micrographs were consecutively photographed from each treated eye and from each untreated monkey. The photographs were taken by four independent investigators, and the quantifications were performed by two of them. For quantification of the areas, image analysis software (iTEM, Olympus Soft Imaging Solutions, Muenster, Germany) was used. The area fraction of the choriocapillaris is expressed as an area in μm^2 occupied by the capillaries per µm length of Bruch's membrane.

Areas within the plasma of the choriocapillaris with free haemoglobin, which stained as blue as the red blood cells or darker were quantified in semithin sections.

Quantification of choriocapillaris endothelial cell fenestrations and measurement of endothelial thickness

The number of fenestrae was counted in 283 electron micrographs taken at a magnification of 50 000-fold for ranibizumab-treated eyes and untreated controls. In total, 457 micrographs at a magnification of 30 000 from drug-treated eyes were analysed blinded for fenestrations.

Images obtained for counting the fenestrae of the choriocapillaris were also used to investigate the thickness of its apical endothelial wall. Measurements were performed every 300–400 nm over a length of about 45 µm length (about 80 measurements per animal). Here again the photographs were taken by four independent investigators and the quantifications were performed by two of them. Vessel walls that were thicker than 70 nm were not counted since they were presumed to contain the central part of the cell with its organelles and nuclei and were not representative of fenestrated endothelium.

Statistical analysis

Statistical significance for the comparison of IOP and for the evaluation of the area of the choriocapillaris was determined by using the Dunnett's test and the JMP10.0 statistical program (SAS, Heidelberg, Germany). $p<0.05$ was considered statistically significant.

For the measurement of free haemoglobin and endothelial thickness in the choriocapillaris, statistical analysis was performed using the Wilcoxon test for non-parametric data sets (JMP 10.0). The null hypothesis was that controls and treated animals showed the same characteristics, for example, CC apical walls of anti-VEGF-treated animals had the same thickness as those of control animals. The alternative hypothesis was that they differ. All p values <0.05 were stated as significantly different (error probability 5%).

RESULTS

Ophthalmic examinations

Funduscopy, FA and SD-OCT

Funduscopic (figure 1A,C), FA (figure 1B,D) and SD-OCT (figure 1E) images did not show abnormalities or blood vessel leakage in any of the eyes injected with ranibizumab (figure 1A, B) or aflibercept (figure 1C–E) at the different time points, nor in any of the control eyes.

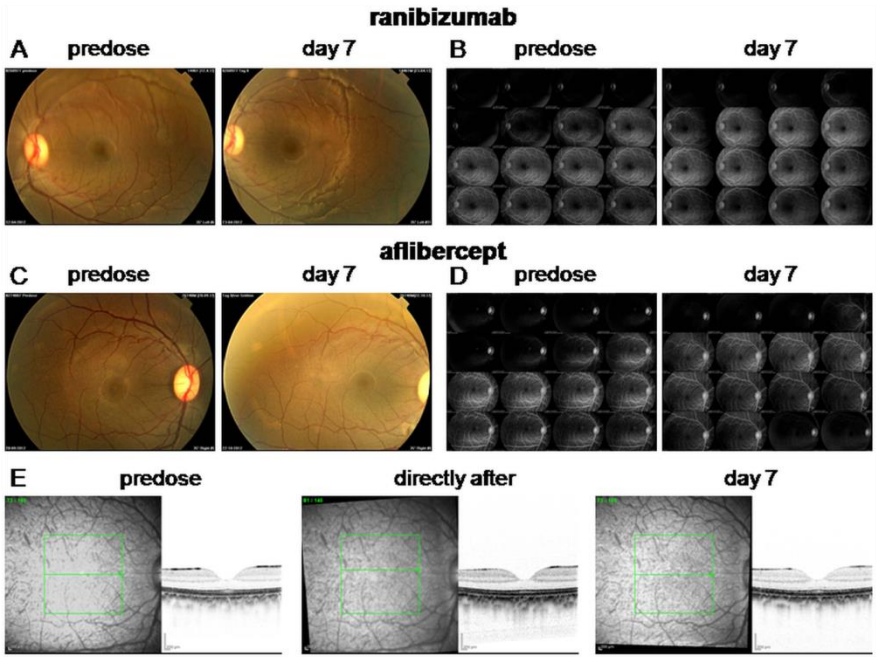

Figure 1 Fundus, fluorescein angiography (FA) and spectral-domain-optical coherence tomography (SD-OCT) photographs before and after injection of ranibizumab and aflibercept. Typical fundus photographs (A) and a series of FA pictures (B) of the same left eye of a monkey before and 7 days after injection of ranibizumab are shown. Typical fundus photographs (C), a series of FA pictures (D) and SD-OCT (E) of the same right eye of a monkey before and 7 days after injection of aflibercept are shown. The time point directly after injection of aflibercept is also shown in the OCT (E). The bright structures appearing in several fundus photographs near the blood vessels are reflection artefacts.

Intraocular pressure

The IOP was measured in a predose phase (2 weeks before the study began), just before administration of the drugs, directly and 10 min afterwards, and 1 and 7 days afterwards (on the day of necropsy). The mean values (MV) as well as the SD were calculated (figure 2). The values obtained in the predose phase and just before the administration of the drugs were pooled since in both cases the animals were untreated. The MV±SD of the untreated animals (15.3±4 mm Hg) was compared with the MV ±SD of the treated animals for each time point. The IOP increased significantly directly after administration of the drugs (30.6±14.5 after ranibizumab (R) (p=1.4E-06) and 50.3±11.5 after aflibercept (A) (p=5.7E-19)). Ten minutes after administration of the drugs, the IOP returned to baseline (18.8±5.5 after ranibizumab and 14.4±3.3 after aflibercept). One day after injection of ranibizumab, the IOP decreased significantly (9.5 ±1.1; p=0.007), whereas the decrease of the IOP after aflibercept's injection was not statistically significant (11±7; p=0.06). Seven days after injection of aflibercept, the IOP was significantly reduced (10.4±3.1; p=0.02) compared with the IOP of untreated animals, whereas it normalised to baseline 7 days after ranibizumab injection (19.4±3.8; p=0.06). There was no statistically significant difference between the IOP of untreated eyes 7 days after the beginning of the study (19.8±1.8) versus the IOP of untreated eyes at the beginning of the study.

Immunohistochemistry

Ranibizumab and aflibercept

Retinal sections were checked for their immune reactivity against ranibizumab and aflibercept. In untreated controls, no specific staining was found in either the retina or the choroid (not shown). Just one day after injection, ranibizumab and aflibercept immune reactivity were already observed in eyes injected with ranibizumab and aflibercept respectively but with distinct distribution patterns (figure 3A,B). Ranibizumab permeated the retina via intercellular clefts (figure 3A), whereas aflibercept was taken up by ganglion cells, cells of the inner and outer retinal layers and the RPE (figure 3B). Local accumulation in retinal and choroidal vessels was observed for both drugs (figure 3A,C, D vs 3B,E,F). Ranibizumab immune reactivity was reduced after 7 days compared with day 1 (figure 3D vs 3C) while aflibercept (figure 3F vs 3E) showed no changes.

Glial acidic fibrillary protein (GFAP)

After GFAP staining in untreated controls, longitudinal astrocytes became visible and were localised in the inner retinal layers close to the ganglion cells and in the vicinity of retinal vessels (figure 4A). One and seven days after injection of ranibizumab and aflibercept, Mueller cells in the middle of the retina became positive for GFAP, indicating a mild activation of Mueller cells (figure 4B,C).

Vimentin

After vimentin staining in untreated controls, Mueller cells appeared in a longitudinal orientation between inner limiting membranes (ILM) and outer limiting membranes and their end-feet formed a continuous layer facing the ILM (figure 4D). One and seven days after injection of ranibizumab and aflibercept, vimentin was overexpressed (figure 4E,F) compared with untreated eyes, confirming activation of Mueller cells.

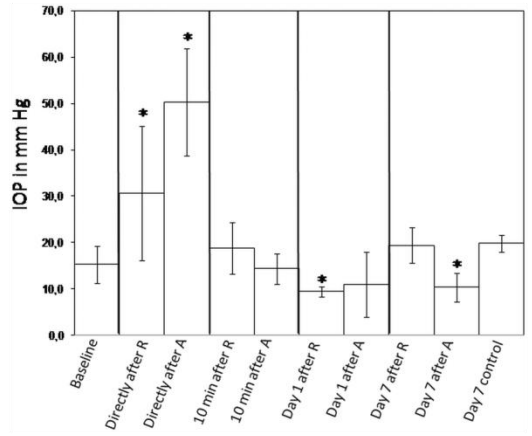

Figure 2 Measurement of the intraocular pressure (IOP) at different time points. The IOP was measured in all monkey eyes during the predose phase (2 weeks before the study started) as well as before administration of the drugs, and the values were pooled in order to obtain the IOP baseline. The IOP was measured directly after and 10 min after injection of ranibizumab (R) and aflibercept (A) respectively in eight eyes. The IOP was also measured on day 1 in four eyes for R and A as well as on day 7 in four eyes for R and A and in two untreated control eyes. IOP mean values±SDs are presented. Asterisks indicate statistical significance compared with the baseline IOP (*p<0.05).

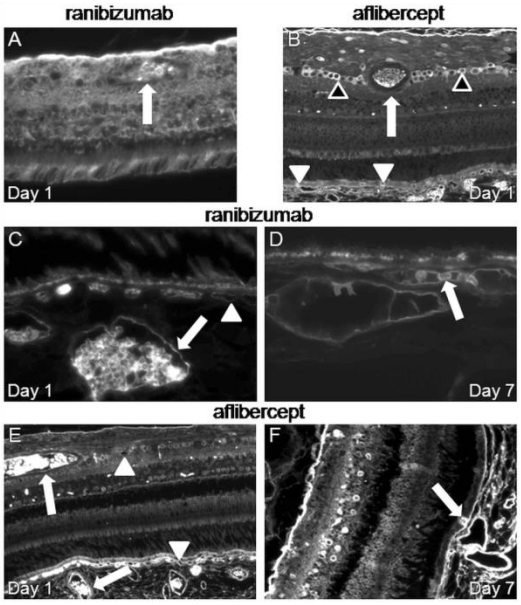

Figure 3 Fluorescence microscopy of the immune histochemical localisation of ranibizumab and aflibercept. One day after injection, ranibizumab (A) permeated the retina via intercellular clefts, whereas aflibercept (B) was taken up by ganglion cells (black arrowheads), cells of the inner and outer retinal layers and retinal pigment epithelium (RPE) (white arrowheads). Both drugs were localised in retinal (A,B) and in choroidal vessels (C,E). A heterogeneous staining was observed for both drugs in individual vessels. It was locally attached to the vessel walls occupying substantial parts of the vessel lumen (arrows in A–C, E). Seven days after injection, ranibizumab immune reactivity (D) in choroidal vessels was reduced compared with aflibercept immune reactivity (F). Note the strong aflibercept immune reactivity in some RPE cells (F, white arrow) and the adherence of ranibizumab (D, white arrow) to the surface of erythrocytes.

Iba-1 and HIF1-α

Macrophages and microglia cells were not affected by ranibizumab or aflibercept. As in untreated controls (figure 4G), Iba-1-positive cells were located in the plexiform layer and the ganglion cell layer (GCL) of the neural retina. There were no significant changes throughout the observation period in the retinas (figure 4H,I).

Independent of the treatments, HIF-1α was never expressed (not shown).

Light microscopy

In semithin sections of untreated eyes (not shown) and ranibizumab-treated eyes (figure 5A), the choriocapillaris as well as choroidal vessels showed well-defined lumina and contained loosely packed erythrocytes. Individual erythrocytes can be clearly recognised when photographed at a magnification of 600-fold (figure 5A). However, ranibizumab at small foci activated thrombocytes and induced fibrin formation in deeper choroidal vessels one day after injection (figure 5A, see also figure 6A at high resolution). Seven days after injection of ranibizumab, stasis and haemolysis were occasionally observed in the choriocapillaris (figure 5B). In contrast, on 1 as well as 7 days after injection, aflibercept treatment had already caused stasis and haemolysis in most parts of the investigated choriocapillaris (figure 5C–E). The RPE was hypertrophic compared with the RPE after ranibizumab treatment (figure 5C vs 5D) or no treatment (not shown). Moreover, dark blue RPE cells were found beside normal pale blue RPE cells (figure 5B,E) and contained lysed mitochondria, indicating individual RPE cell death. However, the photoreceptors showed a normal morphology indicating that they were not affected by the treatment (figure 5D,E). There were no morphological differences observed in the RPE and choroid between foveal and extrafoveal semithin sections. Moreover, in semithin sections from all treated eyes, the lumina of the choriocapillaris were smaller compared with control eyes, as shown in the quantification below (figure 5F).

Quantification of the area occupied by the choriocapillaris and of free haemoglobin

The area (in μm^2) occupied by the choriocapillaris per μm length of Bruch's membrane was significantly reduced in eyes treated with ranibizumab and aflibercept 1 and 7 days after injection compared with the untreated controls (figure 5F). The median of the area occupied by the choriocapillaris in the untreated eyes was 3.9 μm^2, whereas it was 3.2 and 2.9 μm^2 1 day after injection of ranibizumab and aflibercept and 2.1 and 2.1 μm^2 7 days after injection of ranibizumab and aflibercept, respectively. Application of Dunnett's test revealed that the decrease of the choriocapillaris was significant in the eyes 1 day after ranibizumab injection ($p=0.01$) as well as 7 days afterwards and also 1 and 7 days after aflibercept injection ($p<0.001$). These findings confirmed the reduction of the choriocapillaris area 1 and 7 days after injection of both drugs.

Free haemoglobin that stained the plasma as dark or darker than the red blood cells was not observed in the plasma of the choriocapillaris of untreated monkeys. After aflibercept treatment, the part of the area with haemolytic plasma in the

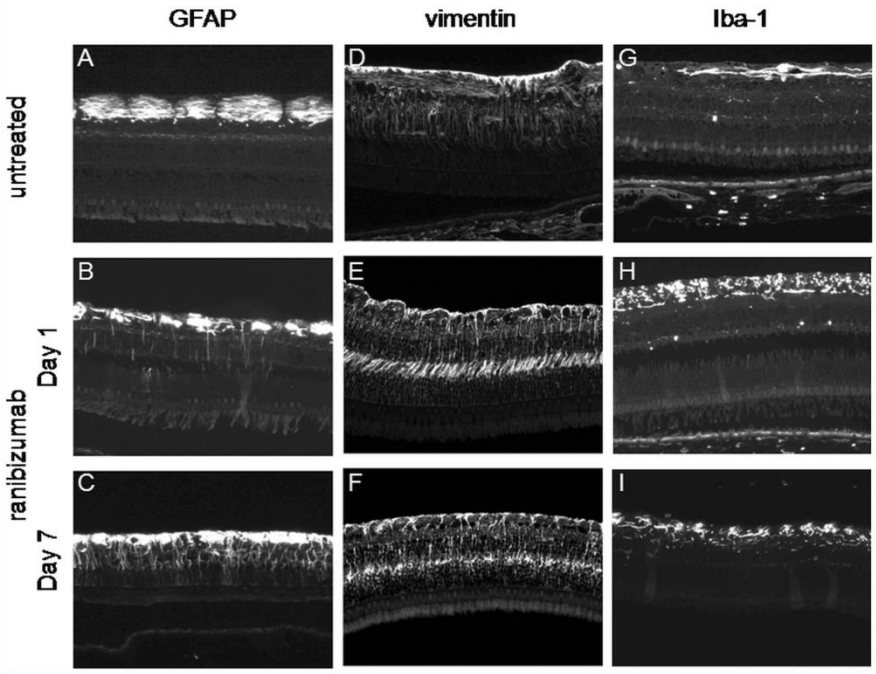

Figure 4 Fluorescence microscopy of retinas after staining for glial acidic fibrillary protein (GFAP) (A–C), vimentin (D–F) and Iba-1 (G–I). Images of untreated eyes are shown for GFAP, vimentin and Iba-1 stainings in A, D and G, respectively. One (B, E and H) and seven (C, F and I) days after injection of ranibizumab, retinas labelled with GFAP, vimentin and Iba-1 are shown in B–C), EF and H–I, respectively. The micrographs presented for ranibizumab treatment are also representative for the staining for GFAP, vimentin and Iba-1 observed after injection of aflibercept. Activated Mueller cells were present after treatment with both drugs 1 and 7 days after injection, whereas astrocytes and microglia cells were not affected.

choriocapillaris was 80.1±4.7% after 1 day and 87.5±3.9% after 7 days. After ranibizumab treatment, the percentage part of the area with haemolytic plasma in the choriocapillaris was 54.6 ±5.7% after 1 day and 49.4±5.1% after 7 days. According to the Wilcoxon test, the differences between aflibercept and ranibizumab were significant with $p<0.0002$ and $p<0.0001$ 1 and 7 days after injection (figure 5G).

Electron microscopy

In order to obtain more information, the eyes were inspected by electron microscopy. The fibrin formation found in deeper choroidal vessels 1 day after ranibizumab injection (figure 5A) can be clearly observed in figure 6A,B. In figure 6A, it was obvious that erythrocytes established contact with thrombocytes. With a higher magnification (figure 6B), a clear binding between an activated thrombocyte and an erythrocyte can be seen. Thrombocytes were activated as judged by their pseudopodia and formation of fibrin, identified by its ultrastructure.[24] Local electron densities were detected exceptionally between an endothelial cell and an erythrocyte after ranibizumab treatment (figure 6C). Erythrocytes often had many holes (figure 6D) of different sizes or were shrinking or blebbing. This phenomenon is well known as eryptosis and was observed after both drug treatments. Filamentary material representing protein complexes was much more obvious after aflibercept treatment (figure 6E). It was never observed in blood plasma of the controls (not shown). After aflibercept treatment, stasis, swelling of erythrocytes and haemolysis were observed in most parts of the choriocapillaris (figure 6F,G) as well as in choroidal veins (figure 6G) but not in the immediate neighbouring arteries. Extravasal-free haemoglobin could be observed as well (figure 6G,H). The presence of haemoglobin was confirmed by energy-dispersive X-ray spectroscopy, which revealed a high level of iron in this electron-dense material compared with areas with normal brighter plasma (not shown). By zooming into the area of figure 6G where extracellular haemoglobin was present (figure 6H), pathological signs like vacuoles in endothelium and dead cells close to the blood vessel were observed. Haemoglobin was also detected within Bruch's membrane and the intercellular clefts of RPE cells between the basal labyrinth and the tight junctions (not shown). Individual RPE cells were completely filled with free haemoglobin (figure 6I), indicating cell death. Microangiopathy was detected as the endothelium was irregular and swollen (figure 6J). None of the above-described characteristics were found in the controls (not shown).

Quantification of choriocapillaris endothelial cell fenestrations and measurement of endothelial thickness

In untreated animals, 90.6±9.2 fenestrae were counted per 25 μm endothelial cell length (figure 7A). After ranibizumab treatment, the number of fenestration (mean value±SD) in the choriocapillaris per 25 μm endothelial cell length facing Bruch's membrane was 34.3±1.9 1 day after injection and 23.7±2.2 after 7 days (figure 7B). After aflibercept treatment, the endothelium was incomplete (extremely thin) and the plasma membranes of the endothelial cells were not clearly recognisable (figure 7C). The number of fenestrations was reduced to 21.9 ±22 and 9.5±14 after 1 and 7 days respectively after aflibercept treatment.

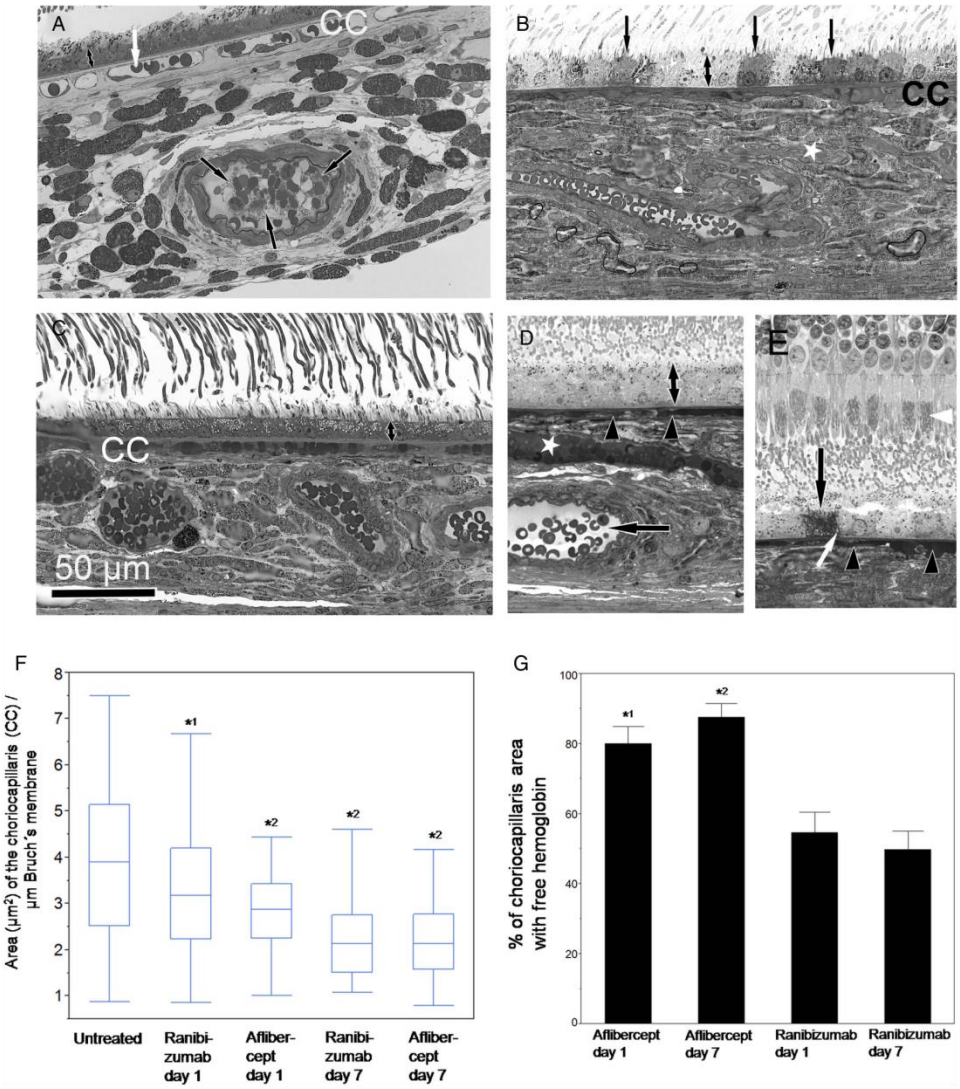

Figure 5 Light microscopy (A–E) and quantification of the choriocapillaris area (F) and of free haemoglobin (G) in ranibizumab and aflibercept-treated eyes 1 and 7 days after injection. (A) Light microscopy of an eye treated with ranibizumab 1 day after injection. The choriocapillaris (CC) contains loosely arranged erythrocytes (white arrow) and open vessel lumina. A deeper choroidal arteriole shows distinct erythrocytes within a wide open vessel lumen but also contact between erythrocytes and thrombocytes leading to fibrin formation (black arrows), as also shown in figure 6A,B at higher magnification. (B) Light microscopy of an eye treated with aflibercept 1 day after injection. The choriocapillaris (CC) and a deeper vessel (asterisk) were homogenously filled with blood cells. Individual dark grey-coloured retinal pigment epithelium (RPE) cells (arrows) were found next to normal pale grey RPE cells indicating RPE cell death as clearly shown in figure 6I. Hypertrophy of the RPE was also observed after aflibercept treatment (double arrow in A vs B). (C) Light microscopy of an eye treated with ranibizumab 7 days after injection. Stasis and haemolysis were occasionally observed in the choriocapillaris (CC). (D,E) Light microscopy of an eye treated with aflibercept 7 days after injection. The choriocapillaris (arrowheads in D and E) and a deeper vessel (asterisk in D) were homogenously filled with blood cells. In a deeper choroidal artery, haemolysis is absent as indicated by normal plasma density (arrow in D). Hypertrophy of RPE was observed (compare double arrow in C vs D) as well as individual dead RPE cells (arrow in E) containing swollen mitochondria (white arrow, see also figure 6I for higher magnification) facing healthy photoreceptors with well-preserved mitochondria (white arrowhead). (F) Quantification of the choriocapillaris area (in μm^2) in semithin sections photographed at a magnification of 600-fold. Results are shown in a box-plot diagram. Application of Dunnett's test demonstrated that the choriocapillaris area was significantly reduced 1 and 7 days after injection of ranibizumab and aflibercept compared with the untreated controls ($^{*1}p=0.01$, $^{*2}p<0.001$). (G) Quantification of the choriocapillaris area (in %) with free haemoglobin. Mean values±SDs are shown. In untreated eyes, free haemoglobin was not observed in the choriocapillaris. Application of Wilcoxon test indicated that the percentage of choriocapillaris area with free haemoglobin was significantly enhanced after aflibercept treatment compared with ranibizumab treatment on days 1 and 7 ($^{*1}p<0.0002$ (day1), $^{*2}p<0.0001$ (day 7)).

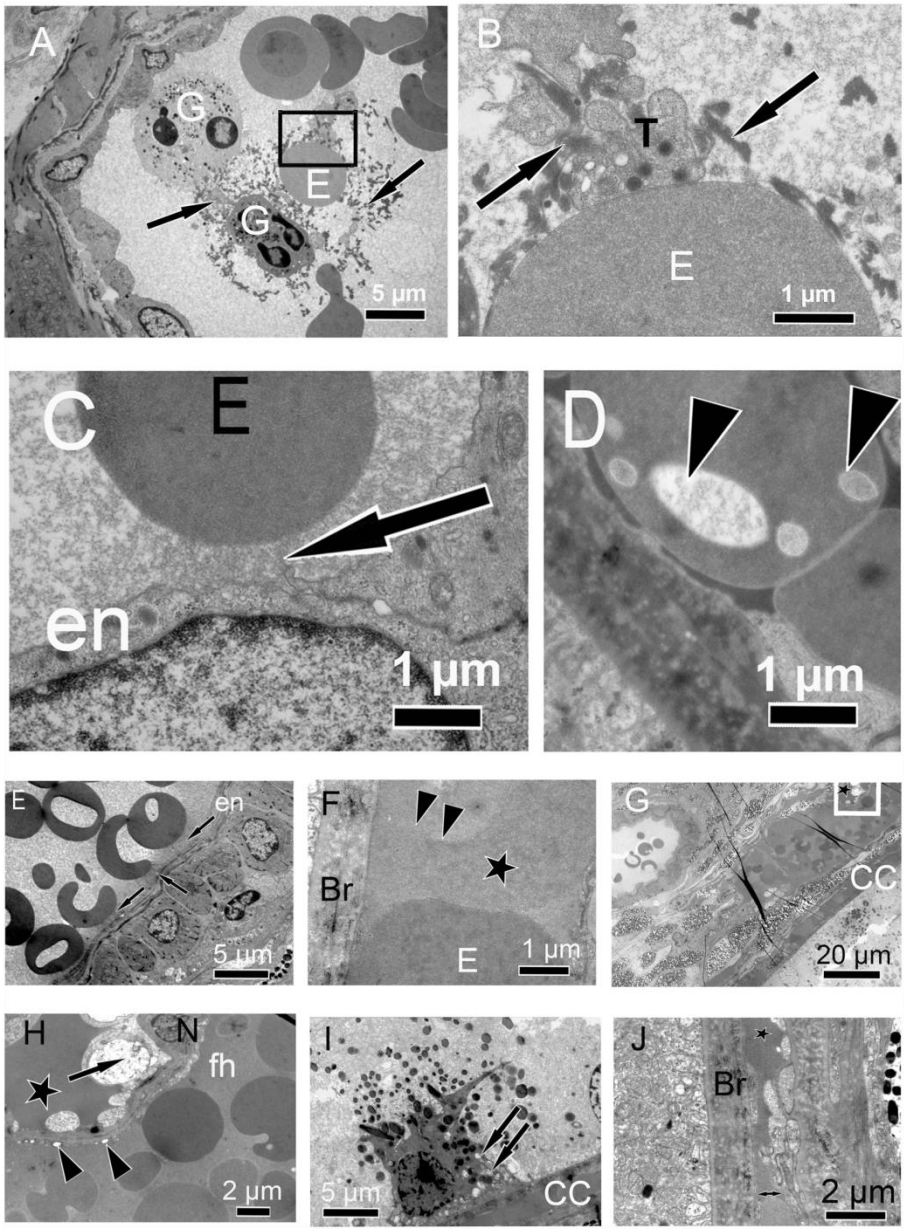

Figure 6 Electron micrographs of eyes injected with ranibizumab (A–D) and aflibercept (E–J). (A) One day after injection of ranibizumab, activated thrombocytes interacted with erythrocytes (E) and granulocytes (G) and were involved in the formation of fibrin (arrows). (B) is a higher magnification of the black square in (A). A clear binding between a thrombocyte (T) and an erythrocyte (E) as well as fibrin (arrows) is shown. (C) Electron-dense material (arrow) is attached to the endothelial wall of a blood vessel (en) and an erythrocyte (E). (D) Eryptosis, as indicated by many holes of different sizes (arrow heads) inside an erythrocyte, is shown. (E) After aflibercept injection, felt-like fibrous material was abundant in choroidal blood vessels. Electron-dense fibrous material is shown attached to the vessel wall between the endothelium (en) and erythrocytes or between erythrocytes (arrows). (F) Haemolysis in the choriocapillaris is visible. The upper erythrocyte is deformed and reveals unusual irregularities in electron density (asterisk) compared with the erythrocyte below (E). The cell membrane is absent to the left of the arrowheads. The Bruch's membrane (Br) is intact. (G) Stasis in the choriocapillaris (CC) is obvious; the erythrocytes are densely packed, filling the entire choriocapillaris lumen. Haemolysis is present in the CC and in a choroidal vein. Extracellular haemoglobin (asterisk) is also seen, and this particular region is shown with a higher magnification in (H). The electron-dense stripes are artificially caused by folds in the section. (H) Free haemoglobin in the plasma (asterisk) and vacuoles (arrow heads) in the endothelium are present, indicating endothelial damage. A nucleus (arrow) of a dead endothelial cell is located close to a nucleus (N) of a healthy smooth muscle cell. Free haemoglobin (fh) is also present within the venule. (I) A retinal pigment epithelium cell is filled with haemoglobin and has swollen mitochondria (arrows) representing a dead cell. (J) Microangiopathy (double arrow) characterised by an irregular and swollen endothelium can be clearly seen. Free haemoglobin (asterisk) is also present. The lumen of this choriocapillaris is collapsed. Bruch's membrane (Br) is electron-dense due to the uptake of free haemoglobin.

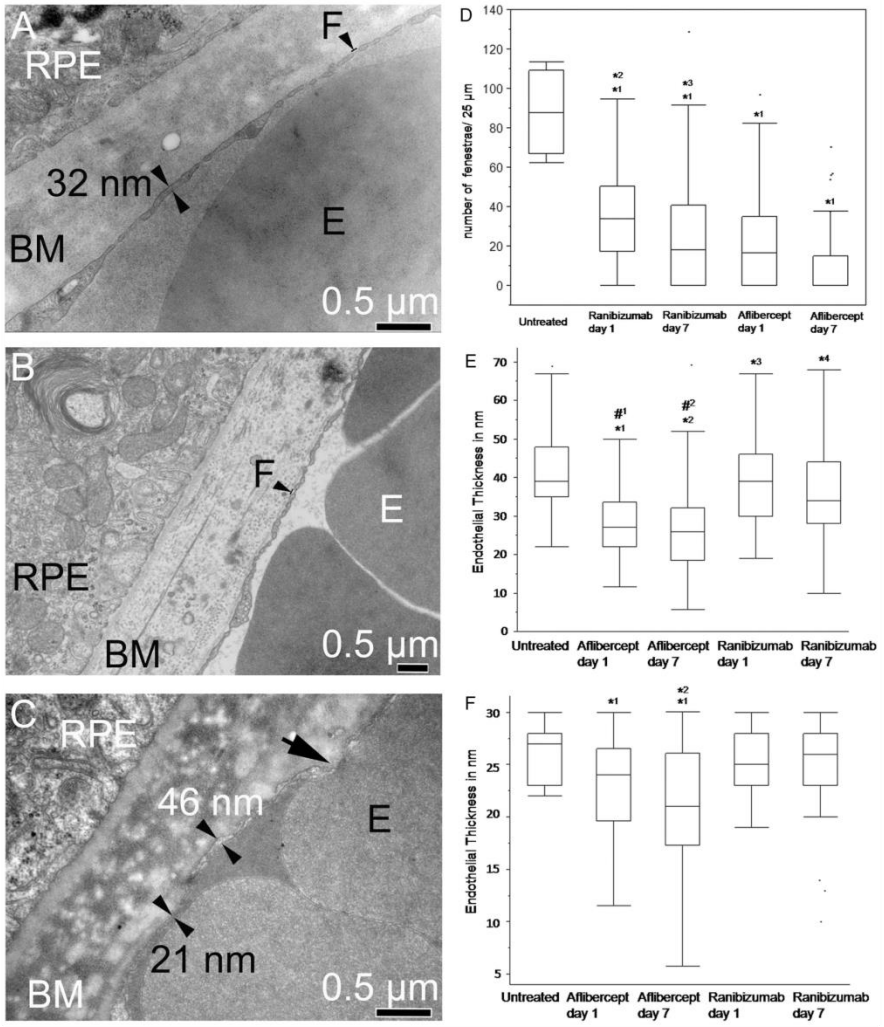

Figure 7 Choriocapillaris endothelial cell fenestrations and endothelial thickness. (A) Electron micrograph of a control animal shows regular and even choriocapillaris endothelium thickness with many fenestrations (F). (B) Electron micrograph of a ranibizumab-treated animal shows normal fenestrations. (C) The electron micrograph of an animal treated with aflibercept shows an extremely thin endothelium (21 nm). The black arrow shows an area where the different membranes from the red blood cell and the endothelium are not identifiable. In contrast, the membranes can be clearly recognised at the sites indicated by the double arrowheads. (D) Quantification of choriocapillaris endothelial cell fenestrations. The number of fenestrations was significantly reduced after treatments with both drugs ($^{*1}p<0.0001$) compared with the controls. Moreover, after aflibercept treatment, the number of fenestrations was significantly reduced compared with ranibizumab treatment on both days ($^{*2}p<0.001$ (day 1), $^{*3}p<0.001$ (day 7)). (E) Measurement of the choriocapillaris wall thickness up to 70 nm. All treated animals show thinner choriocapillaris walls compared with controls ($^{*1}p<0.0001$, $^{*2}p<0.0001$, $^{*3}p=0.03$, $^{*4}p<0.0001$,). Moreover, aflibercept-treated animals also show a significant reduction of the choriocapillaris walls compared with ranibizumab-treated animals ($^{\#1}p<0.0001$, $^{\#2}p<0.0001$). (F) Measurement of the choriocapillaris wall thickness up to 30 nm. While control and ranibizumab-treated animals show similar wall thicknesses, aflibercept-treated animals on days 1 and 7 show severe thinning compared with the control ($^{*1}p<0.04$). The endothelial thickness was also significantly reduced after aflibercept treatment on day 7 compared with day 1 ($^{*2}p=0.02$).

According to the Wilcoxon test, the number of fenestrae was significantly reduced after treatments with both drugs ($p<0.0001$) compared with the controls (figure 7D). The reduction of fenestration was significantly more prominent after aflibercept treatment compared with ranibizumab on both days ($p<0.0001$).

The mean thickness and SD of the endothelial wall in the control was found to be 41.4±10 nm (median 39 nm), whereas it was 38.3±11 nm (median 39 nm) and 36.5±12 nm (median 34 nm) 1 and 7 days after ranibizumab injection and 28.4 ±9 nm (median 27 nm) and 27±11 nm (median 26 nm) 1 and 7 days after aflibercept treatment (figure 7A–C). All treated animals showed significantly decreased vessel wall thicknesses as compared with the control (figure 7E). Aflibercept-treated animals showed even thinner walls than ranibizumab-treated animals ($p<0.0001$).

The vessel thickness that was thinner than 30 nm was investigated separately. Figure 7F shows that controls and animals treated with ranibizumab for 1 or 7 days showed similar thicknesses of 25–26 nm in the mean, while aflibercept-treated animals showed significantly reduced CC thicknesses of 21–23 nm in the mean ($p<0.04$). Moreover, the endothelia of aflibercept-treated animals on day 7 were thinner than those of aflibercept on day 1 ($p=0.02$).

DISCUSSION

A dramatic elevation of the IOP was observed directly after the intravitreal injection of the drugs, but it returned to normal values (between 10 and 20 mm Hg) within 10 min (figure 2). Immediate short-term elevations of the IOP after such injections are a known phenomenon.[25] The main reason for IOP elevation is the sudden addition of fluid to the relatively small volume of the vitreous cavity. Such elevations are usually transient. On days 1 (for ranibizumab) and 7 (for aflibercept) after administration of the drugs, the IOP declined significantly compared with the IOP of untreated animals. However, these reduced IOP values were still normal and they were probably due to both the normal diurnal IOP fluctuation under the influence of repeated anaesthesia induced by intramuscular ketamine, which is known to produce significant IOP declines.[26]

Ophthalmological examinations, including funduscopy, FA and SD-OCT, did not show any pathological effects of drug treatments (figure 1). FA and SD-OCT are non-invasive techniques that permit the in vivo follow-up but present limitations in sensitivity regarding the morphological details compared with histology and particularly electron microscopy. Indeed, only histology with glutaraldehyde-fixed tissues in combination with thin sectioning permitted the detection of all the effects of intravitreally injected ranibizumab and aflibercept on the retina and choroid described in this study and may explain why this kind of 'early' alteration representing the first events of geographic atrophy was never observed in patients. We demonstrated that ranibizumab permeated the retina through intercellular spaces, whereas aflibercept was taken up by neuronal and RPE cells, which contrasts with the belief that aflibercept diffuses through the eye without being metabolised.[3] Aflibercept also induced hypertrophy of the RPE and individual RPE cell death, protein complex formation and more haemolysis, whereas eryptosis was observed after treatment with both drugs (table 1).

The finding that aflibercept-induced protein complex formation is not surprising since it was already found in a high concentration in individual ocular blood vessels 1 day after injection (figure 3E). In the blood vessels, aflibercept can bind to endothelial cells with the endothelial Fc receptor as discussed in the scenario shown in figure 8.

Table 1 Summary of the key effects observed in monkey eyes after intravitreal injection of ranibizumab and aflibercept

	Ranibizumab	Aflibercept
Intracellular uptake in retinal cells	No	Yes
RPE cell death and hypertrophy	No	Yes
Haemolysis	X	XXX
Protein complex formation	No	Yes
Reduction of the choriocapillaris area (CC)	Yes	Yes
Reduction of CC endothelial cell fenestrations	Yes	Yes
Reduction of CC endothelial thickness	X	XXX

RPE, retinal pigment epithelium; X, occasionally seen; XXX, often seen. The difference between X and XXX is statistically significant.

A direct comparison and quantification of the immune reactivity were not possible as distinct antibodies were used for the detection of ranibizumab and aflibercept. The high concentration of both drugs in individual retinal and choroidal vessels can be easily explained by the fact that 50% of intravitreally injected ranibizumab reached the circulation after 2 days[27] and that the half-life of unbound aflibercept is 1–3 days in the blood, whereas VEGF-bound aflibercept has a half-life of 18 days.[3] Moreover, the VEGF concentration in the choriocapillaris must be high in order to maintain the fenestrations. Thus, it is likely that a high concentration of aflibercept as well as ranibizumab and VEGF could coincide in the choriocapillaris in the first days after injection. In previous monkey studies investigating the effect of intravitreally injected bevacizumab,[18 19] protein complexes were also found that were more frequent (figures 5D,E in ref. [18]) than after aflibercept treatment (figure 6D). After ranibizumab, only local densities were occasionally observed (figure 6C). The differences between the three drugs can perhaps be explained in part through the fact that one molecule of bevacizumab can simultaneously bind two VEGF dimers, whereas two ranibizumab molecules can bind one VEGF dimer, and aflibercept can bind VEGF-A and placental growth factor dimers in a 1-to-1 ratio.[3] In the case of bevacizumab, the formation of protein complexes was investigated in vivo and in vitro[20 28] and it was shown that they can result from the binding between VEGF, bevacizumab and heparin (figure 8A). In vitro, the same constellation with ranibizumab instead of bevacizumab did not induce formation of protein complexes.[28] Regarding aflibercept, it is unclear whether the VEGF dimer is completely inside the trap or whether a part of the VEGF dimer is still accessible (figure 8B). If a part of the VEGF dimer is still accessible, heparin can be bound by VEGF via its heparin-binding sites as well as by the Fc fragment of aflibercept[29] leading to protein complex formation. A hypothetical scenario of protein interaction with anti-VEGF drugs is shown in figure 8A–C.

Strong haemolysis in the choriocapillaris and in deeper choroidal vessels as well as the presence of extracellular haemoglobin known to be toxic[30] were other important aspects in which aflibercept differs from ranibizumab and the controls. Ranibizumab-treated eyes showed weaker haemolysis. Aflibercept, like bevacizumab, is produced in Chinese hamster ovary (CHO) cells and therefore contains sugar residues in contrast to ranibizumab, which is produced in *Escherichia coli*. Thus, it is possible that the Fc domain and sugar residues[31 32] of aflibercept (and on bevacizumab[21]) facilitate interference of the VEGF trap with the physiological metabolism or functioning of cells and can result in complement-mediated red blood cell death.

The results of our quantitative analysis of the area occupied by the choriocapillaris show that a single injection of aflibercept as well as ranibizumab induces a measurable reduction in choriocapillaris density. A reduction of the lumina of the choriocapillaris was also found after bevacizumab treatment.[19] This finding is not surprising since VEGF plays a crucial role in the maintenance of the choriocapillaris.[33] The choriocapillaris has been shown to be very vulnerable to VEGF inhibition. Indeed, decreased fenestrations and vessel occlusion were observed after one intravitreal injection of anti-VEGF (bevacizumab) in primate eyes[17] and in this study after one injection of both drugs, but

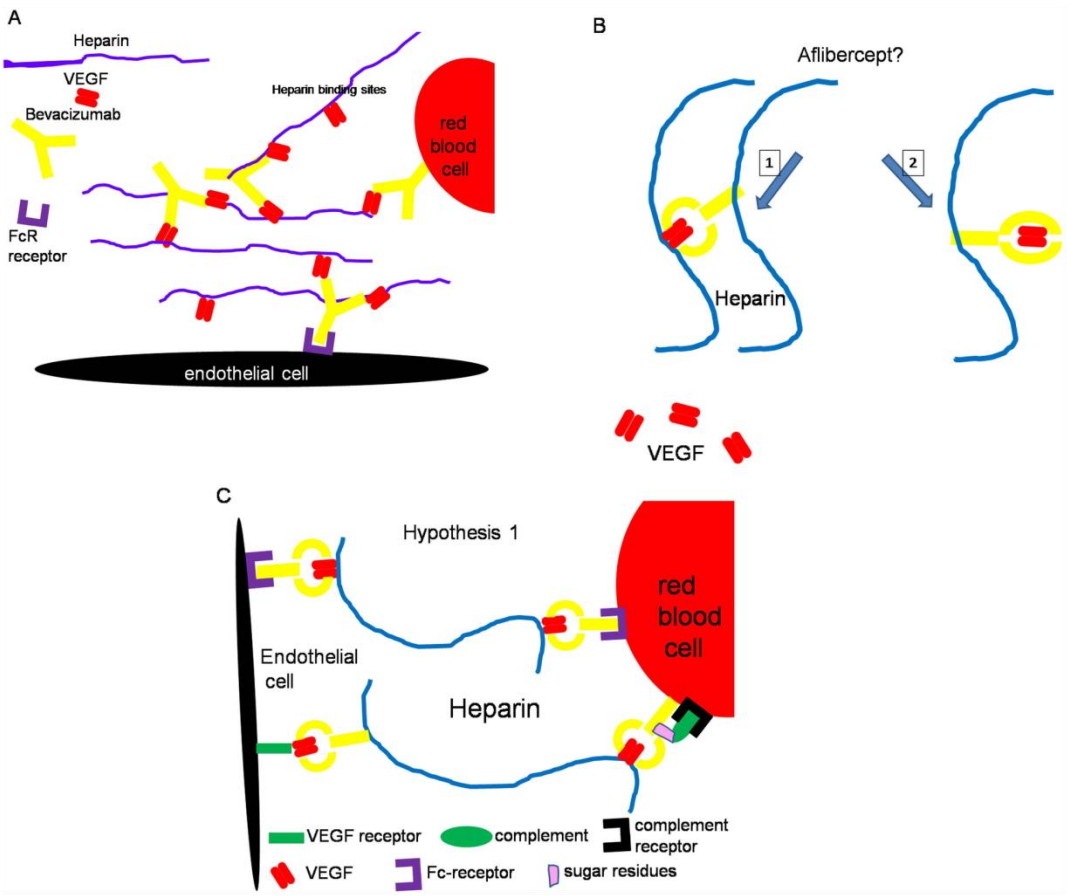

Figure 8 Diagrams depicting proposed mechanisms for formation of protein complexes. (A) Bevacizumab was recently shown to form immune complexes with vascular endothelial growth factor (VEGF) and heparin via the Fcγ receptor and to bind also to endothelial and red blood cells. (B) In the case of aflibercept, it is unclear whether a part of the VEGF dimer is still accessible (hypothesis 1) or whether the VEGF dimer is completely sequestrated inside the VEGF trap (hypothesis 2). The second hypothesis does not account for the formation of protein complexes between endothelial and red blood cells. (C) The first hypothesis permits an explanation of the formation of protein complexes at the interface of red blood cells and endothelial cells involving heparin, VEGF and Fc receptors. VEGF-bound aflibercept can, on the one hand, bind to endothelial cells via interactions between the Fc fragment of aflibercept and the Fc receptor (FcR) present on the surface of endothelial cells, and. on the other hand, through interaction between VEGF and VEGF receptors on the surface of endothelial cells. Moreover, heparin, which binds VEGF and Fc fragments from the endothelial side, can also bind other VEGF from VEGF-bound aflibercept that are attached to the surface of red blood cells, for example, via Fc–FcR interactions[42] and/or via binding between complement and complement receptors.[43] According to hypothesis 2, heparin can only bind to the Fc fragment of aflibercept as no VEGF is accessible.

was particularly prominent after aflibercept treatment. Therefore, it is questionable as to what extent the chronic use of anti-VEGF therapies in the eye may influence the integrity of the choriocapillaris, particularly in the case of aflibercept, which has a higher binding affinity for VEGF-A isoforms in addition to its ability to bind VEGF-B and PlGF.

Besides, it was suggested that decreasing choriocapillaris membrane thickness is responsible for a lower count of fenestrations in anti-VEGF-treated animals. Measurement of the endothelial wall thicknesses of control and anti-VEGF-treated animals yielded a significant decrease in the treated animals compared with the control. This difference was even more obvious when focusing on the areas that were thinner than 30 nm. Here, the aflibercept-treated animals showed distinct thinning compared with all other samples, with aflibercept day 7 reaching a mean value of 21±6 nm. This implies that the two lipid layers of the membrane (each about 10 nm thick) contained no cytoplasmic lumen in these areas (figure 7C). Severe thinning of the apical endothelium is supposed to be the reason for the problems in counting the fenestration in these animals (figure 7C).

Here we show for the first time that both drugs interact particularly with red blood cells of the choriocapillaris. Eryptosis, the suicidal death of erythrocytes, is a well-known phenomenon and characterised by erythrocytes shrinkage, blebbing and phospholipid scrambling of the cell membrane.[34] It can be induced experimentally by IgG antibodies.[35] The milder form of red blood cell damage was observed after both drug treatments, whereas swelling and death of red blood cells indicated by haemolysis and free extravasal haemoglobin were more predominant after aflibercept treatment. We were surprised to

detect so much extravasal haemoglobin, which was at the same level as after bevacizumab treatment.[17] Free haemoglobin is toxic[30] and may have induced the alterations in RPE and endothelial cells. It is likely that the protein-coated and affected erythrocytes were lysed particularly within the choriocapillaris because they were exposed to additional shear stress at this site. Although our results suggest impairment of blood flow in choroidal vessels, we observed healthy photoreceptors, indicated by mitochondria with a well-preserved structure, facing dead RPE cells (figure 5E). It is well known that photoreceptors can perform anaerobic metabolism,[36–40] thus they can survive hypoxic conditions. The retina probably can tolerate slight hypoxic conditions better than being separated from the RPE by subretinal oedema[41] or stressed by intraretinal fluid. Thus, a reduction of blood flow will reduce leakage and reduction of leakage will reduce intraretinal and subretinal oedema formation. The retina can reattach to the RPE or lose intraretinal fluid, and this event improves the function of the retina and subsequently the visual acuity. The disappearance of oedema observed after anti-VEGF therapy is indeed a key event in the improvement of vision.

To summarise, ranibizumab and aflibercept reduced the lumen of the choriocapillaris in the same manner. Haemolysis and microangiopathy were more pronounced after aflibercept treatment, whereas formation of protein complexes as well as RPE hypertrophy, and cell death, which represents the first event of geographic atrophy, was only observed after aflibercept treatment. From a theoretical point of view, it is not an advantage that aflibercept has an Fc fragment because it may cause unpredictable reactions with other molecules and cells. The clinical significance and relation of these findings to the Fc domain or to other characteristics of aflibercept remain to be investigated.

Correction notice This article has been corrected since it was published Online First. In Table 1, the 'Reduction of CC endothelial cell fenestrations' row, 'Aflibercept' column, this has been amended to 'Yes'.

Acknowledgements The authors thank Sigrid Schultheiss for excellent technical assistance.

Contributors No contributors.

Funding This study was supported by a research grant from Novartis Pharma GmbH.

Competing interests The study was supported by Novartis Pharma AG.

Provenance and peer review Not commissioned; externally peer reviewed.

REFERENCES

1 Ferris FL 3rd, Fine SL, Hyman L. Age-related macular degeneration and blindness due to neovascular maculopathy. *Arch Ophthalmol* 1984;102:1640–2.
2 D'Amato RJ, Adamis AP. Angiogenesis inhibition in age-related macular degeneration. *Ophthalmology* 1995;102:1261–2.
3 Stewart MW. Clinical and differential utility of VEGF inhibitors in wet age-related macular degeneration: focus on aflibercept. *Clin Ophthalmol* 2012;6:1175–86.
4 Kliffen M, Sharma HS, Mooy CM, *et al*. Increased expression of angiogenic growth factors in age-related maculopathy. *Br J Ophthalmol* 1997;81:154–62.
5 Ryan SJ. Subretinal neovascularization. Natural history of an experimental model. *Arch Ophthalmol* 1982;100:1804–9.
6 Yi X, Ogata N, Komada M, *et al*. Vascular endothelial growth factor expression in choroidal neovascularization in rats. *Graefes Arch Clin Exp Ophthalmol* 1997;235:313–19.
7 Baffi J, Byrnes G, Chan CC, *et al*. Choroidal neovascularization in the rat induced by adenovirus mediated expression of vascular endothelial growth factor. *Invest Ophthalmol Vis Sci* 2000;41:3582–9.
8 Spilsbury K, Garrett KL, Shen WY, *et al*. Overexpression of vascular endothelial growth factor (VEGF) in the retinal pigment epithelium leads to the development of choroidal neovascularization. *Am J Pathol* 2000;157:135–44.
9 Wang F, Rendahl KG, Manning WC, *et al*. AAV-mediated expression of vascular endothelial growth factor induces choroidal neovascularization in rat. *Invest Ophthalmol Vis Sci* 2003;44:781–90.
10 Lebherz C, Maguire AM, Auricchio A, *et al*. Nonhuman primate models for diabetic ocular neovascularization using AAV2-mediated overexpression of vascular endothelial growth factor. *Diabetes* 2005;54:1141–9.
11 Papadopoulos N, Martin J, Ruan Q, *et al*. Binding and neutralization of vascular endothelial growth factor (VEGF) and related ligands by VEGF Trap, ranibizumab and bevacizumab. *Angiogenesis* 2012;15:171–85.
12 Chong V. Biological, preclinical and clinical characteristics of inhibitors of vascular endothelial growth factors. *Ophthalmologica* 2012;227(Suppl 1):2–10.
13 Browning DJ, Kaiser PK, Rosenfeld PJ, *et al*. Aflibercept for age-related macular degeneration: a game-changer or quiet addition? *Am J Ophthalmol* 2012;154:222–6.
14 Ferrara N, Damico L, Shams N, *et al*. Development of ranibizumab, an anti-vascular endothelial growth factor antigen binding fragment, as therapy for neovascular age-related macular degeneration. *Retina* 2006;26:859–70.
15 Ohr M, Kaiser PK. Aflibercept in wet age-related macular degeneration: a perspective review. *Ther Adv Chronic Dis* 2012;3:153–61.
16 Heiduschka P, Fietz H, Hofmeister S, *et al*. Penetration of bevacizumab through the retina after intravitreal injection in the monkey. *Invest Ophthalmol Vis Sci* 2007;48:2814–23.
17 Peters S, Heiduschka P, Julien S, *et al*. Ultrastructural findings in the primate eye after intravitreal injection of bevacizumab. *Am J Ophthalmol* 2007;143:995–1002.
18 Schraermeyer U, Julien S. Effects of bevacizumab in retina and choroid after intravitreal injection into monkey eyes. *Expert Opin Biol Ther* 2013;13:157–67.
19 Schraermeyer U, Julien S. Formation of immune complexes and thrombotic microangiopathy after intravitreal injection of bevacizumab in the primate eye. *Graefes Arch Clin Exp Ophthalmol* 2012;250:1303–13.
20 Meyer T, Robles-Carrillo L, Robson T, *et al*. Bevacizumab immune complexes activate platelets and induce thrombosis in FCGR2A transgenic mice. *J Thromb Haemost* 2009;7:171–81.
21 Meyer CH, Holz FG. Preclinical aspects of anti-VEGF agents for the treatment of wet AMD: ranibizumab and bevacizumab. *Eye (Lond)* 2011;25:661–72.
22 Daha NA, Banda NK, Roos A, *et al*. Complement activation by (auto-) antibodies. *Mol Immunol* 2011;48:1656–65.
23 Nguyen DC, Scinicariello F, Attanasio R. Characterization and allelic polymorphisms of rhesus macaque (Macaca mulatta) IgG Fc receptor genes. *Immunogenetics* 2011;63:351–62.
24 Hall CE, Slayter HS. The fibrinogen molecule: its size, shape, and mode of polymerization. *J Biophys Biochem Cytol* 1959;5:11–16.
25 Mojica G, Hariprasad SM, Jager RD, *et al*. Short-term intraocular pressure trends following intravitreal injections of ranibizumab (Lucentis) for the treatment of wet age-related macular degeneration. *Br J Ophthalmol* 2008;92:584.
26 Bunch TJ, Tian B, Seeman JL, *et al*. Effect of daily prolonged ketamine anesthesia on intraocular pressure in monkeys. *Curr Eye Res* 2008;33:946–53.
27 Gaudreault J, Fei D, Rusit J, *et al*. Preclinical pharmacokinetics of Ranibizumab (rhuFabV2) after a single intravitreal administration. *Invest Ophthalmol Vis Sci* 2005;46:726–33.
28 Julien S, Biesemeier A, Schraermeyer U. In vitro induction of protein complexes between bevacizumab, VEGF-A165 and heparin: explanation for deposits observed on endothelial veins in monkey eyes. *Br J Ophthalmol* 2013;97:511–17.
29 Levy DE, Horner AA, Solomon A. Immunoglobulin-sulfated polysaccharide interactions. Binding of agaropectin and heparin by human IgG proteins. *J Exp Med* 1981;153:883–96.
30 Schaer DJ, Buehler PW, Alayash AI, *et al*. Hemolysis and free hemoglobin revisited: exploring hemoglobin and hemin scavengers as a novel class of therapeutic proteins. *Blood* 2013;121:1276–84.
31 Malaise MG, Franchimont P, Mahieu PR. The ability of normal human monocytes to phagocytose IgG-coated red blood cells is related to the number of accessible galactosyl and mannosyl residues in the Fc domain of the anti-red blood cell IgG antibody molecules. *J Immunol Methods* 1989;119:231–9.
32 Forthal DN, Gach JS, Landucci G, *et al*. Fc-glycosylation influences Fcgamma receptor binding and cell-mediated anti-HIV activity of monoclonal antibody 2G12. *J Immunol* 2010;185:6876–82.
33 Saint-Geniez M, Kurihara T, Sekiyama E, *et al*. An essential role for RPE-derived soluble VEGF in the maintenance of the choriocapillaris. *Proc Natl Acad Sci USA* 2009;106:18751–6.
34 Lang F, Qadri SM. Mechanisms and significance of eryptosis, the suicidal death of erythrocytes. *Blood Purif* 2012;33:125–30.
35 Attanasio P, Shumilina E, Hermle T, *et al*. Stimulation of eryptosis by anti-A IgG antibodies. *Cell Physiol Biochem* 2007;20:591–600.
36 Hsu SC, Molday RS. Glycolytic enzymes and a GLUT-1 glucose transporter in the outer segments of rod and cone photoreceptor cells. *J Biol Chem* 1991;266:21745–52.
37 Nihira M, Anderson K, Gorin FA, *et al*. Primate rod and cone photoreceptors may differ in glucose accessibility. *Invest Ophthalmol Vis Sci* 1995;36:1259–70.
38 Fliesler SJ, Richards MJ, Miller CY, *et al*. In vitro metabolic competence of the frog retina: effects of glucose and oxygen deprivation. *Exp Eye Res* 1997;64:683–92.

39 Winkler BS, Dang L, Malinoski C, *et al*. An assessment of rat photoreceptor sensitivity to mitochondrial blockade. *Invest Ophthalmol Vis Sci* 1997;38:1569–77.
40 Zak PP, Kapustina NV, Ostrovskii MA. [High resistance of the rat retina rods to hypoxia]. *Ross Fiziol Zh Im I M Sechenova* 2001;87:1534–9.
41 Keane PA, Patel PJ, Liakopoulos S, *et al*. Evaluation of age-related macular degeneration with optical coherence tomography. *Surv Ophthalmol* 2012;57:389–414.
42 Horn S, Bashan N, Gopas J. Phagocytosis of phenylhydrazine oxidized and G-6-PD-deficient red blood cells: the role of cell-bound immunoglobulins. *Blood* 1991;78:1818–25.
43 Taylor RP, Horgan C, Hooper M, *et al*. Dynamics of interaction between complement-fixing antibody/dsDNA immune complexes and erythrocytes. In vitro studies and potential general applications to clinical immune complex testing. *J Clin Invest* 1985;75:102–11.

3.3.2 The effects of VEGF-A-inhibitors aflibercept and ranibizumab on the ciliary body and iris of monkeys.

Authors: Ludinsky M.*, Christner S.*, Su N., Taubitz T., Tschulakow A., Biesemeier A., Julien-Schraermeyer S., Schraermeyer U.

*Maximilian Ludinsky and Sarah Christner are both first authors.

Published in *Graefe's archive for clinical and experimental ophthalmology* in 2016

DOI: 10.1007/s00417-016-3344-8

Declaration of own contributions:

The manuscript was planned by Prof. Dr. Ulrich Schraermeyer and PD Dr. Sylvie Julien-Schraermeyer. Experimental procedures and data acquisition were performed by Maximilian Ludinsky, Nan Su and me, I performed the sample preparation (tissue preparation, embedding and sectioning). Data was analysed by Maximilian Ludinsky, Dr. Sarah Christner, Nan Su, Dr. Alexander Tschulakow and Prof. Dr. Schraermeyer. The manuscript was written by Maximilian Ludinsky, Dr. Sarah Christner and Nan Su. I proof-read the manuscript with the other authors and performed the revision in collaboration with Maximilian Ludinsky, Dr. Sarah Christner, PD Dr. Antje Biesemeier and PD Dr. Sylvie Julien-Schraermeyer.

Graefes Arch Clin Exp Ophthalmol
DOI 10.1007/s00417-016-3344-8

BASIC SCIENCE

The effects of VEGF-A-inhibitors aflibercept and ranibizumab on the ciliary body and iris of monkeys

Maximilian Ludinsky[1] · Sarah Christner[1] · Nan Su[1] · Tatjana Taubitz[1] · Alexander Tschulakow[1] · Antje Biesemeier[1] · Sylvie Julien-Schraermeyer[1] · Ulrich Schraermeyer[1,2]

Received: 3 December 2015 / Revised: 28 March 2016 / Accepted: 4 April 2016
© Springer-Verlag Berlin Heidelberg 2016

Abstract
Purpose To investigate the effects of intravitreal ranibizumab (Lucentis®) and aflibercept (Eylea®) on the ciliary body and the iris of 12 cynomolgus monkeys with regard to the fenestrations of their blood vessels.
Materials and methods Structural changes in the ciliary body and in the iris were investigated with light, fluorescent, and transmission electron microscopy (TEM). The latter was used to specifically quantify fenestrations of the endothelium of blood vessels after treatment with aflibercept and ranibizumab. Each of the two ciliary bodies treated with aflibercept and the two treated with ranibizumab and their controls were examined after 1 and 7 days respectively. Ophthalmological investigations including funduscopy and intraocular pressure measurements were also applied.
Results Ophthalmological investigations did not reveal any changes within the groups. Both drugs reduced the VEGF concentration in the ciliary body pigmented epithelium. The structure of the ciliary body was not influenced, while the posterior pigmented epithelium of the iris showed vacuoles after aflibercept treatment. Ranibizumab was mainly concentrated on the surface layer of the ciliary epithelium, in the blood vessel walls and the lumen of some of the blood vessels, and in the cells of the epithelium of the ciliary body. Aflibercept was more concentrated in the stroma and not in the cells of the epithelium, but as with ranibizumab, also in the blood vessel walls and some of their lumina, and again on the surface layer of the epithelium. Both aflibercept-and ranibizumab-treated eyes showed a decreased number of fenestrations of the capillaries in the ciliary body compared to the untreated controls. On day 1 and day 7, aflibercept had fewer fenestrations than the ranibizumab samples of the same day.
Conclusions Both aflibercept and ranibizumab were found to reach the blood vessel walls of the ciliary body, and effectively reduced their fenestrations. Aflibercept might eliminate VEGF to a greater extent, possibly due to a higher elimination of fenestrations in a shorter time. Moreover, the vacuoles found in the iris need further research, in order to evaluate whether they carry a possible pathological potential.

Keywords Aflibercept · Ranibizumab · Anti-VEGF therapy · Ciliary body · Iris · Fenestration · Blood vessels · Electron microscopy

Introduction

Anti-vascular endothelial growth factor (VEGF) therapy is currently used to treat uncontrolled neovascularisation in the eye, e.g., with age-related macular degeneration (AMD), diabetic macular oedema or retinal vein occlusion [1], glaucoma [2], iris rubosis [3], and others [4, 5]. Especially for the treatment of wet AMD, four different VEGF inhibitors are available and delivered by intravitreal injections: ranibizumab (Lucentis®), aflibercept (Eylea®), pegaptanib (Macugen®) and for off-label use, bevacizumab (Avastin®) [6]. The effects of these therapies on the retina have meanwhile been studied quite thoroughly. The decrease of fenestrations in the choriocapillaris [7–9] of monkeys treated with ranibizumab, bevacizumab, or aflibercept respectively was remarkable. However, the effects of intravitreal ranibizumab and

Maximilian Ludinsky and Sarah Christner are first authors.

✉ Ulrich Schraermeyer
ulrich.schraermeyer@med.uni-tuebingen.de; http://www.ocutox.de

[1] Section of Experimental Vitreoretinal Surgery, Centre for Ophthalmology, Schleichstrasse 12/1, 72076 Tuebingen, Germany

[2] STZ OcuTox Preclinical Drug Assessment, Hechingen, Germany

Published online: 22 April 2016

Reprinted by permission from Springer Nature Customer Service Centre GmbH: Springer, Graef Arch Clin Exp, The effects of VEGF-A-inhibitors aflibercept and ranibizumab on the ciliary body and iris of monkeys, Ludinsky et al., 2016

aflibercept on other ocular tissues like the ciliary body have not yet been studied, and will be presented in this work.

The ciliary body is located right behind the iris, and is nourished by the same blood vessels which also nourish the iris. It consists of smooth muscle fibers and the ciliary processes, which are connected by zonular fibers to the crystalline lens, and are thus able to change the latter's shape for the purpose of focusing, a process known as accommodation [10]. The epithelium of the ciliary processes consists of a pigmented outside layer and a non-pigmented inside layer, connected by gap-junctions. It is this structure which releases a transparent liquid into the eye called the aqueous humour, whose in- and outflow maintains the intraocular eye pressure (IOP). In the ciliary processes, there are lots of fenestrated capillaries whose fenestrations are permeable for water and smaller hydrophilic structures [11]. It has already been shown that VEGF blockade can also reduce the number of fenestrations in the ciliary body [12].

The VEGF family is important for lymphangiogenesis, vasculogenesis, and angiogenesis [13]. The mammalian VEGF family presently contains five members: VEGF-A, placenta growth factor (PlGF), VEGF-B, VEGF-C, and VEGF-D (reviewed by [14]). VEGF-A plays an important role in vascular development and in diseases involving abnormal growth of blood vessels. Clinical studies have shown the significance of VEGF-A in ocular neovascularization, such as diabetic retinopathy and age-related macular degeneration, with the use of VEGF-A neutralizing antibodies [15]. VEGF is a glycosylated, multifunctional cytokine which consists of dimeric polypeptides, and executes its effects through receptors mainly expressed on the vascular endothelium. It also stimulates lymphocyte activation and chemotaxis, and increases microvascular permeability [16].

In previous studies, our group investigated the effects of bevacizumab [17], ranibizumab, and aflibercept [8] on the retina–choroid interface of cynomolgus monkeys. Systemical effects of aflibercept and ranibizumab were studied by also analysing the kidneys of these animals [18]. The same monkeys were used in this work to investigate the effects of aflibercept and ranibizumab on the ciliary body, and in particular on the fenestrations of the capillaries of the same individuals.

Materials and methods

Animals and study protocol

In this study, we used new tissue samples taken from the same monkeys we had used in a previous study to investigate the effects of intravitreal ranibizumab and aflibercept on the retina-choroid complex [8]. The materials and methods applied in vivo are thus repeated here as follows.

Twelve cynomolgus monkeys (*Macaca fascicularis*, aged 3 to 10 years) were raised at the Covance Laboratories (Muenster, Germany) under standard conditions. The monkeys in this study were an average of 5.5 years old for the aflibercept group, and an average of 6.5 years old for the ranibizumab group. Animals were housed and handled in strict accordance with good animal practice under supervision of veterinarians, and were monitored for evidence of disease and changes in attitude, appetite, or behaviour suggestive of illness. Handling and housing of the animals at Covance Laboratories GmbH was done in accordance with the German Animal Welfare Act. For the notice of approval by the appropriate institutional animal care and use committee, please see Covance Studies 8260977 and 8274007.

Intravitreal injection of ranibizumab, aflibercept, and aflibercept vehicle

The animals were sedated by intramuscular injection of medetomidine (Domitor) and ketamine hydrochloride. Before injection, the eyes were examined for any signs of inflammation. Pupils were dilated (mydriasis with 1 % tropicamide) and anesthetized (proxymetacaine; Proparakain-pos 0.5 %; Ursapharm). The conjunctival and corneal surface was disinfected (povidone–iodine 10 %). After sterile coating and insertion of a lid speculum, 50 µl of ranibizumab (10 mg/ml), aflibercept (40 mg/ml) and aflibercept vehicle (10 mM sodium phosphate, 40 mM sodium chloride, 0.03 % polysorbate 20, and 5 % sucrose, pH 6.2) were intravitreally injected using a 27-gauge canula. When removing the syringe, the injection site was compressed with forceps to prevent reflux. A topical antibiotic (gentamicin) was administered. Animals were monitored for signs of inflammation until sacrificed.

Ophthalmic examinations

For all ophthalmic examinations, a mydriatic agent (tropicamide) and a local ophthalmic anaesthetic (proxymetacaine) were instilled in the eyes of the sedated animals before examination.

Funduscopy and fluorescein angiography (FA)

Fundus photographs and FA were obtained for all animals once during the pre-dose phase and on the day of necropsy. For FA, an indwelling catheter was inserted and fluorescein was injected intravenously. A series of images immediately after injection and 10 min thereafter was performed. The equipment used was a digital stationary fundus camera (TRC-50 ex; Topcon, Tokyo, Japan).

Reprinted by permission from Springer Nature Customer Service Centre GmbH: Springer, Graef Arch Clin Exp, The effects of VEGF-A-inhibitors aflibercept and ranibizumab on the ciliary body and iris of monkeys, Ludinsky et al., 2016

Spectral-domain optical coherence tomography (SD-OCT)

SD-OCT was obtained for all animals once during the pre-dose phase, directly after injection (only for aflibercept and its vehicle) and on the day of necropsy. The equipment used was Spectralis™ HRA + OCT (Heidelberg Engineering, Heidelberg, Germany).

Intraocular pressure (IOP)

Measurement of IOP was performed in all animals once during the pre-dose phase, before administration of the drugs, directly after administration, 10 min after administration and on the day of necropsy by using TonoVet® (Kruuse, Langeskov, Denmark). Two readings were obtained per eye for each time point, and the mean IOP value was calculated and reported in millimetres of mercury (mm Hg).

Enucleation and post mortem analyses

On days 1 and 7 after intravitreal injection, the animals were sacrificed under general anaesthesia, i.e., intramuscular injection of ketamine hydrochloride followed by an intravenous sodium pentobarbitone (Lethabarb®, Virbac, Australia) overdose. The eyes were enucleated 5 min post-mortem and cleaned of orbital tissue, and were slit carefully at the limbus without damaging the ora serrata. Then 25 µl of the fixative were carefully injected into the vitreous before the eyes were fixed at 4 °C by immersion into 5 % glutaraldehyde in 0.1 M cacodylate buffer (pH 7.4, Sigma, St. Louis, MO, USA) overnight for electron microscopy or into 4 % formalin in PBS (Carl Roth, Karlsruhe, Germany) for immunohistochemistry. The eyes of three healthy monkeys without treatment, or with infection of aflibercept vehicle, were handled in the same manner.

Immunohistochemistry with paraffin embedded sections

Enucleated eyes were fixed in formalin, embedded in paraffin wax, cut into 4-µm sections and deparaffinised according to standard procedures.

Localisation of drug in the ciliary body (fluorescence microscopy)

Ranibizumab and aflibercept were detected respectively using a goat antiserum to human Fab of IgG (GAHu/Fab/7S, dilution 1:250; Nordic Immunological Laboratories, Tilburg, The Netherlands) and a goat anti-human IgG-Fc antibody (NB7446, dilution 1:200, Novus Biologicals Europe, Cambridge, UK), each with a cy3-rabbit anti-goat antibody as a secondary antibody (305-167-003, dilution 1:400, Jackson ImmunoResearch Europe, Suffolk, UK). Stained sections were embedded (FluorSave; Calbiochem, La Jolla, CA, USA) and inspected with a fluorescence microscope (Axioplan2; Carl Zeiss, Oberkochen, Germany).

Localisation of VEGF in the ciliary body (light microscopy)

Monoclonal mouse anti-human vascular endothelial growth factor, Clone VG1, which labels the VEGF-165, VEGF-121, and VEGF-189 isoforms of vascular endothelial growth factor (DakoCytomation Denmark, Code No.M7273), dilution 1:150, was used as a first antibody and detected with REAL™ Detection System, Alkaline Phosphatase/RED, Rabbit/Mouse(Code k5005,Dako), dilution 1:25 and inspected with a light microscope (Axioskop; Carl Zeiss, Oberkochen, Germany).

Light and electron microscopy (LM and EM) of plastic sections from the ciliary body

Glutaraldehyde fixed specimens were post-fixed with 1 % OsO_4 at room temperature in 0.1 M cacodylate buffer (pH 7.4), stained with uranyl acetate, and embedded in Epon after dehydration in a graded series of ethanol and propylene oxide. Semi-thin sections were stained with toluidine blue and examined by light microscopy (Zeiss Axioplan2 imaging, Zeiss, Jena, Germany). For electron microscopy, the sections were cut ultrathin and analysed with a Zeiss 900 electron microscope (Zeiss, Jena, Germany). For every eye at each time point (days 1 to 7 and control), two different regions of interest were chosen. One piece of tissue was taken in which both ciliary body and iris were visible.

Quantification of the endothelial fenestration in the ciliary body

A transmission electron microscope was used for counting the fenestrations per µm of endothelium in the ciliary body. The ciliary bodies were investigated for blood vessels, which were photographed. Depending on the size of the blood vessels, lower magnifications from 1,100× up to 7,000× were used so that the whole blood vessel could be seen on the image and the length of its endothelium could be measured (Fig. 1). For counting the fenestrations, images of the fenestrated parts of the endothelium were taken at 20,000× magnification (Fig. 2). For quantification of the length of endothelium and of fenestrae, image analysis software (iTEM, Olympus Soft Imaging Solutions, Muenster, Germany) was used.

Semi-quantification of VEGF staining in the ciliary body

From each specimen, one eye was investigated for VEGF analysis (two samples per time point). One section was analysed for each eye. Each section was photographed at

Reprinted by permission from Springer Nature Customer Service Centre GmbH: Springer, Graef Arch Clin Exp, The effects of VEGF-A-inhibitors aflibercept and ranibizumab on the ciliary body and iris of monkeys, Ludinsky et al., 2016

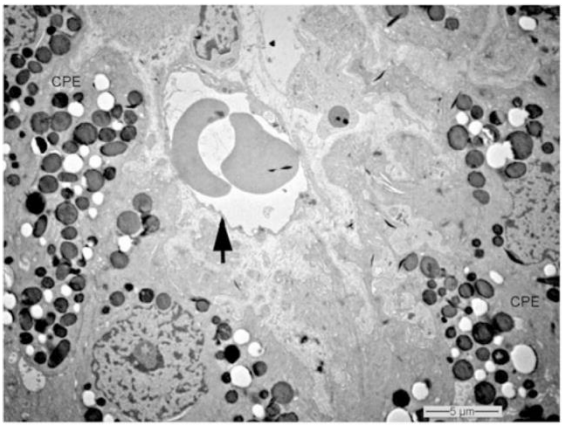

Fig. 1 Overview of a blood vessel (*black arrow* indicates vessel wall) in the ciliary body treated with aflibercept on day 1; TEM, magnification ×3,000; *CPE* ciliary pigmented epithelium

630-fold magnification, using a Zeiss Axioscope light microsope with AxioVision software.

For each section, four photos were taken, which almost covered the whole pigmented epithelium of the ciliary body. So for every sample, eight photos were analysed.

Statistical analysis

Whole blood vessels were investigated for endothelial length and number fenestrations. As vessels always show a fenestrated area and a non-fenestrated area, fenestrations were normalized to fenestrations/10 μm of fenestrated endothelium. Statistical significance for the comparison of aflibercept and ranibizumab to the controls was determined by using the Dunnett's test and the JMP10 statistical program (SAS, Heidelberg, Germany). $P<0.05$ was considered statistically significant.

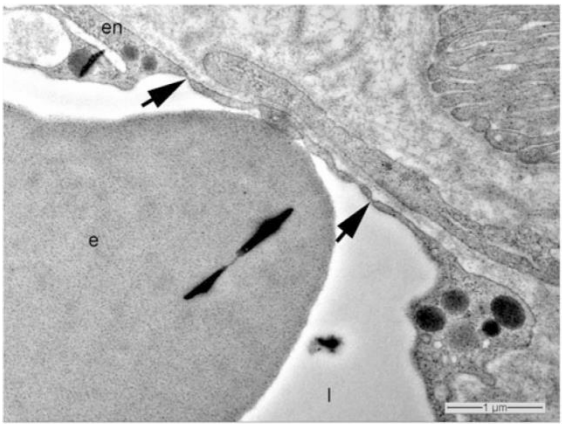

Fig. 2 Detail of endothelium with fenestrations (*black arrows*), aflibercept day 1. TEM, magnification ×20,000; *e* erythrocyte, *en* endothelium, *l* lumen

To quantify the staining in the pigmented epithelium of the ciliary body we used the "colour cube based" function in the Image-Pro Plus software. Statistical testing was performed using JMP10 software as described above.

Results

Ophthalmic examinations (FA, SD-OCT, IOP)

The results from the in-vivo ophthalmological examinations have already been published [8]. In brief, FA and SD-OCT analyses did not show any drug-related changes. The intraocular pressure (IOP), baseline 10–20 mm Hg, was raised immediately after intravitreal injection up to 31 ± 14 mm Hg in the ranibizumab-treated group, and up to 50 ± 12 mm Hg in the aflibercept-treated group. Both regained normal levels after 10 min (ranibizumab 19 ± 6 mm Hg, aflibercept 14 ± 3 mm Hg) and further stabilized after day 1 (ranibizumab 10 ± 1 mm Hg, aflibercept 11 ± 7 mm Hg) and day 7 (ranibizumab 19 ± 4 mm Hg, aflibercept 10 ± 3 mm Hg).

Localisation of drug in the ciliary body (fluorescence immunohistochemistry)

The distribution of aflibercept and ranibizumab within the different structures of the ciliary body were not different; however, the staining of aflibercept was a bit stronger (data not shown). The aflibercept-treated ciliary bodies were intensively stained in the walls of blood vessels, also including the lumen of some, but not all, of these blood vessels. Further staining was detectable on the surface layer of the epithelium and in the connective tissues surrounding the vascular plexus. The ciliary muscle tissue was more weakly stained, as was the cytoplasm of the epithelium, but not their nuclei. The ranibizumab-treated ciliary bodies showed a staining similar to the aflibercept ciliary bodies, on the surface layer of the epithelium and the walls of blood vessels including some of their lumina. The ciliary muscle and the vascular layer were also stained more weakly. We did also not find any significant changes in the distribution of staining between day 1 and day 7 samples.

Localisation of VEGF in the ciliary body (light microscopical immunohistochemistry)

In the paraffin-embedded samples, no histological changes were detected in the ciliary body after intravitreal aflibercept and ranibizumab as compared to the controls.

Within the pigmented epithelium of the ciliary body, all samples were checked for their amount of VEGF using immunohistochemistry. The pigmented epithelium of the ciliary body of untreated monkeys was intensely stained, while both

Reprinted by permission from Springer Nature Customer Service Centre GmbH: Springer, Graef Arch Clin Exp, The effects of VEGF-A-inhibitors aflibercept and ranibizumab on the ciliary body and iris of monkeys, Ludinsky et al., 2016

aflibercept- and ranibizumab-treated groups showed less VEGF immunoreactivity at all time points (Fig. 3; all p values <0.0001). VEGF levels of samples treated with ranibizumab or aflibercept did not change after day 1 or 7 respectively.

Structural changes in ciliary body and iris (LM and EM of plastic sections)

Investigating the semi-thin sections of whole eye preparations in the light microscope did not show any significant changes in the ciliary body. However, since the iris was shown in the same sections and did show differences between aflibercept- and ranibizumab-treated samples, it was analysed as well using both light and electron microscopy (Fig. 4). In all aflibercept-treated samples, clearly visible vacuoles showed up throughout the posterior pigmented epithelium of the iris as shown in Fig. 4b and c. Neither the controls nor the ranibizumab-treated samples showed these vacuoles in either light or electron microscopical evaluations. The vacuoles in the iris in the aflibercept group showed up on day 1 and did not appear to change in the samples taken at day 7.

The transition zone between the pigmented iris epithelium and the unpigmented ciliary epithelium was evaluated as well, and didn't show pathological changes in any of the samples. We also couldn't find any other ultrastructural alterations in the area covering the iris and ciliary body.

Quantification of fenestrations in blood vessels of the ciliary body (EM)

The fenestrations of the endothelium decreased in all aflibercept- as well as in all ranibizumab-treated samples compared to controls. On day 1, the aflibercept samples had an average fenestration rate of 2.7 per 10 μm of endothelium, and

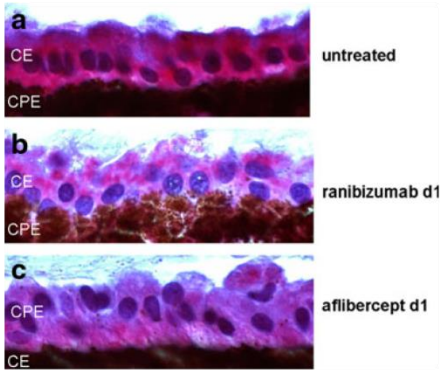

Fig. 3 Reduction of VEGF staining (*red*) after treatment with ranibizumab and aflibercept. Light micrographs of (**a**) untreated control eye (**b**) eye treated with ranibizumab on day 1 (**c**) eye treated with aflibercept on day 1; *CE* ciliary unpigmented epithelium, *CPE* ciliary pigmented epithelium

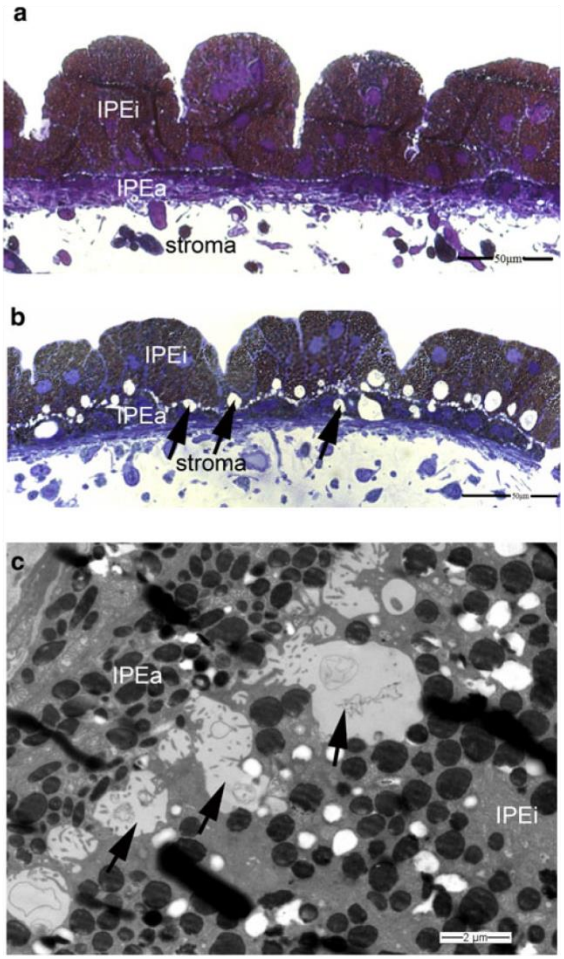

Fig. 4 Effect of ranibizumab (**a**) and aflibercept (**b**, **c**) on the iris pigmented epithelium. **a** Ranibizumab-treated iris day 7 without vacuoles. Semi-thin section, light microscope, magnification ×100. **b** Aflibercept-treated iris day 1 showing vacuoles between the pigment cells (*black arrows*). Semi-thin section, light microscope, magnification ×100. **c** Aflibercept-treated iris day 1 with vacuoles (*black arrows*); TEM, magnification ×7,000; *IPEa* anterior iris pigment epithelium, *IPEi* interior iris pigment epithelium

on day 7 lower 2.5 fenestrations per 10 μm. The ranibizumab-treated samples had an average of 2.9 fenestrations per 10 μm on day 1 and an average of 2.6 fenestrations per 10 μm on day 7. Both ranibizumab values are higher than the aflibercept values of the same day. Compared to the control's average of 3.8 fenestrations per 10 μm, the samples with VEGF-inhibitors showed a significant decrease of fenestrations in aflibercept on day 1 and 7 and in ranibizumab on day 7. Exemplary images of the clear differences in fenestrations before and after treatment can be seen in Fig. 5. The box plot shows the statistical analysis. The ranibizumab-treated group of day 1 is not significantly different as compared to the controls ($p = 0.1$), whereas the other groups (ranibizumab day 7,

Reprinted by permission from Springer Nature Customer Service Centre GmbH: Springer, Graef Arch Clin Exp, The effects of VEGF-A-inhibitors aflibercept and ranibizumab on the ciliary body and iris of monkeys, Ludinsky et al., 2016

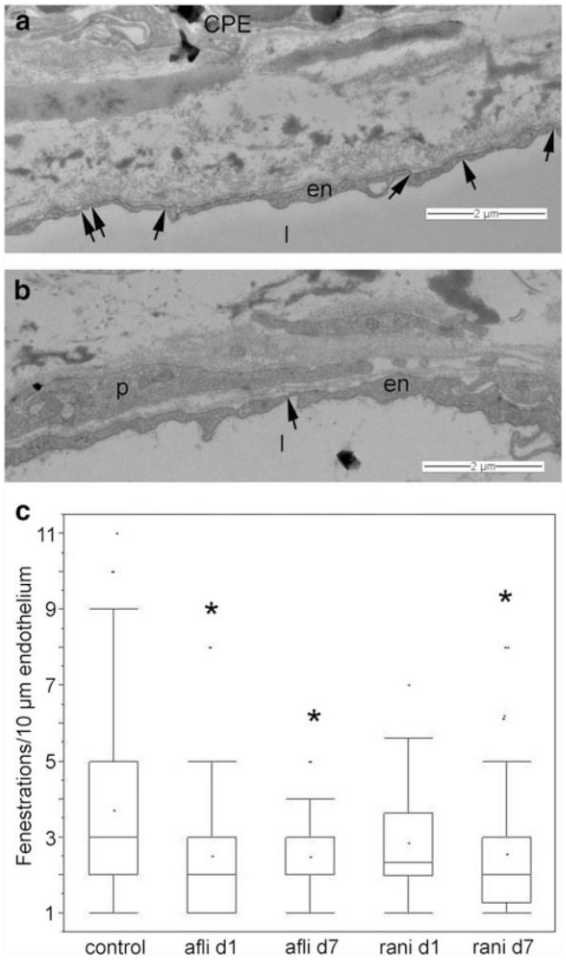

Fig. 5 Fenestration in ciliary blood vessels. **a** Endothelium with a lot of fenestrations (*black arrows*) in an untreated blood vessel of the ciliary body. **b** Endothelium with significantly less fenestrations (*black arrow*) in a ranibizumab-treated sample after day 7; TEM, magnification ×12,000. **c** Box-plot of average fenestrations per 10 µm. Lines extending vertically from the boxes (*whiskers*) indicate the variability outside the upper and lower quartiles and individual points marking outliers. * statistically significant to control group ($p < 0.05$). *CPE* ciliary pigmented epithelium, *en* endothelium, *l* lumen

$p = 0.0003$; aflibercept day 1, $p = 0.007$: aflibercept day 7, $p = 0.053$) had a lower p-value than 0.05, thus showed significant changes.

Discussion

It has been shown before that VEGF-A inhibition leads to a degeneration of blood vessels [19, 20], and since an unusual growth of new blood vessels is characteristic for neovascular age-related macular degeneration (wet AMD) [21], this effect was identified as being an adequate way to treat this disease [22]. Apart from wet AMD, VEGF-dependant ischemic retinopathies going along with pathological neovascularization of the anterior segment of the eye have been described. This is for example the case in rubeosis iridis, which is characterized by a neovascularization of the iris and represents a complication of diabetic retinopathy or central vein occlusion. In consequence, neovascular glaucoma may occur. In a previous study, our group showed that intravitreally injected bevacizumab penetrates quickly not only into the posterior segment of the eye but also into the iris, anterior chamber angle, and ciliary body, and accumulates particularly in blood-vessel walls [23]. Bevacizumab has already been used intracamerally and intravitreally for the adjuvant treatment of rubeosis iridis and neovascular glaucoma, with promising results [3, 24–26]. Recently, papers describing the use of ranibizumab injections for the treatment of these diseases have been published [27, 28], but to our knowledge, no trials have yet been performed with aflibercept. Our results show that the VEGF-A inhibitors ranibizumab and aflibercept both reduce the amount of VEGF in the ciliary pigmented epithelium, and also reduce the number of fenestrations in the blood vessels of the ciliary body, without significant changes in the ultrastructure. We further demonstrate that aflibercept administration resulted in a lower number of fenestrations both after day 1 and day 7 compared to ranibizumab. Since fenestrations can be induced by VEGF-A in vitro and in vivo [29, 30], and an inhibition of VEGF eliminates fenestrations in the choriocapillaris, the ciliary body, and even in endothelial cells of the glomeruli of the kidney [7, 9, 12, 18, 31], the loss of them here can be seen as a proof of activity of the drugs in the ciliary body.

All morphological changes observed in the eye and other tissues have always been related to not only the physiological situation but also the age of the subject. For example, in the retina it is known that physiological aging processes include steady loss of photoreceptors, thickening of Bruch's membrane, thinning of the choroid, and forming of hard drusen in the periphery [32]. For increased pigmentation of the trabecular meshwork of the iris and ciliary body, an increase in the resistance to the outflow of aqueous humour with an increased risk of glaucoma are described. Moreover, the iris tends to become less reactive with age and loses pigment, and also the shape and tone of ciliary body changes with age [33]. Taken into account that the average life expectancy of humans in the developed countries is about 77 years [34], and that the average life span of *Macaca fascicularis* is 31 years [35], then the human equivalent age of the study subjects with an average of 5.5 years for aflibercept-treated and an average of 6.5 years for ranibizumab-treated monkeys is 13.8 and 16 years respectively. Thus, none of the described aging changes have been observed in our study, and the vacuoles found in the iris of aflibercept samples cannot be related to the age of the monkeys. However, the loss of fenestrations in the

Reprinted by permission from Springer Nature Customer Service Centre GmbH: Springer, Graef Arch Clin Exp, The effects of VEGF-A-inhibitors aflibercept and ranibizumab on the ciliary body and iris of monkeys, Ludinsky et al., 2016

ciliary body can have negative effects on the function of the ciliary body, e.g., defects of the pigmented epithelial layer, as observed by others after VEGF-A neutralization [12]. A greater loss of fenestrations, as we saw it in the aflibercept treated ciliary bodies, might thus not be desirable, as irreversible damage of the ciliary body can cause prolonged ocular hypotony and phthisis bulbi [36]. By contrast, we did not find a significant amount of microthrombi in the blood vessels after VEGF-A inhibition, as our group previously observed in the choriocapillaris and choroidal vessels after intravitreal bevacizumab injection [37]. Another clinical complication has been documented before, when a 65-year-old patient with unilateral exudative age-related macular degeneration showed a focal atrophic area in the ciliary body corresponding to the site of the intravitreal bevacizumab injection [38]. Another group found a decrease in retrobulbar blood flow after intravitreal bevacizumab injections [39]. VEGF inhibitors also lead to several other defects in various other cell types, for example signs of thrombotic microangiopathy in the glomerular endothelium [40], a decreased vascular perfusion in the choroid plexus of the brain [41], and an increased apoptosis in the neuronal retina of the eye [42]. However, in the retina–choroid complex, there were indications that the fenestrations in the choriocapillaris recovered from the VEGF blockade after day 14 [7]. In a different study, where VEGF-A inhibition led to blood vessel degeneration in pancreas, thyroid, adrenal cortex, pituitary, choroid plexus, small-intestinal villi, and epididymal adipose tissue, the vessels also recovered 14 days after the inhibition was stopped [43]. On the other hand—as described above—a higher effectivity in eliminating fenestrations in the ciliary body can be a desirable effect in the treatment of iris neovascularization and neovascular glaucoma and in lowering IOP.

Furthermore, we found vacuoles in the posterior pigmented epithelium of the iris in the aflibercept-treated samples, but not in the ranibizumab-treated ones. To our knowledge, this is the first time this has been found in the iris after intravitreal injection with aflibercept or other VEGF-A inhibitors. Vacuolization of the iris pigmented epithelium has been found before in 40 % of enucleated eyes of patients with diabetic diseases, and it was also discovered that the material in the vacuoles was glycogen [44]. The vacuoles can also be called microcysts of the iris pigmented epithelium (MIPE), and have been found in enucleated eyes of patients with several different diseases, not necessarily associated with the eye, such as alveolar cell carcinoma of the lung, prostatic adenocarcinoma, or acute lymphocytic leukemia [45]. The material inside the vacuoles was not identified in this study, but microcysts were found in other compartments of the eye, such as the non-pigmented epithelium of the ciliary body [45], which was not the case in our samples of the ciliary body. Microcysts have been identified as a common pathological feature associated with many disorders and in patients who have been on high-dosage corticosteroids, and the speculative conclusion was drawn that neoplasms might alter the body's metabolism and lead to fluid accumulation in the pigmented epithelium of the iris [45]. Oedema have been found in the macula as a result of branch retinal vein occlusion, which is the second most common major retinal vascular disease, causing decreased visual acuity [46]. Interestingly, the VEGF-A inhibitor bevacizumab showed beneficial effects on macular oedema caused by branch retinal vein occlusion [47] as well as ranibizumab, which can also be used for macular oedema caused by diabetes [48]. In contrast, in our study, the VEGF-A inhibitor aflibercept might cause oedema in the iris. Macular oedema have also been found as a result of retinitis pigmentosa, where changes in the retinal pigmented epithelium take place, endangering the blood–retinal barrier, causing a subretinal leakage and therefore macular oedema [49]. However, new research in this area might be indicated to get more insight into the influence of the vacuoles in the iris after intravitreal aflibercept injection.

Our immunohistochemical localisation of aflibercept and ranibizumab showed no histological changes compared to the controls, which is in agreement with other studies with bevacizumab where this also did not occur [50]. However, we already saw an intense staining after the first day, showing that both intravitreally injected drugs penetrate the ciliary body well and fast. In all our samples, ranibizumab and aflibercept could be mostly located in the walls of blood vessels, being the place of secretion and binding of VEGF to its receptors on the vascular endothelial cells. This seems to be the optimal place for the best effect of the VEGF inhibitors [51]. Despite this, we found staining in other compartments of the ciliary body, where their impact remains theoretical. For example, the immunoreactivity of aflibercept and ranibizumab in the lumen of the blood vessels could lead to the conclusion that there is a quick distribution, but also a quick elimination of the intravascular drugs. But since there are aggregations of this type only in some, but not all, blood vessels, circulation might not be disturbed in these vessels. The same effect in the ciliary body has been shown before, with intravitreal bevacizumab injection [23]. The effects and distribution of the intravascular drugs throughout the whole body, especially on other structures with fenestrations like the glomerular endothelium of the kidney, is an interesting topic for further research. Our group recently published a study in which the kidneys of the animals studied in this work were analysed. Interestingly, both drugs could be detected within the capillaries of the glomeruli, and fenestration changes in the glomerular endothelium differed from those observed in the walls of blood vessels in the ciliary body as described above [18]. The drug staining on the surface of the epithelium might indicate the penetration through these tissues and even the stroma, as seen after intravitreal injections with bevacizumab [23].

Reprinted by permission from Springer Nature Customer Service Centre GmbH: Springer, Graef Arch Clin Exp, The effects of VEGF-A-inhibitors aflibercept and ranibizumab on the ciliary body and iris of monkeys, Ludinsky et al., 2016

In conclusion, aflibercept might eliminate more fenestrations than ranibizumab. Whether this is desirable or not remains subject to discussion, and will depend on the treated ocular disease and its desired effect. Moreover, the role of the vacuoles in the iris should be clarified, as well as some other effects, where VEGF-A plays some other important roles, such as in photoreceptors and Müller cells. There, increased apoptosis was noticed after VEGF-A inhibition, which in an experiment with mice led to a degraded retinal function [42]. Another experiment where VEGF-A inhibition was paired with ischemia led to retinal ganglion cell death [52]. Furthermore, VEGF improved the survival of retinal pigmented epithelium cells under oxidative stress [53], and provided neuroprotection [54]. A more effective VEGF neutralization, as provided by aflibercept, might be beneficial for treating the wet form of AMD or rubeosis iridis/neovascular glaucoma, but with regard to all of the preceding aspects, further research is needed to rule out any unexpected side-effects.

Compliance with ethical standards

Funding Novartis provided financial support in the form of a honorarium for author US.

The sponsor had no role in the design or conduct of this research.

Conflict of interest All authors certify that they have no affiliations with or involvement in any organization or entity with any financial interest (such as honoraria; educational grants; participation in speakers' bureaus; membership, employment, consultancies, stock ownership, or other equity interest; and expert testimony or patent-licensing arrangements) other then stated below, or non-financial interest (such as personal or professional relationships, affiliations, knowledge, or beliefs) in the subject matter or materials discussed in this manuscript. STZ OcuTox Preclinical Drug Assessment provided support in the form of an honorarium for author US, but did not have any additional role in the study design, data collection and analysis, decision to publish, or preparation of the manuscript.

Animal experiments Ethical approval: All applicable international, national, and/or institutional guidelines for the care and use of animals were followed.

All procedures performed in studies involving animals were in accordance with the ethical standards of the institution at which the studies were conducted (Covance Studies 8260977 and 8274007).

References

1. Tah V, Orlans HO, Hyer J, Casswell E, Din N, Sri Shanmuganathan V, Ramskold L, Pasu S (2015) Anti-VEGF therapy and the retina: an update. J Ophthalmol: 627674. doi 10.1155/2015/627674
2. Bikbov MM, Babushkin AE, Orenburkina OI (2012) Anti-VEGF-agents in treatment of neovascular glaucoma. Vestn Oftalmol 128: 50–53
3. Grisanti S, Biester S, Peters S, Tatar O, Ziemssen F, Bartz-Schmidt KU, Tuebingen Bevacizumab Study G (2006) Intracameral bevacizumab for iris rubeosis. Am J Ophthalmol 142:158–160. doi:10.1016/j.ajo.2006.02.045
4. Tolentino M (2011) Systemic and ocular safety of intravitreal anti-VEGF therapies for ocular neovascular disease. Surv Ophthalmol 56:95–113. doi:10.1016/j.survophthal.2010.08.006
5. Barkmeier AJ, Akduman L (2009) Bevacizumab (Avastin) in ocular processes other than choroidal neovascularization. Ocul Immunol Inflamm 17:109–117. doi:10.1080/09273940802596534
6. Cheung LK, Eaton A (2013) Age-related macular degeneration. Pharmacotherapy 33:838–855. doi:10.1002/phar.1264
7. Peters S, Heiduschka P, Julien S, Ziemssen F, Fietz H, Bartz-Schmidt KU, Tubingen Bevacizumab Study G, Schraermeyer U (2007) Ultrastructural findings in the primate eye after intravitreal injection of bevacizumab. Am J Ophthalmol 143:995–1002. doi:10.1016/j.ajo.2007.03.007
8. Julien S, Biesemeier A, Taubitz T, Schraermeyer U (2014) Different effects of intravitreally injected ranibizumab and aflibercept on retinal and choroidal tissues of monkey eyes. Br J Ophthalmol 98: 813–825. doi:10.1136/bjophthalmol-2013-304019
9. Ford KM, Saint-Geniez M, Walshe T, Zahr A, D'Amore PA (2011) Expression and role of VEGF in the adult retinal pigment epithelium. Invest Ophthalmol Vis Sci 52:9478–9487. doi:10.1167/iovs.11-8353
10. Helmholtz H (1855) Ueber die Accommodation des Auges. Graefes Arch Clin Exp Ophthalmol 1:1–74. doi:10.1007/BF02720789
11. Welsch U, Deller T (2010) Lehrbuch Histologie. Urban & Fischer Verlag/Elsevier, Munich, pp 210, 504
12. Ford KM, Saint-Geniez M, Walshe TE, D'Amore PA (2012) Expression and role of VEGF–a in the ciliary body. Invest Ophthalmol Vis Sci 53:7520–7527. doi:10.1167/iovs.12-10098
13. Shibuya M, Claesson-Welsh L (2006) Signal transduction by VEGF receptors in regulation of angiogenesis and lymphangiogenesis. Exp Cell Res 312:549–560. doi:10.1016/j.yexcr.2005.11.012
14. Ferrara N (2009) Vascular endothelial growth factor. Arterioscler Thromb Vasc Biol 29:789–791. doi:10.1161/ATVBAHA.108.179663
15. Wolf S (2008) Current status of anti-vascular endothelial growth factor therapy in Europe. Jpn J Ophthalmol 52:433–439. doi:10.1007/s10384-008-0580-4
16. Schlingemann RO, van Hinsbergh VW (1997) Role of vascular permeability factor/vascular endothelial growth factor in eye disease. Br J Ophthalmol 81:501–512
17. Schraermeyer U, Julien S (2013) Effects of bevacizumab in retina and choroid after intravitreal injection into monkey eyes. Expert Opin Biol Ther 13:157–167. doi:10.1517/14712598.2012.748741
18. Tschulakow A, Christner S, Julien S, Ludinsky M, van der Giet M, Schraermeyer U (2014) Effects of a single intravitreal injection of aflibercept and ranibizumab on glomeruli of monkeys. PLoS One 9, e113701. doi:10.1371/journal.pone.0113701
19. Folkman J (1971) Tumor angiogenesis: therapeutic implications. N Engl J Med 285:1182–1186. doi:10.1056/NEJM197111182852108
20. Folkman J (1992) Angiogenesis—retrospect and outlook. EXS 61: 4–13
21. Fine SL, Berger JW, Maguire MG, Ho AC (2000) Age-related macular degeneration. N Engl J Med 342:483–492. doi:10.1056/NEJM200002173420707
22. Nguyen DH, Luo J, Zhang K, Zhang M (2013) Current therapeutic approaches in neovascular age-related macular degeneration. Discov Med 15:343–348
23. Peters S, Heiduschka P, Julien S, Bartz-Schmidt KU, Schraermeyer U (2008) Immunohistochemical localisation of intravitreally injected bevacizumab in the anterior chamber angle, iris and ciliary body of the primate eye. Br J Ophthalmol 92:541–544. doi:10.1136/bjo.2007.133496

Reprinted by permission from Springer Nature Customer Service Centre GmbH: Springer, Graef Arch Clin Exp, The effects of VEGF-A-inhibitors aflibercept and ranibizumab on the ciliary body and iris of monkeys, Ludinsky et al., 2016

24. Yazdani S, Hendi K, Pakravan M (2007) Intravitreal bevacizumab (Avastin) injection for neovascular glaucoma. J Glaucoma 16:437–439. doi:10.1097/IJG.0b013e3180457c47
25. Wolf A, von Jagow B, Ulbig M, Haritoglou C (2011) Intracameral injection of bevacizumab for the treatment of neovascular glaucoma. Ophthalmologica 226:51–56. doi:10.1159/000327364
26. Ghanem AA, El-Kannishy AM, El-Wehidy AS, El-Agamy AF (2009) Intravitreal bevacizumab (avastin) as an adjuvant treatment in cases of neovascular glaucoma. Middle East African J Ophthalmol 16:75–79. doi:10.4103/0974-9233.53865
27. Luke J, Nassar K, Luke M, Grisanti S (2013) Ranibizumab as adjuvant in the treatment of rubeosis iridis and neovascular glaucoma—results from a prospective interventional case series. Graefes Arch Clin Exp Ophthalmol 251:2403–2413. doi:10.1007/s00417-013-2428-y
28. Tu Y, Fay C, Guo S, Zarbin MA, Marcus E, Bhagat N (2012) Ranibizumab in patients with dense cataract and proliferative diabetic retinopathy with rubeosis. Oman J Ophthalmol 5:161–165. doi:10.4103/0974-620X.106099
29. Esser S, Wolburg K, Wolburg H, Breier G, Kurzchalia T, Risau W (1998) Vascular endothelial growth factor induces endothelial fenestrations in vitro. J Cell Biol 140:947–959
30. Roberts WG, Palade GE (1995) Increased microvascular permeability and endothelial fenestration induced by vascular endothelial growth factor. J Cell Sci 108(Pt 6):2369–2379
31. Inai T, Mancuso M, Hashizume H, Baffert F, Haskell A, Baluk P, Hu-Lowe DD, Shalinsky DR, Thurston G, Yancopoulos GD, McDonald DM (2004) Inhibition of vascular endothelial growth factor (VEGF) signaling in cancer causes loss of endothelial fenestrations, regression of tumor vessels, and appearance of basement membrane ghosts. Am J Pathol 165:35–52. doi:10.1016/S0002-9440(10)63273-7
32. Ardeljan D, Chan CC (2013) Aging is not a disease: distinguishing age-related macular degeneration from aging. Prog Retin Eye Res 37:68–89. doi:10.1016/j.preteyeres.2013.07.003
33. Salvi SM, Akhtar S, Currie Z (2006) Ageing changes in the eye. Postgrad Med J 82:581–587. doi:10.1136/pgmj.2005.040857
34. Roser M (2016) Life Expectancy. http://ourworldindata.org/data/population-growth-vital-statistics/life-expectancy/. Accessed 25 Mar 2016
35. Cawthon LK (2006) Primate Factsheets: long-tailed macaque (Macaca fascicularis) Taxonomy, Morphology, & Ecology. <http://pin.primate.wisc.edu/factsheets/entry/long-tailed_macaque>. Accessed 2016 March 21. Wisconsin Primate Research Center (WPRC) Library at the University of Wisconsin-Madison
36. Jovanovik-Pandova L, Watson PG, Liu C, Chan WY, de Wolff-Rouendaal D, Barthen ER, Emmanouilidis-van der Spek K, Jager MJ (2006) Ciliary tissue transplantation in the rabbit. Exp Eye Res 82:247–257. doi:10.1016/j.exer.2005.06.019
37. Schraermeyer U, Julien S (2012) Formation of immune complexes and thrombotic microangiopathy after intravitreal injection of bevacizumab in the primate eye. Graefe's archive for clinical and experimental ophthalmology. Graefes Arch Clin Exp Ophthalmol 250:1303–1313. doi:10.1007/s00417-012-2055-z
38. Martel JN, Han Y, Lin SC (2011) Severe intraocular pressure fluctuation after intravitreal anti-vascular endothelial growth factor injection. Ophthalmic Surg Lasers Imaging : Off J Int Soc Imaging Eye 42:e100–e102. doi:10.3928/15428877-20111006-02
39. Mete A, Saygili O, Mete A, Bayram M, Bekir N (2010) Effects of intravitreal bevacizumab (Avastin) therapy on retrobulbar blood flow parameters in patients with neovascular age-related macular degeneration. J Clin Ultrasound 38:66–70. doi:10.1002/jcu.20650
40. Eremina V, Jefferson JA, Kowalewska J, Hochster H, Haas M, Weisstuch J, Richardson C, Kopp JB, Kabir MG, Backx PH, Gerber HP, Ferrara N, Barisoni L, Alpers CE, Quaggin SE (2008) VEGF inhibition and renal thrombotic microangiopathy. N Engl J Med 358:1129–1136. doi:10.1056/NEJMoa0707330
41. Maharaj AS, Walshe TE, Saint-Geniez M, Venkatesha S, Maldonado AE, Himes NC, Matharu KS, Karumanchi SA, D'Amore PA (2008) VEGF and TGF-beta are required for the maintenance of the choroid plexus and ependyma. J Exp Med 205:491–501. doi:10.1084/jem.20072041
42. Saint-Geniez M, Maharaj AS, Walshe TE, Tucker BA, Sekiyama E, Kurihara T, Darland DC, Young MJ, D'Amore PA (2008) Endogenous VEGF is required for visual function: evidence for a survival role on muller cells and photoreceptors. PLoS One 3, e3554. doi:10.1371/journal.pone.0003554
43. Kamba T, Tam BY, Hashizume H, Haskell A, Sennino B, Mancuso MR, Norberg SM, O'Brien SM, Davis RB, Gowen LC, Anderson KD, Thurston G, Joho S, Springer ML, Kuo CJ, McDonald DM (2006) VEGF-dependent plasticity of fenestrated capillaries in the normal adult microvasculature. Am J Physiol Heart Circ Physiol 290:H560–576. doi:10.1152/ajpheart.00133.2005
44. Yanoff M, Fine BS, Berkow JW (1970) Diabetic lacy vacuolation of iris pigment epithelium; a histopathologic report. Am J Ophthalmol 69:201–210
45. Fischer R, Henkind P, Gartner S (1979) Microcysts of the human iris pigment epithelium. Br J Ophthalmol 63:750–753
46. Aref AA, Scott IU (2011) Management of macular edema secondary to branch retinal vein occlusion: an evidence-based update. Adv Ther 28:28–39. doi:10.1007/s12325-010-0089-3
47. Lee K, Jung H, Sohn J (2014) Comparison of injection of intravitreal drugs with standard care in macular edema secondary to branch retinal vein occlusion. Korean J Ophthalmol : KJO 28:19–25. doi:10.3341/kjo.2014.28.1.19
48. Schmidt-Erfurth U, Lang GE, Holz FG, Schlingemann RO, Lanzetta P, Massin P, Gerstner O, Bouazza AS, Shen H, Osborne A, Mitchell P, Group RES (2014) Three-year outcomes of individualized ranibizumab treatment in patients with diabetic macular edema: the RESTORE extension study. Ophthalmology 121:1045–1053. doi:10.1016/j.ophtha.2013.11.041
49. Barge S, Rothwell R, Sepulveda P, Agrelos L (2013) Intravitreal and subtenon depot triamcinolone as treatment of retinitis pigmentosa associated cystoid macular edema. Case Rep Ophthalmol Med 2013:591681. doi:10.1155/2013/591681
50. Sugimoto Y, Mochizuki H, Miyagi H, Kawamata S, Kiuchi Y (2013) Histological findings of uveal capillaries in rabbit eyes after multiple intravitreal injections of bevacizumab. Curr Eye Res 38:487–496. doi:10.3109/02713683.2013.763990
51. Simorre-Pinatel V, Guerrin M, Chollet P, Penary M, Clamens S, Malecaze F, Plouet J (1994) Vasculotropin-VEGF stimulates retinal capillary endothelial cells through an autocrine pathway. Invest Ophthalmol Vis Sci 35:3393–3400
52. Nishijima K, Ng YS, Zhong L, Bradley J, Schubert W, Jo N, Akita J, Samuelsson SJ, Robinson GS, Adamis AP, Shima DT (2007) Vascular endothelial growth factor-A is a survival factor for retinal neurons and a critical neuroprotectant during the adaptive response to ischemic injury. Am J Pathol 171:53–67. doi:10.2353/ajpath.2007.061237
53. Byeon SH, Lee SC, Choi SH, Lee HK, Lee JH, Chu YK, Kwon OW (2010) Vascular endothelial growth factor as an autocrine survival factor for retinal pigment epithelial cells under oxidative stress via the VEGF-R2/PI3K/Akt. Invest Ophthalmol Vis Sci 51:1190–1197. doi:10.1167/iovs.09-4144
54. Beazley-Long N, Hua J, Jehle T, Hulse RP, Dersch R, Lehrling C, Bevan H, Qiu Y, Lagreze WA, Wynick D, Churchill AJ, Kehoe P, Harper SJ, Bates DO, Donaldson LF (2013) VEGF-A165b is an endogenous neuroprotective splice isoform of vascular endothelial growth factor A in vivo and in vitro. Am J Pathol 183:918–929. doi:10.1016/j.ajpath.2013.05.031

Reprinted by permission from Springer Nature Customer Service Centre GmbH: Springer, Graef Arch Clin Exp, The effects of VEGF-A-inhibitors aflibercept and ranibizumab on the ciliary body and iris of monkeys, Ludinsky et al., 2016

3.3.3 Effects of intravitreally injected Fc fragment on rat eyes.

Authors: Taubitz T., Steinbrenner L. P., Tschulakow A. V., Biesemeier A., Julien-Schraermeyer S., Schraermeyer U.

Published in *Graefe's archive for clinical and experimental ophthalmology* in 2016

DOI: 10.1007/s00417-016-3511-y

Declaration of own contributions:

The manuscript was planned by Prof. Dr. Ulrich Schraermeyer and PD Dr. Sylvie Julien-Schraermeyer. The experiments were performed by me, Dr. Laura-Pia Steinbrenner, Dr. Alexander Tschulakow and Prof. Dr. Schraermeyer. I performed the biotinylation of the Fc fragments, assisted during the intravitreal injection and did part of the sample preparation (tissue preparation, embedding and sectioning). Data acquisition was done by Dr. Laura-Pia Steinbrenner, PD Dr. Antje Biesemeier and me. Data interpretation was done by Prof. Dr. Schraermeyer, Dr. Laura-Pia Steinbrenner, PD Dr. Antje Biesemeier and me. The manuscript was written by Prof. Dr. Ulrich Schraermeyer and proof-read by me and the other authors. Manuscript revision was done by PD Dr. Antje Biesemeier and me.

Graefes Arch Clin Exp Ophthalmol
DOI 10.1007/s00417-016-3511-y

BASIC SCIENCE

Effects of intravitreally injected Fc fragment on rat eyes

Tatjana Taubitz[1] · Laura-Pia Steinbrenner[1] · Alexander V. Tschulakow[1] · Antje Biesemeier[1] · Sylvie Julien-Schraermeyer[1] · Ulrich Schraermeyer[1,2]

Received: 23 June 2016 / Revised: 14 September 2016 / Accepted: 3 October 2016
© Springer-Verlag Berlin Heidelberg 2016

Abstract
Purpose Anti-vascular endothelial growth factor (VEGF) drugs are used to treat neovascular eye diseases. Some of these drugs contain Fc fragments (Fc), but it is unknown how their mode of action is influenced by Fc. Therefore, this study investigated the effects of Fc on rat eyes after intravitreal injection.
Methods Eighteen Long–Evans rats were intravitreally injected with sterile, biotin-labeled rat Fc (9.1 μg in 5 μl PBS). For control, 5 μl PBS was injected in another nine rats. Animals were sacrificed between 1 and 3 days (group 1), 7 days (group 2), and 14 days (group 3) after injection. The right eyes were examined by electron microscopy (EM). The left eyes were stained by immunohistochemistry to investigate the distribution of Fc and the presence of macrophages.
Results After 1 day, Fc had penetrated into the anterior chamber and the retina up to the inner nuclear layer, and was located especially in retinal vessels. High numbers of infiltrating cells were present within the vitreous, around the ciliary body, anterior chamber and inside the retina 1–3 days after Fc injection ($p < 0.02$ group 1 vs. control). Immunohistochemistry and EM showed that they were macrophages or granulocytes in close association with Fc. Ultrastructurally, there were effects on the blood vessels such as thrombocyte activation and fibrin formation.
Conclusions Biotin labeling is ideal for investigating the distribution of intravitreally injected proteins in ocular tissue. Fc fragments at a dose corresponding to their concentration in standard AMD treatments induced inflammation, and particularly the attraction of immune-competent cells. This may be associated with the risk of inflammation or endophthalmitis after anti-VEGF treatment, and needs further investigation.

Keywords Fc fragment · Anti-VEGF therapy · Intravitreal injection · Endophthalmitis

Electronic supplementary material The online version of this article (doi:10.1007/s00417-016-3511-y) contains supplementary material, which is available to authorized users.

✉ Antje Biesemeier
antje.biesemeier@med.uni-tuebingen.de

Ulrich Schraermeyer
http://www.ocutox.com

[1] Centre for Ophthalmology, Division of Experimental Vitreoretinal Surgery, Schleichstrasse 12/1, Tuebingen, Germany

[2] STZ OcuTox Preclinical Drug Assessment, Hechingen, Germany

Introduction

The eye is an immune-privileged organ, which means that immune responses are usually suppressed [1, 2]. Nevertheless, side effects including inflammation and sterile endophthalmitis have been observed after intravitreal application of full-length antibodies [3, 4].

Fc receptors (Fc = fragment crystallizable) are present in more or less all parts of the eye, including the outer nuclear layer, Müller cells, nerve fiber and photoreceptor layers, and the pigment epithelium (RPE) of the retina, but also in the ciliary body, cornea, trabecular meshwork, choroid and iris [5]. In humans, an age-related decrease in Fcγ receptor expression has been shown [5], and may play a role in the pathogenesis of age-related macular degeneration (AMD) and its treatment. Indeed, Fc-containing anti-vascular endothelial growth factor (VEGF) therapeutics (bevacizumab [Avastin®, Genentech/Roche], aflibercept [Eylea®, Regeneron/Bayer]) are used as standard therapy in AMD and could affect treatment outcome [6–11].

Published online: 17 October 2016

Reprinted by permission from Springer Nature Customer Service Centre GmbH: Springer, Graef Arch Clin Exp, Effects of intravitreally injected Fc fragment on rat eyes, Taubitz et al., 2016

Bevacizumab is a humanized monoclonal antibody that inhibits all isoforms of VEGF-A [12, 13], while aflibercept is a recombinant fusion protein containing VEGF receptor sequences (VEGFR1 and VEGFR2) fused to an IgG backbone [14]. Aflibercept binds to all VEGF-A isoforms, VEGF-B and placental growth factor [13]. Both drugs contain the human Fc fragment. A third anti-VEGF drug, ranibizumab (Lucentis®, Genentech/Novartis), is a humanized monoclonal antibody fragment (Fab) [15]. Ranibizumab inhibits all VEGF-A isoforms [13], but in contrast to bevacizumab, lacks the Fc fragment.

Fc-containing anti-VEGF therapeutics have been reported to induce protein complexes [6] and platelet activation [16] in vitro, while ranibizumab did not [6, 16]. In addition, bevacizumab was found to induce platelet aggregation, degranulation and thrombosis via complex formation with VEGF and heparin and activation of the platelet FcγRIIa receptor [17]. Bevacizumab accumulates in RPE cells in vitro, whereas ranibizumab does not [18]. Research has shown that this difference in pharmacokinetics is because bevacizumab is recognized by the neonatal Fc receptor and thus transported into the RPE cells [19, 20]. Whether intravitreally administered anti-VEGF therapeutics with an Fc fragment really cause greater ocular and/or systemic adverse effects is still under debate, since study results are conflicting [21–24].

Therefore, the present study was performed to investigate the effects of intravitreally administered isolated Fc fragment on rat eyes. Since, in a therapeutic context, injection of human Fc fragment containing anti-VEGF drugs is of interest for patient treatment, we performed our study in rats with their respective rat Fc fragment.

Methods

Animals

Six-week-old Long–Evans rats ($n = 27$) were purchased from Janvier Labs, Le Genest-Saint-Isle, France. Animals were kept under 12-h on-off cyclic lighting and provided with water and food ad libitum. All procedures involving animals were in accordance with the German laws governing the use of experimental animals and were previously approved by the local authorities (Regierungspraesidium Tuebingen; AK02/14). All efforts were made to minimize suffering.

Biotinylation of Fc fragment

Fc fragment from rat IgG (ChromPure Rat IgG, Fc Fragment; Jackson ImmunoResearch, West Grove, PA, USA) was obtained as a 2.4-mg/ml solution in a 0.25 M saline solution buffered with 0.01 M sodium phosphate (pH 7.6). The solution was concentrated to approximately 100 µl by ultrafiltration using a Thermo Scientific™ Pierce™ Concentrator 9k MWCO (Thermo Fisher Scientific, Waltham, MA, USA). Biotinylation was performed with the BiotinTag™ Micro Biotinylation Kit (Sigma-Aldrich, St. Louis, MO, USA) according to the manufacturer's instructions. Briefly, the biotinylation reagent (BAC-Sulfo-NHS) was reconstituted with sodium phosphate buffer (pH 7.2), and 10 µl of the biotinylation reagent solution was added to the Fc fragment and incubated for 30 min at room temperature. Excess biotinylation reagent was removed by loading the reaction mixture onto MicroSpin G-50 columns and eluting the labeled protein with phosphate-buffered saline (PBS). The concentration of the labeled protein was determined with the Bicinchoninic Acid Protein Assay Kit (Sigma-Aldrich, St. Louis, MO, USA), according to the manufacturer's instructions. In brief, the biotinylated Fc fragment and a diluted series of bovine serum albumin (BSA) solution as a standard were mixed with freshly prepared working solution containing copper sulfate and bicinchoninic acid, and incubated in a 96-well plate at room temperature for 2 h. Absorption was measured at 562 nm with a microplate reader (Synergy HT; BioTek, Winooski, VT, USA). The Fc fragment solution was sterile-filtered before injection into the eyes.

Intravitreal injection

Eighteen rats were anaesthetized using a mixture of ketamine and xylazine (WDT, Garbsen, Germany), and an intravitreal injection of sterile 9.1-µg biotin-labeled Fc from rats in 5 µl PBS was administered in both eyes of each animal using an UltraMicroPump III microsyringe injector with a Micro4 controller. The pump was equipped with a NanoFil 100-µL syringe loaded with the labeled Fc fragment. A 34-gauge beveled needle was connected to the syringe with SilFlex tubing and a needle holder. All instruments were obtained from World Precision Instruments, Sarasota, FL, USA. The advantage of this system is accurate and repetitive injection. The injection volume was 5 µl per eye and the injection rate was 2 µl/s. For control, 5 µl sterile PBS was injected into the eyes of another nine rats. Eleven animals treated with Fc fragment and six PBS-treated animals were sacrificed 1–3 days (group 1) after injection, and another five and three animals, respectively, 7 days (group 2) after injection. Two rats were sacrificed 14 days after Fc fragment injection (group 3).

Tissue preparation

On days 1–3 (group 1), 7 (group 2) and 14 (group 3) after intravitreal injection, the animals were sacrificed by cervical dislocation under general anesthesia using a mixture of ketamine and xylazine (WDT, Garbsen, Germany). The eyes were enucleated immediately post mortem and cleaned of orbital tissue. Right eyes were fixed for electron microscopy in 5 %

Reprinted by permission from Springer Nature Customer Service Centre GmbH: Springer, Graef Arch Clin Exp, Effects of intravitreally injected Fc fragment on rat eyes, Taubitz et al., 2016

glutaraldehyde in 0.1 M cacodylate buffer (pH 7.4; Sigma-Aldrich, St. Louis, MO, USA). Left eyes were fixed for immunohistochemistry in 4.5 % formalin (Carl Roth, Karlsruhe, Germany).

Immunohistochemistry

Eyes were fixed in formalin, embedded in paraffin wax, cut into 5-µm sections and deparaffinized according to standard procedures.

Biotinylated Fc fragments were detected using a streptavidin alkaline phosphatase detection kit (RED Rabbit/Mouse K5005; Dako, Glostrup, Denmark) or a Cy3-conjugated AffiniPure Goat Anti-Rat IgG (H+L) antibody (112-165-143; Jackson ImmunoResearch, West Grove, PA, USA, 1:250), according to the manufacturer's protocol. Sections were counterstained with hematoxylin solution modified according to Gill III for microscopy (Merck, Darmstadt, Germany).

For detection of macrophages, sections were incubated for 1 h with Mouse Anti-Rat CD-68 antibodies (MCA 341R; AbD Serotec/Bio-Rad, Kidlington, Oxford, UK) 1:100 and stained with Goat Anti-Mouse IgG (H+L) Cy3 Conjugate (81-6515; Invitrogen, Carlsbad, CA, USA) 1:100 diluted 30 min at room temperature. Dilution was performed with antibody diluent with background-reducing components (Dako S3022) at room temperature.

Sections were mounted on Superfrost Plus slides (Langenbrinck, Emmendingen, Germany) using FluorSave (Calbiochem, La Jolla, CA, USA) and inspected with a fluorescence microscope (ZEISS Axioplan 2; Carl Zeiss, Jena, Germany).

Light and electron microscopy

After fixation in glutaraldehyde for 30 min, the corneas were carefully removed from the bulbi, and the fixation was continued overnight. Specimens were post-fixed with 1 % OsO_4 at room temperature in 0.1 M cacodylate buffer (pH 7.4), stained with uranyl acetate, and embedded in Epon after dehydration in a graded series of ethanol and propylene oxide. Semi-thin sections were stained with toluidine blue and examined by light microscopy (ZEISS Axioplan 2; Zeiss, Jena, Germany). For electron microscopy, ultra-thin sections were cut and were analyzed with a ZEISS EM 900 electron microscope.

Quantification of infiltrating cells in the vitreous–retinal interface

Cells that were present within the vitreous close to the retina were counted in semi-thin sections.

Quantification of macrophages in the vitreous and retina

CD68-positive cells that were present within the vitreous close to the retina were counted in paraffin sections.

Statistical analysis

Statistical significance for the evaluation of the occurrence of macrophages in the vitreous was determined by using Dunnett's test and the JMP11.0 statistical program (SAS Institute Inc., Cary, NC, USA). The null hypothesis was that the treated samples were not histologically different from the PBS controls. All p values < 0.05 were considered to indicate significant difference (error probability 5 %).

Results

Detection of Fc fragments and macrophages by immunohistochemistry

Between 1 and 3 days after injection, Fc fragments were detected within the vitreous, often associated with fibrous material (Fig. 1a). Fc fragments were also present in infiltrating cells within the vitreous (Fig. 1b and e), and around the ciliary body (Fig. 1c) and the anterior chamber (Fig. 1c). One day after injection, the Fc fragments were localized in infiltrating cells (Fig. 1e) and the inner retina (Fig. 1b). However, 2 and 3 days after injection, Fc fragments permeated the retina and were taken up by ganglion cells and cells of the inner nuclear layer (Fig. 1a). In addition, Fc fragments were clearly detectable within the retinal vessels (Fig. 1a). Infiltrating cells were very prominent between 1 and 3 days after injection of Fc fragments (Fig. 1a, b, c, and e), and CD68 labeling identified many of them as macrophages (Fig. 1f). These macrophages also infiltrated the retina (Fig. 1f). At 7 and 14 days after injection, the Fc fragments disappeared from the vitreous (not shown) but were still detectable in the RPE (Fig. 1d). In PBS-injected rats, staining for biotin was completely negative in sections from all eyes (Supplementary Figure 1).

Light microscopy of semi-thin sections

After Fc fragment injection, all three groups showed infiltrating cells within the vitreous and thrombocyte activation in the retinal vessels (Fig. 2). Infiltrating cells were most frequent in treated group 1.

Electron microscopy

At the electron microscopic level, the loosely aggregating thrombocytes (Fig. 3a and c), unknown fibrous material, fibrin (Fig. 3b) and granulocytes fixed in the state of degranulation

Reprinted by permission from Springer Nature Customer Service Centre GmbH: Springer, Graef Arch Clin Exp, Effects of intravitreally injected Fc fragment on rat eyes, Taubitz et al., 2016

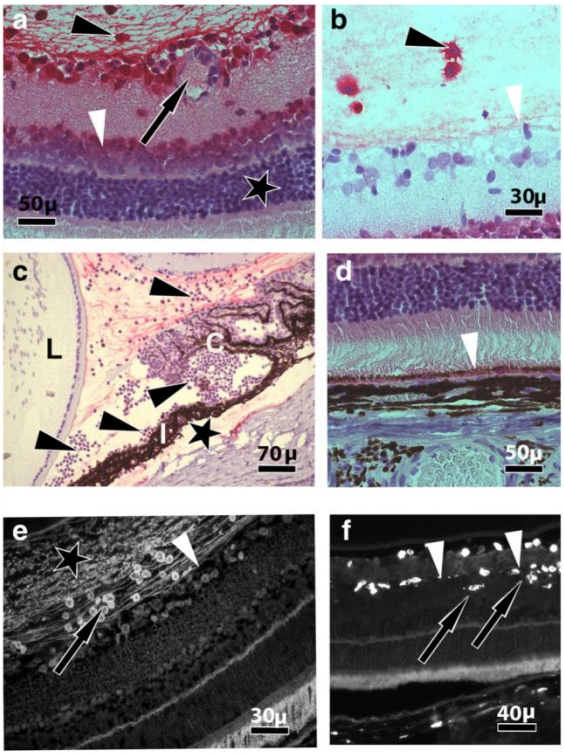

Fig. 1 Distribution of Fc fragments and infiltrating cells by light and fluorescence microscopy. **a** 3 days after injection, biotinylated Fc fragments (*red*) can be detected within the vitreous, often associated with fibrous material as visualized with streptavidin alkaline-phosphatase stain. Fc fragments are present in infiltrating cells within the vitreous (*black arrowhead*). Fc fragment penetrated the retina up to the inner nuclear layer (*white arrowhead*). The permeating Fc fragments do not reach the photoreceptor nuclei (*asterisk*). The lumen of a retinal vessel (*arrow*) contains Fc fragments. The same is true for ganglion cells to the left and right of this vessel. **b** 1 day after injection, the Fc fragments are localized to the inner limiting membrane (*white arrowhead*) and cells infiltrating the vitreous (*black arrowhead*). **c** 1 day after injection, red-labeled Fc fragments are seen within the space between lens (*L*) and ciliary body (*C*) in the anterior chamber (*asterisk*). Many infiltrating cells (*arrowheads*) can be seen around the ciliary body and attached to the iris (*I*). **d** 7 days after injection, the Fc fragments disappeared from the vitreous (not shown), but were still detectable in the retinal pigment epithelium (*white arrowhead*). **e** A fluorescent light micrograph 1 day after injection shows cells infiltrating the vitreous (*arrow*) that have taken up anti-rat IgG-labeled Fc fragments and are associated with fibers. Fc fragments are also seen in the central vitreous (*asterisk*). The inner limiting membrane is marked by an *arrowhead*. **f** These infiltrating cells (1 day after infection) were identified by CD68 labeling as macrophages. The macrophages also infiltrated the retina (*arrows*). The inner limiting membrane (ILM) is marked by *arrowheads*, and macrophages are seen on both sides of the ILM within the retina and within the vitreous

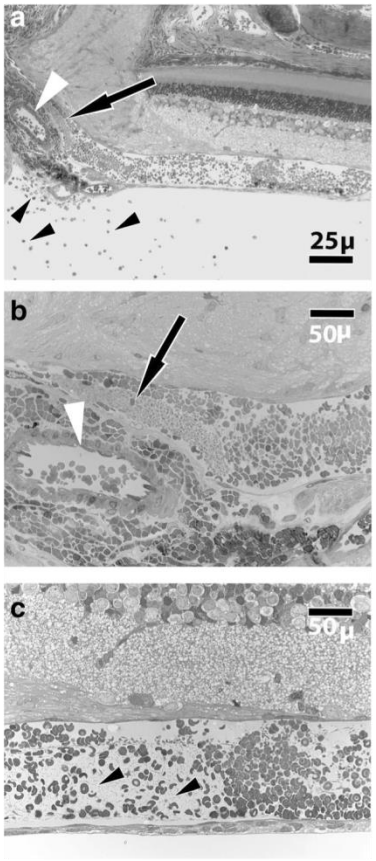

Fig. 2 Light microscopy of the distribution of infiltrating cells and thrombocytes in the inner retina. **a** Infiltrating cells within the vitreous are shown 1 day after Fc fragment injection (*black arrowheads*). Loosely aggregating thrombocytes are marked by an *arrow* within the central vein (higher magnification in **b**). The central artery is marked by a *white arrowhead*. For additional details, see electron microscopy image in Fig. 3a. **c** 1 day after injection, fibrin fibers (*arrowheads*) can already be detected within the central vein by light microscopy. The diameter of the central vein appears enlarged

(Fig. 3c) were regularly seen in retinal veins of all groups after Fc fragment treatment. After the injection of PBS, these findings were only infrequently observed. Microparticles were also observed after Fc injection in all groups (Fig. 3b), but were observed in the respective PBS-injected controls in retinal and choroidal vessels as well (not significant). In untreated Long–Evans rats, we never noticed such an accumulation of microparticles (not shown).

In a few cases in groups 2 and 3, unusual electron-dense material accumulated within the subretinal space and the vitreous, as shown in an example from group 3 (Fig. 4). This electron-dense material penetrated the retina and was localized close to the retinal veins (Fig. 4b). At higher magnification, vesicular transport (transcytosis) of this material through smooth muscle cells and endothelium into the lumen of the veins was clearly seen (not shown). As this phenomenon was only infrequently observed, it was not further investigated.

The most prominent finding after Fc fragment treatment was cellular infiltration of the vitreous and retina (Fig. 5).

Reprinted by permission from Springer Nature Customer Service Centre GmbH: Springer, Graef Arch Clin Exp, Effects of intravitreally injected Fc fragment on rat eyes, Taubitz et al., 2016

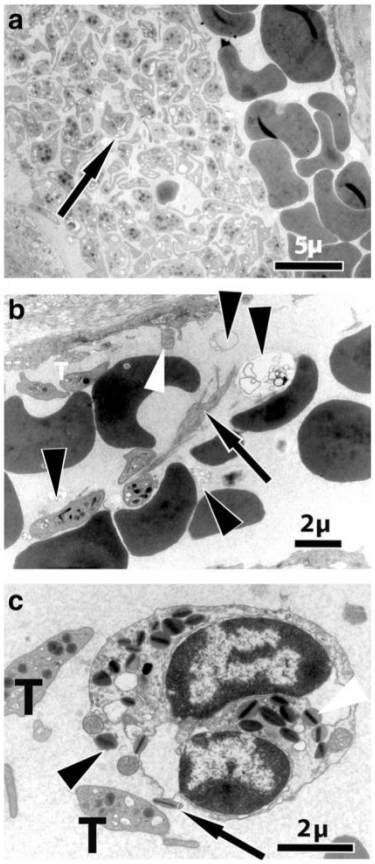

Fig. 3 Electron microscopy of thrombotic events and inflammation within retinal vessels. **a** Loosely aggregating thrombocytes, marked by an *arrow* within the central vein, 1 day after Fc fragment injection. **b** Unknown fibrous material (*arrow*), thrombocytes (*white T*) and microparticles (*black arrowheads*) 14 days after injection. The endothelium has unusual projections (*white arrowhead*) towards the vessel lumen. **c** An eosinophil granulocyte has been fixed in the state of degranulation in a retinal vein, 14 days after Fc fragment injection. The plasma membrane is partly missing (*black arrowhead*). Eosinophilic granules are seen free in the lumen (*arrow*) but also within the cell (*white arrowhead*). Activated thrombocytes (*T*) are also present

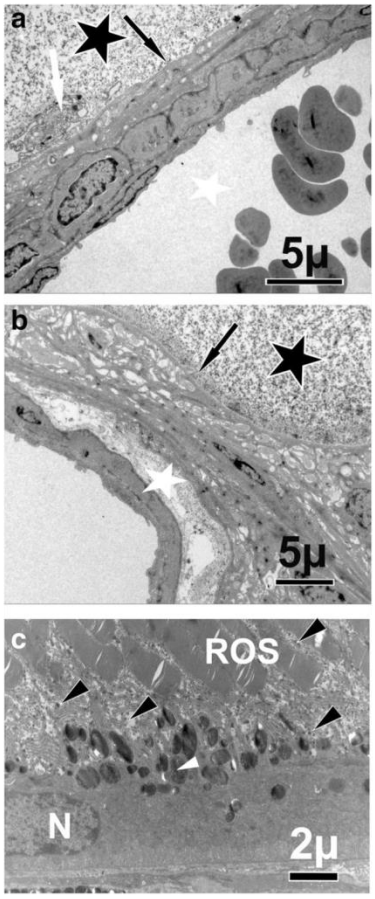

Fig. 4 Electron microscopy of electron-dense material in the vitreous and retina 14 days after intravitreal injection of Fc fragment. **a** An electron micrograph shows unusual electron-dense material which accumulated within the vitreous (*black asterisk*) from an Fc-treated rat. This material is probably transported into the vessel lumen (*white asterisk*) but cannot be recognized at this magnification. The ILM (*black arrow*) is well preserved, but a damaged cell (*white arrow*) is attached to it. **b** Electron-dense particles are localized in the vitreous (*black asterisk*) and in the space around the central retinal vein (*white asterisk*). The ILM (*black arrow*) is well preserved. **c** Very unusual electron-dense particles of unknown origin are shown in the subretinal space between the rod outer segments (ROS) and attached to the microvilli of the RPE (*black arrowheads*). The nucleus of this RPE cell is marked by an *N*, and a melanosome by a *white arrowhead*. The outer segments appear healthy

The cells were frequently seen within damaged retinal cells close to the inner limiting membrane (Fig. 5a and c). Some of them were clearly identified as granulocytes by the morphology of their nuclei (Fig. 5a). Eosinophil granulocytes were also detected infiltrating the retina. These cells can be clearly recognized by the typical morphology of their granules, as shown in Fig. 3c. Others resembled macrophages, judging by the "U" shape of their nuclei (Fig. 5c and d). Macrophages within the vitreous were highly activated, which was indicated by the formation of microvilli (Fig. 5b and d). Infiltrating cells were only infrequently seen after PBS injection. The number of these cells is quantified in Fig. 6.

Fourteen days after Fc treatment, cells attached to the inner limiting membrane and collagen fibers were seen within the vitreous (Fig. 5e).

Quantification of infiltrating cells in the vitreous–retinal interface

Cells that were present within the vitreous close to the retina were counted in semi-thin sections. Fc fragment injection significantly ($p < 0.02$) enhanced the number of infiltrating cells

Reprinted by permission from Springer Nature Customer Service Centre GmbH: Springer, Graef Arch Clin Exp, Effects of intravitreally injected Fc fragment on rat eyes, Taubitz et al., 2016

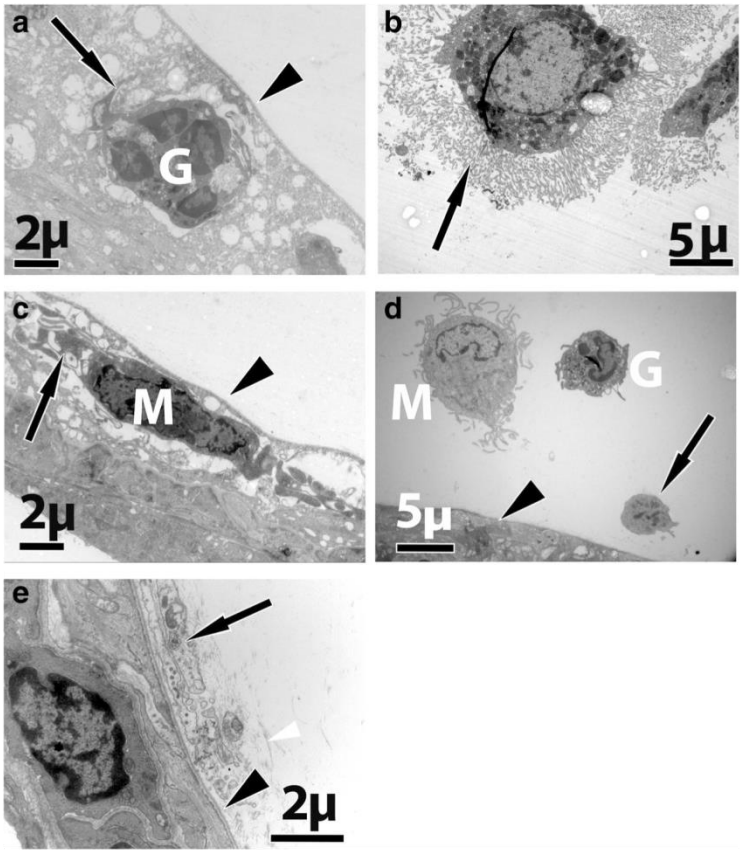

Fig. 5 Electron microscopy of infiltrating cells. **a** The most prominent finding 1 day after Fc fragment treatment is cellular infiltration of the vitreous and retina, as shown here in an electron micrograph. The cell in the ganglion cell layer can be clearly identified as a granulocyte (*G*) by the morphology of the nucleus. Microvilli (*arrow*) of this granulocyte are within a damaged retinal cell close to the inner limiting membrane (*arrowhead*). **b** A macrophage within the vitreous is highly activated, which is indicated by the formation of microvilli (*arrow*), 1 day after injection. **c** This micrograph reveals a cell with microvillar (*arrow*) projections within a retinal cell 1 day after Fc treatment. The cell is probably a macrophage (*M*) infiltrating the retina close to the inner limiting membrane (*arrowhead*). **d** An activated macrophage (*M*) with a U-shaped nucleus and a granulocyte (*G*) and a third cell (*arrow*) are infiltrating the vitreous close to the ILM (*arrowhead*) 2 days after injection. **e** 14 days after Fc treatment, cells (*arrow*) are attached to the inner limiting membrane (*black arrowhead*), and newly formed collagen fibers (*white arrowhead*) are seen within the vitreous

in group 1 (Fig. 6). The type of infiltrating cell was not distinguished ($n = 6$ eyes/group).

Quantification of macrophages in the vitreous

To identify the number of CD68-positive macrophages within the group of infiltrating cells observed in the Fc-treated rats, all CD68-positive and -negative cells were counted along the vitreoretinal interface in central paraffin sections of whole eyes of two to three rats in each group. Both CD68-positive and -negative infiltrating cells were most prominent in the Fc-treated group1 (both $p < 0.05$ compared to PBS control in group 1, Fig. 7). Note that the majority of infiltrating cells were found to be CD68-positive (ratio 2.88 in group1, 7.67 in group 2).

Discussion

To our knowledge, this is the first study that has investigated the role of isolated Fc fragments after intravitreal injection. There is clear evidence that Fc fragments have multiple effects on eye tissues that are not yet understood in detail. It is well known, however, that Fc receptors are involved in the pharmacokinetics of therapeutic IgG in eye tissue and play an important role in eliminating intravitreally administered full-length IgG antibodies across the blood–retinal barrier into the systemic blood system [19].

Previous work has shown that Fc-containing anti-VEGF drugs preferentially accumulate in endothelial and RPE cells with prolonged treatment time. This implies potential side effects in the treatment of AMD and diabetic retinopathy, both

Reprinted by permission from Springer Nature Customer Service Centre GmbH: Springer, Graef Arch Clin Exp, Effects of intravitreally injected Fc fragment on rat eyes, Taubitz et al., 2016

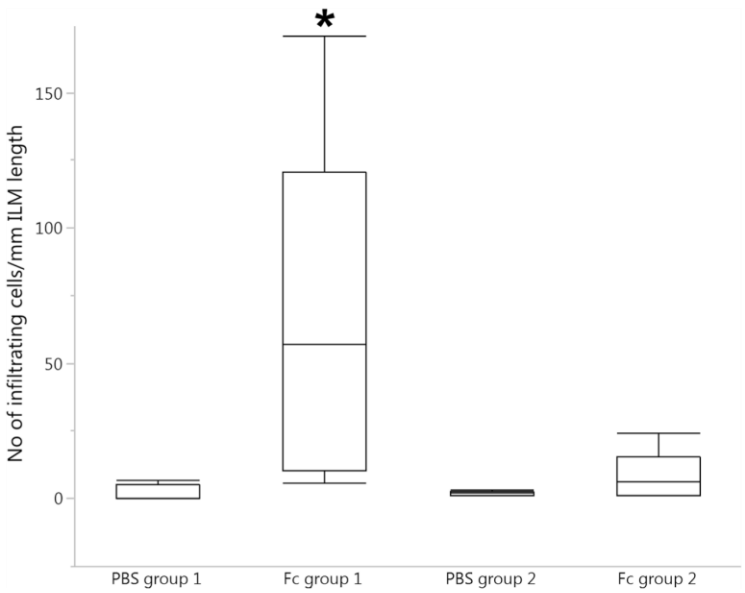

Fig. 6 Quantification of infiltrating cells in the vitreous–retinal interface. Cells that were present within the vitreous close to the retina were counted in semi-thin sections, and their number is given per millimeter of inner limiting membrane length. The type of cell was not distinguished. Fc fragment injection significantly ($p < 0.02$) enhanced the number of infiltrating cells in group 1 (n = 6 eyes/group)

of which are to be applied over several years [10, 11]. Indeed, Fc fragments were found to induce platelet aggregation, degranulation and thrombosis through complex formation with VEGF and activation of the platelet FcγRIIa receptor, and this can provide an explanation for the thrombotic events observed in vivo after bevacizumab [8, 9, 17, 25] and aflibercept [7] treatment of patients with AMD.

Endothelial cells in mammals also express the endocytic Fcγ receptor IIb2 [26] and the neonatal Fc receptor [27]. Fc fragment binding stimulates phagocytosis of waste material [26]. In this manner, endothelial cells can communicate directly with Fc fragments, resulting in the clearance of the drugs from the eye [19]. Additionally, the RPE has been shown to express Fc receptors and to take up Fc-containing drugs such as bevacizumab and aflibercept via membrane-stranding Fcγ and intracellular neonatal Fc receptors [20].

The present findings are in accordance with common knowledge about the interaction of Fc fragments and Fc receptors. Stimulation and modulation of cellular immune reactivity is the natural function of Fc fragments, and phagocytes, including epithelial cells, are also known to express Fcγ receptors [28]. Thus, it is not surprising that Fc fragments induced cellular activation of macrophages and granulocytes in the vitreous and retina.

This study demonstrates uptake of Fc fragments into the retina and the bloodstream of retinal vessels within the first

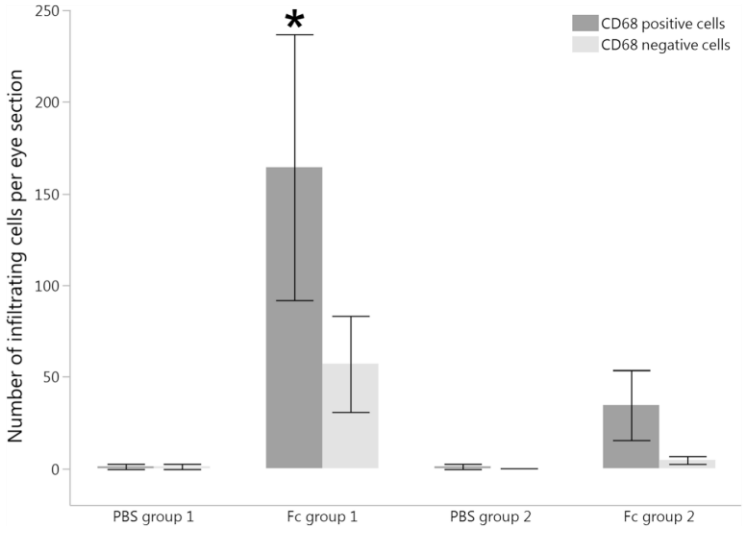

Fig. 7 Quantification of macrophages in the vitreous. CD68-positive and CD68-negative infiltrating cells were counted along the vitreoretinal interface in paraffin sections. In group 1, Fc treatment resulted in greater accumulation of CD68-positive macrophages compared to PBS treatment (*$p < 0.05$). The ratio between stained and unstained infiltrating cells was 2.88 for Fc group1 and 7.67 for Fc group 2

Reprinted by permission from Springer Nature Customer Service Centre GmbH: Springer, Graef Arch Clin Exp, Effects of intravitreally injected Fc fragment on rat eyes, Taubitz et al., 2016

3 days after injection. Alteration of the serum composition in general, and by Fc fragments in particular, can activate platelets and induce fibrin formation, which was frequently observed in this study. Microparticles are also strongly correlated with thrombotic events, but whether they are risk factors or results of thrombosis is under discussion [29]. Thus, the alterations in the retinal veins, including activation of platelets, fibrin formation and degranulation of granulocytes, are not surprising. These observations are also in accordance with our previous findings in monkey studies [7–9].

Exclusively after Fc fragment injection, immune cells infiltrated the retina and vitreous and were found to be associated with damaged retinal cells (Fig. 5a and c). At least two thirds of the infiltrating cells in the vitreous were CD68-positive monocytes/macrophages. The remnant CD68-negative infiltrating cells are assumed to be lymphocytes or granulocytes, as shown in Fig. 5a and d. Infiltrating cells, both CD68-positive and -negative, were most prominent on day 1, and diminished over time.

The present study also shows that biotinylation is a suitable method for investigating the transport and turnover of intravitreally injected proteins and excludes cross reactions with endogenous immune globulins in the eye.

In conclusion, intravitreal injection of Fc fragments at a dose corresponding to the Fc fragment portion in standard treatments in AMD patients induced multiple reactions in rats within the first 3 days—particularly the attraction of immune-competent cells, which may be associated with the risk of inflammation or endophthalmitis, and thus warrants further investigation.

Acknowledgments We thank Monika Rittgarn and Sigrid Schultheiss for technical assistance and Judith Birch for proofreading. This study was supported by Novartis.

Compliance with ethical standards

Funding Novartis provided financial support in the form of research grant funding. The sponsor had no role in the design or conduct of this research.

Conflict of interest All authors certify that they have no affiliations with or involvement in any organization or entity with any financial interest (such as honoraria; educational grants; participation in speakers' bureaus; membership, employment, consultancies, stock ownership, or other equity interest; or expert testimony or patent-licensing arrangements) or non-financial interest (such as personal or professional relationships, affiliations, knowledge or beliefs) in the subject matter or materials discussed in this manuscript.

Ethical approval All applicable international, national, and institutional guidelines for the care and use of animals were followed. All procedures performed in studies involving animals were in accordance with the ethical standards of the institution at which the studies were conducted.

References

1. Ferguson TA, Griffith TS (2006) A vision of cell death: Fas ligand and immune privilege 10 years later. Immunol Rev 213:228–238. doi:10.1111/j.1600-065X.2006.00430.x
2. Taylor AW (2009) Ocular immune privilege. Eye (Lond) 23:1885–1889. doi:10.1038/eye.2008.382
3. Agrawal S, Joshi M, Christoforidis JB (2013) Vitreous inflammation associated with intravitreal anti-VEGF pharmacotherapy. Mediators Inflamm 2013:943409. doi:10.1155/2013/943409
4. Hahn P, Yashkin AP, Sloan FA (2016) Effect of prior anti-VEGF injections on the risk of retained lens fragments and endophthalmitis after cataract surgery in the elderly. Ophthalmology 123:309–315. doi:10.1016/j.ophtha.2015.06.040
5. Tripathi RC, Borisuth NS, Tripathi BJ (1991) Mapping of Fc gamma receptors in the human and porcine eye. Exp Eye Res 53:647–656
6. Julien S, Biesemeier A, Schraermeyer U (2012) In vitro induction of protein complexes between bevacizumab, VEGF-A165 and heparin: explanation for deposits observed on endothelial veins in monkey eyes. Br J Ophthalmol. doi:10.1136/bjophthalmol-2012-302308
7. Julien S, Biesemeier A, Taubitz T, Schraermeyer U (2014) Different effects of intravitreally injected ranibizumab and aflibercept on retinal and choroidal tissues of monkey eyes. Br J Ophthalmol 98:813–825. doi:10.1136/bjophthalmol-2013-304019
8. Schraermeyer U, Julien S (2013) Effects of bevacizumab in retina and choroid after intravitreal injection into monkey eyes. Expert Opin Biol Ther 13:157–167. doi:10.1517/14712598.2012.748741
9. Schraermeyer U, Julien S (2012) Formation of immune complexes and thrombotic microangiopathy after intravitreal injection of bevacizumab in the primate eye. Graefes Arch Clin Exp Ophthalmol 250:1303–1313. doi:10.1007/s00417-012-2055-z
10. Lang GE, Lang GK, Deissler HL (2015) Basic in vitro studies on VEGF inhibition with aflibercept: similarities and differences to other VEGF-binding therapeutic proteins. Klin Monbl Augenheilkd 232:295–302. doi:10.1055/s-0034-1383142
11. Deissler HL, Lang GK, Lang GE (2016) Internalization of bevacizumab by retinal endothelial cells and its intracellular fate: evidence for an involvement of the neonatal Fc receptor. Exp Eye Res 143:49–59. doi:10.1016/j.exer.2015.10.007
12. Presta LG, Chen H, O'Connor SJ, Chisholm V, Meng YG, Krummen L, Winkler M, Ferrara N (1997) Humanization of an anti-vascular endothelial growth factor monoclonal antibody for the therapy of solid tumors and other disorders. Cancer Res 57:4593–4599
13. Papadopoulos N, Martin J, Ruan Q, Rafique A, Rosconi MP, Shi E, Pyles EA, Yancopoulos GD, Stahl N, Wiegand SJ (2012) Binding and neutralization of vascular endothelial growth factor (VEGF) and related ligands by VEGF Trap, ranibizumab and bevacizumab. Angiogenesis 15:171–185. doi:10.1007/s10456-011-9249-6
14. Ohr M, Kaiser PK (2012) Aflibercept in wet age-related macular degeneration: a perspective review. Ther Adv Chronic Dis 3:153–161. doi:10.1177/2040622312446007
15. Ferrara N, Damico L, Shams N, Lowman H, Kim R (2006) Development of ranibizumab, an anti-vascular endothelial growth factor antigen binding fragment, as therapy for neovascular age-related macular degeneration. Retina 26:859–870. doi:10.1097/01.iae.0000242842.14624.e7
16. Nomura Y, Kaneko M, Miyata K, Yatomi Y, Yanagi Y (2015) Bevacizumab and Aflibercept activate platelets via FcγRIIa. Invest Ophthalmol Vis Sci 56:8075–8082. doi:10.1167/iovs.15-17814
17. Meyer T, Robles-Carrillo L, Robson T, Langer F, Desai H, Davila M, Amaya M, Francis JL, Amirkhosravi A (2009) Bevacizumab

Reprinted by permission from Springer Nature Customer Service Centre GmbH: Springer, Graef Arch Clin Exp, Effects of intravitreally injected Fc fragment on rat eyes, Taubitz et al., 2016

immune complexes activate platelets and induce thrombosis in FCGR2A transgenic mice. J Thromb Haemost 7:171–181. doi:10.1111/j.1538-7836.2008.03212.x
18. Klettner AK, Kruse ML, Meyer T, Wesch D, Kabelitz D, Roider J (2009) Different properties of VEGF-antagonists: Bevacizumab but not Ranibizumab accumulates in RPE cells. Graefes Arch Clin Exp Ophthalmol 247:1601–1608. doi:10.1007/s00417-009-1136-0
19. Kim H, Robinson SB, Csaky KG (2009) FcRn receptor-mediated pharmacokinetics of therapeutic IgG in the eye. Mol Vis 15:2803–2812
20. Dithmer M, Hattermann K, Pomarius P, Aboul Naga SH, Meyer T, Mentlein R, Roider J, Klettner A (2016) The role of Fc-receptors in the uptake and transport of therapeutic antibodies in the retinal pigment epithelium. Exp Eye Res 145:187–205. doi:10.1016/j.exer.2015.12.013
21. Tolentino M (2011) Systemic and ocular safety of intravitreal anti-VEGF therapies for ocular neovascular disease. Surv Ophthalmol 56:95–113. doi:10.1016/j.survophthal.2010.08.006
22. Schmucker C, Ehlken C, Agostini HT, Antes G, Ruecker G, Lelgemann M, Loke YK (2012) A safety review and meta-analyses of bevacizumab and ranibizumab: off-label versus goldstandard. PLoS One 7, e42701. doi:10.1371/journal.pone.0042701
23. van der Reis MI, La Heij EC, De Jong-Hesse Y, Ringens PJ, Hendrikse F, Schouten JS (2011) A systematic review of the adverse events of intravitreal anti-vascular endothelial growth factor injections. Retina 31:1449–1469. doi:10.1097/IAE.0b013e3182278ab4
24. Modi YS, Tanchon C, Ehlers JP (2015) Comparative safety and tolerability of anti-VEGF therapy in age-related macular degeneration. Drug Saf 38:279–293. doi:10.1007/s40264-015-0273-0
25. Schraermeyer U, Julien S, Biesemeier A, Bartz-Schmidt KU, Wolburg H (2015) A new kind of labyrinth-like capillary is responsible for leakage from human choroidal neovascular endothelium, as investigated by high-resolution electron microscopy. Graefes Arch Clin Exp Ophthalmol 253:681–689. doi:10.1007/s00417-014-2733-0
26. Sorensen KK, McCourt P, Berg T, Crossley C, Le Couteur D, Wake K, Smedsrod B (2012) The scavenger endothelial cell: a new player in homeostasis and immunity. Am J Physiol Regul Integr Comp Physiol 303:R1217–R1230. doi:10.1152/ajpregu.00686.2011
27. Niu N, Zhang J, Sun Y, Wang S, Sun Y, Korteweg C, Gao W, Gu J (2011) Expression and distribution of immunoglobulin G and its receptors in an immune privileged site: the eye. Cell Mol Life Sci 68:2481–2492. doi:10.1007/s00018-010-0572-7
28. Joshi T, Butchar JP, Tridandapani S (2006) Fcgamma receptor signaling in phagocytes. Int J Hematol 84:210–216. doi:10.1532/IJH97.06140
29. Nomura S, Shimizu M (2015) Clinical significance of procoagulant microparticles. J Intensive Care 3:2. doi:10.1186/s40560-014-0066-z

Reprinted by permission from Springer Nature Customer Service Centre GmbH: Springer, Graef Arch Clin Exp, Effects of intravitreally injected Fc fragment on rat eyes, Taubitz et al., 2016

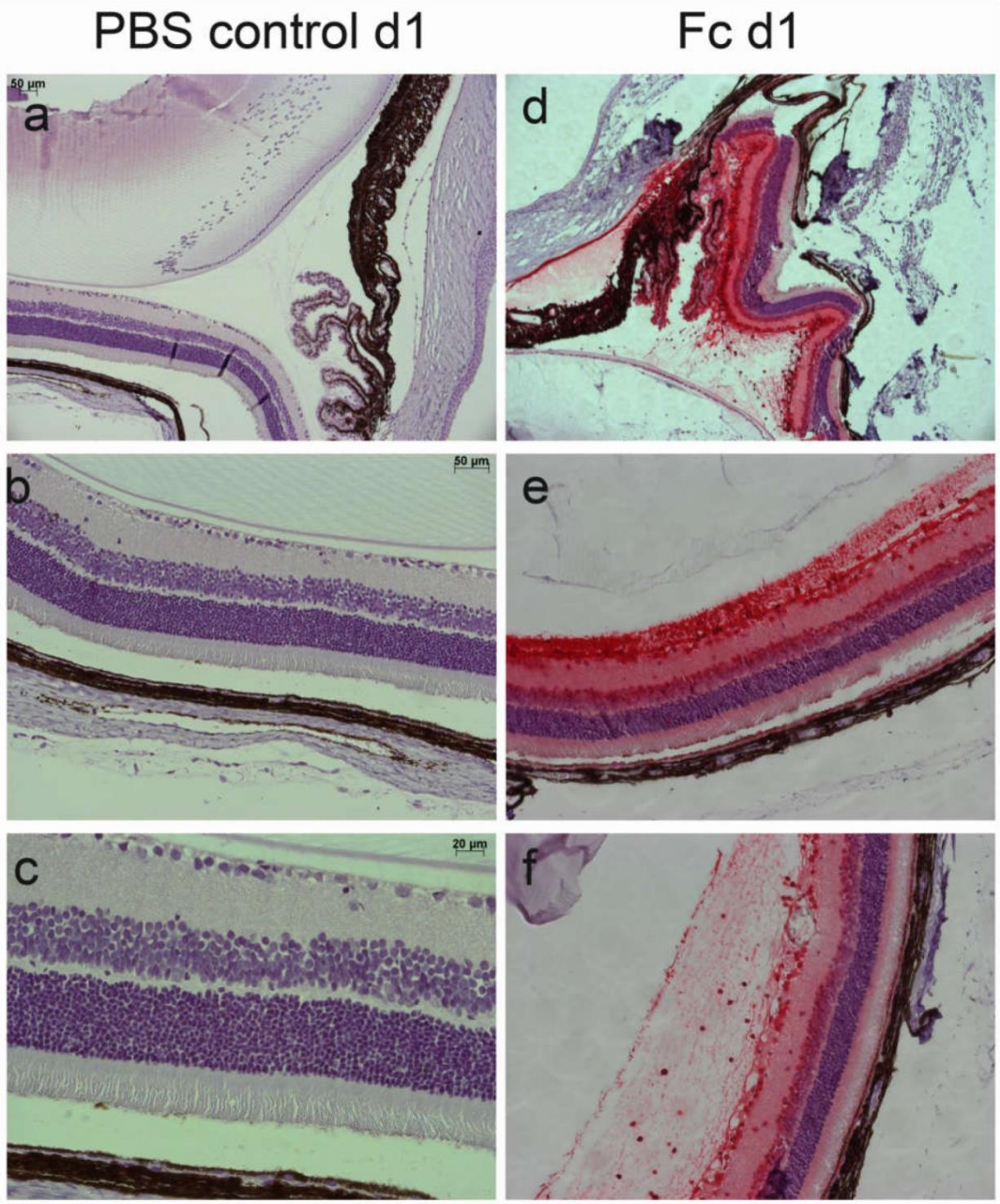

Supplementary figure 1: Distribution of biotinylated Fc fragment (stained with streptavidin-red) in (a-c) PBS control and (d-f) Fc injected LE rats, both 1d after injection. Controls never show any streptavidin stain, while Fc treated animals show staining especially along the inner retina and within cells that infiltrate the vitreous above the retina (e, f) as well as the area around the ciliary body (d). Magnifications a+d 10x, b+e 20x, c+f 20x objective

Reprinted by permission from Springer Nature Customer Service Centre GmbH: Springer, Graef Arch Clin Exp, Effects of intravitreally injected Fc fragment on rat eyes, Taubitz et al., 2016

3.4 Conclusion and future perspectives

Unravelling the pathogenesis of multifactorial diseases, such as AMD, is a complex and challenging task. In addition to several genes involved in the complement system, lipid metabolism, extracellular matrix formation and others [84-87], environmental factors, such as nutrition (e.g. uptake of antioxidants) [110] and habits (e.g. smoking) [211, 212], play an essential role in AMD genesis and progression. All these factors may have an immediate impact on the disease course and maybe even on the route AMD takes – development of the dry or wet form in the final disease stage.

In the present work, a loss of choriocapillaris was identified as the initial step in early stages of AMD [1] (section 3.1.1). In fact, even in healthy aged donor eyes a slight reduction was present [1], as was also described before [161, 162].

For diagnosis and monitoring of retinal alterations in AMD and other retinal diseases, optical coherence tomography (OCT) is routinely employed. In this technique, coherent light is used to generate micrometre-resolution images of optically scattering materials, such as biological tissue. In 2012, an advanced technique, called OCT angiography, was introduced that allows the visualisation of retinal and choroidal blood flow without additional dye injection [213]. Reduction of choriocapillaris density outside of GA has recently been confirmed by OCT angiography and is discussed as potential endpoint for clinical interventional GA trials [214, 215]. Whether choriocapillaris density is also affected in inherited retinal dystrophies is currently unknown, but choroidal vascularity was shown to be reduced in retinitis pigmentosa, cone-rod dystrophy and STGD1 [216].

On a molecular level, reduced blood flow due to a loss of choriocapillaris results in hypoxia, an inadequate supply of oxygen. Furthermore, AMD is characterised by a low chronic inflammation [217]. Elevated cellular metabolism due to inflammation might even increase oxygen consumption, further deteriorating the situation. The group of Prof. Dr. Schraermeyer showed in an *ex vivo* model that under hypoxic conditions, the endothelial cells of the choriocapillaris express Hif-1α and VEGF, lose contact to each other and develop fenestrated microvillar projections into the vessel lumen that can form a labyrinth (Tikhonovich MV, et al. Invest Ophthalmol Vis Sci. 2017;58:ARVO E-Abstract 4078). Capillaries with impaired endothelial cell connections and microvillar projections were previously found in CNV mem-

branes and termed “labyrinth-like capillaries” [218]. Since the labyrinth-like projections prevent cellular blood components, but not plasma, from passing through the vessel, leakages due to insufficient endothelial connections cannot be halted by thrombocytes [218].

In AMD, inflammation is not only limited to the retina and the choroid, but can also be found systemically [219]. Moreover, gout, a systemic inflammatory disease that also promotes oxidative stress, was found to be associated with an elevated risk to develop AMD [220]. Oxidative stress and retinal inflammation were also found in mouse models of STGD1 previously [177, 221] and in the present work [5] (section 3.1.2) .

As aforementioned, melanin is a potent antioxidant that exists in high levels in both the RPE and the melanocytes of the choroid. RPE melanin was shown to be an immune response modulator [222]. Tyrosinase, the key enzyme in melanin biosynthesis, was found to be a potential factor in AMD genetics [86] and prevalence of AMD is lower in individuals of African descent [80, 223, 224]. This highlights the relevance of ocular melanin in health and disease and warrants further investigation. An important limitation of the study presented in section 3.1.2 [5] is that it was not designed to test for melanin effects. In fact, the major goal of this study was an ultrastructural comparison of the STGD1 mouse models to gain more insight into their pathology and to evaluate their strengths and weaknesses as disease models. As previously described in the literature, there were no signs of retinal degeneration in pigmented *Abca4*$^{-/-}$ mice. Albino *Abca4*$^{-/-}$ mice however showed an unexpected earlier onset of retinal degeneration compared to *Abca4*$^{-/-}$.*Rdh8*$^{-/-}$ mice, although *Abca4*$^{-/-}$.*Rdh8*$^{-/-}$ mice have a higher genetic burden that results in high levels of cytotoxic free all-*trans*-retinal [172]. However, earlier onset of retinal degeneration in albino *Abca4*$^{-/-}$ mice is in accordance with the hypothesis that melanin might be a key factor in retinal health. This is supported by the vast literature highlighting the relevance of melanin in the RPE, but nevertheless, future studies are inevitable to elucidate the specific effects of RPE melanin. A main issue in this endeavour is the abundance of melanin in the eye: melanin is not only present in the RPE, but also in the choroid and the iris. Especially the iris melanin may not be overlooked, since more light can travel through albinistic irides, resulting in a higher illumination of the fundus of the eye. This in itself might result in damages that might be falsely attributed to the lack of

RPE melanin. The use of conditional knock-out and knock-in models (for instance, pigmented animals with a conditional knock-out of tyrosinase in the RPE, resulting in albinistic RPE in an otherwise pigmented eye) would be an invaluable asset.

In recent times, the investigation of fundus NIR-AF has attracted attention, since in many retinal diseases, characteristic changes in NIR-AF occur and sometimes even precede changes in SW-AF patterns [67-72]. The work presented in section 3.2.1 [6] shows that not only RPE and choroidal melanin, but also the lipofuscin moiety of melanolipofuscin and lipofuscin granules can emit relevant levels of NIR-AF. The work also demonstrates that both oxidative and photic stress increases melanosome-derived NIR-AF. This suggests that NIR-AF is not an intrinsic property of melanin but should rather be considered to be a marker for aged and/or damaged melanin. The fact that pigmented *Abca4*$^{-/-}$ mice showed higher intensity of NIR-AF than pigmented WT mice, is in accordance with the higher levels of oxidative stress due to accumulation of lipofuscin in these mice. This also supports the notion that ocular melanin can act as a "wear and tear" material that is meant to quench oxidative stress at its own expense and thereby reduce the oxidative burden of the surrounding tissue, as suggested in the study presented in section 3.1.2 [5]. However, future research is needed to investigate whether the NIR-AF signal derived from lipofuscin is in fact due to accumulation of melanin degradation products. Nevertheless, these findings urge to rethink the interpretation of NIR-AF patterns in retinal diseases. Currently, new non-invasive imaging techniques are being developed that for instance are potentially able to distinguish between lipofuscin and melanolipofuscin granules [225, 226]. Such techniques in combination with a refined interpretation of already established techniques, such as NIR-AF, have the potential to advance the understanding of both the biogenesis and the diagnostics of retinal diseases.

However, the influence of melanin is by far not the only open question left in understanding macular degenerative diseases. For instance, a very compelling issue is the question which mechanism triggers the development of either the wet or the dry form of AMD. Furthermore, both AMD and STGD1 patients have high levels of RPE lipofuscin, and even though the lipofuscin component A2E was shown to be pro-angiogenic [54, 55], only patients with wet AMD develop CNV, while CNV was never described in STGD1 and was also not seen in the three STGD1 mouse strains investigated in section 3.1.2 [5]. Even though a plethora of associated genes and an

extensive list of molecular and cellular changes have been identified in AMD, linking the disease to oxidative stress, lipid metabolism and mitochondrial malfunction among others, there is still a lack in understanding how these factors determine the disease progression. Deciphering these interconnections and finding better treatment options will undoubtedly be challenging, but will be invaluable due to the expected rise in AMD patients in future years. But also the pathology of STGD1 leaves a series of open questions that warrant further investigation. The probably most intriguing one is the variety in *ABCA4*-related disease: As mentioned briefly in section 1.4.2, mutations in *ABCA4* are not only found in STGD1, but also in other retinal degenerative diseases, such as cone-rod dystrophy, retinitis pigmentosa and AMD. Therefore, a genotype-phenotype model was suggested [96-100]. In this model, STGD1 is caused by rather mild mutations (e.g. mutations leading to reduced protein functionality) in both alleles or a mild and a severe mutation (e.g. mutations leading to complete loss of function) in one allele of *ABCA4*, respectively. On the other hand, two severe mutations in both alleles of *ABCA4* always lead to autosomal recessive retinitis pigmentosa [97, 101, 183, 184], a disease that has a very different phenotype compared to STGD1: the first clinical symptom is night blindness, followed by progressive loss in peripheral vision and subsequent loss in central vision [227]. How different defects in a single gene can lead to so vastly different diseases is astonishing and not yet understood. A recent study indicates that *Abca4* is not only expressed in photoreceptors, but also in the RPE, and suggests that RPE-ABCA4 is also involved in lipofuscin accumulation [43]. Furthermore, the macula is predominated by cones, while in the periphery only rods exist. Differences in the metabolism of these different photoreceptor species are not yet fully understood but might play a role in the photoreceptor's reaction to various *ABCA4* defects and impaired RPE due to lipofuscin accumulation, and the resulting implications.

Even though the molecular mechanisms in macular degeneration are not yet completely understood, at least for wet AMD the treatment with anti-VEGF compounds turned out to be successful in reversing acute visual distortion due to oedema and reducing disease progression. However, as outlined in the studies presented in section 3.3, anti-VEGF compounds show certain adverse effects that might be mediated by their Fc moiety. There are new anti-VEGF compounds currently under FDA review or in phase III for treatment of wet AMD, namely brolu-

cizumab and abicipar pegol, respectively, both lacking Fc fragments and both with a molecular weight lower than that of ranibizumab. This potentially reduces not only the likeliness of systemic adverse events due to reduced systemic accumulation, but the low molecular weight also gives the possibility of applying high dosages with a single intravitreal injection. This might act as a depot, reducing the re-injection frequency and thus leading to a higher patient compliance, since high-frequent re-injections, as often as monthly, are often perceived as a burden by patients. And in fact, phase III trials of brolucizumab showed that 50% of treated eyes could be maintained on an every-12-weeks dosing scheme [142]. But the relevance of the Fc fragment is also considered in other therapeutic approaches: For instance, in the bispecific antibody faricimab that is targeted against both VEGF and Ang-2, the Fc fragment is engineered to prohibit binding to all Fcγ receptors and the neonatal Fc receptor, reducing systemic availability and inflammatory potential [145].

However, some studies suggest that prolonged anti-VEGF treatment results in development of geographic atrophy, leading to a disease state for which no treatment option exists, but the available data is still inconclusive [117-119]. VEGF is not only a major player in the development of CNV, but is also essential for the stability of the choriocapillaris [203]. And indeed, short-term effects of anti-VEGF treatment on the choriocapillaris in humans have been reported [228] and were also evident in monkey eyes treated with bevacizumab [150] or treated with either aflibercept or ranibizumab, as described in section 3.3.1 [2]. Since the choriocapillaris is already impaired in still healthy areas of wet AMD, as shown in section 3.1.1 [1], it is plausible that any further disturbances can be detrimental for the choriocapillaris. Current pre-clinical and clinical studies therefore also focus on other growth factors involved in CNV formation and stability, such as Ang-2 and pigment epithelium-derived factor (PEDF). A new treatment approach is for instance the stabilization of CNV-vessels (such as the above mentioned “labyrinth-like capillaries”) to prevent leakage as well as oedema formation and support the physiological function of the CNV as a “wound healing reaction” (Julien S, et al. IOVS 2019;60:ARVO E-Abstract 366). This approach is supported by the finding of morphologically healthy photoreceptors and RPE cells which are nourished by underlying morphologically functional CNV vessels, in the midst of retinal scar tissue, as reported in section 3.1.1 [1].

For the treatment of dry AMD and STGD1, several therapy approaches are under clinical investigation, but none are close to market maturity yet. In a further project, which is not presented in this thesis, my colleagues and I investigate a substance called soraprazan (IUPAC name: (7R,8R,9R)-7-(2-methoxyethoxy)-2,3-dimethyl-9-phenyl-7,8,9,10-tetrahydroimidazo[1,2-h][1,7]naphthyridin-8-ol; also called Remofuscin) that is capable to remove existing lipofuscin *in vivo* from the RPE of monkeys after oral treatment [229]. In this project, we aim to investigate whether a local application (intravitreal injection) of soraprazan can remove lipofuscin from the eyes of STGD1 model mice. Furthermore, toxicity, as well as morphologic and functional rescue are in the focus of this study. Since data acquisition and evaluation is still ongoing, no peer-reviewed publication exists, but parts of the preliminary data were presented at the annual meeting of the Association for Research in Vision and Ophthalmology (ARVO), the world's largest vision research organisation (Taubitz T, et al. IOVS 2015;56:ARVO E-Abstract 4199; Taubitz T, et al. IOVS 2017;58:ARVO E-Abstract 257; Fang Y, et al. IOVS 2017;58:ARVO E-Abstract 256). The data show that intravitreally applied soraprazan can remove lipofuscin from the RPE of pigmented *Abca4*$^{-/-}$ mice at dosages that result in no toxic effects towards the retina and RPE as investigated by immunohistochemistry, electron microscopy and electroretinography. Lack of RPE toxicity was corroborated in cell culture experiments performed on primary RPE cells isolated from pigmented *Abca4*$^{-/-}$ mice. Data also point to a reduction of oxidative stress markers and to a deceleration of the retinal degeneration after a single intravitreal application of the compound in *Abca4*$^{-/-}$.*Rdh8*$^{-/-}$ mice. Rescue effects were also evident in a light toxicity model where soraprazan reduced the retinal degeneration of light-exposed pigmented *Abca4*$^{-/-}$ mice after a single intravitreal application compared to control. Meanwhile, in April 2019, a multi-national phase II study started to evaluate the safety and efficacy of oral soraprazan in patients with STGD1 (EudraCT number: 2018-001496-20).

A benefit of the lipofuscin removal route for treatment is the lack of necessity for long-term or early start of treatment, especially for dry AMD patients: therapeutic approaches that rely on prevention of bisretinoid formation have to be applied early in life before considerable amounts of lipofuscin have accumulated (e.g. gene therapy) or have to be used continuously (e.g. visual cycle inhibitors). This is a highly valuable route for patients with STGD1, since they experience high

lipofuscin amounts due to forced lipofuscin accumulation early in life. However, AMD is not caused by genetic factors, but merely the risk to develop AMD is dependent on genetics, so approaches like gene therapy might only play a minor role in AMD therapy. Furthermore, since there is currently no way to predict whether an individual will develop AMD, preventive approaches like visual cycle inhibitors might be of limited practicality for AMD treatment. Indeed, a phase 2 study with the visual cycle modulator fenretinide failed to show a visual benefit after a 2-year-treatment with 300 mg daily oral administration in dry AMD patients with geographic atrophy [230].

However, small molecules that are capable to eliminate lipofuscin, as for example the compound soraprazan [229] and cyclodextrins as described by Nociari et al. [231], have not only a high potential value in treatment of AMD, but also for STGD1: many parents of children affected from STGD1 are not aware they are carriers of *ABCA4* mutations and that their children might inherit a blinding disease. Therefore, many patients are at the earliest diagnosed when they are already experiencing the first signs of vision loss, which rules out any preventive treatment. These patients might benefit from an immediate reduction of their lipofuscin load, decelerating progression of retinal degeneration. In a subsequent step, other currently investigated treatment options that prevent future lipofuscin accumulation could be applied as a long-term remedy.

4 References

1. Biesemeier, A., et al., *Choriocapillaris breakdown precedes retinal degeneration in age-related macular degeneration.* Neurobiol Aging, 2014. **35**(11): p. 2562-73.
2. Julien, S., et al., *Different effects of intravitreally injected ranibizumab and aflibercept on retinal and choroidal tissues of monkey eyes.* Br J Ophthalmol, 2014. **98**(6): p. 813-25.
3. Ludinsky, M., et al., *The effects of VEGF-A-inhibitors aflibercept and ranibizumab on the ciliary body and iris of monkeys.* Graefes Arch Clin Exp Ophthalmol, 2016. **254**(6): p. 1117-25.
4. Taubitz, T., et al., *Effects of intravitreally injected Fc fragment on rat eyes.* Graefes Arch Clin Exp Ophthalmol, 2016. **254**(12): p. 2401-2409.
5. Taubitz, T., et al., *Ultrastructural alterations in the retinal pigment epithelium and photoreceptors of a Stargardt patient and three Stargardt mouse models: indication for the central role of RPE melanin in oxidative stress.* PeerJ, 2018. **6**: p. e5215.
6. Taubitz, T., et al., *Age, lipofuscin and melanin oxidation affect fundus near-infrared autofluorescence.* EBioMedicine, 2019. **48**: p. 592-604.
7. Hoon, M., et al., *Functional architecture of the retina: development and disease.* Prog Retin Eye Res, 2014. **42**: p. 44-84.
8. Strauss, O., *The retinal pigment epithelium in visual function.* Physiol Rev, 2005. **85**(3): p. 845-81.
9. Kiser, P.D. and K. Palczewski, *Retinoids and Retinal Diseases.* Annu Rev Vis Sci, 2016. **2**: p. 197-234.
10. Kanow, M.A., et al., *Biochemical adaptations of the retina and retinal pigment epithelium support a metabolic ecosystem in the vertebrate eye.* Elife, 2017. **6**.
11. Kevany, B.M. and K. Palczewski, *Phagocytosis of retinal rod and cone photoreceptors.* Physiology (Bethesda), 2010. **25**(1): p. 8-15.
12. Young, R.W., *The renewal of photoreceptor cell outer segments.* J Cell Biol, 1967. **33**(1): p. 61-72.
13. Curcio, C.A. and C.L. Millican, *Basal linear deposit and large drusen are specific for early age-related maculopathy.* Arch Ophthalmol, 1999. **117**(3): p. 329-39.
14. Buschini, E., et al., *Age related macular degeneration and drusen: neuroinflammation in the retina.* Prog Neurobiol, 2011. **95**(1): p. 14-25.
15. Wangsa-Wirawan, N.D. and R.A. Linsenmeier, *Retinal oxygen: fundamental and clinical aspects.* Arch Ophthalmol, 2003. **121**(4): p. 547-57.
16. Bhutto, I. and G. Lutty, *Understanding age-related macular degeneration (AMD): relationships between the photoreceptor/retinal pigment epithelium/Bruch's membrane/choriocapillaris complex.* Mol Aspects Med, 2012. **33**(4): p. 295-317.
17. Ollivier, F.J., et al., *Comparative morphology of the tapetum lucidum (among selected species).* Vet Ophthalmol, 2004. **7**(1): p. 11-22.
18. Hu, D.N., J.D. Simon, and T. Sarna, *Role of ocular melanin in ophthalmic physiology and pathology.* Photochem Photobiol, 2008. **84**(3): p. 639-44.
19. Schraermeyer, U. and K. Heimann, *Current understanding on the role of retinal pigment epithelium and its pigmentation.* Pigment Cell Res, 1999. **12**(4): p. 219-36.
20. Smith-Thomas, L., et al., *Human ocular melanocytes and retinal pigment epithelial cells differ in their melanogenic properties in vivo and in vitro.* Curr Eye Res, 1996. **15**(11): p. 1079-91.
21. Miyamoto, M. and T.B. Fitzpatrick, *On the nature of the pigment in retinal pigment epithelium.* Science, 1957. **126**(3271): p. 449-50.
22. Sarna, T., *Properties and function of the ocular melanin--a photobiophysical view.* J Photochem Photobiol B, 1992. **12**(3): p. 215-58.
23. Dorey, C.K., X. Torres, and T. Swart, *Evidence of melanogenesis in porcine retinal pigment epithelial cells in vitro.* Exp Eye Res, 1990. **50**(1): p. 1-10.
24. Peters, S., et al., *Subretinal injection of rod outer segments leads to an increase in the number of early-stage melanosomes in retinal pigment epithelial cells.* Ophthalmic Res, 2000. **32**(2-3): p. 52-6.
25. Schraermeyer, U., *Transformation of albumin into melanin by hydroxyl radicals.* Comp Biochem Physiol C Pharmacol Toxicol Endocrinol, 1994. **108**(3): p. 281-8.
26. Herman, K.G. and R.H. Steinberg, *Melanosome metabolism in the retinal pigmented epithelium of the opossum.* Cell Tissue Res, 1982. **227**(3): p. 485-507.
27. Poliakov, E., et al., *Multiple A2E treatments lead to melanization of rod outer segment-challenged ARPE-19 cells.* Mol Vis, 2014. **20**: p. 285-300.
28. Weiter, J.J., et al., *Retinal pigment epithelial lipofuscin and melanin and choroidal melanin in human eyes.* Invest Ophthalmol Vis Sci, 1986. **27**(2): p. 145-52.
29. Ito, S., et al., *Photoaging of human retinal pigment epithelium is accompanied by oxidative modifications of its eumelanin.* Pigment Cell Melanoma Res, 2013. **26**(3): p. 357-66.
30. Hill, H.Z., *The function of melanin or six blind people examine an elephant.* Bioessays, 1992. **14**(1): p. 49-56.
31. Bustamante, J., et al., *Role of melanin as a scavenger of active oxygen species.* Pigment Cell Res, 1993. **6**(5): p. 348-53.
32. Tada, M., M. Kohno, and Y. Niwano, *Scavenging or quenching effect of melanin on superoxide anion and singlet oxygen.* J Clin Biochem Nutr, 2010. **46**(3): p. 224-8.

33. Burke, J.M., et al., *Dynamic analyses reveal cytoprotection by RPE melanosomes against non-photic stress.* Mol Vis, 2011. **17**: p. 2864-77.
34. Zareba, M., et al., *Photic injury to cultured RPE varies among individual cells in proportion to their endogenous lipofuscin content as modulated by their melanosome content.* Invest Ophthalmol Vis Sci, 2014. **55**(8): p. 4982-90.
35. Biesemeier, A., et al., *UV-A induced oxidative stress is more prominent in naturally pigmented aged human RPE cells compared to non-pigmented human RPE cells independent of zinc treatment.* J Photochem Photobiol B, 2008. **90**(2): p. 113-20.
36. Dontsov, A.E., R.D. Glickman, and M.A. Ostrovsky, *Retinal pigment epithelium pigment granules stimulate the photo-oxidation of unsaturated fatty acids.* Free Radic Biol Med, 1999. **26**(11-12): p. 1436-46.
37. Rozanowski, B., et al., *The phototoxicity of aged human retinal melanosomes.* Photochem Photobiol, 2008. **84**(3): p. 650-7.
38. Tsybovsky, Y., R.S. Molday, and K. Palczewski, *The ATP-binding cassette transporter ABCA4: structural and functional properties and role in retinal disease.* Adv Exp Med Biol, 2010. **703**: p. 105-25.
39. Terman, A. and U.T. Brunk, *Lipofuscin: mechanisms of formation and increase with age.* APMIS, 1998. **106**(2): p. 265-76.
40. Ng, K.P., et al., *Retinal pigment epithelium lipofuscin proteomics.* Mol Cell Proteomics, 2008. **7**(7): p. 1397-405.
41. Sparrow, J.R., et al., *The bisretinoids of retinal pigment epithelium.* Prog Retin Eye Res, 2012. **31**(2): p. 121-35.
42. Boyer, N.P., et al., *Lipofuscin and N-retinylidene-N-retinylethanolamine (A2E) accumulate in retinal pigment epithelium in absence of light exposure: their origin is 11-cis-retinal.* J Biol Chem, 2012. **287**(26): p. 22276-86.
43. Lenis, T.L., et al., *Expression of ABCA4 in the retinal pigment epithelium and its implications for Stargardt macular degeneration.* Proc Natl Acad Sci U S A, 2018.
44. Sundelin, S., et al., *Lipofuscin accumulation in cultured retinal pigment epithelial cells reduces their phagocytic capacity.* Curr Eye Res, 1998. **17**(8): p. 851-7.
45. Wihlmark, U., et al., *Lipofuscin accumulation in cultured retinal pigment epithelial cells causes enhanced sensitivity to blue light irradiation.* Free Radic Biol Med, 1997. **22**(7): p. 1229-34.
46. Biesemeier, A., U. Schraermeyer, and O. Eibl, *Chemical composition of melanosomes, lipofuscin and melanolipofuscin granules of human RPE tissues.* Exp Eye Res, 2011. **93**(1): p. 29-39.
47. Biesemeier, A., et al., *Transition metals and trace elements in the retinal pigment epithelium and choroid: correlative ultrastructural and chemical analysis by analytical electron microscopy and nano-secondary ion mass spectrometry.* Metallomics, 2018. **10**(2): p. 296-308.
48. Schutt, F., et al., *Isolation of intact lysosomes from human RPE cells and effects of A2-E on the integrity of the lysosomal and other cellular membranes.* Graefes Arch Clin Exp Ophthalmol, 2002. **240**(12): p. 983-8.
49. Sparrow, J.R., et al., *A2E, a lipofuscin fluorophore, in human retinal pigmented epithelial cells in culture.* Invest Ophthalmol Vis Sci, 1999. **40**(12): p. 2988-95.
50. Vives-Bauza, C., et al., *The age lipid A2E and mitochondrial dysfunction synergistically impair phagocytosis by retinal pigment epithelial cells.* J Biol Chem, 2008. **283**(36): p. 24770-80.
51. Holz, F.G., et al., *Inhibition of lysosomal degradative functions in RPE cells by a retinoid component of lipofuscin.* Invest Ophthalmol Vis Sci, 1999. **40**(3): p. 737-43.
52. Finnemann, S.C., L.W. Leung, and E. Rodriguez-Boulan, *The lipofuscin component A2E selectively inhibits phagolysosomal degradation of photoreceptor phospholipid by the retinal pigment epithelium.* Proc Natl Acad Sci U S A, 2002. **99**(6): p. 3842-7.
53. Suter, M., et al., *Age-related macular degeneration. The lipofusion component N-retinyl-N-retinylidene ethanolamine detaches proapoptotic proteins from mitochondria and induces apoptosis in mammalian retinal pigment epithelial cells.* J Biol Chem, 2000. **275**(50): p. 39625-30.
54. Iriyama, A., et al., *A2E, a pigment of the lipofuscin of retinal pigment epithelial cells, is an endogenous ligand for retinoic acid receptor.* J Biol Chem, 2008. **283**(18): p. 11947-53.
55. Iriyama, A., et al., *A2E, a component of lipofuscin, is pro-angiogenic in vivo.* J Cell Physiol, 2009. **220**(2): p. 469-75.
56. Sparrow, J.R., J. Zhou, and B. Cai, *DNA is a target of the photodynamic effects elicited in A2E-laden RPE by blue-light illumination.* Invest Ophthalmol Vis Sci, 2003. **44**(5): p. 2245-51.
57. van der Burght, B.W., et al., *Early changes in gene expression induced by blue light irradiation of A2E-laden retinal pigment epithelial cells.* Acta Ophthalmol, 2013. **91**(7): p. e537-45.
58. Schutt, F., et al., *Photodamage to human RPE cells by A2-E, a retinoid component of lipofuscin.* Invest Ophthalmol Vis Sci, 2000. **41**(8): p. 2303-8.
59. Sparrow, J.R. and B. Cai, *Blue light-induced apoptosis of A2E-containing RPE: involvement of caspase-3 and protection by Bcl-2.* Invest Ophthalmol Vis Sci, 2001. **42**(6): p. 1356-62.
60. Sparrow, J.R., K. Nakanishi, and C.A. Parish, *The lipofuscin fluorophore A2E mediates blue light-induced damage to retinal pigmented epithelial cells.* Invest Ophthalmol Vis Sci, 2000. **41**(7): p. 1981-9.

61. Ach, T., et al., *Quantitative autofluorescence and cell density maps of the human retinal pigment epithelium.* Invest Ophthalmol Vis Sci, 2014. **55**(8): p. 4832-41.
62. Schmitz-Valckenberg, S., et al., *Fundus autofluorescence imaging: review and perspectives.* Retina, 2008. **28**(3): p. 385-409.
63. Keilhauer, C.N. and F.C. Delori, *Near-infrared autofluorescence imaging of the fundus: visualization of ocular melanin.* Invest Ophthalmol Vis Sci, 2006. **47**(8): p. 3556-64.
64. Weinberger, A.W., et al., *Fundus near infrared fluorescence correlates with fundus near infrared reflectance.* Invest Ophthalmol Vis Sci, 2006. **47**(7): p. 3098-108.
65. Yung, M., M.A. Klufas, and D. Sarraf, *Clinical applications of fundus autofluorescence in retinal disease.* Int J Retina Vitreous, 2016. **2**: p. 12.
66. Paavo, M., et al., *Mutations in GPR143/OA1 and ABCA4 Inform Interpretations of Short-Wavelength and Near-Infrared Fundus Autofluorescence.* Invest Ophthalmol Vis Sci, 2018. **59**(6): p. 2459-2469.
67. Pilotto, E., et al., *Short wavelength fundus autofluorescence versus near-infrared fundus autofluorescence, with microperimetric correspondence, in patients with geographic atrophy due to age-related macular degeneration.* Br J Ophthalmol, 2011. **95**(8): p. 1140-4.
68. Cideciyan, A.V., et al., *Predicting Progression of ABCA4-Associated Retinal Degenerations Based on Longitudinal Measurements of the Leading Disease Front.* Invest Ophthalmol Vis Sci, 2015. **56**(10): p. 5946-55.
69. Gibbs, D., et al., *Retinal pigment epithelium defects in humans and mice with mutations in MYO7A: imaging melanosome-specific autofluorescence.* Invest Ophthalmol Vis Sci, 2009. **50**(9): p. 4386-93.
70. Duncker, T., et al., *Comparison of near-infrared and short-wavelength autofluorescence in retinitis pigmentosa.* Invest Ophthalmol Vis Sci, 2013. **54**(1): p. 585-91.
71. Birtel, J., et al., *Near-Infrared Autofluorescence in Choroideremia: Anatomic and Functional Correlations.* Am J Ophthalmol, 2018. **199**: p. 19-27.
72. Skondra, D., et al., *Near infrared autofluorescence imaging of retinal diseases.* Semin Ophthalmol, 2012. **27**(5-6): p. 202-8.
73. Hendrickson, A., *Organization of the Adult Primate Fovea*, in *Macular Degeneration*, P.L. Penfold and J.M. Provis, Editors. 2005, Springer Berlin Heidelberg: Berlin, Heidelberg. p. 1-23.
74. Curcio, C.A. and K.A. Allen, *Topography of ganglion cells in human retina.* J Comp Neurol, 1990. **300**(1): p. 5-25.
75. Jager, R.D., W.F. Mieler, and J.W. Miller, *Age-related macular degeneration.* N Engl J Med, 2008. **358**(24): p. 2606-17.
76. Altschwager, P., et al., *Juvenile Macular Degenerations.* Semin Pediatr Neurol, 2017. **24**(2): p. 104-109.
77. Silva, R., *Myopic maculopathy: a review.* Ophthalmologica, 2012. **228**(4): p. 197-213.
78. Li, J., R.C. Tripathi, and B.J. Tripathi, *Drug-induced ocular disorders.* Drug Saf, 2008. **31**(2): p. 127-41.
79. Diaz, R.I., et al., *Ocular histoplasmosis syndrome.* Surv Ophthalmol, 2015. **60**(4): p. 279-95.
80. Wong, W.L., et al., *Global prevalence of age-related macular degeneration and disease burden projection for 2020 and 2040: a systematic review and meta-analysis.* Lancet Glob Health, 2014. **2**(2): p. e106-16.
81. Chakravarthy, U., et al., *Clinical risk factors for age-related macular degeneration: a systematic review and meta-analysis.* BMC Ophthalmol, 2010. **10**: p. 31.
82. Chew, E.Y., et al., *Risk of advanced age-related macular degeneration after cataract surgery in the Age-Related Eye Disease Study: AREDS report 25.* Ophthalmology, 2009. **116**(2): p. 297-303.
83. de Koning-Backus, A.P.M., et al., *Intake of vegetables, fruit, and fish is beneficial for Age-related Macular Degeneration.* Am J Ophthalmol, 2018.
84. DeAngelis, M.M., et al., *Genetics of age-related macular degeneration (AMD).* Hum Mol Genet, 2017. **26**(R1): p. R45-R50.
85. Herrmann, P., F.G. Holz, and P. Charbel Issa, *[Etiology and pathogenesis of age-related macular degeneration].* Ophthalmologe, 2013. **110**(4): p. 377-87; quiz 388-9.
86. Holliday, E.G., et al., *Insights into the genetic architecture of early stage age-related macular degeneration: a genome-wide association study meta-analysis.* PLoS One, 2013. **8**(1): p. e53830.
87. Fritsche, L.G., et al., *Age-related macular degeneration: genetics and biology coming together.* Annu Rev Genomics Hum Genet, 2014. **15**: p. 151-71.
88. Laude, A., et al., *Polypoidal choroidal vasculopathy and neovascular age-related macular degeneration: same or different disease?* Prog Retin Eye Res, 2010. **29**(1): p. 19-29.
89. Wong, C.W., et al., *Age-related macular degeneration and polypoidal choroidal vasculopathy in Asians.* Prog Retin Eye Res, 2016. **53**: p. 107-139.
90. Brandl, C., et al., *Features of Age-Related Macular Degeneration in the General Adults and Their Dependency on Age, Sex, and Smoking: Results from the German KORA Study.* PLoS One, 2016. **11**(11): p. e0167181.
91. Korb, C.A., et al., *Prevalence of age-related macular degeneration in a large European cohort: results from the population-based Gutenberg Health Study.* Graefes Arch Clin Exp Ophthalmol, 2014. **252**(9): p. 1403-11.
92. Blacharski, P., *Fundus flavimaculatus*, in *Retinal Dystrophies and Degenerations.* , D.A. Newsome, Editor. 1988, Raven Press: New York. p. 135-159.

93. Stargardt, K., *Über familiäre, progressive Degeneration in der Maculagegend des Auges.* Albrecht von Graefes Archiv für Ophthalmologie, 1909. **71**(3): p. 534-550.
94. Allikmets, R., et al., *A photoreceptor cell-specific ATP-binding transporter gene (ABCR) is mutated in recessive Stargardt macular dystrophy.* Nat Genet, 1997. **15**(3): p. 236-46.
95. The Human Gene Mutation Database, *Mutations in ABCA4,* 2019. Available at *http://www.hgmd.cf.ac.uk* (accessed 13 August 2019).
96. Klevering, B.J., et al., *The spectrum of retinal phenotypes caused by mutations in the ABCA4 gene.* Graefes Arch Clin Exp Ophthalmol, 2005. **243**(2): p. 90-100.
97. Martinez-Mir, A., et al., *Retinitis pigmentosa caused by a homozygous mutation in the Stargardt disease gene ABCR.* Nat Genet, 1998. **18**(1): p. 11-2.
98. Cideciyan, A.V., et al., *ABCA4 disease progression and a proposed strategy for gene therapy.* Hum Mol Genet, 2009. **18**(5): p. 931-41.
99. Allikmets, R., et al., *Mutation of the Stargardt disease gene (ABCR) in age-related macular degeneration.* Science, 1997. **277**(5333): p. 1805-7.
100. Mullins, R.F., et al., *Autosomal recessive retinitis pigmentosa due to ABCA4 mutations: clinical, pathologic, and molecular characterization.* Invest Ophthalmol Vis Sci, 2012. **53**(4): p. 1883-94.
101. van Driel, M.A., et al., *ABCR unites what ophthalmologists divide(s).* Ophthalmic Genet, 1998. **19**(3): p. 117-22.
102. Rozet, J.M., et al., *Spectrum of ABCR gene mutations in autosomal recessive macular dystrophies.* Eur J Hum Genet, 1998. **6**(3): p. 291-5.
103. Fishman, G.A., *Historical evolution in the understanding of Stargardt macular dystrophy.* Ophthalmic Genet, 2010. **31**(4): p. 183-9.
104. Lindner, M., et al., *Differential Disease Progression in Atrophic Age-Related Macular Degeneration and Late-Onset Stargardt Disease.* Invest Ophthalmol Vis Sci, 2017. **58**(2): p. 1001-1007.
105. Westeneng-van Haaften, S.C., et al., *Clinical and genetic characteristics of late-onset Stargardt's disease.* Ophthalmology, 2012. **119**(6): p. 1199-210.
106. Molday, R.S. and K. Zhang, *Defective lipid transport and biosynthesis in recessive and dominant Stargardt macular degeneration.* Prog Lipid Res, 2010. **49**(4): p. 476-92.
107. Yang, Z., et al., *Mutant prominin 1 found in patients with macular degeneration disrupts photoreceptor disk morphogenesis in mice.* J Clin Invest, 2008. **118**(8): p. 2908-16.
108. Goldberg, A.F., O.L. Moritz, and D.S. Williams, *Molecular basis for photoreceptor outer segment architecture.* Prog Retin Eye Res, 2016. **55**: p. 52-81.
109. Bhattacharya, S., et al., *Prominin-1 Is a Novel Regulator of Autophagy in the Human Retinal Pigment Epithelium.* Invest Ophthalmol Vis Sci, 2017. **58**(4): p. 2366-2387.
110. Age-Related Eye Disease Study Research, G., *A randomized, placebo-controlled, clinical trial of high-dose supplementation with vitamins C and E, beta carotene, and zinc for age-related macular degeneration and vision loss: AREDS report no. 8.* Arch Ophthalmol, 2001. **119**(10): p. 1417-36.
111. Teussink, M.M., et al., *The effect of light deprivation in patients with Stargardt disease.* Am J Ophthalmol, 2015. **159**(5): p. 964-72 e2.
112. Waugh, N., et al., *Treatments for dry age-related macular degeneration and Stargardt disease: a systematic review.* Health Technol Assess, 2018. **22**(27): p. 1-168.
113. Lim, L.S., et al., *Age-related macular degeneration.* Lancet, 2012. **379**(9827): p. 1728-38.
114. Joussen, A.M. and N. Bornfeld, *The treatment of wet age-related macular degeneration.* Dtsch Arztebl Int, 2009. **106**(18): p. 312-7.
115. Pozarowska, D. and P. Pozarowski, *The era of anti-vascular endothelial growth factor (VEGF) drugs in ophthalmology, VEGF and anti-VEGF therapy.* Cent Eur J Immunol, 2016. **41**(3): p. 311-316.
116. Eandi, C.M., et al., *Treatment for neovascular age related macular degeneration: The state of the art.* Eur J Pharmacol, 2016. **787**: p. 78-83.
117. Gemenetzi, M., A.J. Lotery, and P.J. Patel, *Risk of geographic atrophy in age-related macular degeneration patients treated with intravitreal anti-VEGF agents.* Eye (Lond), 2017. **31**(1): p. 1-9.
118. Grunwald, J.E., et al., *Risk of geographic atrophy in the comparison of age-related macular degeneration treatments trials.* Ophthalmology, 2014. **121**(1): p. 150-161.
119. Horani, M., S. Mahmood, and T.M. Aslam, *Macular Atrophy of the Retinal Pigment Epithelium in Patients with Neovascular Age-Related Macular Degeneration: What is the Link? Part I: A Review of Disease Characterization and Morphological Associations.* Ophthalmol Ther, 2019. **8**(2): p. 235-249.
120. Stefanini, F.R., J.F. Arevalo, and M. Maia, *Bevacizumab for the management of diabetic macular edema.* World J Diabetes, 2013. **4**(2): p. 19-26.
121. Rosenfeld, P.J., A.A. Moshfeghi, and C.A. Puliafito, *Optical coherence tomography findings after an intravitreal injection of bevacizumab (avastin) for neovascular age-related macular degeneration.* Ophthalmic Surg Lasers Imaging, 2005. **36**(4): p. 331-5.
122. Lu, X. and X. Sun, *Profile of conbercept in the treatment of neovascular age-related macular degeneration.* Drug Des Devel Ther, 2015. **9**: p. 2311-20.
123. Nguyen, C.L., et al., *Anti-vascular endothelial growth factor for neovascular age-related macular degeneration: a meta-analysis of randomized controlled trials.* BMC Ophthalmol, 2018. **18**(1): p. 130.
124. Modi, Y.S., C. Tanchon, and J.P. Ehlers, *Comparative safety and tolerability of anti-VEGF therapy in age-related macular degeneration.* Drug Saf, 2015. **38**(3): p. 279-93.

125. Bakall, B., et al., *Aflibercept therapy for exudative age-related macular degeneration resistant to bevacizumab and ranibizumab.* Am J Ophthalmol, 2013. **156**(1): p. 15-22 e1.
126. Garcia-Layana, A., et al., *Treatment of Exudative Age-related Macular Degeneration: Focus on Aflibercept.* Drugs Aging, 2015. **32**(10): p. 797-807.
127. Gasperini, J.L., et al., *Bevacizumab and ranibizumab tachyphylaxis in the treatment of choroidal neovascularisation.* Br J Ophthalmol, 2012. **96**(1): p. 14-20.
128. Ho, V.Y., et al., *Short-term outcomes of aflibercept for neovascular age-related macular degeneration in eyes previously treated with other vascular endothelial growth factor inhibitors.* Am J Ophthalmol, 2013. **156**(1): p. 23-28 e2.
129. Yonekawa, Y., et al., *Conversion to aflibercept for chronic refractory or recurrent neovascular age-related macular degeneration.* Am J Ophthalmol, 2013. **156**(1): p. 29-35 e2.
130. Pikkel, J. and S. Attas, *"What should I inject next?" Challenging treatment decisions in the multiple anti-VEGF: a review of publications exploring anti-VEGF switching for nAMD.* Int Ophthalmol, 2018. **38**(5): p. 2031-2039.
131. Chin-Yee, D., et al., *A systematic review of as needed versus treat and extend ranibizumab or bevacizumab treatment regimens for neovascular age-related macular degeneration.* Br J Ophthalmol, 2016. **100**(7): p. 914-917.
132. Gemenetzi, M. and P.J. Patel, *A Systematic Review of the Treat and Extend Treatment Regimen with Anti-VEGF Agents for Neovascular Age-Related Macular Degeneration.* Ophthalmol Ther, 2017. **6**(1): p. 79-92.
133. Mantel, I., *Optimizing the Anti-VEGF Treatment Strategy for Neovascular Age-Related Macular Degeneration: From Clinical Trials to Real-Life Requirements.* Transl Vis Sci Technol, 2015. **4**(3): p. 6.
134. Kozak, I., S.S. Shoughy, and D.U. Stone, *Intravitreal Antiangiogenic Therapy of Uveitic Macular Edema: A Review.* J Ocul Pharmacol Ther, 2017. **33**(4): p. 235-239.
135. Wu, A.L. and W.C. Wu, *Anti-VEGF for ROP and Pediatric Retinal Diseases.* Asia Pac J Ophthalmol (Phila), 2018. **7**(3): p. 145-151.
136. Krick, T.W. and N.M. Bressler, *Recent clinically relevant highlights from the Diabetic Retinopathy Clinical Research Network.* Curr Opin Ophthalmol, 2018. **29**(3): p. 199-205.
137. Cheung, C.M.G., et al., *Myopic Choroidal Neovascularization: Review, Guidance, and Consensus Statement on Management.* Ophthalmology, 2017. **124**(11): p. 1690-1711.
138. Rodrigues, G.B., et al., *Neovascular glaucoma: a review.* Int J Retina Vitreous, 2016. **2**: p. 26.
139. Gunther, J.B. and M.M. Altaweel, *Bevacizumab (Avastin) for the treatment of ocular disease.* Surv Ophthalmol, 2009. **54**(3): p. 372-400.
140. Grisanti, S., et al., *Intracameral bevacizumab for iris rubeosis.* Am J Ophthalmol, 2006. **142**(1): p. 158-60.
141. Hussain, R.M. and T.A. Ciulla, *Emerging vascular endothelial growth factor antagonists to treat neovascular age-related macular degeneration.* Expert Opin Emerg Drugs, 2017. **22**(3): p. 235-246.
142. Dugel, P.U., et al., *HAWK and HARRIER: phase 3, multicenter, randomized, double-masked trials of brolucizumab for neovascular age-related macular degeneration.* Ophthalmology, 2019.
143. Novartis AG, *Novartis announces FDA filing acceptance and Priority Review of brolucizumab (RTH258) for patients with wet AMD,* 2019. Available at *https://www.novartis.com/news/media-releases/novartis-announces-fda-filing-acceptance-and-priority-review-brolucizumab-rth258-patients-wet-amd* (accessed 02 May 2019).
144. Klaassen, I., C.J. Van Noorden, and R.O. Schlingemann, *Molecular basis of the inner blood-retinal barrier and its breakdown in diabetic macular edema and other pathological conditions.* Prog Retin Eye Res, 2013. **34**: p. 19-48.
145. Regula, J.T., et al., *Targeting key angiogenic pathways with a bispecific CrossMAb optimized for neovascular eye diseases.* EMBO Mol Med, 2016. **8**(11): p. 1265-1288.
146. Sahni, J., et al., *Simultaneous Inhibition of Angiopoietin-2 and Vascular Endothelial Growth Factor-A with Faricimab in Diabetic Macular Edema: BOULEVARD Phase 2 Randomized Trial.* Ophthalmology, 2019.
147. Tolentino, M., *Systemic and ocular safety of intravitreal anti-VEGF therapies for ocular neovascular disease.* Surv Ophthalmol, 2011. **56**(2): p. 95-113.
148. Ladas, I.D., et al., *Safety of repeat intravitreal injections of bevacizumab versus ranibizumab: our experience after 2,000 injections.* Retina, 2009. **29**(3): p. 313-8.
149. Julien, S., A. Biesemeier, and U. Schraermeyer, *In vitro induction of protein complexes between bevacizumab, VEGF-A(1)(6)(5) and heparin: explanation for deposits observed on endothelial veins in monkey eyes.* Br J Ophthalmol, 2013. **97**(4): p. 511-7.
150. Schraermeyer, U. and S. Julien, *Formation of immune complexes and thrombotic microangiopathy after intravitreal injection of bevacizumab in the primate eye.* Graefes Arch Clin Exp Ophthalmol, 2012. **250**(9): p. 1303-13.
151. Schraermeyer, U. and S. Julien, *Effects of bevacizumab in retina and choroid after intravitreal injection into monkey eyes.* Expert Opin Biol Ther, 2013. **13**(2): p. 157-67.
152. Peters, S., et al., *Ultrastructural findings in the primate eye after intravitreal injection of bevacizumab.* Am J Ophthalmol, 2007. **143**(6): p. 995-1002.

153. European Medicines Agency, *Summary of product characteristics for Avastin,* 2019. Available at *https://www.ema.europa.eu/en/documents/product-information/avastin-epar-product-information_en.pdf* (accessed 02 May 2019).
154. Avery, R.L., et al., *Systemic pharmacokinetics following intravitreal injections of ranibizumab, bevacizumab or aflibercept in patients with neovascular AMD.* Br J Ophthalmol, 2014. **98**(12): p. 1636-41.
155. Jampol, L.M., et al., *Plasma Vascular Endothelial Growth Factor Concentrations after Intravitreous Anti-Vascular Endothelial Growth Factor Therapy for Diabetic Macular Edema.* Ophthalmology, 2018.
156. Moja, L., et al., *Systemic safety of bevacizumab versus ranibizumab for neovascular age-related macular degeneration.* Cochrane Database Syst Rev, 2014(9): p. CD011230.
157. Hanhart, J., D.S. Comaneshter, and S. Vinker, *Mortality after a cerebrovascular event in age-related macular degeneration patients treated with bevacizumab ocular injections.* Acta Ophthalmol, 2018.
158. Kwon, J.W., D. Jee, and T.Y. La, *The association between myocardial infarction and intravitreal bevacizumab injection.* Medicine (Baltimore), 2018. **97**(13): p. e0198.
159. Jonas, J.B., C.M.G. Cheung, and S. Panda-Jonas, *Updates on the Epidemiology of Age-Related Macular Degeneration.* Asia Pac J Ophthalmol (Phila), 2017.
160. Hogan, M.J., *Bruch's membrane and disease of the macula. Role of elastic tissue and collagen.* Trans Ophthalmol Soc U K, 1967. **87**: p. 113-61.
161. McLeod, D.S., et al., *Relationship between RPE and choriocapillaris in age-related macular degeneration.* Invest Ophthalmol Vis Sci, 2009. **50**(10): p. 4982-91.
162. Ramrattan, R.S., et al., *Morphometric analysis of Bruch's membrane, the choriocapillaris, and the choroid in aging.* Invest Ophthalmol Vis Sci, 1994. **35**(6): p. 2857-64.
163. Friedman, E., *A hemodynamic model of the pathogenesis of age-related macular degeneration.* Am J Ophthalmol, 1997. **124**(5): p. 677-82.
164. Machalinska, A., et al., *[Elevated level of circulating endothelial cells as an exponent of chronic vascular dysfunction in the course of AMD].* Klin Oczna, 2011. **113**(7-9): p. 228-32.
165. Verhoeff, F.H. and H.P. Grossman, *The Pathogenesis of Disciform Degeneration of the Macula.* Trans Am Ophthalmol Soc, 1937. **35**: p. 262-94.
166. Grossniklaus, H.E. and W.R. Green, *Choroidal neovascularization.* Am J Ophthalmol, 2004. **137**(3): p. 496-503.
167. Chen, K.G., P.G. Christakis, and E.Y. Chew, *10-Year Follow-up of a Subclinical Choroidal Neovascular Membrane in a Patient with Age-Related Macular Degeneration.* Retin Cases Brief Rep, 2018.
168. Treister, A.D., et al., *Prevalence of Subclinical CNV and Choriocapillaris Nonperfusion in Fellow Eyes of Unilateral Exudative AMD on OCT Angiography.* Transl Vis Sci Technol, 2018. **7**(5): p. 19.
169. Birnbach, C.D., et al., *Histopathology and immunocytochemistry of the neurosensory retina in fundus flavimaculatus.* Ophthalmology, 1994. **101**(7): p. 1211-9.
170. Bonilha, V.L., et al., *Retinal Histopathology in Eyes from a Patient with Stargardt disease caused by Compound Heterozygous ABCA4 Mutations.* Ophthalmic Genet, 2016. **37**(2): p. 150-60.
171. Eagle, R.C., Jr., et al., *Retinal pigment epithelial abnormalities in fundus flavimaculatus: a light and electron microscopic study.* Ophthalmology, 1980. **87**(12): p. 1189-200.
172. Maeda, A., et al., *Retinopathy in mice induced by disrupted all-trans-retinal clearance.* J Biol Chem, 2008. **283**(39): p. 26684-93.
173. Radu, R.A., et al., *Light exposure stimulates formation of A2E oxiranes in a mouse model of Stargardt's macular degeneration.* Proc Natl Acad Sci U S A, 2004. **101**(16): p. 5928-33.
174. Weng, J., et al., *Insights into the function of Rim protein in photoreceptors and etiology of Stargardt's disease from the phenotype in abcr knockout mice.* Cell, 1999. **98**(1): p. 13-23.
175. Charbel Issa, P., et al., *Fundus autofluorescence in the Abca4(-/-) mouse model of Stargardt disease--correlation with accumulation of A2E, retinal function, and histology.* Invest Ophthalmol Vis Sci, 2013. **54**(8): p. 5602-12.
176. Radu, R.A., et al., *Accelerated accumulation of lipofuscin pigments in the RPE of a mouse model for ABCA4-mediated retinal dystrophies following Vitamin A supplementation.* Invest Ophthalmol Vis Sci, 2008. **49**(9): p. 3821-9.
177. Radu, R.A., et al., *Complement system dysregulation and inflammation in the retinal pigment epithelium of a mouse model for Stargardt macular degeneration.* J Biol Chem, 2011. **286**(21): p. 18593-601.
178. Mao, H., et al., *Mitochondrial oxidative stress in the retinal pigment epithelium leads to localized retinal degeneration.* Invest Ophthalmol Vis Sci, 2014. **55**(7): p. 4613-27.
179. Seo, S.J., et al., *Pathological consequences of long-term mitochondrial oxidative stress in the mouse retinal pigment epithelium.* Exp Eye Res, 2012. **101**: p. 60-71.
180. Zhao, Z., et al., *Age-related retinopathy in NRF2-deficient mice.* PLoS One, 2011. **6**(4): p. e19456.
181. Fujihara, M., et al., *Chronic cigarette smoke causes oxidative damage and apoptosis to retinal pigmented epithelial cells in mice.* PLoS One, 2008. **3**(9): p. e3119.
182. Zhang, N., et al., *Protein misfolding and the pathogenesis of ABCA4-associated retinal degenerations.* Hum Mol Genet, 2015. **24**(11): p. 3220-37.
183. Cremers, F.P., et al., *Autosomal recessive retinitis pigmentosa and cone-rod dystrophy caused by splice site mutations in the Stargardt's disease gene ABCR.* Hum Mol Genet, 1998. **7**(3): p. 355-62.

184. Shroyer, N.F., et al., *Null missense ABCR (ABCA4) mutations in a family with stargardt disease and retinitis pigmentosa.* Invest Ophthalmol Vis Sci, 2001. **42**(12): p. 2757-61.
185. Maeda, A., et al., *Involvement of all-trans-retinal in acute light-induced retinopathy of mice.* J Biol Chem, 2009. **284**(22): p. 15173-83.
186. Chen, Y., et al., *Mechanism of all-trans-retinal toxicity with implications for stargardt disease and age-related macular degeneration.* J Biol Chem, 2012. **287**(7): p. 5059-69.
187. Danciger, M., et al., *New retinal light damage QTL in mice with the light-sensitive RPE65 LEU variant.* Mamm Genome, 2004. **15**(4): p. 277-83.
188. Elleder, M. and J. Borovansky, *Autofluorescence of melanins induced by ultraviolet radiation and near ultraviolet light. A histochemical and biochemical study.* Histochem J, 2001. **33**(5): p. 273-81.
189. Kayatz, P., et al., *Oxidation causes melanin fluorescence.* Invest Ophthalmol Vis Sci, 2001. **42**(1): p. 241-6.
190. Sarna, T., et al., *Loss of melanin from human RPE with aging: possible role of melanin photooxidation.* Exp Eye Res, 2003. **76**(1): p. 89-98.
191. Wakamatsu, K., et al., *UVA-induced oxidative degradation of melanins: fission of indole moiety in eumelanin and conversion to benzothiazole moiety in pheomelanin.* Pigment Cell Melanoma Res, 2012. **25**(4): p. 434-45.
192. Dontsov, A.E., N.L. Sakina, and M.A. Ostrovsky, *Loss of Melanin by Eye Retinal Pigment Epithelium Cells Is Associated with Its Oxidative Destruction in Melanolipofuscin Granules.* Biochemistry (Mosc), 2017. **82**(8): p. 916-924.
193. Fang, Y., et al., *Fundus autofluorescence, spectral-domain optical coherence tomography, and histology correlations in a Stargardt disease mouse model.* FASEB J, 2020. **34**(3): p. 3693-3714.
194. Schraermeyer, U. and H. Stieve, *A newly discovered pathway of melanin formation in cultured retinal pigment epithelium of cattle.* Cell Tissue Res, 1994. **276**(2): p. 273-9.
195. Feeney, L., *Lipofuscin and melanin of human retinal pigment epithelium. Fluorescence, enzyme cytochemical, and ultrastructural studies.* Invest Ophthalmol Vis Sci, 1978. **17**(7): p. 583-600.
196. Heiduschka, P., et al., *Penetration of bevacizumab through the retina after intravitreal injection in the monkey.* Invest Ophthalmol Vis Sci, 2007. **48**(6): p. 2814-23.
197. Heiduschka, P., et al., *Bevacizumab (avastin) does not harm retinal function after intravitreal injection as shown by electroretinography in adult mice.* Retina, 2008. **28**(1): p. 46-55.
198. Julien, S., et al., *Immunohistochemical localisation of intravitreally injected bevacizumab at the posterior pole of the primate eye: implication for the treatment of retinal vein occlusion.* Br J Ophthalmol, 2008. **92**(10): p. 1424-8.
199. Peters, S., et al., *Immunohistochemical localisation of intravitreally injected bevacizumab in the anterior chamber angle, iris and ciliary body of the primate eye.* Br J Ophthalmol, 2008. **92**(4): p. 541-4.
200. Meyer, T., et al., *Bevacizumab immune complexes activate platelets and induce thrombosis in FCGR2A transgenic mice.* J Thromb Haemost, 2009. **7**(1): p. 171-81.
201. Scappaticci, F.A., et al., *Arterial thromboembolic events in patients with metastatic carcinoma treated with chemotherapy and bevacizumab.* J Natl Cancer Inst, 2007. **99**(16): p. 1232-9.
202. Schraermeyer, U., et al., *Intravitreal injection of Fc-fragments has multiple adverse effects on retina and choroid.* Investigative Ophthalmology & Visual Science, 2015. **56**(7): p. 1511-1511.
203. Saint-Geniez, M., et al., *An essential role for RPE-derived soluble VEGF in the maintenance of the choriocapillaris.* Proc Natl Acad Sci U S A, 2009. **106**(44): p. 18751-6.
204. Janssens, K., T. Zeyen, and J. Van Calster, *Anterior segment ischemia with rubeosis iridis after a circular buckling operation treated successfully with an intravitreal bevacizumab injection: a case report and review of the literature.* Bull Soc Belge Ophtalmol, 2012(319): p. 5-9.
205. Sigford, D.K., et al., *Global reported endophthalmitis risk following intravitreal injections of anti-VEGF: a literature review and analysis.* Clin Ophthalmol, 2015. **9**: p. 773-81.
206. Liu, L., *Pharmacokinetics of monoclonal antibodies and Fc-fusion proteins.* Protein Cell, 2018. **9**(1): p. 15-32.
207. Jafari, R., et al., *Fc-fusion Proteins in Therapy: An Updated View.* Curr Med Chem, 2017. **24**(12): p. 1228-1237.
208. Dedania, V.S. and S.J. Bakri, *Systemic safety of intravitreal anti-vascular endothelial growth factor agents in age-related macular degeneration.* Curr Opin Ophthalmol, 2016. **27**(3): p. 224-43.
209. Schmucker, C., et al., *A safety review and meta-analyses of bevacizumab and ranibizumab: off-label versus goldstandard.* PLoS One, 2012. **7**(8): p. e42701.
210. van der Reis, M.I., et al., *A systematic review of the adverse events of intravitreal anti-vascular endothelial growth factor injections.* Retina, 2011. **31**(8): p. 1449-69.
211. Chen, Y., et al., *Assessing susceptibility to age-related macular degeneration with genetic markers and environmental factors.* Arch Ophthalmol, 2011. **129**(3): p. 344-51.
212. Thornton, J., et al., *Smoking and age-related macular degeneration: a review of association.* Eye (Lond), 2005. **19**(9): p. 935-44.
213. Jia, Y., et al., *Split-spectrum amplitude-decorrelation angiography with optical coherence tomography.* Opt Express, 2012. **20**(4): p. 4710-25.
214. Kvanta, A., et al., *Optical Coherence Tomography Angiography of the Foveal Microvasculature in Geographic Atrophy.* Retina, 2017. **37**(5): p. 936-942.

215. Sacconi, R., et al., *Optical Coherence Tomography Angiography in Geographic Atrophy.* Retina, 2017.
216. Wei, X., et al., *Choroidal structural analysis and vascularity index in retinal dystrophies.* Acta Ophthalmol, 2018.
217. Kaarniranta, K. and A. Salminen, *Age-related macular degeneration: activation of innate immunity system via pattern recognition receptors.* J Mol Med (Berl), 2009. **87**(2): p. 117-23.
218. Schraermeyer, U., et al., *A new kind of labyrinth-like capillary is responsible for leakage from human choroidal neovascular endothelium, as investigated by high-resolution electron microscopy.* Graefes Arch Clin Exp Ophthalmol, 2015. **253**(5): p. 681-9.
219. Scholl, H.P., et al., *Systemic complement activation in age-related macular degeneration.* PLoS One, 2008. **3**(7): p. e2593.
220. Singh, J.A. and J.D. Cleveland, *Gout and the risk of age-related macular degeneration in the elderly.* PLoS One, 2018. **13**(7): p. e0199562.
221. Sawada, O., et al., *All-trans-retinal induces Bax activation via DNA damage to mediate retinal cell apoptosis.* Exp Eye Res, 2014. **123**: p. 27-36.
222. Yacout, S.M., S.F. Elsawa, and E.R. Gaillard, *Calf melanin immunomodulates RPE cell attachment to extracellular matrix protein.* Graefes Arch Clin Exp Ophthalmol, 2018.
223. Klein, R., et al., *Prevalence of age-related macular degeneration in the US population.* Arch Ophthalmol, 2011. **129**(1): p. 75-80.
224. Fisher, D.E., et al., *Incidence of Age-Related Macular Degeneration in a Multi-Ethnic United States Population: The Multi-Ethnic Study of Atherosclerosis.* Ophthalmology, 2016. **123**(6): p. 1297-308.
225. Ben Ami, T., et al., *Spatial and Spectral Characterization of Human Retinal Pigment Epithelium Fluorophore Families by Ex Vivo Hyperspectral Autofluorescence Imaging.* Transl Vis Sci Technol, 2016. **5**(3): p. 5.
226. Tong, Y., et al., *Hyperspectral Autofluorescence Imaging of Drusen and Retinal Pigment Epithelium in Donor Eyes with Age-Related Macular Degeneration.* Retina, 2016. **36 Suppl 1**: p. S127-S136.
227. Martinez-Mir, A., et al., *A new locus for autosomal recessive retinitis pigmentosa (RP19) maps to 1p13-1p21.* Genomics, 1997. **40**(1): p. 142-6.
228. Lee, B., et al., *Short-term effects of anti-vascular endothelial growth factor on peripapillary choroid and choriocapillaris in eyes with neovascular age-related macular degeneration.* Graefes Arch Clin Exp Ophthalmol, 2019.
229. Julien, S. and U. Schraermeyer, *Lipofuscin can be eliminated from the retinal pigment epithelium of monkeys.* Neurobiol Aging, 2012. **33**(10): p. 2390-7.
230. Hussain, R.M., et al., *Pharmacotherapy of retinal disease with visual cycle modulators.* Expert Opin Pharmacother, 2018. **19**(5): p. 471-481.
231. Nociari, M.M., et al., *Beta cyclodextrins bind, stabilize, and remove lipofuscin bisretinoids from retinal pigment epithelium.* Proc Natl Acad Sci U S A, 2014. **111**(14): p. E1402-8.

5 Publications and presentations

5.1 Peer-reviewed publications

Boll, B., Taubitz, T. & Heide, L. **Role of MbtH-like proteins in the adenylation of tyrosine during aminocoumarin and vancomycin biosynthesis**. *The Journal of biological chemistry* 286, 36281-36290, DOI: 10.1074/jbc.M111.288092 (2011).

Biesemeier, A., Taubitz, T., Julien, S., Yoeruek, E. & Schraermeyer, U. **Choriocapillaris breakdown precedes retinal degeneration in age-related macular degeneration.** *Neurobiology of aging* 35, 2562-2573, DOI: 10.1016/j.neurobiolaging.2014.05.003 (2014).

Julien, S., Biesemeier, A., Taubitz, T. & Schraermeyer, U. **Different effects of intravitreally injected ranibizumab and aflibercept on retinal and choroidal tissues of monkey eyes.** *The British journal of ophthalmology* 98, 813-825, DOI: 10.1136/bjophthalmol-2013-304019 (2014).

Ludinsky, M., Christner, S., Su, N., Taubitz, T., Tschulakow, A., Biesemeier, A., Julien-Schraermeyer, S. & Schraermeyer, U. **The effects of VEGF-A-inhibitors aflibercept and ranibizumab on the ciliary body and iris of monkeys.** *Graefe's archive for clinical and experimental ophthalmology* 254, 1117-1125, DOI: 10.1007/s00417-016-3344-8 (2016).

Taubitz, T., Steinbrenner, L. P., Tschulakow, A. V., Biesemeier, A., Julien-Schraermeyer, S. & Schraermeyer, U. **Effects of intravitreally injected Fc fragment on rat eyes.** *Graefe's archive for clinical and experimental ophthalmology* 254, 2401-2409, DOI: 10.1007/s00417-016-3511-y (2016).

Taubitz, T., Tschulakow, A. V., Tikhonovich, M., Illing, B., Fang, Y., Biesemeier, A., Julien-Schraermeyer, S. & Schraermeyer, U. **Ultrastructural alterations in the retinal pigment epithelium and photoreceptors of a Stargardt patient and three Stargardt mouse models: indication for the central role of RPE melanin in oxidative stress.** *PeerJ* 6, e5215, DOI: 10.7717/peerj.5215 (2018).

Taubitz, T., Fang, Y., Biesemeier, A., Julien-Schraermeyer, S. & Schraermeyer, U. **Age, lipofuscin and melanin oxidation affect fundus near-infrared autofluorescence.** *EBioMedicine* 48, 592-604, DOI: 10.1016/j.ebiom.2019.09.048 (2019).

Fang Y., Tschulakow A., Taubitz T., Illing B., Biesemeier A., Julien-Schraermeyer S., Radu R. A., Jiang Z., & Schraermeyer U. **Correlation between *in vivo* and *ex vivo* assessments in a mouse model of advanced Stargardt disease.** *FASEB journal* 34, 3693-3714, DOI: 10.1096/fj.201901784RR (2020).

5.2 Conference abstracts

Biesemeier, A., Taubitz, T. & Schraermeyer, U. **Egg or hen: Use of combined light and electron microscopy to reveal whether CC breakdown precedes RPE degeneration in AMD.** *Investigative ophthalmology & visual science* 54, 3200-3200 (2013).

Annual meeting of ARVO in Seattle, Washington, USA (2013)

Schraermeyer, U., Taubitz, T., Steinbrenner, L. P., Peters, T., Biesemeier, A. K., Rittgarn, M., Schultheiss, S., Tschulakow, A. & Julien, S. **Intravitreal injection of Fc-fragments has multiple adverse effects on retina and choroid.** *Investigative ophthalmology & visual science* 56, 1511-1511 (2015).

Annual meeting of ARVO in Denver, Colorado, USA (2015)

Taubitz, T., Peters, T., Pöschel, S., Tschulakow, A., Rittgarn, M., Schultheiss, S., Schenke-Layland, K., Burnet, M., Julien, S. & Schraermeyer, U. **Removal of lipofuscin from the RPE of *Abca4*$^{-/-}$ mice with THPE: quantitative and toxicity studies.** *Investigative ophthalmology & visual science* 56, 4199-4199 (2015).

Annual meeting of ARVO in Denver, Colorado, USA (2015)

Taubitz, T., Fang, Y., Rittgarn, M., Schraermeyer, U. & Julien-Schraermeyer, S. **Testing a new pharmacological therapy approach for the removal of lipofuscin *in vitro*: results from a newly established culture of aged primary Stargardt mouse model RPE cells and aged primary human RPE cells.** *Investigative ophthalmology & visual science* 58, 257-257 (2017).

Annual meeting of ARVO in Baltimore, Maryland, USA (2017)

Fang, Y., Tschulakow, A., Tikhonovich, M., Taubitz, T., Illing, B., Schultheiss, S., Schraermeyer, U. & Julien-Schraermeyer, S. **Preclinical results of a new pharmacological therapy approach for Stargardt disease and dry age-related macular degeneration.** *Investigative ophthalmology & visual science* 58, 256-256 (2017).

Annual meeting of ARVO in Baltimore, Maryland, USA (2017)

Schraermeyer, U., Fang, Y., Taubitz, T., Tschulakow, A. **Degradation of lipofuscin in Stargardt mice can be enhanced by the superoxide generator riboflavin - a hypothesis for melanolipofuscin formation**. *Investigative ophthalmology & visual science* 60, 1912-1912 (2019).

Annual meeting of ARVO in Vancouver, Canada (2019)

Fang, Y., Tschulakow, A., Taubitz, T., Illing, B., Burda, A., Biesemeier, A., Julien-Schaermeyer, S., Schraermeyer, U. **Short-wavelength and near-infrared fundus autofluorescence in blue light-illuminated *Abca4*$^{-/-}$ mice and a patient with Stargardt disease.** *Investigative ophthalmology & visual science* 60, 5982-5982 (2019).

Annual meeting of ARVO in Vancouver, Canada (2019)

5.3 Poster presentations

Taubitz, T., Steinbrenner, L. P., Tschulakow, A., Biesemeier, A., Julien-Schraermeyer, S. & Schraermeyer, U. **Intravitreal injection of Fc fragment leads to attraction of immune-competent cells**

Makula Update in Hannover (2017)

Taubitz, T., Fang, Y., Rittgarn, M., Schraermeyer, U. & Julien-Schraermeyer, S. **Die Entfernung des Alterspigmentes Lipofuszin aus dem retinalen Pigmentepithel *in vitro***

Makula Update in Leipzig (2018)

6 Danksagung

Mein Dank gebührt zuallererst Prof. Dr. Ulrich Schraermeyer, der mich bereits als kleine Studentin auf der Suche nach einem Praktikumsplatz in seiner Gruppe willkommen hieß und nur durch dessen Anregungen, Betreuung und Geduld diese Arbeit überhaupt entstehen konnte.

Weiterhin bedanke ich mich bei Prof. Dr. Michael Duszenko und Prof. Dr. Thomas Langmann für die Erstellung der Gutachten.

Ebenfalls bedanken muss ich mich bei PD Dr. Sylvie Julien-Schraermeyer, die mir von Anfang an eine treue Ratgeberin und in den letzten Jahren auch eine wundervolle Büromitbewohnerin war, die immer ein offenes Ohr hatte. Je te remercie du fond du cœur!

Ebenso viel Dank schulde ich PD Dr. Antje Biesemeier für Rat, Tat und Amüsement, sowohl im, als auch außerhalb des Labors. Ich wünsch Dir alles Gute in Luxemburg!

Auch bei meinen übrigen Kollegen aus der Sektion bedanke ich mich sehr für die freundschaftliche Atmosphäre und die wundervolle Zusammenarbeit mit ihnen. Daher ein herzliches Danke an Dr. Alexander Tschulakow, Yuan Fang, Judith Birch, Antonina Burda, Shan Liu, Lei Xi, Kun Wang, Yanan Lyu und Harsh Thakkar. Der Dank gilt genauso den Ehemaligen, Dr. Laura Steinbrenner, Marina Tikhonovich, Dr. Sarah Christner, Maximilian Ludinsky, Miroslava Mingyarova, Nan Su, Bowen Cao und allen anderen, selbst den Praktikanten (und waren sie noch so kurz da), die ich hier nicht alle aufzählen kann.

Drei Namen fehlen bei der Auflistung der Ehemaligen allerdings mit Absicht: Bei Sigrid Schultheiß, Monika Rittgarn und Dr. Barbara Illing möchte ich mich ganz besonders bedanken, da ich von ihnen technisch und wissenschaftlich, nicht zuletzt aber auch menschlich, unfassbar viel gelernt habe. Euch dreien Danke, Danke, und Danke!

Allen ehemaligen und aktuellen Kollegen im Breuninger Bau und in der Augenklinik danke ich für all die Ratschläge, Hilfestellungen und angenehmen Gespräche, die sich im Lauf der Jahre angesammelt haben.

Ein besonderes Dankeschön gilt den Spendern und ihren Angehörigen, die dazu bereit waren ihr Gewebe nach dem Tod der Wissenschaft zur Verfügung zu stellen.

Nicht zuletzt möchte ich meinen Freunden und meiner Familie für ihre Unterstützung und ihren Glauben an mich danken. Insbesondere gilt dieser Dank Hildor Suter für sein geduldiges Zuhören und seine unendliche Faszination für Wissenschaft, die mich selbst an schlechten Tagen wieder angesteckt hat, und meinen Eltern Monika und Hans-Peter Taubitz, die mir in weiser Voraussicht schon als Kind ein Spielzeug-Mikroskop zu Weihnachten schenkten. Der folgende Satz ist das absolute Klischee jeder Danksagung, aber… Ohne Euch wäre diese Arbeit nicht möglich gewesen. Danke.